5-2013

A New Species of Teleoceras from the Late Miocene Gray Fossil Site, with Comparisons to Other North American Hemphillian Species

Rachel A. Short
East Tennessee State University

A New Species of *Teleoceras* from the Late Miocene Gray Fossil Site, with Comparisons to Other North American Hemphillian Species

A thesis

presented to

the faculty of the Department of Geosciences

East Tennessee State University

In partial fulfillment

of the requirements for the degree

Master of Science in Geosciences

by

Rachel A. Short

May 2013

Steven C. Wallace, chair

Blaine W. Schubert

Jim I. Mead

Keywords: Gray Fossil Site, *Teleoceras*, Morphology, Post-cranial

ABSTRACT

A New Species of *Teleoceras* from the Late Miocene Gray Fossil Site, with Comparisons to Other North American Hemphillian Species

by

Rachel A. Short

A thorough morphological description of *Teleoceras* material from the Gray Fossil Site, Gray, Tennessee is provided. This is the only record of a browsing *Teleoceras* and, as a late Hemphillian locality, represents 1 of the youngest populations. Linear measurements of post-cranial elements indicate proportional differences between *Teleoceras* from the Gray Fossil Site and those from other Hemphillian localities. These differences are more pronounced in the elements of the forelimb than in those of the hind limb. Statistical analyses of post-cranial elements from 3 Hemphillian species of *Teleoceras* suggest that these differences should not be used to separate species. However, the elements do typically sort well by fossil locality, which suggests that post-cranial morphology is plastic enough to become modified within a population. Furthermore, dental morphology comparisons with the holotypes of these species indicate that the GFS rhino represents a previously undescribed species.

ACKNOWLEDGEMENTS

I would like to thank my committee members, Drs. Steven Wallace, Blaine Schubert, and Jim Mead, for their help and encouragement along the way. A big thank you goes to Sandy Swift for always being available (and willing!) to reassure me. Thank you to all of the staff at the Gray Fossil Site, especially Brian Compton for making the excavation map for me, Shawn Haugrud for making the fossils look so wonderful, and Brett Woodward for access to specimens. I thank Jeff Supplee for always being interested in my work and providing an outlet for me to talk about it. I would also like to thank the following museum staffs for access to specimens and assistance with research: Drs. Richard Hulbert, Jr. and Jonathan Bloch (FLMNH); Charyl Ito and Kathy Hollis (NMNH); Judy Galkin, Ruth O'Leary, and Alana Gishlick (AMNH); Logan Ivy and Dr. Richard Stucky (DMNS); and Dr. Laura Wilson (SMNH). Also, this work would not have been possible without funding from the Center of Excellence in Paleontology and the Department of Geosciences at ETSU.

I have to thank my fellow graduate students for making the past 2 years so much fun, especially Laura Gilmore who was the best thesis buddy ever! I must thank my family for supporting me and understanding my want to move so far away from home to study rhino fossils. Finally, I give an enormous thank you to Jeff Martin who put up with my craziness for the last year while I finished this project. I'll return the favor next year!

TABLE OF CONTENTS

LIST OF TABLES

Table Page

LIST OF FIGURES

Figure Page

CHAPTER 1

INTRODUCTION

Teleoceras (Perissodactyla, Rhinocerotidae) is a wide-spread Miocene rhinoceros that has been reported at nearly all fossil localities from the early Barstovian to the late Hemphillian Land Mammal Age (Prothero 1998, 2005). In 2000, fossils were found during road construction in Gray, Tennessee (see summary in Schubert 2011) and, in 2004, 2 complete rhinoceros skeletons (ETMNH 609 and ETMNH 601; Appendix 1) were discovered at the Gray Fossil Site (GFS). These specimens were referred to *Teleoceras* cf. *T. hicksi* (Wallace 2006) (FIG. 1). To date, GFS has a minimum of 5 individuals of *Teleoceras* based on 4 adult left astragali and a juvenile, possibly fetal, tibia and fibula pair (Wallace 2006); however, this number is expected to increase as excavations continue.

Figure 1. Mounted skeleton of ETMNH 609 at the East Tennessee State University and General Shale Brick Museum and Visitor's Center at the Gray Fossil Site. Photo courtesy of Steven Wallace.

With the Pipe Creek Sinkhole of Indiana, which has some fragmentary *Teleoceras* sp. material, GFS is the only wholly terrestrial Hemphillian fossil locality east of the Mississippi River that is not in Florida (Farlow et al. 2001, Prothero 2005) (Fig. 2). Thus, GFS provides an excellent opportunity to study the more northern and eastern fauna of North America during an important time of environmental changes. Wallace and Wang (2004) dated GFS to 4.5-7 Ma (Late Hemphillian) and Strömberg and McInerney (2011) determined that GFS represents a forested setting that coincides with and follows the spread of grasslands in North America.

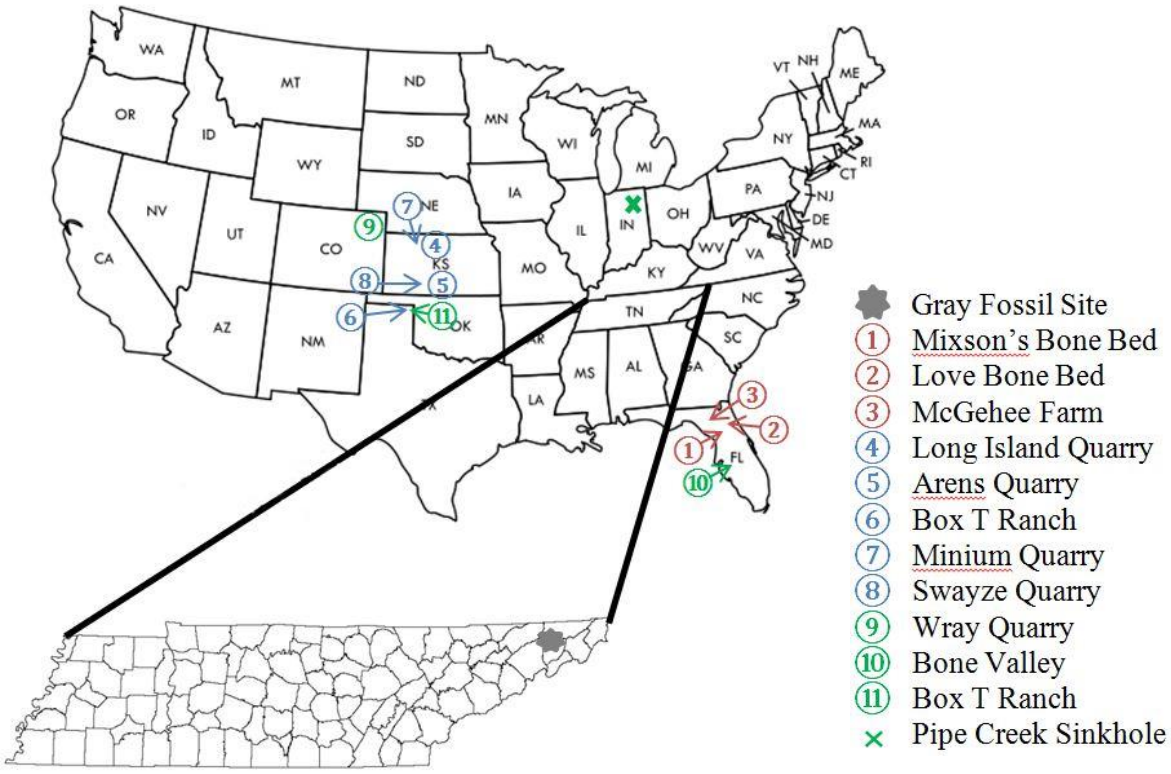

Figure 2. Map of the contiguous United States showing the Gray Fossil Site, Pipe Creek Sinkhole, and other Hemphillian localities with *Teleoceras* fossils that are included in this study. Numbers 1-11 are comparative localities used in this study and numbers 1, 4, and 9 are the type localities for their respective species. Colors: red, *T. proterum*; blue, *T. fossiger*; green, *T. hicksi*.

Given the importance of the fossil locality, it is critical to understand which *Teleoceras* species is found at GFS. In the history of rhino phylogenetics, most work has focused primarily on skulls and dentition, which has caused much confusion and uncertainty (Prothero 2005) so that some fossils have been named solely on chronology rather than morphology (Richard Hulbert 2012, pers. comm.). In the course of these craniodental studies, very little work has been done on post-cranial elements beyond the basic dimensions and even less has involved proportions within these elements (Mead 2000, Prothero 2005). With complete skeletons available at GFS, this is something that is examined here. This study includes a thorough morphological description of the *Teleoceras* sample from GFS and an analysis of post-cranial proportions within the Hemphillian species.

Review of Rhinocerotoidea and *Teleoceras*

Hyrachus, the most ancestral taxon of the Superfamily Rhinocerotoidea (Prothero et al. 1986), appeared in North America from Europe during the Late Wasatchian-Early Bridgerian Land Mammal Ages (Prothero et al. 1989). Rhinocerotoidea includes 3 families: Amynodontidae, Hyracodontidae, and Rhinocerotidae (Prothero et al. 1986). Radinsky (1966:637) defined Rhinocerotidae as including only those with "chisel-shaped I^1/hypertrophied, lanceolate I_2 tusks" and their descendants. With this, Radinsky (1966) moved multiple taxa to Hyracodontidae and made Rhinocerotidae monophyletic, so that Rhinocerotidae only contains the descendants of the *Epiaceratherium-Trigonias* lineages, which originated in the Oligocene.

In North America, the first true Rhinocerotidae is from the Duchesnean Land Mammal Age Clarno Formation of Oregon (Prothero 1998). Within Rhinocerotidae, there are currently 4 subfamilies: Rhinocerotinae, Diceratheriinae, Menoceratinae, and Aceratheriinae (Prothero 1998,

2005) (Fig. 3). At one time, Teleoceratinae was a fifth subfamily but has been reduced to a tribe, Teleoceratini, which was first placed within Rhinocerotinae (Prothero 1986). Later, Cerdeño (1995) moved Teleoceratini to Aceratheriinae and expanded the tribe to include *Aphelops* and *Chilotherium*, leaving Rhinocerotinae to include only the extant rhinoceroses (Prothero et al. 1989). Most recently and followed here, Prothero (2005) describes Teleoceratini, excluding *Aphelops* and *Chilotherium*, as a sister group to the Aceratheriinae.

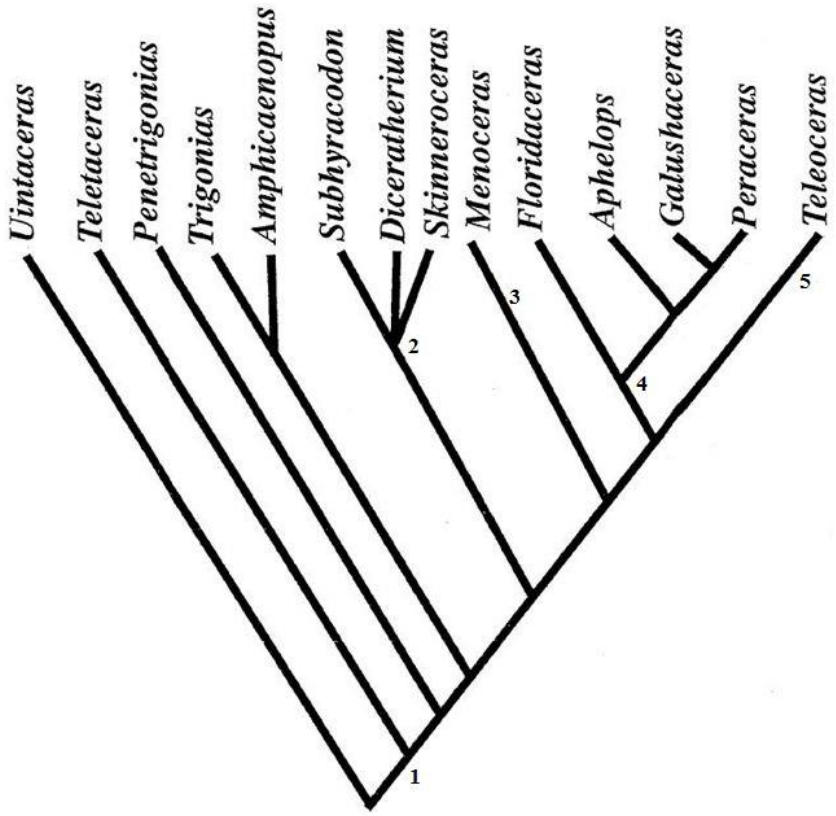

Figure 3. Phylogenetic tree of Rhinocerotidae. Nodes: 1. Rhinocerotidae; 2. Diceratheriinae; 3. Menoceratiinae; 4. Aceratheriinae; and 5. Teleoceratini. Modified from Prothero (2005).

By the early Miocene, Diceratheriinae and Menoceratinae were the only North American rhino subfamilies but were extinct by end of the Hemingfordian Land Mammal Age (Prothero

1998). At the time of this extinction, the Aceratheriinae and the Teleoceratini, emigrated from Europe as part of what Prothero et al. (1989) refer to as the "great Burdigalian-Hemingfordian interchange" (Prothero 1998). Teleoceratini is primarily represented by *Brachypotherium* in Europe and only by *Teleoceras* in North America (Prothero 2005). *Teleoceras major* from the Loup Fork Beds of Sheridan County, Nebraska is the type species of the genus (Hatcher 1894a). Hatcher (1894b) recognized that *Teleoceras* was neither an ancestor of the extant rhinos of the Eastern Hemisphere nor a direct migrant from Eurasia but that it represents a wholly North American lineage. Prothero (2005:94) lists 6 synapomorphies for the Teleoceratini and 11 characters of *Teleoceras* (Table 1).

Table 1. Synapomorphies of Teleoceratini and characters of *Teleoceras* from Prothero (2005:94)

A.	**Synapomorphies of Teleoceratini**
1.	short, stumpy limbs with robust, flattened carpals, tarsals, and metapodials
2.	a very brachycephalic skull with a flaring lambdoid crest and broad zygomatic arches
3.	nasals that are U-shaped in cross-section, with or without a small terminal horn
4.	a nasal incision retracted to anterior P3 (not as far as in aceratheriines)
5.	a strong, lobal antecrochet on the upper molars
6.	an elongate calcaneal tuber
B.	**Characters of *Teleoceras***
1.	hypsodont teeth
2.	strong antecrochets
3.	greatly reduced premolars with deciduous first premolars lost and occasional loss of second premolars
4.	thick cement on teeth
5.	narrow nasals with strongly downturned lateral edges
6.	enlarged premaxilla and upper first incisor
7.	broad zygomatic arches
8.	flaring lambdoid crests (skull semicircular in posterior view)
9.	small terminal nasal horn and fused nasals
10.	lower second incisor (tusk) shaped like a teardrop in cross-section
11.	teleoceratine body proportions of a barrel-shaped trunk and short, robust limbs

The appearance of *Teleoceras* has been used, along with a number of other taxa, to indicate the beginning of the late Hemingfordian (He_2) (Tedford et al. 2004). Because the genus is so prolific during the Miocene, the 9 current species are often used as taxa for biochronology (Prothero 2005). Five of these species are found at localities older than the Hemphillian—*T. americanum* (Yatkola and Tanner, 1979), *T. medicornutum* Osborn, 1904, *T. meridianum* (Leidy, 1865), *T. brachyrhinum* Prothero, 2005, and *T. major* Hatcher, 1894a. However, the 4 other species—*T. proterum* (Leidy, 1885), *T. fossiger* (Cope, 1878), *T. hicksi* Cook, 1927, and *T. guymonense* Prothero, 2005—are found at Hemphillian localities (Fig. 4).

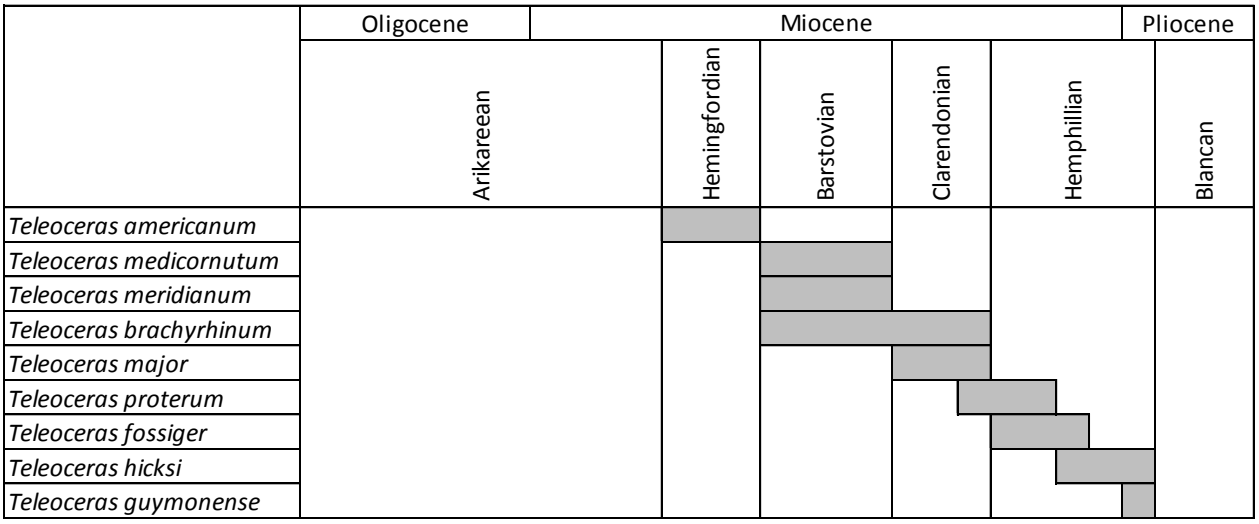

Figure 4. *Teleoceras* species along a timeline of associated land mammal ages

Gray Fossil Site

At GFS, Tennessee, fossil material is found in lacustrine sediments, including clays, silts, and sands, that filled a former sinkhole in the Knox Group Limestone (Wallace and Wang 2004). Originally, the sinkhole formed a pond that may have served as a watering hole for local fauna

(Wallace et al. 2002). Initial estimates placed the size of the deposit at 4.5 acres and 35 m thick (Wallace et al. 2002) but subsequent estimates have included 1.8-2.0 ha and 39 m thick (Wallace and Wang 2004), 2.6 ha and 40 m thick (Shunk et al. 2006), and less than 2 ha and approximately 30 m thick (Shunk et al. 2009). Because of the small surface area to volume ratio, Shunk et al. (2009) suggests that the watering hole was anoxic especially at the bottom. This environment allowed the fossils to be well-preserved without much disruption.

Sediments filled the sinkhole pond in fine laminations with isolated gravels (Wallace and Wang 2004). It has been estimated that the sinkhole filled in a span of 4500-11000 years (Shunk et al. 2009); further sedimentation analyses are reported by Shunk et al. (2006, 2009). However, attempts at geochemical dating have been unsuccessful as have paleomagnetic studies (Shunk et al. 2006). Due to a topographic reversal, the deposit became a high point in which the fossils were discovered (see summary in Schubert 2011). Recently, it was postulated that the locality was not 1 sinkhole but a series of sinkholes that formed independently (Zobaa et al. 2011).

Pollen studies suggest that GFS represents an arboreal setting with *Quercus* and *Carya* comprising 70% of the flora (Wallace and Wang 2004; Ochoa et al. 2012). It has been hypothesized that the local area was a forested 'refugium' during the spread of grasslands in the Miocene (Wallace and Wang 2004; DeSantis and Wallace 2008). Despite being deposited during a time of climate change when grasslands were spreading, it is believed that the environment at GFS remained a C3 forest throughout its depositional history (Wallace and Wang 2004; DeSantis and Wallace 2008). Taxa from GFS are of North American and Eurasian lineages and, though there are genera, including *Arctomeles* and *Pristinailurus*, from cool habitats, there are also genera from warm habitats, including *Alligator*, *Tapirus*, and *Heloderma* (Wallace and

Wang 2004; Mead et al. 2012). Atypically for a fossil deposit of this age, limited horse material has been recovered (Wallace and Hulbert 2009); moreover, there is little evidence of other animals normally associated with the Great Plains or the Gulf Coast (Wallace and Wang 2004).

Because of the fauna present, the GFS site is biochronologically dated to the North American Hemphillian Land Mammal Age, which spans approximately 4.8-9.0 Ma (Tedford et al. 2004). The beginning of the Hemphillian is marked by the first appearances of Edentata (specifically, *Pliometanastes*), *Paramicrotoscoptes*, *Kansasimys*, *Pliotomodon*, *Lemoynea*, and *Crusafontina*; amongst the autochthonous fauna, the appearance of *Teleoceras fossiger* marks the early Hemphillian (Tedford et al. 2004). However, the date of GFS can be narrowed to the late or latest Hemphillian (He_3 and He_4), which begins at approximately 7.5 Ma and ends with the Hemphillian at 4.8 Ma (Tedford et al. 2004). Because of the presence of *Teleoceras* and *Plionarctos*, the locality has been biochronologically dated to 4.5-7.0 Ma, which is supported by the other fauna of the locality, including *Tapirus polkensis*, *Megatylopus*, Gomphotheriidae, and Tayassuidae (Wallace and Wang 2004; DeSantis and Wallace 2008).The end of the Hemphillian of North America is defined by the extinction of Rhinocerotidae, including *Teleoceras*, Plesiosoricidae, Mylagaulidae, Protoceratidae, Dromomerycidae, *Plesiogulo*, *Pliotaxidea*, *Carpocyon*, *Borophagus secundus*, *Machairodus*, *Gomphotherium*, *Dinohippus*, *Astrohippus*, *Neohipparion*, and *Hexomeryx* (Tedford et al. 2004).

CHAPTER 2

METHODS

Morphology

Morphological descriptions of the GFS population were written with the aid of Barone (1999), Flower (1876), McFadyean (1908), Osborn (1898a), and Prothero (2005). Dental morphology is modified from Garutt (1994) and Prothero (2005) (Fig. 5). Using the measurements provided by Prothero (2005), linear measurements of cranial, dental, and some post-cranial elements were taken twice with an error of 1.0 mm. If the first 2 measurements had an error greater than 1.0 mm, a third measurement was taken and the 2 with the least difference were used. If an error less than 1.0 mm was not achieved in 3 attempts, all 3 were discarded and the process was restarted. Measurements taken with a measuring box were recorded to the nearest 10^{th} of a millimeter while those taken with calipers were recorded to the nearest 100^{th} of a millimeter. The data collected from the GFS specimens were plotted in bar graphs with data from Prothero (2005).

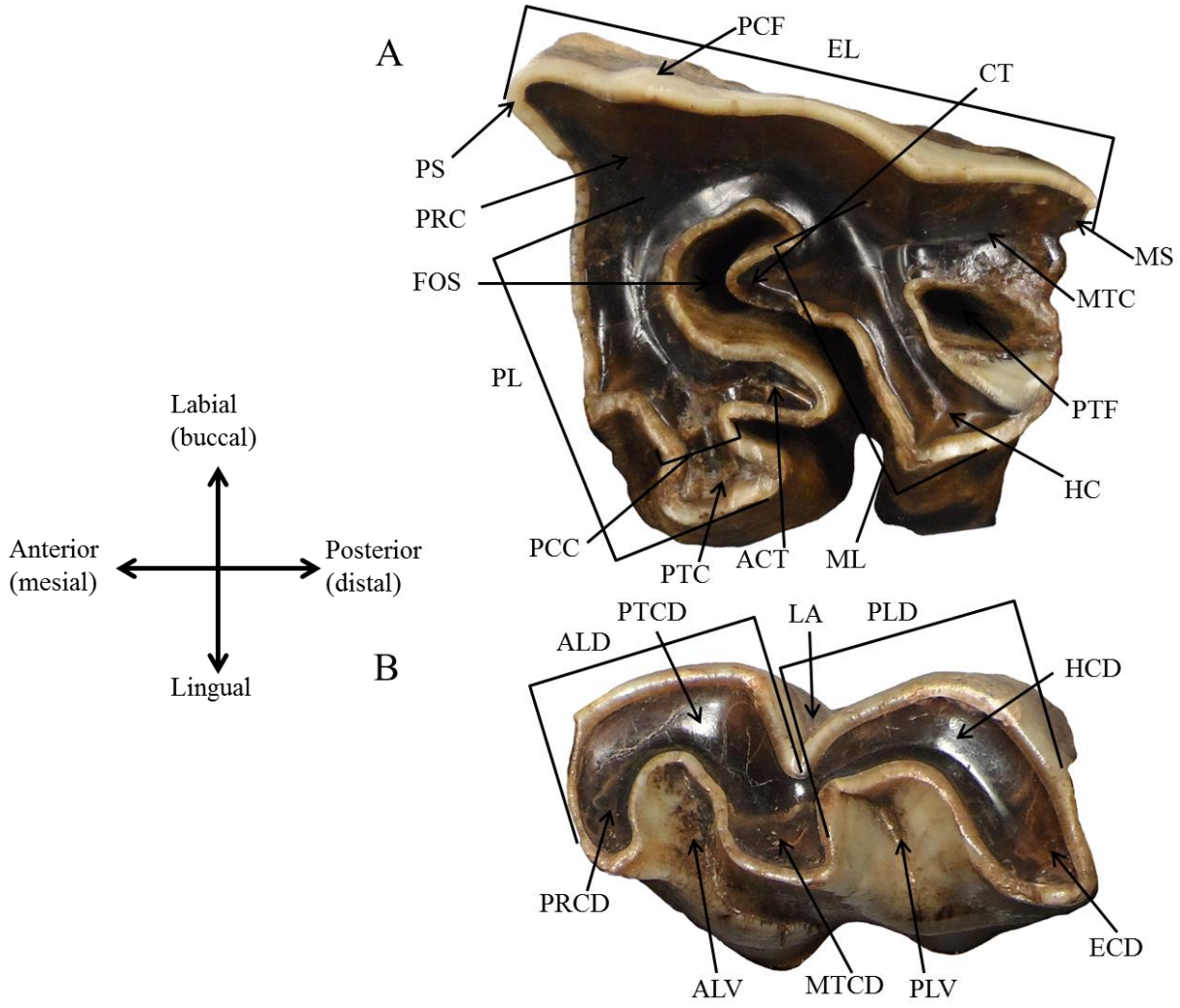

Figure 5. Dental nomenclature. A, Upper left second molar of ETMNH 601; B, Lower right second molar of ETMNH 601. Abbreviations: ACT, antecrochet; ALD, anterior lophid; ALV, anterior lingual valley; CT, crochet; ECD, entoconid; EL, ectoloph; FOS; fossette; HC, hypocone; HCD, hypoconid; LA, labial angle; ML, metaloph; MS, metastyle; MTC, metacone; MTCD, metaconid; PCC, protocone constriction; PCF, paracone fold; PLD, posterior lophid; PL, protoloph; PLV, posterior lingual valley; PRC, paracone; PRCD, paraconid; PS, parastyle; PTC, protocone; PTCD, protoconid; PTF, post-fossette.

Paleobiology

Sex of the skeletons was determined using Osborn (1898a, 1898b) and Voorhies and Stover (1978). Following Mihlbachler (2003) and Hagge (2010), an age determination scheme by Hitchins (1978) for the browsing *Diceros bicornis* (black rhinoceros) was used to determine the age of these 2 *Teleoceras* individuals. So as to not assume that *Teleoceras* had the same life span as *Diceros*, Mihlbachler (2003) adjusted the age groups provided by Hitchins (1978) into life span percentages to assign approximate ages to the rhinos from Love Bone Bed and Mixson's Bone Bed. This percentage scheme is used here to determine an approximate age stage for the 2 skeletons from GFS.

Museums and Species

In addition, comparative data were collected during visits to the Florida Museum of Natural History (FLMNH), the American Museum of Natural History (AMNH), the National Museum of Natural History (NMNH), the Denver Museum of Nature and Science (DMNS), and the Sternberg Museum of Natural History (SNHM). During these museum visits, it was possible to examine the holotypes of the species of interest and to make morphological comparisons with the GFS specimens. Because GFS is known to be Hemphillian, only Hemphillian species, specifically *Teleoceras proterum*, *T. fossiger*, and *T. hicksi*, were included in this study. A fourth Hemphillian species, *T. guymonense*, was excluded from this study because it is a dwarf species and because extremely poor preservation has resulted in most specimens being left in their field jackets. In the study here, fossil localities and their respective species are from Prothero (2005).

Teleoceras proterum specimens are from Mixson's Bone Bed, Love Bone Bed, and McGehee Farm (Prothero 2005) (Fig. 6). Mixson's Bone Bed (MBB) is the type locality of *T. proterum* and is an early Hemphillian deposit of clay sediments in Levy County, Florida (Leidy

1896; Prothero 2005). Love Bone Bed (LBB) is a late Clarendonian locality of fluvial sediments in the Alachua Formation in Alachua County, Florida (Webb et al. 1981; Prothero 2005). McGehee Farm (MF) is another early to middle Hemphillian locality in Florida (Prothero 2005).

Figure 6. Mounted skeleton of *Teleoceras proterum* at FLMNH

Teleoceras fossiger specimens are from Long Island Quarry, Arens Ranch, Box T Ranch, Minium Quarry, and Swayze Quarry (Prothero 2005) (Fig. 7). Long Island Quarry (LIQ) is a middle Hemphillian deposit of sand sediments in Phillips County, Kansas (Sternberg 1905; Prothero 2005). Because the holotype skull from Beaver Creek, Decatur County, Kansas lacks data, LIQ is typically considered the representative locality for the species (Prothero 2005) as it will be here. Arens Ranch (here Arens Quarry, AQ) is an early Hemphillian locality in the

Ogallala Formation of Clark County, Kansas (Prothero 2005). Box T Ranch (BTR) is an early Hemphillian locality in the Ogallala Formation of Lipscomb County, Texas (Prothero 2005). Minium Quarry (MQ) is a middle Hemphillian locality in the Ogallala Formation of Graham County, Kansas (Thomasson et al. 1990; Churchill 1992; Prothero 2005; Mullin 2006). Swayze Quarry (SQ) is another early Hemphillian locality in the Ogallala Formation of Clark County, Kansas (Liggett 1994; Prothero 2005).

Figure 7. Mounted skeleton of *Teleoceras fossiger* at NMNH

Teleoceras hicksi specimens are from Wray Quarry, Box T Ranch, and Bone Valley (Prothero 2005) (Fig. 8). Wray Quarry (WQ) is the type locality of *T. hicksi* and is a middle to late Hemphillian deposit of sands and gravels in the Ogallala Formation of Yuma County, Colorado (Cook 1922; Prothero 2005). Box T Ranch (BTRh) is a middle to late Hemphillian locality in the Hemphill Beds of Lipscomb County, Texas (Prothero 2005). Both *T. fossiger* and *T. hicksi* are found at Box T Ranch but come from different sites on the ranch (Prothero 2005).

Bone Valley (BV) is a formation in Polk County, Florida whose upper section is late Hemphillian fluvioestuarine sediments that contain fossils of the Palmetto Fauna (Prothero 2005; Webb et al. 2008).

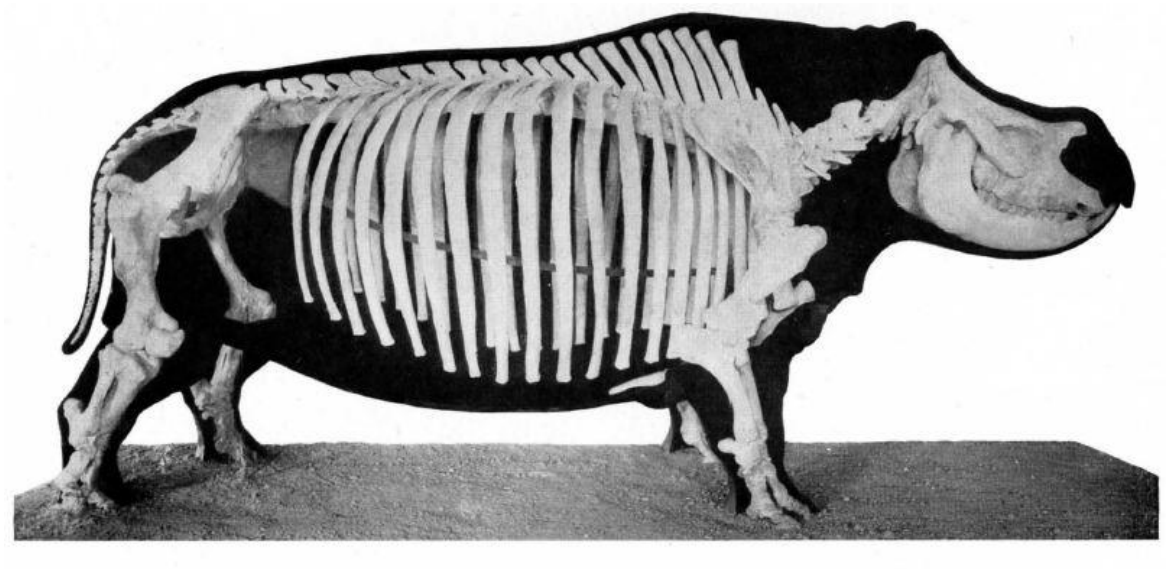

Figure 8. Mounted skeleton of *Teleoceras hicksi*. Modified from Cook (1927).

Post-Cranial Comparisons

For this study, 8 post-cranial elements were included—humerus, radius, ulna, third metacarpal, femur, tibia, calcaneum, and third metatarsal—because they were believed to be the best suited for defining post-cranial differences.

Age and Sexual Dimorphism

Because nearly all of the material is disassociated, there was no way to determine a precise age or sex of the specimens. For the first concern, only those elements with completely fused epiphyseal plates were included in this study. Complete fusion indicates adulthood and,

thus, reduces the influence of ontogenetic changes. Sexual dimorphism was not as easy to account for. Although Mead (2000) found significant sexual dimorphism in the post-crania of *Teleoceras major* from the Poison Ivy Quarry in Nebraska, Mihlbachler (2001) found little sexual dimorphism in *T. proterum* from Love Bone Bed and Mixson's Bone Bed suggesting a greater likelihood in Great Plains *Teleoceras*. This was further supported by Mullin (2006), who tentatively described sexual dimorphism in some *T. fossiger* elements from the Swayze and Minium Quarries. In the current study, the sample sizes from each locality are not large enough to statistically determine the presence of sexual dimorphism.

Measurements

Including the 33 post-cranial elements measured from GFS, 463 additional bones were examined and measured. In the analyses, each skeleton from GFS was represented by only 1 of each element to prevent data duplication. Of the original 463 comparative bones, only 282 (56%) were able to be included in further analyses because of insufficient data. Including all 8 bones of interest, a total of 70 linear measurements were taken using calipers and a measuring box (Appendix 3). Measurements followed the procedure discussed previously. Incomplete specimens were included as much as possible but unavailable measurements were omitted and questionable measurements were treated as a least measurement and are marked with an asterisk (Appendix 4).

For further study, these measurements were used in their original state and as standardized data. Standardization was performed by dividing the measurement of interest by the length of the element. Elements, such as the humerus, with a 'greatest length' longer than the 'articular length' were standardized using the articular length.

Statistical Analyses

Statistical analyses using both unstandardized and standardized data were performed using Microsoft Excel and IBM SPSS Statistics 20. In all, 268 analyses were done with the 2 programs. First, bivariate plots, using both sets of data, were compared to the data provided by Prothero (2005). Then, Principle Components Analyses (PCA) and Discriminant Function Analyses (DA) were performed on data by element. A PCA uses the given data set to show variation among the individual specimens by constructing principal components that are independent and can be plotted on the axes of a graph to clarify differences within the sample. In this case, PCA was chosen to elucidate variation between species. A DA uses the given data set and assigned groupings of knowns to place an unknown in the appropriate group and to produce discriminant functions that can be plotted on the axes of a graph. In this study, DA was chosen to determine placement of the unknown GFS rhino among the knowns of previously determined species.

Both PCA and DA were conducted in 3 different sets of analyses. In the first analysis, specimens from all of the localities, including GFS, were analyzed using selected measurements. Because of fragmentary specimens, it was necessary to exclude some measurements to maintain a large sample that included all of the localities. It was also necessary to exclude some specimens in order to include some of the measurements. Next, only the type localities and GFS were analyzed using the same selected measurements. Then, the type localities and GFS were analyzed using the full suite of measurements and only those specimens that were complete enough to be included. PCA was also performed on the 3 type localities to determine if these occupy different morphospaces. Finally, each locality of interest was treated individually as an

unknown with the 3 type localities as knowns. This was done to determine if any of the localities could be assigned to the type locality of their respective species using post-cranial elements. Throughout, these analyses, each element was evaluated to determine if any were more successful than others at species assignment.

Abbreviations

Museums

Abbreviations: AMNH, American Museum of Natural History, New York City, New York; GFS, East Tennessee State University and General Shale Brick Natural History Museum and Visitor's Center at the Gray Fossil Site, Gray, Tennessee; DMNS, Denver Museum of Nature and Science, Denver, Colorado; FLMNH, Florida Museum of Natural History, Gainesville, Florida; NMNH, National Museum of Natural History, Smithsonian Institution, Washington, D.C.; and SNHM, Sternberg Museum of Natural History, Fort Hays, Kansas.

Fossil Collections

Abbreviations: DMNH, Denver Museum of Natural History Collection at DMNS; ETMNH, East Tennessee Museum of Natural History Collection at GFS; F:AM, Frick Collection at AMNH; FHSM VP, Fort Hays Sternberg Museum Vertebrate Paleontology Collection at SNHM; UF, University of Florida Collection at FLMNH; UF/TRO, University of Florida/Timberlane Research Organization Collection at FLMNH; USNM PAL, United States National Museum Paleontology Collection at NMNH; and USNM V, United States National Museum Vertebrate Collection at NMNH.

Localities

Abbreviations: AQ, Arens Quarry, Texas; BTR, Box T Ranch, Texas, *Teleoceras fossiger*; BTRh, Box T Ranch, Texas, *Teleoceras hicksi*; BV, Bone Valley (Palmetto Fauna), Florida; GFS, Gray Fossil Site, Tennessee; LBB, Love Bone Bed, Florida; LIQ, Long Island Quarry, Kansas; MBB, Mixson's Bone Bed, Florida; MF, McGehee Farm, Florida; MQ, Minium Quarry, Kansas; SQ, Swayze Quarry, Kansas; and WQ, Wray Quarry (primarily Beecher Island sites), Colorado.

CHAPTER 3

TELEOCERAS OF THE GRAY FOSSIL SITE

In addition to the 2 complete skeletons mentioned previously, there is an assortment of unassociated material (Appendix 2) that produces a minimum number of 5 individuals based on 4 left astragali and a juvenile tibia and fibula (Fig. 9). This material will be addressed within the appropriate sections; however, the 2 complete skeletons (ETMNH 609 and ETMNH 601) are the primary focus of this discussion. ETMNH 609 is the smaller and more complete of the 2 skeletons because it is only missing the distal phalanx of the left hind fourth digit. ETMNH 601 is larger but less complete than ETMNH 609.

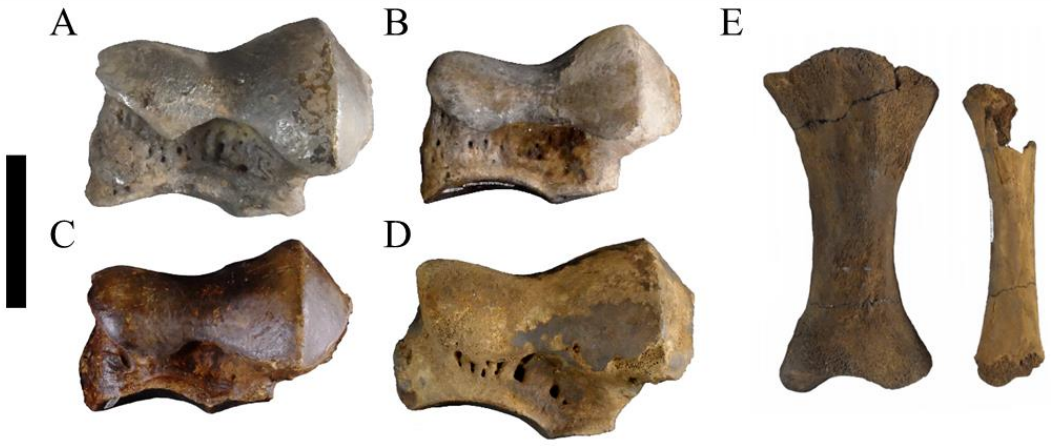

Figure 9. Specimens that produce a minimum number of 5 *Teleoceras* individuals at GFS. A, left astragalus, ETMNH 601; B, left astragalus, ETMNH 609; C, left astragalus, ETMNH 1901; D, left astragalus, ETMNH 6647; E, juvenile tibia and fibula, ETMNH 1902. Scale bar = 5 cm.

Sex and Age of the Complete Skeletons

Using dental features, it is possible to determine the age and sex of *Teleoceras*. At GFS, both skeletons are males based on the presence of enlarged tusk-like lower second incisors (Fig.

10) in contrast to the smaller incisors seen in females (Osborn 1898a, 1898b). This distinction was later confirmed when a pregnant *T. major* with small tusks was uncovered at Ashfall Fossil Beds, Nebraska (Voorhies and Stover 1978) and has now become widely accepted as a reliable way to determine the sex of *Teleoceras*. Thus, unless our population varies from the standard pattern of rhinoceroses, both skeletons represent male individuals.

Figure 10. Lower tusks of the 2 skeletons from GFS. The large size suggests that both are males. A, ETMNH 609; B, ETMNH 601. Scale bar = 10 cm.

Both of these skeletons are adults based on the degree of epiphyseal fusion and tooth wear. Using Hitchins (1978), the upper tooth row of ETMNH 609 matches age class XI and the lower tooth row matches age class X. The obviously older ETMNH 601 matches age class XIII

on the upper teeth and age class XII on the lower teeth. Mihlbachler (2003) discussed that there are some inconsistencies between *Teleoceras* and the ages provided by Hitchins (1978), which is most likely why the uppers and lowers fall into different age classes. Using Mihlbachler's (2003) life span percentages, ETMNH 609 was at the beginning of an age class marking 25-35% of its potential life span and ETMNH 601 was at the beginning of an age class marking 35-52% of its potential life span. In *Diceros*, these life span percentages refer to 8-12 years old and 11-18 years old, respectively (Hitchins 1978).

Skull

A significant amount of repair work has been done to reassemble the skull and dentaries of ETMNH 609 (Fig. 11). MagicSculpt, in the same color as the bone, was used in this reconstruction to prepare it for museum display; however, it also makes it difficult to determine where bone is present or missing. Though the skull and dentaries of ETMNH 601 have also been repaired, Butvar-98 and aluminum mesh, instead of MagicSculpt, were used to construct 'walls' across any spaces missing the original bone (Fig. 11). These areas are limited to the orbital walls, the palate, and some smaller areas of bone. This makes the skull morphology of ETMNH 601 much easier to describe than ETMNH 609 and, for this reason, the following descriptions were written almost exclusively using ETMNH 601.

Figure 11. Skulls of the complete skeletons from GFS in right lateral view. A, cranium of ETMNH 609; B, right dentary of ETMNH 609; C, cranium of ETMNH 601; right dentary of ETMNH 601. Scale bar = 10 cm.

Cranium

Nasal. Paired nasal bones articulate medially with each other, posteriorly with the frontals, and ventrally with the maxillae (Fig. 12). An additional specimen, ETMNH 12175 appears to belong to a female because, though the nasals are small, they are fused, which suggests an older but smaller individual. None of the specimens have a visible suture with the frontal but the suture with the maxilla is visible on ETMNH 601. ETMNH 609 has more upturned nasals than the straight nasals that are seen in ETMNH 601.

Figure 12. Nasals of GFS specimens. In dorsal view: A, ETMNH 12175; B, ETMNH 609; C, ETMNH 601. In right lateral view: D, ETMNH 601. In A, B, and C, the scale bar = 10 cm. In D, the scale bar = 10 cm.

At the anterior extent, all of the nasals are round in cross-section and, when visible, are articulated along a zigzag suture (Fig. 13); it has been suggested that this was a strengthening mechanism for use as a battering ram (see summary in Wallace 2011). No evidence of a horn attachment is present on the smooth outer surface of the nasal bones. On the ventral surface of the nasals, the inner surface is concave and has an anteroposterior ethmoid crest. The nasals form the dorsal surface of the round nasal cavity, which is missing the nasal turbinates in both skulls.

Figure 13. Nasals of ETMNH 601 in anterior view. Notice the complex suture marked by the arrow. Scale bar = 1 cm.

Frontal. Paired frontals articulate medially with each other, anteriorly with the nasals and lacrimals and posteriorly with the parietals (Fig. 14). It is not possible to determine articulations within the orbit (OR) and along the temporal fossa (TF) because only the lacrimal sutures are visible on ETMNH 601. There is no evidence of a supra-orbital process; however, there are laterally extending bulbous knobs dorsal to the orbit (DOK). Dorsally, the frontals are flat except for the previously mentioned feature.

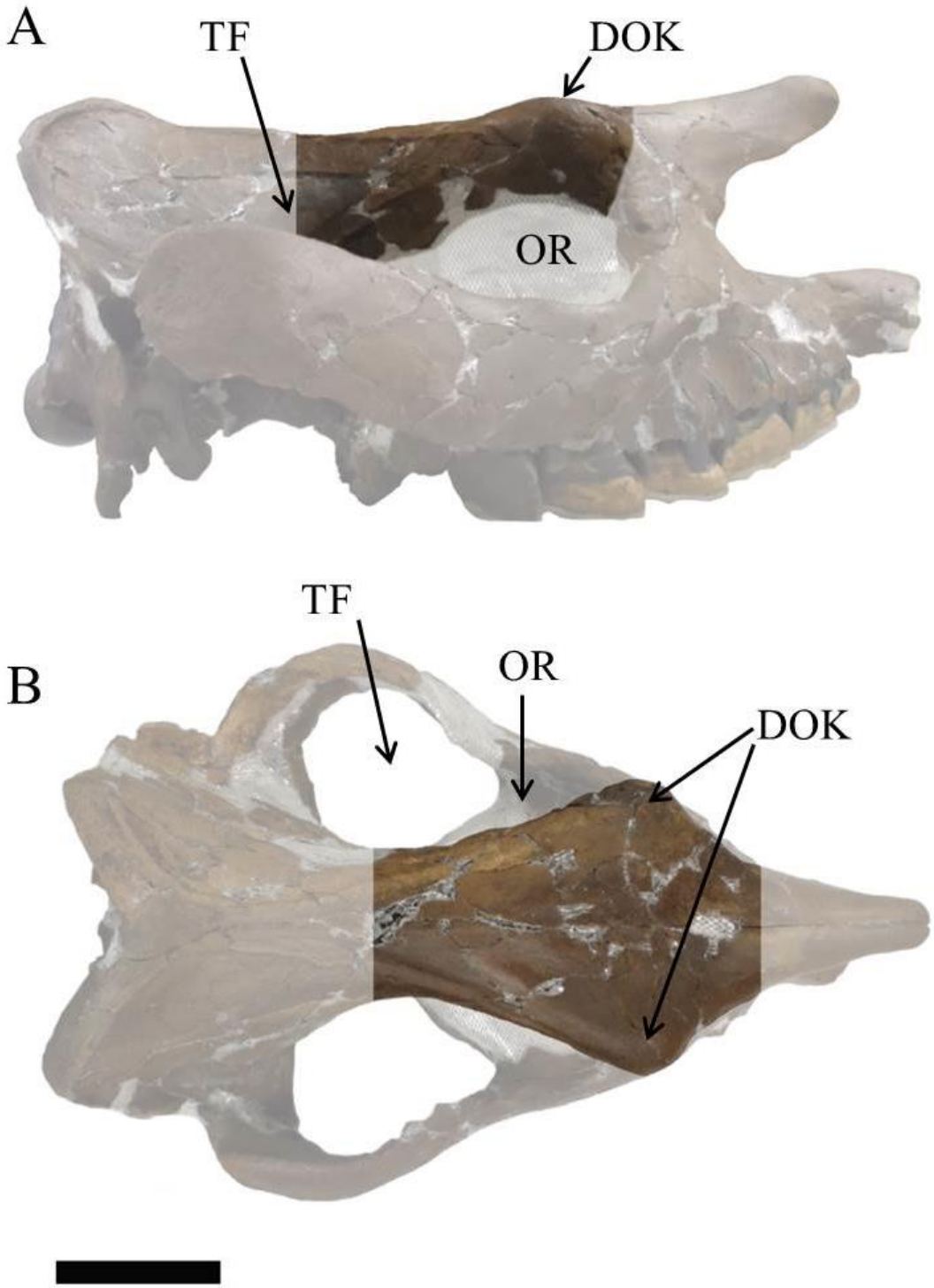

Figure 14. Frontals of ETMNH 601. A, right lateral view; B, dorsal view. Anterior is to the right. Abbreviations: DOK, dorsal orbit knobs; OR, orbit; TF, temporal fossa. Scale bar = 10 cm.

Parietal. Paired parietals articulate medially with each other, anteriorly with the frontal, posteriorly with the occipital, and ventrolaterally with the squamosal (Fig. 15). Neither skull has visible parietal sutures. A broad concavity (CV) is present at the articulation between the squamosal and the parietal dorsal to the external auditory meatus (EAM). Paired temporal crests (TCT) extend posteromedially from the dorsal orbital knobs of the frontals until they nearly merge on the dorsal parietal surface but then split again at the lambdoid crest (LCT). These crests are only slightly raised but are more pronounced on ETMNH 609. The dorsal surface of the parietals is covered with a slight roughness. Laterally, the parietals are inflated around the braincase.

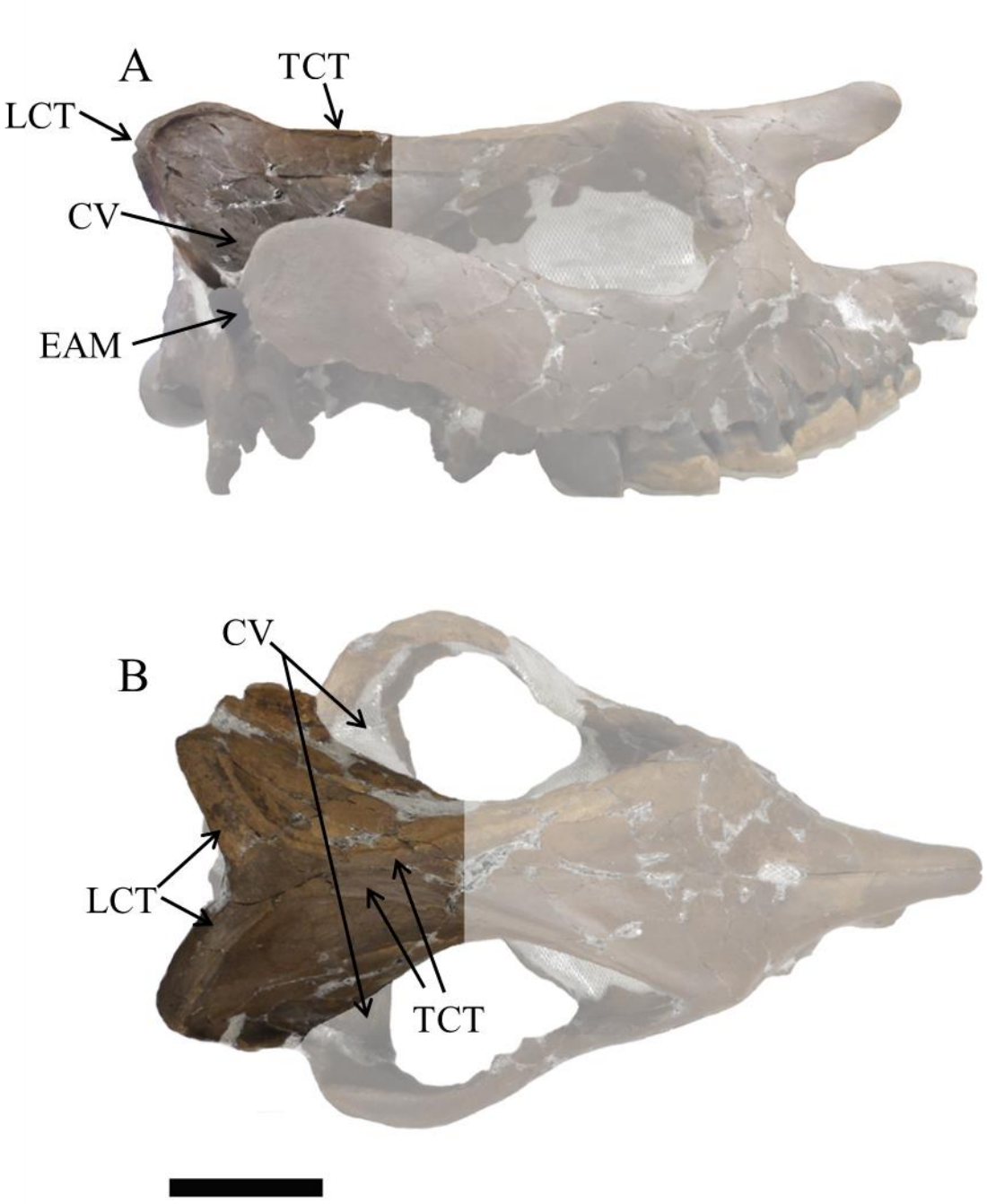

Figure 15. Parietals of ETMNH 601. A, right lateral view; B, dorsal view. Anterior is to the right. Abbreviations: CV, concavity; EAM, external auditory meatus; LCT, lambdoid crest; TCT, temporal crest. Scale bar = 10 cm.

Premaxilla. Paired premaxillae only articulate with the maxillae so that even the right and left premaxillae do not contact (Fig. 16). ETMNH 601 has visible premaxillary sutures with the maxilla. Both premaxillae of ETMNH 609 have been completely reconstructed; however, they have been reconstructed so that the upper tusks occlude with the lower tusks. Those of ETMNH 601 are complete and are close to touching at their anterior-most point. The premaxillae of ETMNH 609 are separated by a larger gap than those of ETMNH 601, which suggests that premaxilla breadth is variable within this population. Anteroventrally directed tusk alveoli (TAL) are present and support the upper first incisors, which are modified into reduced tusks. The premaxillae of ETMNH 601 are medially flattened, laterally flared, dorsally rounded, and posteroventrally pinched. No nasal or palatine processes are present and there is no evidence of an incisive foramen.

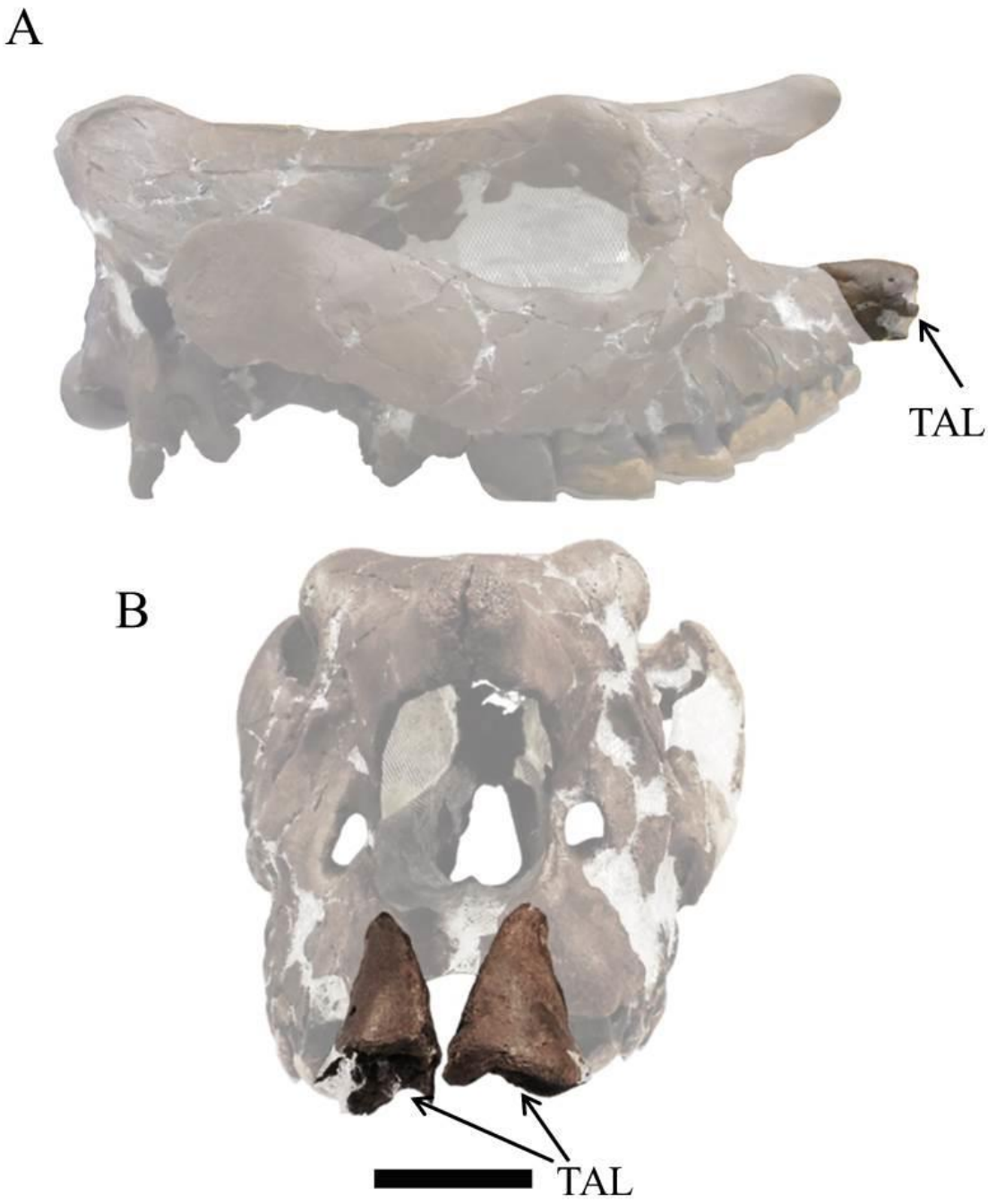

Figure 16. Premaxillae of ETMNH 601. Views: A, right lateral; B, anterior. Abbreviations: TAL, tusk alveolus. Scale bar = 10 cm.

Maxilla. Paired maxillae articulate dorsally with the nasals, anteriorly with the premaxillae, and posteriorly with the jugals, lacrimals, and palatines (Fig. 17). In addition to ETMNH 609 and ETMNH 601, there is a maxilla fragment (ETMNH 13914) with an upper first molar that was found during construction of the Annex Building at GFS. The maxilla supports the entirety of the upper tooth row (TR) except for the tusks. Though the facial surfaces are present, most of the internal maxilla of ETMNH 601 is missing. Between the premaxillae articulations, the maxillae are concave to form a round incisive cleft (IC). On the anterolateral surface, the maxilla has ridges presumably for muscle attachment. Also on the lateral surface, there is a concavity (CV) anterior to the lacrimal and ventral to the nasal. A large infraorbital foramen (IOF) is present above the anterior fourth premolar. Posterolaterally, the maxilla expands to articulate with the jugal. The maxillary tuberosity (MTB) continues posteroventrally to the jugal articulation the end of the tooth row. The superior maxillary sinus is within the maxillary tuberosity. A facial crest (FCT) is present as a groove between the maxillary tuberosity and the jugal articulation. Both ETMNH 601 and ETMNH 609 have anteriorly deep maxillary palates (MPL) that rise to the level of the tooth alveoli at the posterior end. This could provide the animal with a surface for bolus manipulation during mastication.

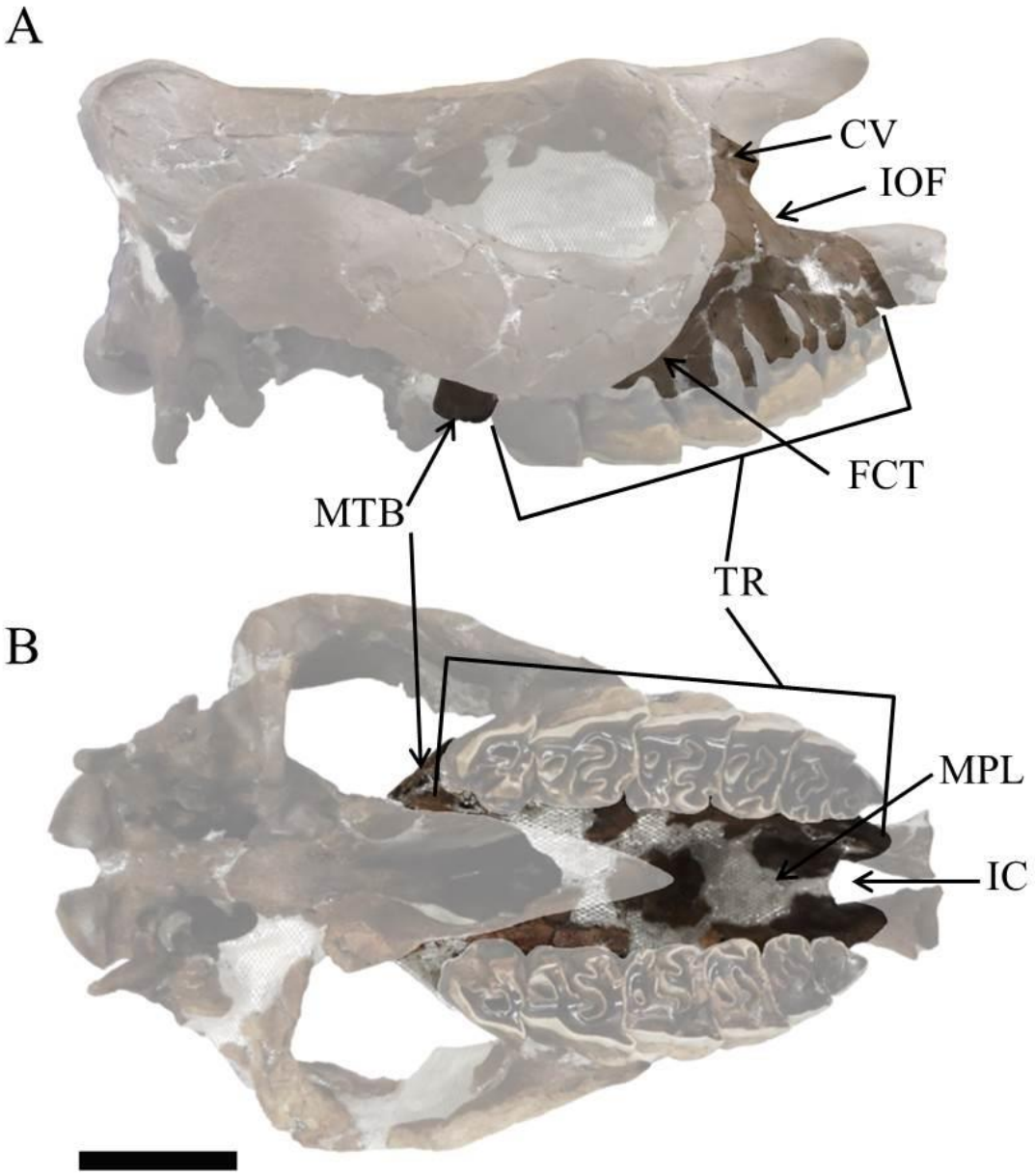

Figure 17. Maxillae of ETMNH 601. Views: A, right lateral; B, ventral. Anterior is to the right. Abbreviations: CV, concavity; FCT, facial crest; IC, incisive cleft; IOF, infraorbital foramen; MPL, maxillary palate; MTB, maxillary tuberosity; TR, tooth row. Scale bar = 10 cm.

Lacrimal. Paired lacrimals articulate dorsally with the nasals and frontals, anteriorly and ventrally with the maxillae, and posteroventrally with the jugals (Fig. 18). All of the lacrimal sutures are visible on ETMNH 601. This is a small round bone that forms the anterior edge of the orbit (OR). While the facial surface (FS) is rugose, the orbital surface (OS) is smooth. There is a small, laterally-directed lacrimal foramen (LF) just beneath a laterally-protruding lacrimal tubercle (LTB). The latter serves as an attachment site for eye muscles.

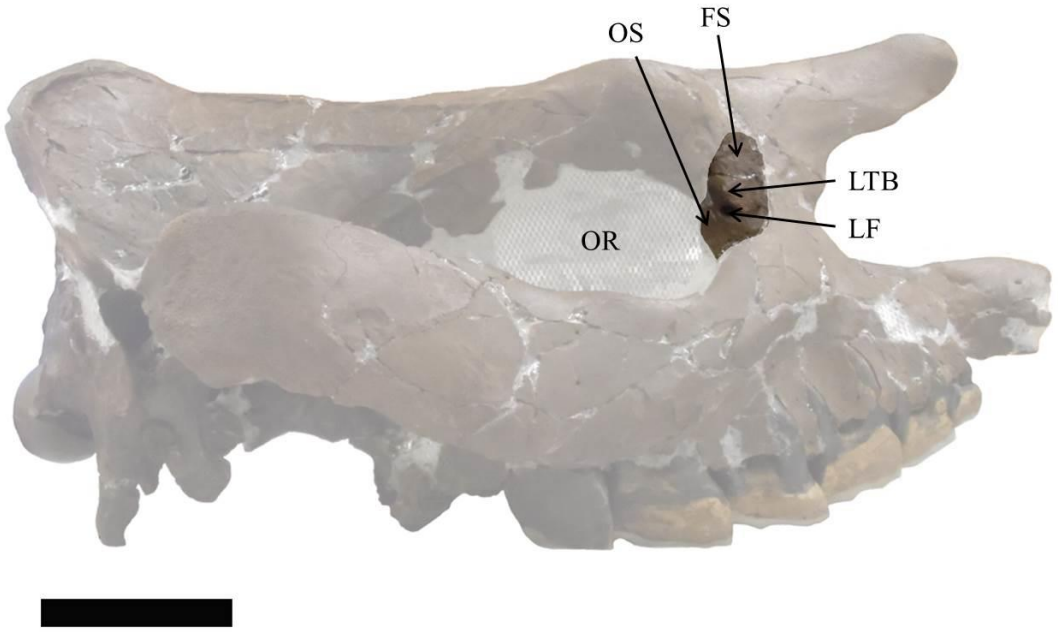

Figure 18. Right lacrimal of ETMNH 601 in lateral view. Abbreviations: FS, facial surface; LF, lacrimal foramen; LTB, lacrimal tuberosity; OR, orbit; OS, orbital surface. Scale bar = 10 cm.

Jugal. Paired jugals articulate anteriorly with the maxillae and posteriorly with squamosals (Fig. 19); both of these sutures are visible on ETMNH 601. At the base, the jugal articulates with the maxilla above the upper first and second molars and, at the apex, the jugal forms a nearly straight articulation with the squamosal. This articulation slants from anterodorsal to posteroventral so that the squamosal is dorsal to the jugal. On each side, the jugal, with the squamosal, forms the broad and rugose zygomatic arch (ZMA). Heavy rugosities on the zygomatic arch, especially the underside, provide attachment surfaces predominantly for the masseter muscle. The facial surface has minimal rugosities. Along the ventral edge of the orbit (OR), the jugal is smooth and, though the jugal does contribute to the orbital floor (OF), most of this is missing.

Figure 19. Jugals of ETMNH 601. Views: A, right lateral; B, ventral. Anterior is to the right. Abbreviations: OF, orbital floor; OR, orbit; ZMA, zygomatic arch. Scale bar = 10 cm.

Squamosal. Paired squamosals articulate dorsally with the parietals, ventrally with the basicranium, anteriorly with the jugals and posteriorly with the occipital (Fig. 20). Sutures are not visible on the ventral surface, so it is difficult to ascertain the individual bones of the basicranium. Only the squamosal suture with the jugal is visible on ETMNH 609. With the jugal, the squamosal makes up the zygomatic arch (ZMA) and, like on the jugal, though the outer surface is smooth, the inner surface is rugose for attachment of the masseter muscle. There is a significant medial curve as the squamosal transitions from the zygomatic arch to the parietal articulation and, in doing so, forms the lateral boundary of the temporal fossa (TF).

A transversely elongate glenoid fossa (GF) has an open angle and is only slightly concave. Anterior to the glenoid fossa, the articular tubercle (ATB) is round but appears to be pinched anteriorly. Post-glenoid processes (PGP) are nearly straight and elongate but are shorter than the paroccipital processes (POC) of the occipital. These 2 processes fuse ventral to the triangular external auditory meatus (EAM) to form the mastoid crest but are then separated by a V-shaped notch. Dorsal to the external auditory meatus, the squamosal and occipital bones fuse to form the lambdoid crest (LCT). There are no external auditory bullae present and there is no evidence that they were present during life either.

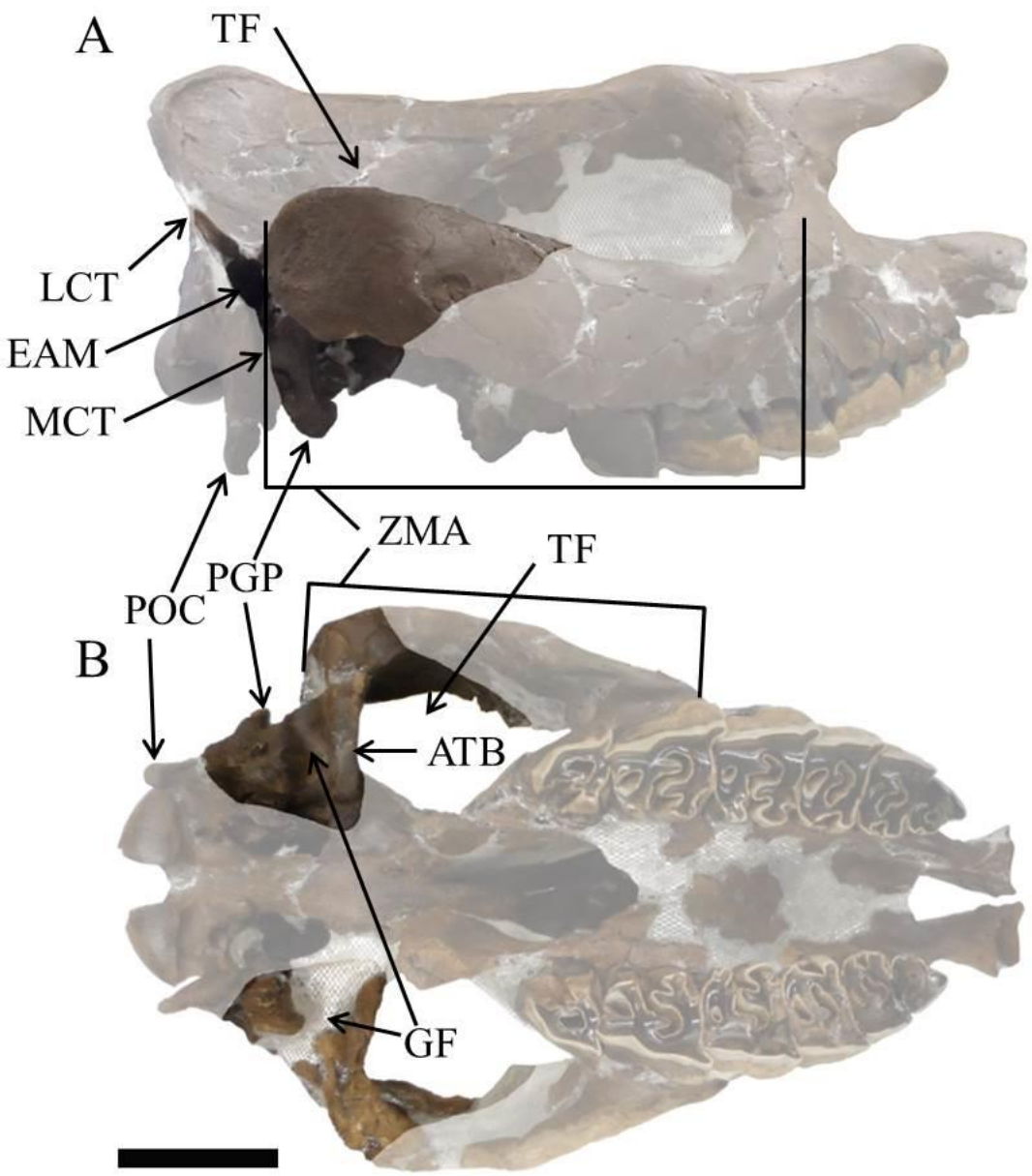

Figure 20. Squamosals of ETMNH 601. Views: A, right lateral; B, ventral; Abbreviations: ATB, anterior tubercle; EAM, external auditory meatus; GF, glenoid fossa; LCT, lambdoid crest; MCT, mastoid crest; PGP, post-glenoid process; POC, paroccipital process; TF, temporal fossa; ZM, zygomatic arch. Scale bar = 10 cm.

Occipital. The unpaired occipital bone articulates anteriorly with the parietals and the basicranium, posteriorly with the atlas, and laterally with the squamosal (Fig. 21). On the posteroventral surface, the triangular (in posterior view), convex occipital condyles (OCD) are lateral to the round foramen magnum (FM). On the ventral surface, the paired hypoglossal foramina (HGF) are anterior to each of the occipital condyles and medial to each paroccipital process (POC). Most of the occipital extends in the same plane as the occipital condyles and only the dorsal-most lambdoid crest (LCT) extends more posteriorly. Edges of the occipital form the lambdoid crest with the squamosal and parietals. At the ventral point of the external auditory meatus (EAM), the lambdoid crest fuses with the mastoid crest (MCT) of the squamosal and then continues as the paroccipital process.

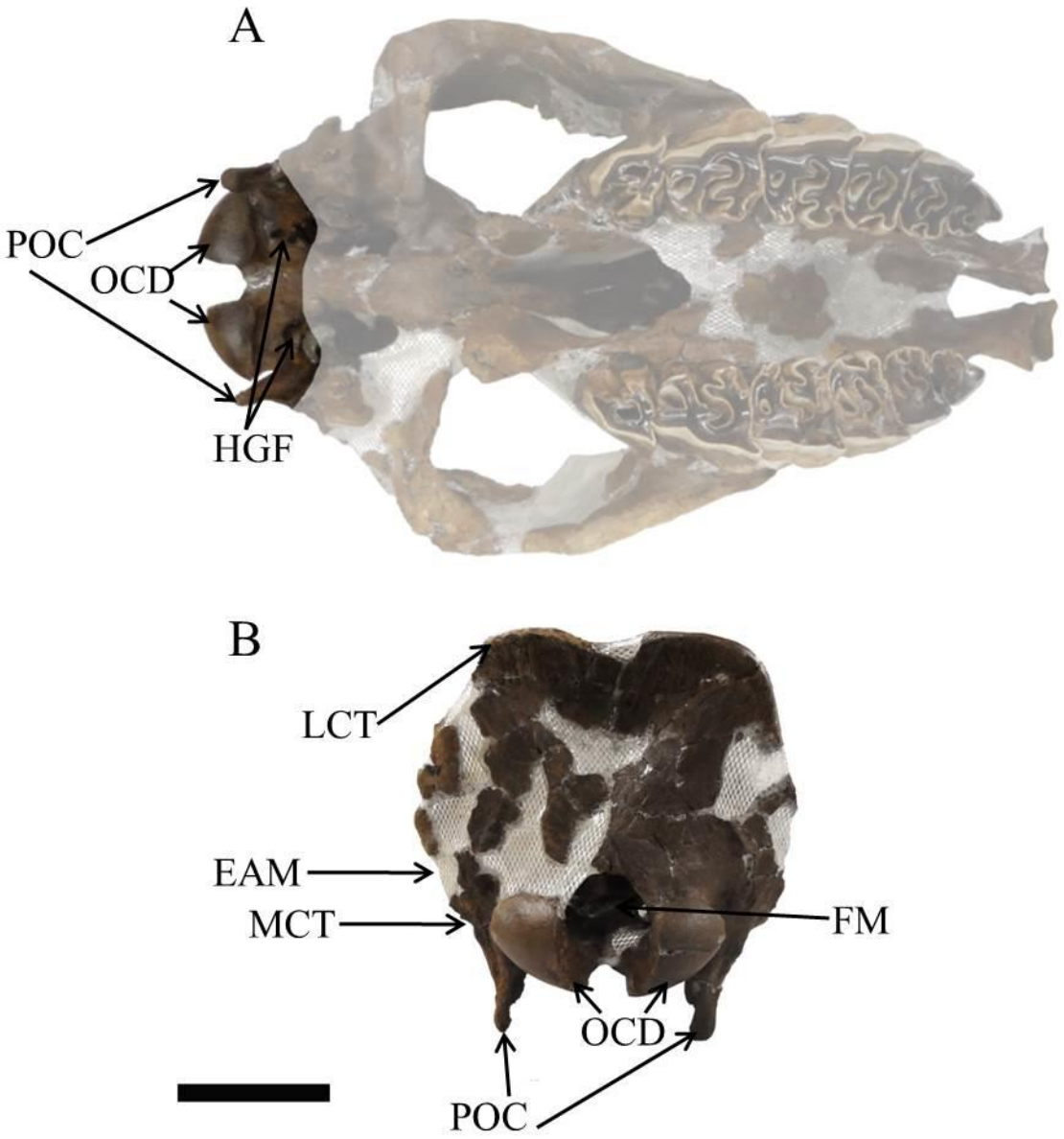

Figure 21. Occipital of ETMNH 601. Views: A, ventral with anterior to the right; B, posterior. Abbreviations: EAM, external auditory meatus; FM, foramen magnum; HGF, hypoglossal foramen; LCT, lambdoid crest; MCT, mastoid crest; OCD, occipital condyles; POC, paroccipital process. Scale bar = 10 cm.

Basicranium. It is impossible to distinguish the bones of this region because of the large amount of fusion, so it will be described here as a region. The basicranium articulates anteriorly with the vomer, posteriorly with the occipital, and laterally with the squamosals and frontals (Fig. 22). Ventrally, the basicranium is in poor condition on both skulls. There is a ventral muscle tubercle (MTB) anterior to what is most likely the articulation between the occipital and the basisphenoid. Each lateral side of this region has an alisphenoid canal (ASC) that is bridged by bone, which is most likely the alisphenoid and which has prominent ridges on the surface. The dorsal opening to this canal is anterior and the ventral opening is posteroventral.

Figure 22. Basicranium region of ETMNH 601. Views: A, ventral; B; right ventrolateral, beneath zygomatic arch. Abbreviations: ASC, alisphenoid canal; MTB, muscle tubercle. Scale bar = 10 cm.

Pterygoid. The paired pterygoids articulate laterally with the palatines but this articulation is not visible in either skull (Fig. 23). Pterygoid processes (PGP) are directed posteroventrally and almost to the height of the third molar.

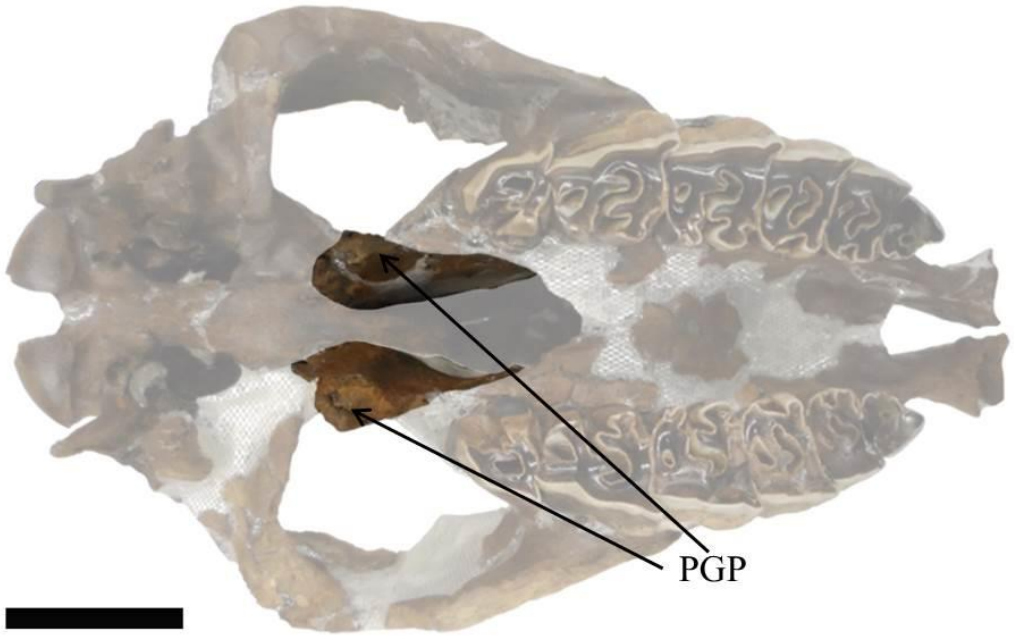

Figure 23. Pterygoids of ETMNH 601 in ventral view. Anterior is to the right. Abbreviation: PGP, pterygoid process. Scale bar = 10 cm.

Palatine. Paired palatines articulate medially with each other, the pterygoids, and the vomer and anteriorly and laterally with the maxillae (Fig. 24). Either the bone is missing or the sutures are completely fused so that these articulations are not visible. Almost all of the palatine of ETMNH 601 has been repaired with mesh making it impossible to describe any morphology.

Figure 24. Palatines of ETMNH 601 in ventral view. Anterior is to the right. Scale bar = 10 cm.

Vomer. The unpaired vomer is missing on both skulls. If it were present, it would articulate posteriorly with the basisphenoid.

Hyoid Apparatus. Both skeletons have hyoids preserved but that of ETMNH 601 is in better condition (Fig. 25). The basihyoid (BAS) is round but is dorsoventrally compressed and lacks a lingual process. Only the left thyrohyoid (THY) of ETMNH 601 is present and it extends posterolaterally from the basihyoid. A rugose knob forms the articulation and the thyrohyoid tapers so that it is mediolaterally compressed. ETMNH 601 is missing both ceratohyoids and only 1 ceratohyoid of ETMNH 609 is present. The ceratohyoid (CER) is a long, round bone that articulates between the basihyoid and the epihyoid; though, no epihyoids are present. Finally, the stylohyoid articulates with the epihyoid and the skull. Pieces of all 4 stylohyoids are present,

though those of ETMNH 601 are in better condition. The stylohyoid (STY) is the largest of the hyoid bones and is mediolaterally compressed with a medial fossa at the proximal end. There are no tympanohyoids present.

Figure 25. Hyoid apparatus of ETMNH 601 with ceratohyoid from ETMNH 609. Image in dorsal view with anterior to the left. Abbreviations: BAS, basihyoid; CER, ceratohyoid; STY, stylohyoid; THY, thyrohyoid. Scale bar = 10 cm.

Mandible

As with the skull, the mandible of ETMNH 609 is heavily repaired with MagicSculpt, which makes a thorough description difficult. Because the mandible of ETMNH 601 was repaired using the same Butvar-98 and aluminum mesh method that was used on the skull, this specimen is used for the description here (Fig. 26). Overall, the mandible is much longer than it is tall and the intermaxillary space (IMS) is 'V'-shaped. A shallow, sloping symphysis (SYM) with a broad lingual surface is present between the dentaries and extends posteriorly to the middle of the lower fourth premolar. The angles of the dentaries (AD) are flared laterally and are rugose, especially on ETMNH 601, which is likely due to increased muscle attachment due

associated with a more advanced age. Each lateral surface has a broad and shallow masseteric fossa (MSF) that is dorsal to the angular rugosities. Those are the only areas of rugosity on the entire body of the dentary. Though there are no angular processes, shallow mandibular incisures (MDI) separate thin, rounded coronoid processes (CNP) from transversely long and convex articular condyles (ACD). Posterior to each articular condyle, there is a second convex surface that merges with the lateral articular condyle and slopes medioventrally. In dorsal view, ETMNH 601 has uneven condyles that are slightly offset from one another, which is consistent with the offset of the skull.

Tusks, which are modified second incisors, are present on the anterior end of the dentary and are directed dorsally and labially from the symphysis. Below the medial edge of these tusks, there is a pair of foramen. A short diastema is transversely pinched behind the tusks and separates the tusks from the lower second premolars. A mental foramen is found below the anterior root of each lower fourth premolar. An inferior maxillary foramen is on the pterygoid fossa (PGF) of the internal surface of the ramus and is at the same level as the tooth row. The tooth row lingually expands the mandibular body, especially at the lower third molar. Behind the lower third premolar, the dentary is flattened to the width of the tooth row but becomes laterally depressed into the inferior maxillary foramen.

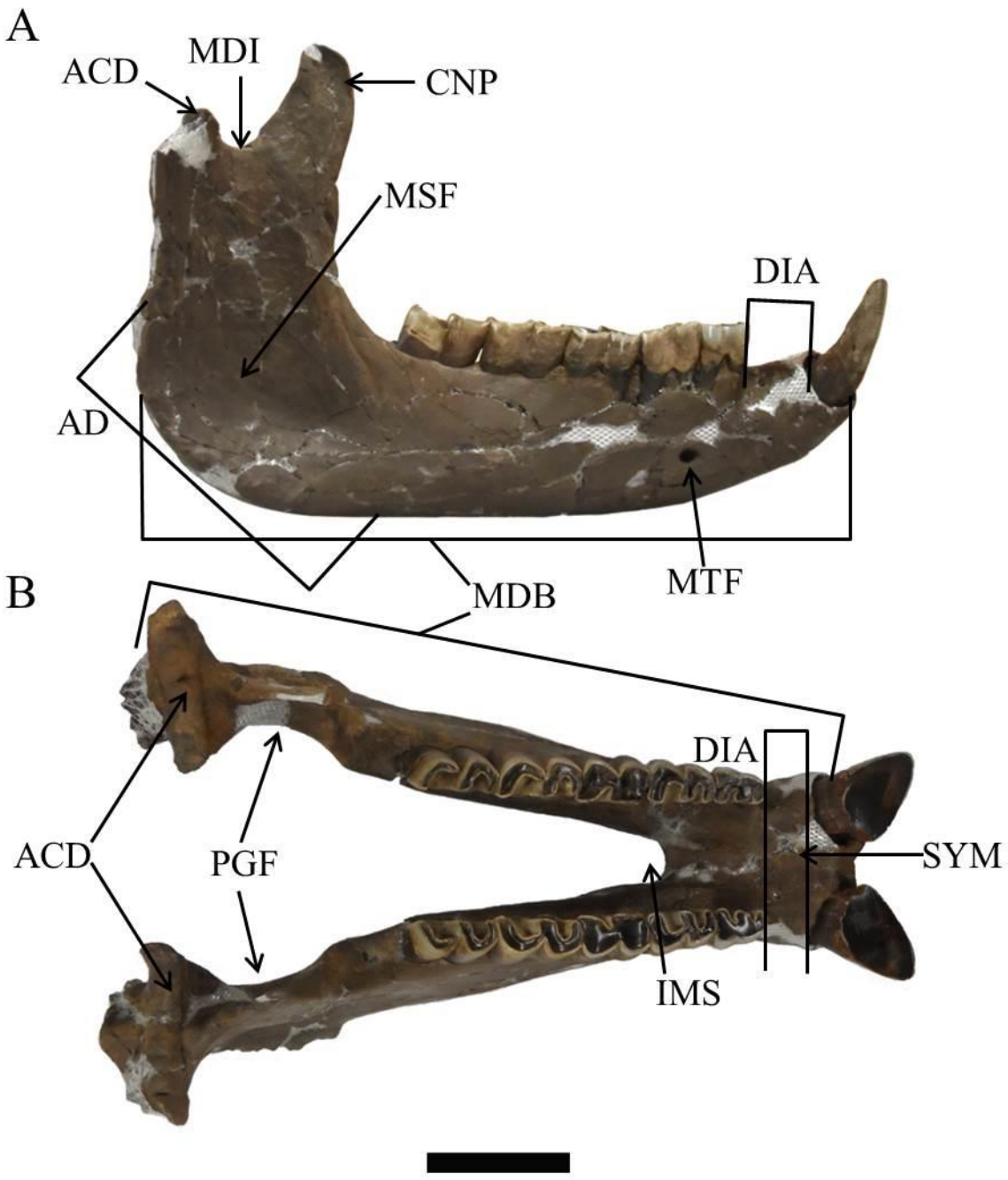

Figure 26. Mandible of ETMNH 601. Views: A, right lateral; B, dorsal. Anterior is to the right. Abbreviations: ACD, articular condyle; AD, angle of dentary; CNP, coronoid process; DIA, diastema; IMS; intermaxillary space; MDB, mandibular body; MDI, mandibular incisure; MSF, masseteric fossa; MTF, mental foramen; PGF, pterygoid fossa; SYM, symphysis. Scale bar = 10 cm.

Dentition

Upper Dentition

The upper teeth appear small when compared to the overall size of the skull (relative to other species of *Teleoceras*). Along each tooth row, there is 1 incisor modified as a tusk and 6 lophodont cheek teeth that can be considered mesodont, even in the less worn ETMNH 609.

Incisors. Upper tusks are modified first incisors that are reduced when compared to the lower tusks (Fig. 27). These upper tusks are ovate, elongate mediodorsally to lateroventrally, and function to hone the lower tusks during occlusion.

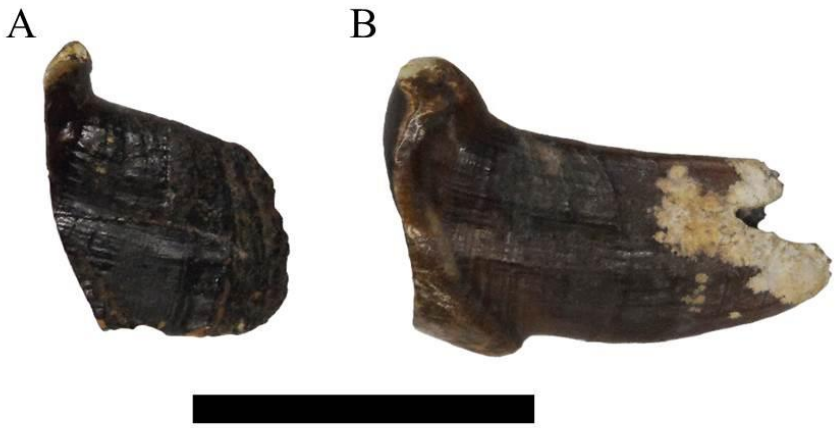

Figure 27. Upper left incisors with occlusal surface to the left. A, ETMNH 601; B, ETMNH 609. Scale bar = 5 cm.

Premolars. In addition to the teeth of the 2 skulls, there is an additional isolated upper premolar fragment in the collections (ETMNH 566). Upper second premolars are reduced and barely make the 'π' shape that is characteristic of rhinoceroses. This feature is more evident in the upper third and fourth premolars (Fig. 28). Though the second premolar (PM^2) is nearly

triangular, the third and fourth premolars (PM^3 and PM^4) are more rectangular with the longest axis oriented labiolingually. All premolars of both ETMNH 609 and ETMNH 601 have lingual merging between the protocone and the metaloph that creates closed fossettes but only the second lacks evidence of an antecrochet. The third premolar has a minimal antecrochet and the fourth has an antecrochet that is nearly as large as the respective crochet. While the second premolars have very small crochets, the third and fourth premolars have large crochets. Only the fourth premolars have a crista; thus, they have pre- and medifossettes. On ETMNH 609, the fossettes have extra protuberances between the crochets and the cristae and between the cristae and the antecrochets. ETMNH 609 has deep, triangular postfossettes on the upper premolars that have been worn to shallow ovals on ETMNH 601.

Shallow depressions are formed by slight cingula on the anterior and lingual surfaces of all upper premolars but become progressively larger through the series. No significant styles are present on the labial surfaces of the second premolars. On the third premolar, a slight parastyle extends beyond the metastyle of the second premolar. This is more pronounced in the fourth premolar. In all of the premolars, the ectoloph is either shorter than or equal in length to the protoloph and metaloph.

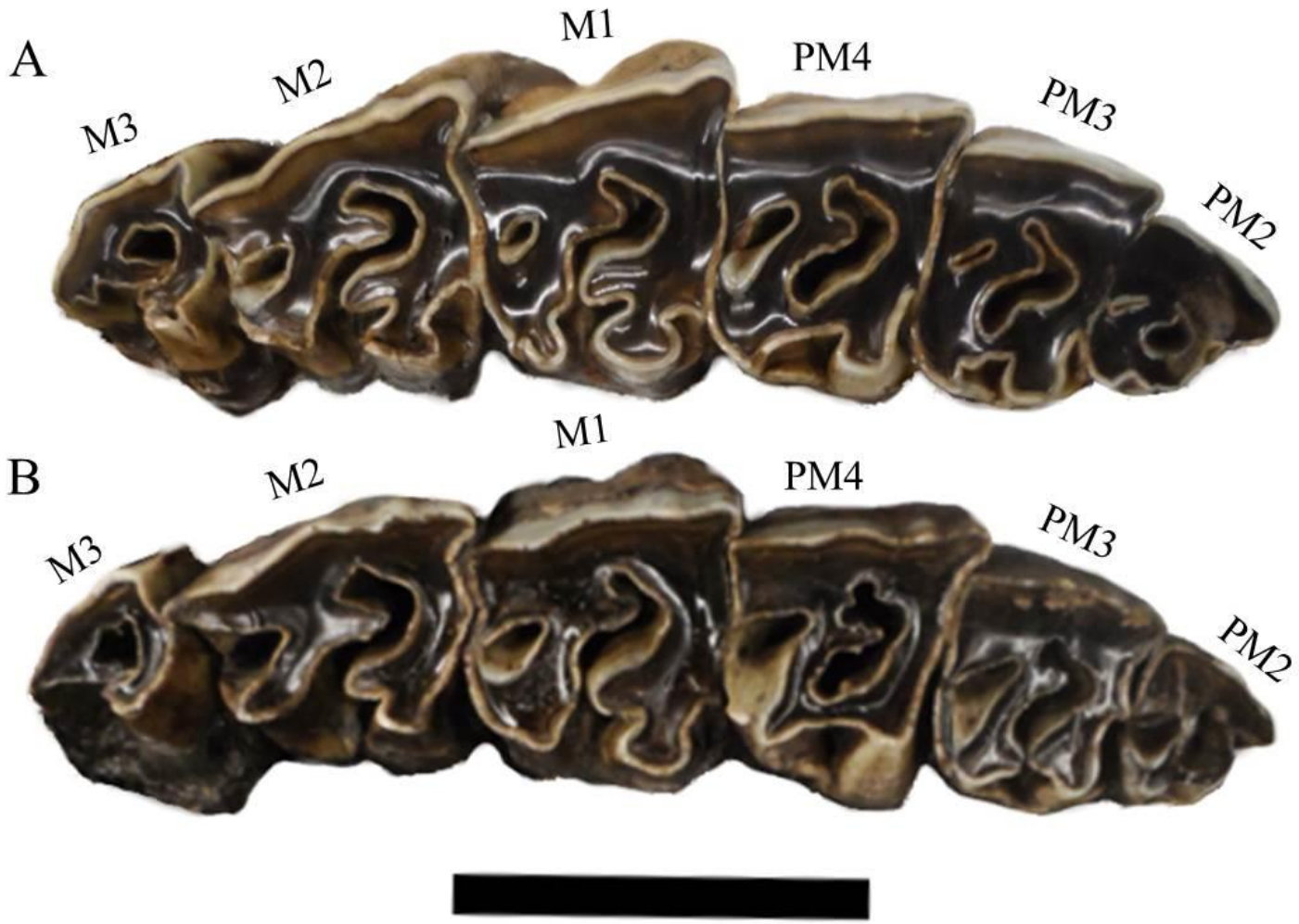

Figure 28. Upper cheek teeth in occlusal view. Anterior is to the right. A, ETMNH 601; B, ETMNH 609. Abbreviations: PM^2, upper second premolar; PM^3, upper third premolar; PM^4, upper fourth premolar; M^1, upper first molar; M^2, upper second molar; M^3, upper third molar. For terminology, see figure 5. Scale bar = 10 cm.

Molars. Isolated upper molars include a right first molar (ETMNH 12487), a partial right molar that might be a first (ETMNH 780), and 1 complete left first molar and 1 partial left first molar (ETMNH 781). Upper third molars (M^3) are reduced to a triangular shape but the first and second molars (M^1 and M^2) are rectangular and, though the first is nearly square, the second molar is longer anteroposteriorly (Fig. 28). Only the third molars have closed fossettes because the crochet is curved within the antecrochet. All of the molars have large crochets and antecrochets, though they are most pronounced on the second molars, and all of them lack cristae. Protocone constriction is found on all of the molars of ETMNH 601 but is only defined on the first molars of ETMNH 609.

First molars have closed postfossettes that have been worn to an oval but second molars have open triangular postfossettes. Shallow depressions are on the lingual and anterior surfaces of the first and second molars, like on the premolars, and are lined by slight cingula. These depressions are not as defined on the molars because wear has not merged the antecrochet with the metaloph. The ectoloph of the second molar is longer than both the protoloph and the metaloph of the same tooth. On the third molar, there is no metaloph and the protoloph and ectoloph are approximately the same length. Prominent parastyles, which extend beyond the metastyle of the anterior tooth, are found on all of the molars. A prominent metastyle is present on all upper molars but especially on the second molars where it extends beyond the posterior extent of the metaloph. All molars have a slight paracone fold on their labial surfaces.

Lower Dentition

Like the upper teeth, the lower teeth appear to be relatively small when compared to the overall size of the skull (again, compared to other species of *Teleoceras*). Along each tooth row,

all 5 mesodont cheek teeth have the ‘W’ shape characteristic of rhinoceroses and lack significant cingula.

Incisors. *Teleoceras* only has the lower second incisors and they have been modified into tusks with a cross-section in the shape of a tear-drop with the ‘point’ directed medially (Fig. 29). There are few isolated fragments of lower tusks are in the collections (ETMNH 3763, ETMNH 5235). The complete tusks of ETMNH 609 and ETMNH 601, there are concave wear surfaces on the lower tusks caused by occlusion with the upper tusks. Compared to ETMNH 601, ETMNH 609 has larger lower incisors because of the less advanced wear. On ETMNH 601, the alveoli for the tusks are much larger than the size of the tusks. Unfortunately, the mesial end of the mandible of ETMNH 609 was reconstructed using MagicSculpt, so it does not provide a comparison with which to judge the odd fit on ETMNH 601 as normal or pathological.

Figure 29. Lower left incisor tusks in occlusal view. A, ETMNH 609; B, ETMNH 601. Scale bar = 10 cm.

Premolars. ETMNH 609 has a small vestigial premolar, first noted by Wallace (2006), which is typically lacking in other species of *Teleoceras* (Prothero, 2005) (Fig. 30). Because of the small sample size, it is not possible to know whether this is an isolated anomaly or an atavism within the population. Two lower premolars are nearly upright and perpendicular to the axis of the dentary (Fig. 31). Both ETMNH 601 and ETMNH 609 have lower third premolars that are heavily worn with the lophids merged. An extremely open angle is present between the 2 lophids but the degree of wear has nearly straightened the labial surface. The anterior and posterior valleys are both sharp 'V's and are of similar depths. The right lower fourth premolar

of ETMNH 609 and both lower fourth premolars of ETMNH 601 have been worn so that the lophids are merged. There is a slight open angle on the labial edges between the lophids. While both the anterior and posterior valleys are sharp ‘V’s, the posterior valley is the deeper of the two.

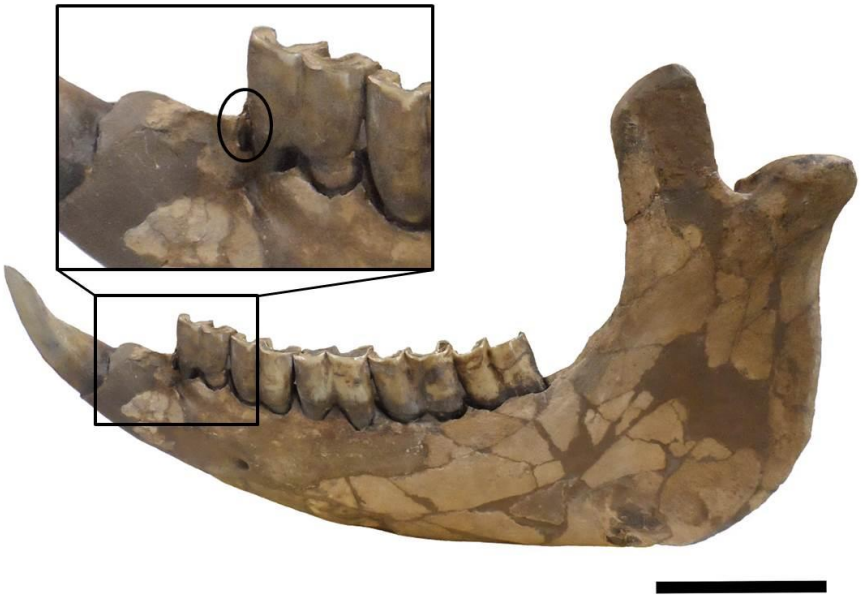

Figure 30. Vestigial left lower second premolar of ETMNH 609. Tooth of interest is indicated by the circle. Scale bar = 10 cm.

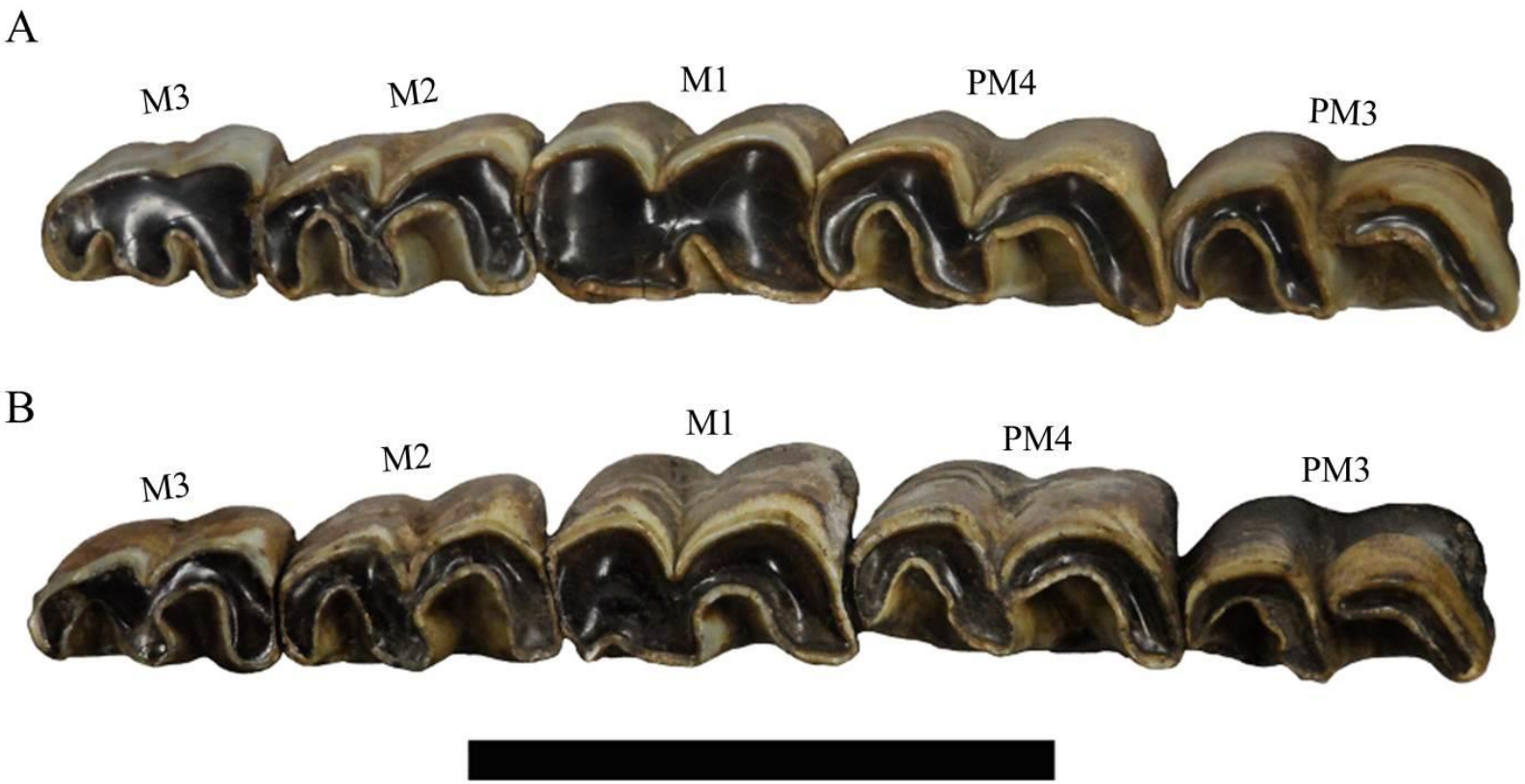

Figure 31. Lower cheek teeth in occlusal view. Anterior is to the right. A, ETMNH 601; B, ETMNH 609. Abbreviations: PM_3, upper third premolar; PM_4, upper fourth premolar; M_1, upper first molar; M_2, upper second molar; M_3, upper third molar. For terminology, see figure 5. Scale bar = 10 cm.

Molars. Three lower molars are slanted mesially and the degree of slant increases toward the distal end of the tooth row (Fig. 31). Both ETMNH 601 and ETMNH 609 have heavy wear on the lower first molars, so the lophids are merged with only a slight open angle on the labial side. The heavy degree of wear has removed the anterior valley on all 4 of the lower first molars. Posteriorly, the remaining valley is a sharp 'V.' The lower second molars of ETMNH 609 are not worn so that the lophids are merged. ETMNH 601 has merged the lophids of the right lower second molar but not of the left. Because of the wear stage variation, the labial angle between the lophids ranges from open to sharp. Anteriorly, the lingual valley is a sharp 'V' with an anterior cingulum that extends ventrally and posteriorly toward the posterior valley, which is a broad 'V.' Excluding the cingulum, the 2 valleys are approximately the same depth. None of the lower third molars have been worn to the extent that the lophids are merged. This produces a sharp angle on the labial side between the lophids. On the lingual side of the lower third molar, the anterior valley is a sharp 'V' and the posterior valley is a broad 'V.' These valleys are approximately the same depth.

Vertebrae

Cervical Vertebrae

Atlas. The atlas articulates anteriorly with the occipital condyles of the skull and posteriorly with the axis (Fig. 32). Differential weathering is obvious in the atlas of ETMNH 609; the reconstructed left side is much smaller and worn than the right, which has a good amount of rugosity present. ETMNH 601 has a more heavily weathered atlas with multiple fractures that were repaired.

The dorsal tubercle (DTB) is a round structure along the midline of the dorsal arch (DA), which is a thin dome that narrows caudally. A minimal ventral tubercle (VTB) mirrors the

odontoid process of the axis. The ventral arch (VA) is more robust, more ‘V’-shaped, and narrows caudally. Thus, the neural canal (NC) is round dorsally and ‘V’-shaped ventrally. At the base of the dorsal arch, lateral vertebral foramina (LVF) are located slightly more cranially than caudally. ETMNH 609 has a furrow for blood vessels and nerves in the right lateral vertebral foramen but, in the left, this has been weathered away.

Transverse processes (TVP) are narrow craniocaudally, long mediolaterally, and thin dorsoventrally. The left transverse process of ETMNH 609 has an unnatural depression of unknown origin near the left lateral vertebral foramen that does not extend through the transverse process to the ventral surface and may be a remnant of weathering or reconstruction. At the lateral-most ends of the transverse processes, there is a great amount of rugosity present on ETMNH 601 that is not present on ETMNH 609. This is most likely an ontogenetic effect because ETMNH 601 is the older and larger of the 2 individuals. On the medioventral surface of the transverse processes, transverse foramina (TVF) are present. No foramen alare are present on the atlases of GFS *Teleoceras*.

Cranial articular surfaces (CRAS) for the occipital condyles are tear-drop shaped and narrow ventromedially. Lateral edges of the articular surfaces extend cranially with a slight dorsal lip. There is a small, indented gap between the cranial articular surfaces on the dorsal arch of ETMNH 609 that is not present on ETMNH 601. Caudal articular surfaces (CAAS) are ovate with the elongated axis extending mediolaterally. Ovate caudal articular surfaces extend laterally to the vertebral foramina.

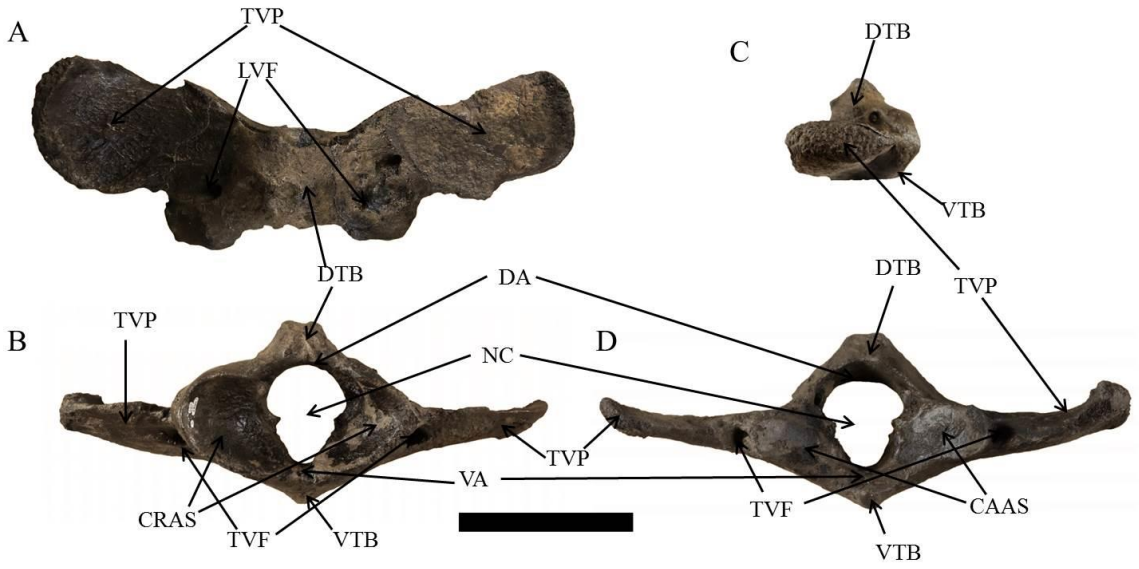

Figure 32. Atlas of ETMNH 609. Views: A, dorsal; B, left lateral; C, anterior; D, posterior. Abbreviations: CAAS, caudal articular surface; CRAS, cranial articular surface; DA, dorsal arch; DTB, dorsal tubercle; LVF, lateral vertebral foramen; NC, neural canal; TVF, transverse foramen; TVP, transverse process; VA, ventral arch; VTB, ventral tubercle. Scale bar = 10 cm.

Axis. The axis articulates anteriorly with the atlas and posteriorly with the third cervical vertebra (Fig. 33). Both ETMNH 609 and ETMNH 601 have nearly complete axes with only minor repairs. The axes are taller and wider than they are long and have large rounded odontoid processes (OP) that articulate with their respective atlases. Caudally, the centrum (CEN) is somewhat concave. A spinous process is non-existent and, while this is possibly the result of weathering, it is unlikely it was ever present. The neural canal (NC) is domed dorsally but flattened ventrally.

Prezygapophyses (PRZ) are expanded mediolaterally. Postzygapophyses (POZ) extend laterally and caudally to form slightly ovate facets. No lateral vertebral foramina are present on the axis but a deep cranial notch (CRN) is. Only minimal transverse processes (TVP) are present.

Transverse foramina (TVF) are not completely closed on ETMNH 609 but are on ETMNH 601 suggesting that this is variable by age. Caudal vertebral notches (CAN) are present as rounded notches between the ventral postzygapophyses and the dorsal centrum. While the centrum's posterior epiphyseal suture (EPS) is visible, it does appear to be fused. ETMNH 601 has completely fused epiphyses.

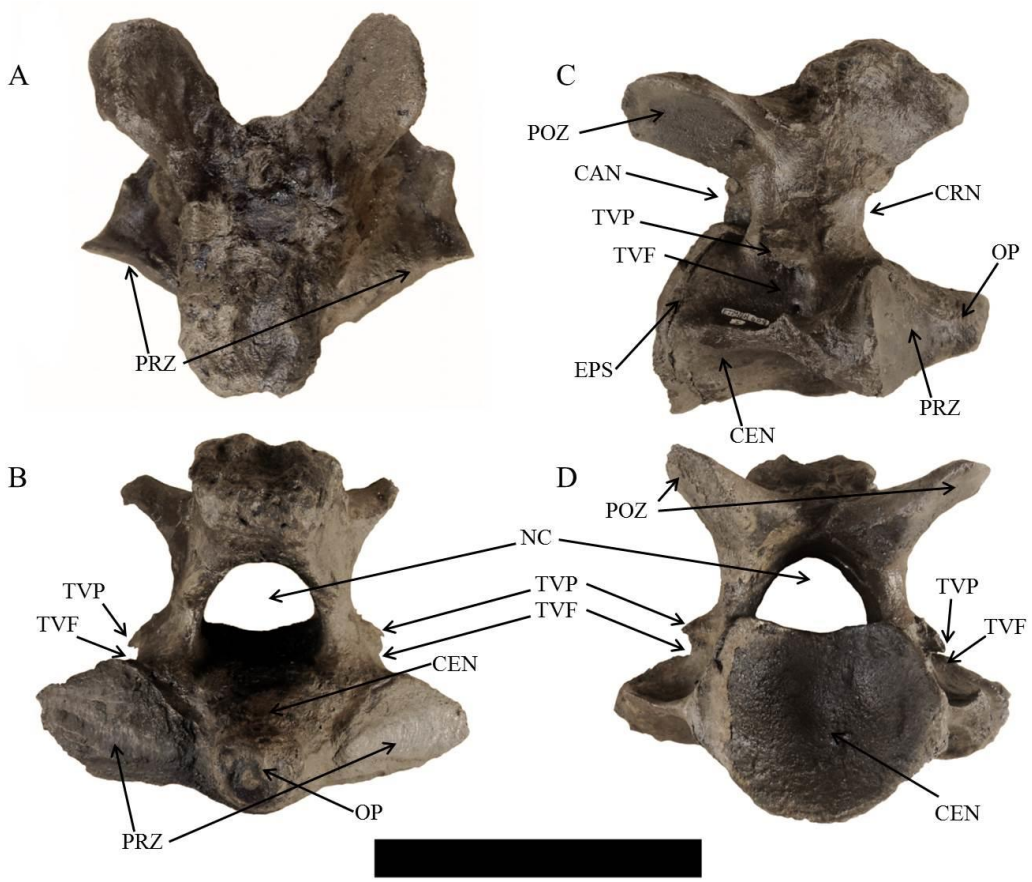

Figure 33. Axis of ETMNH 609. Views: A, dorsal; B, left lateral; C, anterior; D, posterior. Abbreviations: CAN, caudal notch; CEN, centrum; CRN, cranial notch; EPS, epiphyseal suture; NC, neural canal; OP, odontoid process; PRZ, prezygapophyses; POZ, postzygapophyses; TVF, transverse foramen; TVP, transverse process. Scale bar = 10 cm.

Third—Sixth Cervical Vertebrae. Four remaining cervical vertebrae are posterior to the axis and anterior to the first thoracic vertebra (Fig. 34). These cervical vertebrae, identified by the presence of transverse foramina and the lack of rib articular facets, are damaged in both skeletons. Those of ETMNH 609 have been repaired and the 2 most posterior cervicals of ETMNH 601 are fused together and to the first thoracic vertebra. Unlike ETMNH 601, ETMNH 609 does not have completely fused posterior epiphyseal plates and the fourth cervical is missing the posterior plate entirely. Cervical anterior epiphyseal plates are completely fused on both skeletons. Posterior through the cervical series, the neural spines (NS) transition from very little to prominent. The neural canal (NC) is domed dorsally and flattened ventrally along the dorsal centrum (CEN). On the ventral surface of the centra, there is no evidence of any hemal structures.

Round prezygapophyses (PRZ) are present on the dorsal surface of the anterior prominences (APR) of the vertebrae. These articulate with the round postzygapophyses (POZ) that are present on the ventral surface of the posterior prominences (PPR). Posteriorly through the series, the transverse processes (TVP) vary from a small lateral extension on the third cervical vertebra to a larger split process on the sixth cervical vertebra. The characteristic transverse foramina are found just lateral to the centra at the origin of the transverse processes. Though the centra are acoelous, the exaggerated shape resembles opisthocoelous vertebrae. This restricts the range of motion and increases the strength of the neck to support the large head, which was possibly advantageous during aggressive use of the lower tusks.

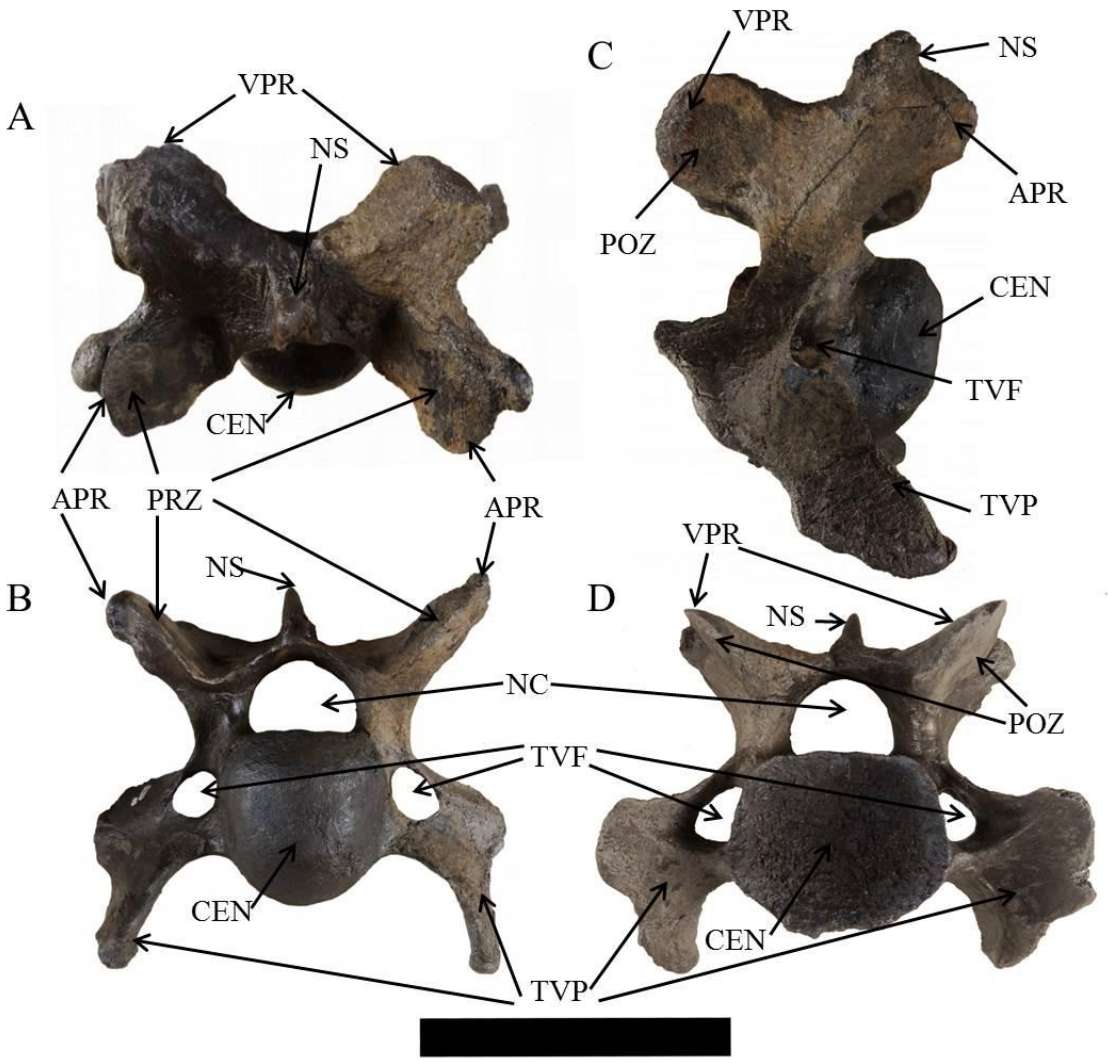

Figure 34. Fourth cervical vertebra of ETMNH 609. Views: A, dorsal; B, right lateral; C, anterior; D, posterior. Abbreviations: APR, anterior prominence; CEN, centrum; NC, neural canal; NS, neural spine; POZ, postzygapophyses; PPR, posterior prominence; PRZ, prezygapophyses; TVF, transverse foramen; TVP, transverse process. Scale bar = 10 cm.

Thoracic Vertebrae

Thoracic vertebrae are posterior to the cervical vertebrae and anterior to the lumbar vertebrae (Fig. 35). In addition to the thoracics of the complete skeletons, there is a neural spine

epiphysis (ETMNH 3751), a neural spine fragment (ETMNH 13510), and 2 complete thoracic vertebrae (ETMNH 3752, ETMNH 12175). ETMNH 609 has 19 thoracic vertebrae, most of which have been at least partially repaired, that articulate with 18 pairs of ribs. The epiphyseal plates of ETMNH 609 are only partially fused and some are separated or missing from their vertebrae. ETMNH 601 has an incomplete thoracic series as only 10 fragmented and concreted vertebrae are present; though, most of the epiphyseal plates are completely fused. Neural spine (NS) height varies throughout the thoracic series to form an arc with the third thoracic as the apex. After the 12th thoracic, the neural spine height becomes consistent. In addition to height, the orientation of the neural spines changes from upright on the first thoracic to posteriorly directed on the last thoracic.

The first through third thoracic vertebrae have prominent transverse processes (TVP) and articulate with reduced ribs. These transverse processes continue the neck support produced by the robust cervical vertebrae. The fourth though 19th thoracic vertebrae have reduced transverse processes and articulate with larger ribs. There are 3 articular surfaces on the second through 18th thoracics—the articular fossa for the anterior rib (AFAR), the articular fossa for the posterior rib (AFPR), and the costal fovea (CF). Throughout the thoracic series, the size and shape of these facets varies and, in some cases, the anterior articular fossa and the costal fovea merge. The first thoracic vertebra lacks the anterior articular fossa and the 19th thoracic lacks the posterior articular fossa. On the posterior surface of each vertebra, caudal notches (CAN) separate the transverse processes from the posterior articular fossae.

At the anterior end of the thoracic series, the first 5 vertebrae have triangular neural canals (NC). From the sixth vertebrae to the posterior end of the series, the neural canal is round.

Along with the change in neural canal shape, the thoracic centra (CEN) also change shape throughout the series from round at the anterior end to heart-shaped at the posterior end. The dorsal vertebral arch (DA)—between the neural spine and the transverse process—is more obtuse in the anterior thoracics and becomes more acute in the posterior thoracics.

On the first 2 thoracic vertebrae, the prezygapophyses (PRZ) resemble those on the cervical vertebrae but, beginning with the third thoracic, the prezygapophyses are reduced in size and are at the base of the anterior neural spine. Through the anteroposterior progression, the dorsal notch (DN) between the prezygapophyses becomes deeper and more pronounced. In the case of the postzygapophyses (POZ), only the first thoracic vertebra resembles the cervical vertebrae. The remaining thoracics have reduced postzygapophyses that are at the base of the posterior neural spine for articulation with the prezygapophyses of the subsequent vertebra.

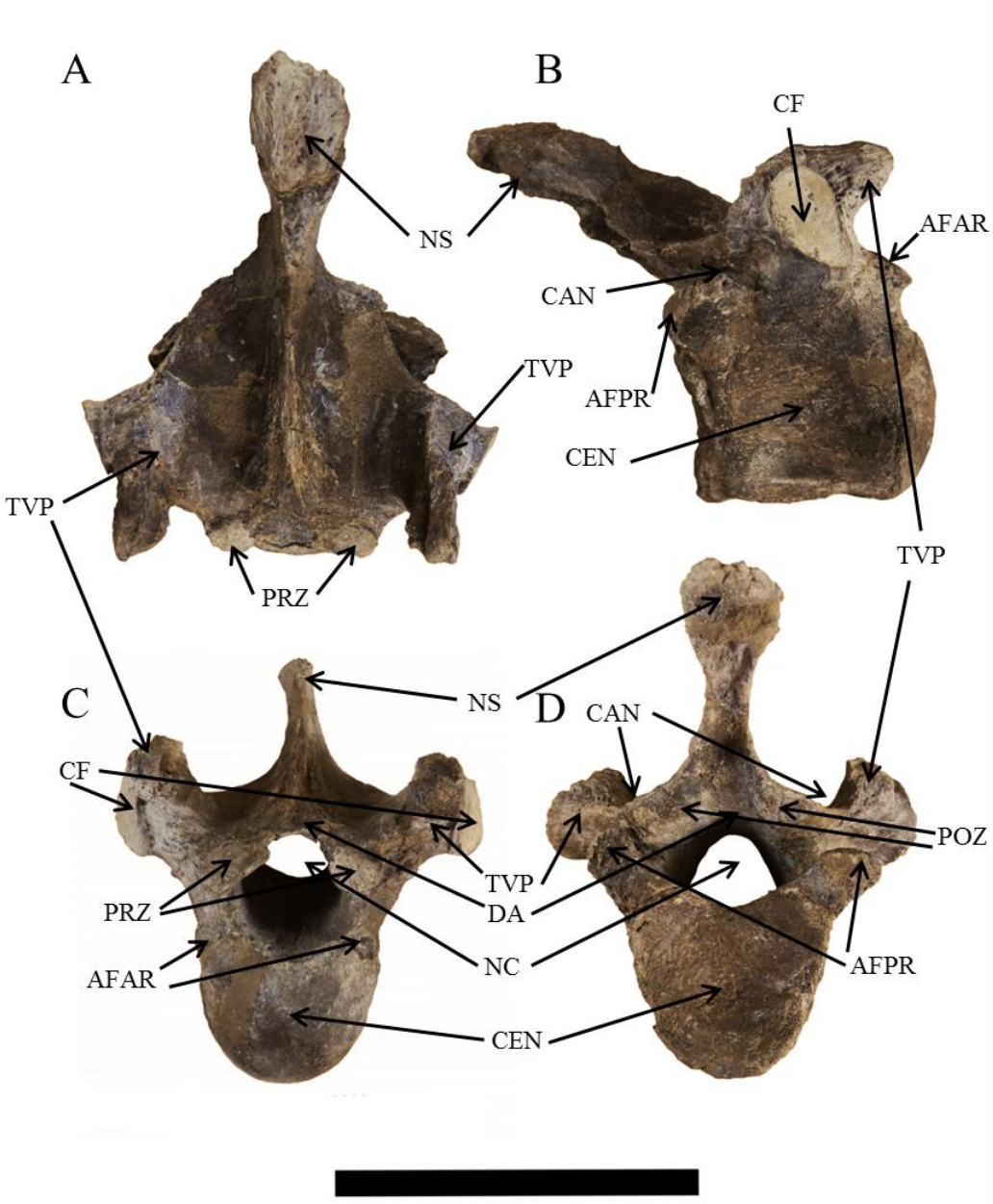

Figure 35. Sixteenth thoracic vertebra of ETMNH 609. Views: A, dorsal; B, right lateral; C, anterior; D, posterior. Abbreviations: AFAR, articular fossa for anterior rib; AFPR, articular fossa for posterior rib; CAN, caudal notch; CEN, centrum; CF, costal fossa; DA, dorsal arch; NC, neural canal; NS, neural spine; POZ, postzygapophyses; PRZ, prezygapophyses; TVP, transverse process. Scale bar = 10 cm.

Lumbar Vertebrae

The lumbar vertebrae are posterior to the thoracic series and anterior to the sacrum (Fig. 36). There are 3 lumbar vertebrae in ETMNH 609; however, none are preserved in ETMNH 601. All 3 lumbar of ETMNH 609 have significant repairs and visible epiphyseal plates, especially the posterior ones. Lumbar neural spines (NS) are thin but anteroposteriorly wide and slanted posteriorly. The neural canal (NC) is more triangular than domed and widens through the series. Lumbar vertebrae have acoelous centra (CEN) that are heart-shaped. The posterior centrum of the last lumbar is oval for articulation with the sacrum.

The first lumbar vertebra has tighter anterodorsal processes for articulation with the last thoracic; these are more wide-set on the last lumbar. Prezygapophyses (PRZ) are small ovals on either side of the medial notch (MN). Postzygapophyses (POZ) are also oval and are on the ventral side of the neural spine and either side of the medial notch. Transverse processes (TVP) are smallest on the first lumbar vertebrae and largest on the second. On the third lumbar, the transverse processes have flat, slightly rugose areas on their dorsal surface for articulation with the wings of the sacrum.

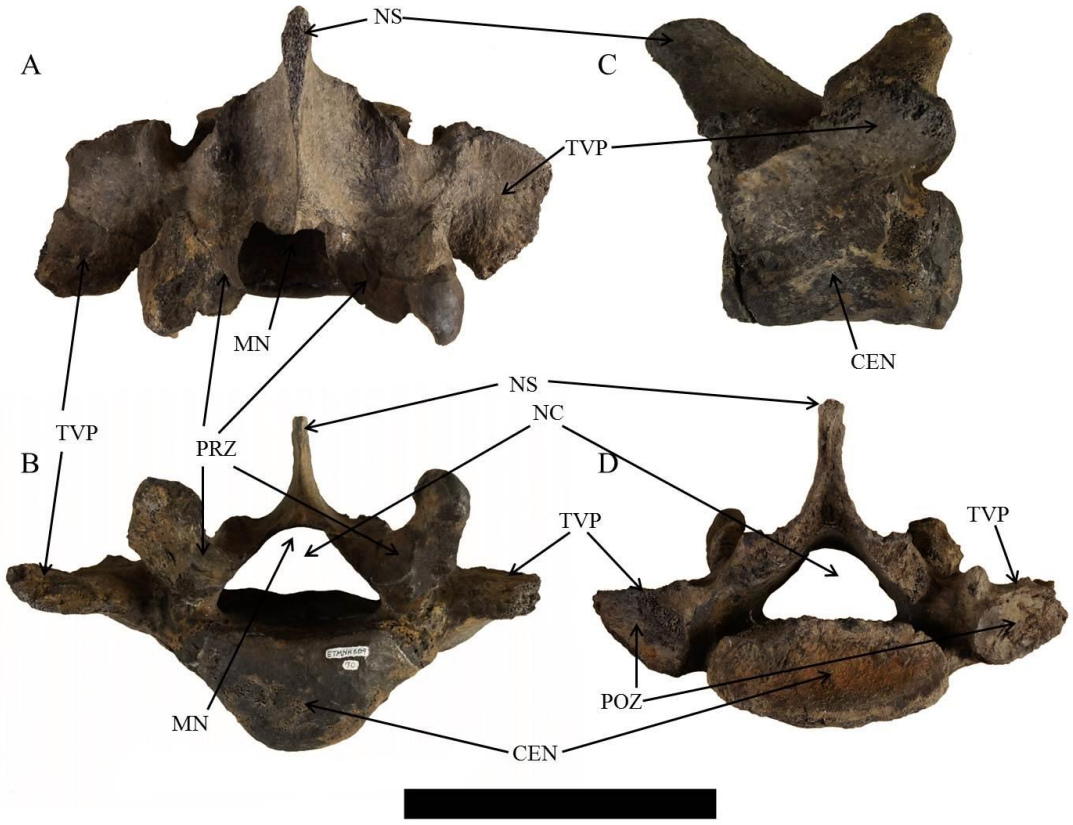

Figure 36. Third lumbar vertebra of ETMNH 609. Views: A, dorsal; B, right lateral; C, anterior; D, posterior. Abbreviations: CEN, centrum; MN, medial notch; NC, neural canal; NS, neural spine; PRZ, prezygapophyses; POZ, postzygapophyses; TVP, transverse process. Scale bar = 10 cm.

Sacrum

The sacrum articulates anteriorly with the third lumbar vertebra, posteriorly with the first caudal vertebra, and laterally with the ilia (Fig. 37). There is very little of the sacrum of ETMNH 601 preserved and not enough to make any morphological observations. The sacrum of ETMNH 609 appears to be generally rugose but there is a great degree of weathering. Restoration of the sacrum left it nearly complete except for a small box of fragments that could

not be included. Four sacral vertebrae (SV1-4) fused to form the triangular sacrum that is wide cranially and narrows caudally. Neural spines (NS) of the first and second sacral vertebrae have fused together while those of the third and fourth are isolated. Three pairs of sacral foramina (SF) are present on either side of the sacrum with 1 between each adjacent pair of sacral vertebra. These are found on both sides of the neural spines but are more visible when viewed ventrally, and they decrease in size caudally.

The neural canal (NC) appears to be triangular but this may be an effect of preservation as the dorsal surface has collapsed into the caudal portion of the canal. Cranial notches (CRN) are half-circles with the left slightly more open than the right. The first sacral vertebra has bulbous prezygapophyses (PRZ) that articulate with the postzygapophyses of the last lumbar vertebra. Oval centra (CEN) are transversely elongated and sagittally shortened. Rugose cranial margins of the sacral wings (SW) are flattened and turned dorsally so that their dorsal surfaces articulate with the ventral ilia. Lateral sacral ridges are not visible but this may be due to weathering rather than a true absence. Caudal notches (CAN) are smaller than cranial notches and form postzygapophyses (POZ) that articulate with the first caudal vertebra.

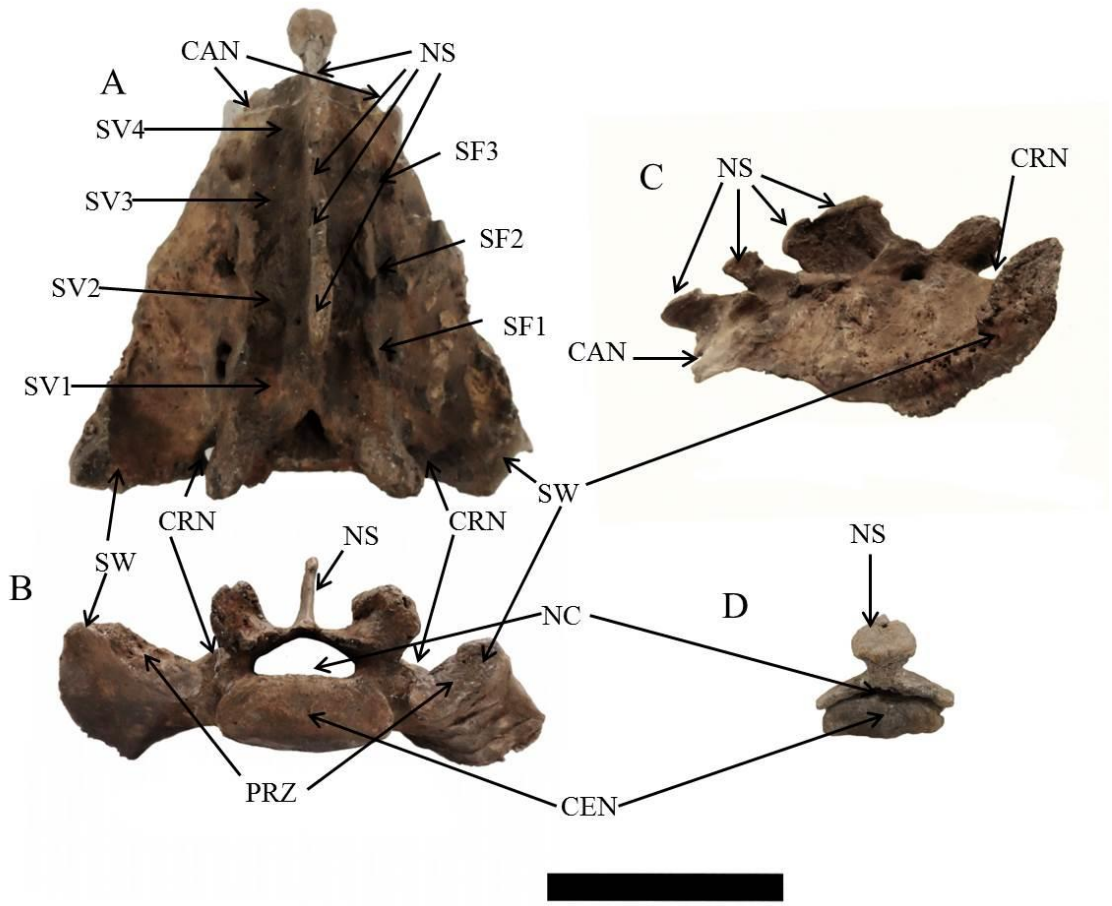

Figure 37. Sacrum of ETMNH 609. Views: A, dorsal; B, right lateral; C, anterior; D, posterior. Abbreviations: CAN, caudal notch; CEN, centrum; CRN, cranial notch; NC, neural canal; NS, neural spine; PRZ, prezygapophyses; SF1-3, sacral foramina 1-3; SV1-4, sacral vertebrae 1-4; SW, sacral wing. Scale bar = 10 cm.

Caudal Vertebrae

ETMNH 609 has 21 caudal vertebrae and ETMNH 601 has 23 (Fig. 38). There are also 2 isolated caudal vertebrae (ETMNH 559 and ETMNH 573). Through the caudal series, the vertebrae change from a typical morphology to being 'blob-like.' The first 4 caudals have distinct neural spines, the fifth and sixth caudals are transitional, and all subsequent caudals lack true neural spines. Transverse processes are present on the anterior caudals and become reduced

to simple protuberances at the 10th caudal before being lost on the 17th caudal. A dorsoventrally compressed, triangular neural canal curves over the centrum on the anterior caudals until it becomes rounded on the sixth caudal. On the 11th caudal, the neural canal is opened by the posterior progression of the dorsal neural canal notch. The first 3 caudal vertebrae have small round remnants of pre- and postzygapophyses but, after the third caudal, the only articulation between caudals occurs at the centra. Posterior caudals have complete epiphyseal fusion and some are fused in both ETMNH 609 and ETMNH 601.

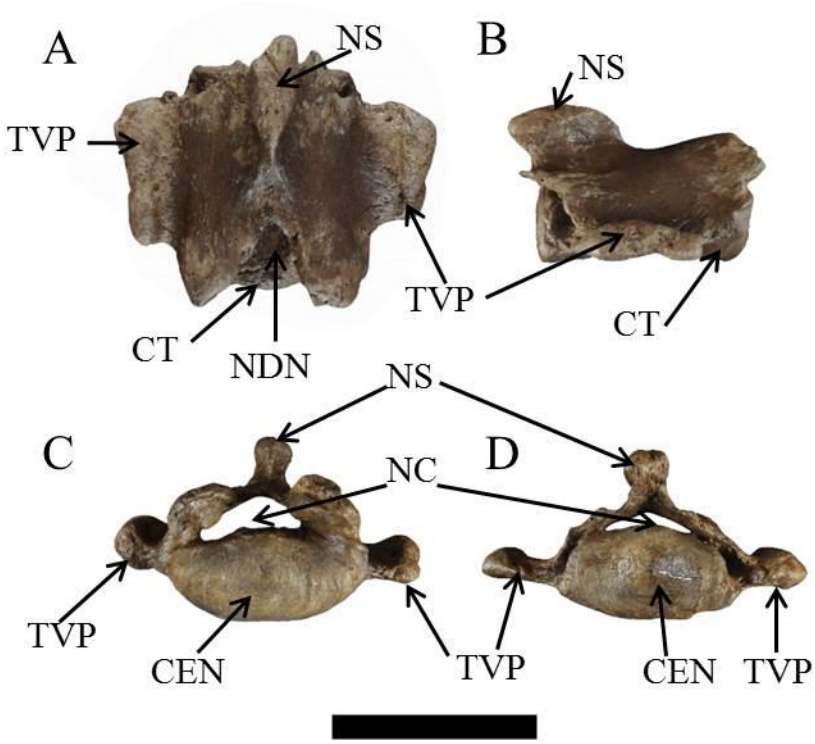

Figure 38. Third caudal vertebra of ETMNH 609. Views: A, dorsal; B, right lateral; C, anterior; D, posterior. Abbreviations: CT, centrum; NC; neural canal; NDN; neural dorsal notch; NS, neural spine; TP, transverse process. Pre- and post-zygapophyses are not visible in this figure. Scale bar = 10 cm.

Other Axial Elements

Sternebrae

There are 3 sternebrae associated with ETMNH 609 but only fragments of ossified cartilage were found with ETMNH 601 (Fig. 39). The sternebrae of ETMNH 609 include 1 long sternebra with a triangular protuberance, 1 short sternebra that appears pinched on the long axis and expanded at both ends, and 1 round ball. These specimens are very porous bone with a different texture than is seen in the other skeletal elements.

Figure 39. Sternebrae of ETMNH 609. Scale bar = 10 cm.

Ribs

ETMNH 609 has 18 pairs of ribs, which is accurate considering the presence of 19 thoracic vertebrae. ETMNH 601 only has incomplete fragments that do not produce an accurate count. There are 19 specimens of rib fragments that are unassociated with the 2 complete skeletons (Appendix 2). Overall, the ribs are rather unremarkable in their morphology; although, ETMNH 601 has 2 ribs with pathologies that are addressed in Gilmore and Wallace (in prep.) (Fig. 40).

Figure 40. Ribs of ETMNH 601 showing pathologies. Photo courtesy of Laura Gilmore. Scale bar = 10 cm.

Ossified Cartilage

Each complete skeleton has pieces of ossified costal that are characteristically very porous. An isolated piece of ossified cartilage has also been found (ETMNH 3752).

Forelimb

Scapula

The scapula articulates distally with the humerus (Fig. 41). Only the right scapula of ETMNH 609 is in good condition. The robust scapulae are nearly triangular in shape with a slightly convex cranial border (CRB) that is rugose, especially at the proximal angle where it meets the heavily rugose vertebral border (VBB). The vertebral border is concave and extends to form a prominent, rugose angle with the rather straight caudal border (CDB). ETMNH 601 has more rugosity along the edges of the scapulae suggesting an ontogenetic progression. A wide scapular neck separates the broad proximal triangle from the distal site of articulation. Two small foramina are present on the cranial edge between the glenoid fossa (GF) and the robust coracoid process (CCP). An ovate and gently concave glenoid fossa forms the distal end of the scapula

and articulates with the humerus. The glenoid fossa has well-defined edges, except the craniolateral edge (CLE), which is modified into a rounded ridge as if the surface has been folded toward the coracoid process to create an extra point of articulation with the proximal head of the humerus.

The scapular spine (SCS) extends nearly the length of the element from just distal of the vertebral point to just proximal of the glenoid fossa. The spine is tall and curves over the infraspinous fossa (ISF) toward the caudal angle. On the left scapula of ETMNH 609, there is a foramen at the base of the spine on the infraspinous fossa. The distal end of the scapular spine is more elevated but it slopes to the level of the fossae as it extends proximally. A heavily rugose spinal tuber (ST) is triangular but has a rounded apex directed caudally. Medially, the underside of the spine is marked by a depression. The supraspinous fossa (SSF) is reduced in size when compared to the infraspinous fossa. Laterally, the supraspinous fossa is depressed near the scapular spine and raised at the cranial border. In the same view, the infraspinous fossa is nearly flat, except for slight raise along the caudal border. Medially, a large, raised ridge is present beginning at the scapular neck and into the infraspinous fossa. Completely visible only on the right scapula of ETMNH 609, this ridge forms a ‘Y’ with the larger of the 2 ridges extending along the scapular spine and the smaller extending into the infraspinous fossa.

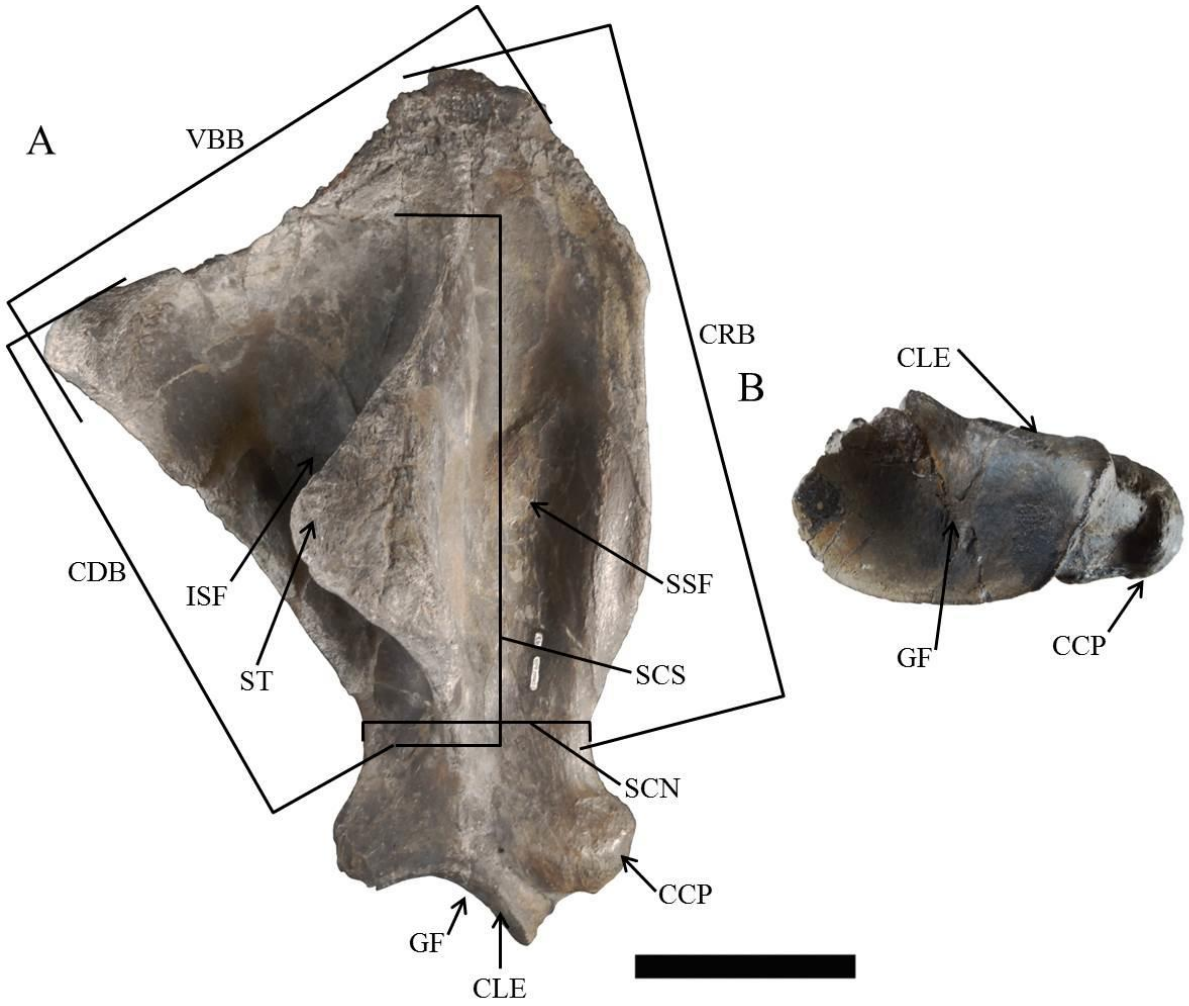

Figure 41. Right scapula of ETMNH 609. Views: A, lateral; B, distal. Abbreviations: CCP, coracoid process; CDB, caudal border; CLE, craniolateral edge; CRB, cranial border; GF, glenoid fossa; ISF, infraspinous fossa; SCN, scapular neck; SCS, scapular spine; SSF, supraspinous fossa; ST, spinous tuber; VBB, vertebral border. Scale bar = 10 cm.

Humerus

The humerus articulates proximally with the scapula and distally with the radius and ulna (Fig. 42). There is a proximal epiphyseal plate with fragments of a right humerus (ETMNH 5057) and the proximal end of another right humerus (ETMNH 6648). Both humeri of ETMNH

609 have been broken across the diaphysis and subsequently repaired; however, the humeri of ETMNH 601 are in worse condition, though they have been reconstructed as much as possible. On the proximal surface, there is a depression posterior (PD) to the lesser and intermediate tuberosities and anterior to the humeral head. This depression articulates with the craniolateral portion of the scapula's glenoid fossa. The smooth and rounded articular head (AH) extends caudally so that it curves onto the posterior surface of the humerus. On this posterior surface, an edge marking the extent of the articular surface forms a lip that extends beyond the diaphyseal surface.

Greater tuberosities are missing from both humeri of ETMNH 601, though the pieces may be present among the associated fragments. On ETMNH 609, the greater tuberosity extends proximomedially and with a distinct curvature. A very shallow groove (GR1) separates the summit (GTS) and the convexity (GTC) of the greater tuberosity; another groove (GR2) separates the intermediate tubercle (IMT) and the summit of the lesser tuberosity (LTS). A number of foramina are found distal to the convexity of the greater tuberosity. Although on the right humerus of ETMNH 609, the intermediate tubercle and the summit of the lesser tuberosity have been reconstructed, these features are still intact on the left humerus. The convexity of the lesser tuberosity (LTC) is a slight knob on the medial side of the humeral head. Both the greater and lesser tuberosities are rugose, which indicates strong muscle attachments. A tightly rounded bicipital groove (BCG) separates the greater tuberosity and the intermediate tubercle. The smooth, rounded intermediate tubercle is not as prominent as that seen in *Equus* and, for that reason, was not considered to be present in rhinos by Hermanson and MacFadden (1992). It is being considered as a feature here because it is distinct from the greater and lesser trochanters

and, within rhinos, *Teleoceras* has a large intermediate tubercle (Mihlbachler 2013, pers. comm.). Hermanson and MacFadden (1992) describe the intermediate tubercle of *Equus* as a passive stay-mechanism in the shoulder to allow the animal to stand for a long period of time without energy exertion (Hermanson and MacFadden 1992).

In medial view, rugosity extends from the lesser tuberosity almost to the medial epicondyle. In lateral view, the deltoid tuberosity (DT) is distal to the greater tuberosity and, though the deltoid tuberosity is small, it is a rugose projection that is directed posteriorly. A pronounced humeral crest (HCT) originates at the deltoid tuberosity and curves distomedially to its insertion at the midline of the distal diaphysis. ETMNH 601 has a more distal extent to the humeral crests, which suggests more pronounced muscle attachment caused by the advanced age and the larger size of the individual. The humeral crest gives the humerus the appearance of being twisted. Posteriorly, the diaphyseal axis extends from the posterior curvature of the humeral head to the distal olecranon fossa (OF). On ETMNH 609, there is a nutrient foramen (HNF) at the midpoint of the posterior diaphysis that is not visible on ETMNH 601.

Anteriorly, a larger, medial coronoid fossa (CF) and a smaller, lateral radial fossa (RF) are proximal to the trochlea and capitulum, respectively. These are not completely distinct but are only divided by a very slight ridge. The wide trochlea (TRO) extends more proximal than the narrow capitulum (CAP), giving the appearance of a rotated articular surface. While the capitulum is only slightly angled from proximolateral to distomedial, the trochlea is more strongly angled along the same axis. The trochlea and capitulum curve around the distal end, narrow, and merge together before terminating at the distal edge of the olecranon fossa. This forms a lip, which is more pronounced along the capitulum, over the epicondyles.

At the distal end, the epicondyles are robust and form the sides of the posterior olecranon fossa without overhanging the fossa. From the lateral epicondyle (LEC) of ETMNH 609, the epicondylar crest (ECC) extends proximally to the midpoint of the posterior diaphysis and projects more laterally than the features at the proximal end. In contrast, the lateral epicondyle of ETMNH 601 does not extend more laterally than the features of the proximal end, specifically the deltoid tuberosity, which indicates that there is a degree of variability in the relative proportions possibly based on size and age of the individuals. In contrast to the expansive lateral epicondyle, the medial epicondyle (MEC) is relatively slender along the side of the olecranon fossa, which is a deep, rounded depression that is proximally open to the diaphysis. The olecranon fossae of ETMNH 601 are not as open as that of ETMNH 609 due to larger epicondyles caused by greater muscle attachment.

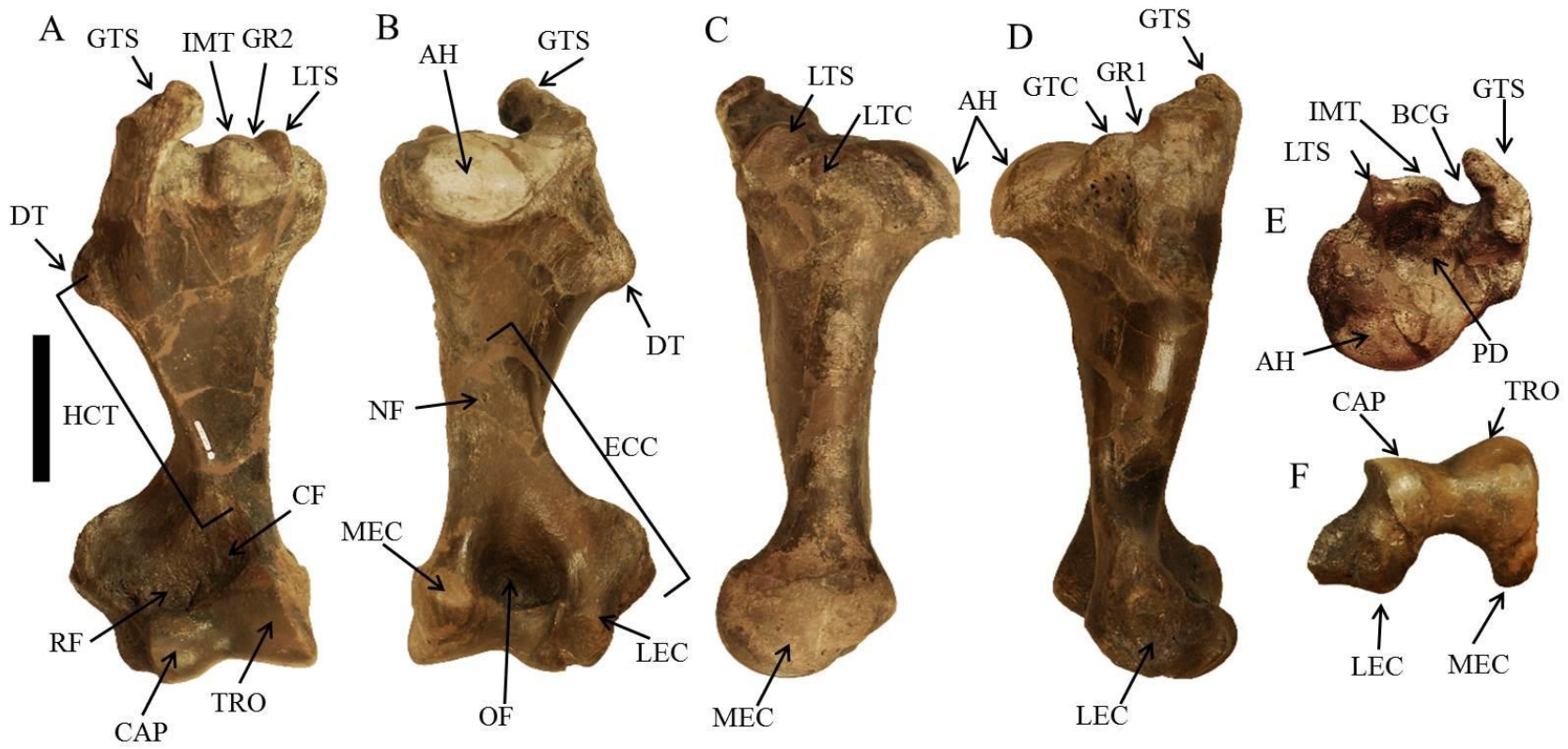

Figure 42. Right humerus of ETMNH 609. Views: A, anterior; B, posterior; C, medial; D, lateral; E, proximal; F, distal. Abbreviations: AH, articular head; BCG, bicipital groove; CAP, capitulum; CF, coronoid fossa; HCT, humeral crest; DT, deltoid tuberosity; ECC, epicondylar crest; HGR1, groove one; GR2, groove two; GTC, greater tuberosity convexity; GTS, greater tuberosity summit; IMT, intermediate tubercle; LEC, lateral epicondyle; LTC, lesser tuberosity convexity; LTS, lesser tuberosity summit; MEC, medial epicondyle; NF, nutrient foramen; OF, olecranon fossa; PD, proximal depression; RF, radial fossa; TRO, trochlea. Scale bar = 10 cm.

Ulna

The ulna articulates proximally with the humerus, anteromedially with the radius, and distally with the cuneiform and, in ETMNH 601, the pisiform (Fig. 43). Additional material includes a right ulna (ETMNH 502) and a fragment of a left ulna (ETMNH 8762). The ulnae of ETMNH 609 and ETMNH 601 have been repaired; although, the olecranon process of the right ulna of ETMNH 601 is unassembled but associated. A long olecranon process (OP) with heavy rugosities and numerous foramina resembles those found in cursorial animals, such as horses. A prominent anconeal process (AP) slants laterally at its proximal point, which is marked with a V-shaped depression. This surface has a slight concave curvature and appears to have a loose articulation with the humerus until the radius is articulated.

A broad trochlear notch (TN) slants laterally at its proximal end. Two articular processes extend from the distal trochlear notch; the medial (MAP) of which is wider and longer than the lateral (LAP). ETMNH 609 has a more distinct medial process than ETMNH 601, which has a medial process that appears only to be a flaring of the anconeal process with little definition. A deep, rugose radial notch (RN) is present between the medial and lateral processes of the trochlear notch. An articular surface for the radius (ASR1) extends from the medial edge of the lateral process of the trochlear notch and into the radial notch.

The diaphysis of the ulna is V-shaped in cross section with the point along the posterior surface and a broad anterior surface with its narrowest point at its proximal end and just distal to the radial notch. Distally, as the diaphysis broadens, the lateral side of the anterior diaphysis is more robust than the medial; however, the medial has more rugosity for radial articulation (ARR). After the widest point of the distal end, the diaphysis narrows to form the styloid process, which articulates with the cuneiform and the radius. In distal view, the articular surface

for the cuneiform (ASC) is slanted from anterolateral to posteromedial with a central concavity that extends parallel to the slant of the facet. On the proximomedial surface of the styloid process (SP), a small facet extends along the medial edge of the ulna providing a point of articulation with the radius (ASR2). ETMNH 601 has an additional distal articular surface for the pisiform that may only be present in older individuals or a subsection of this population.

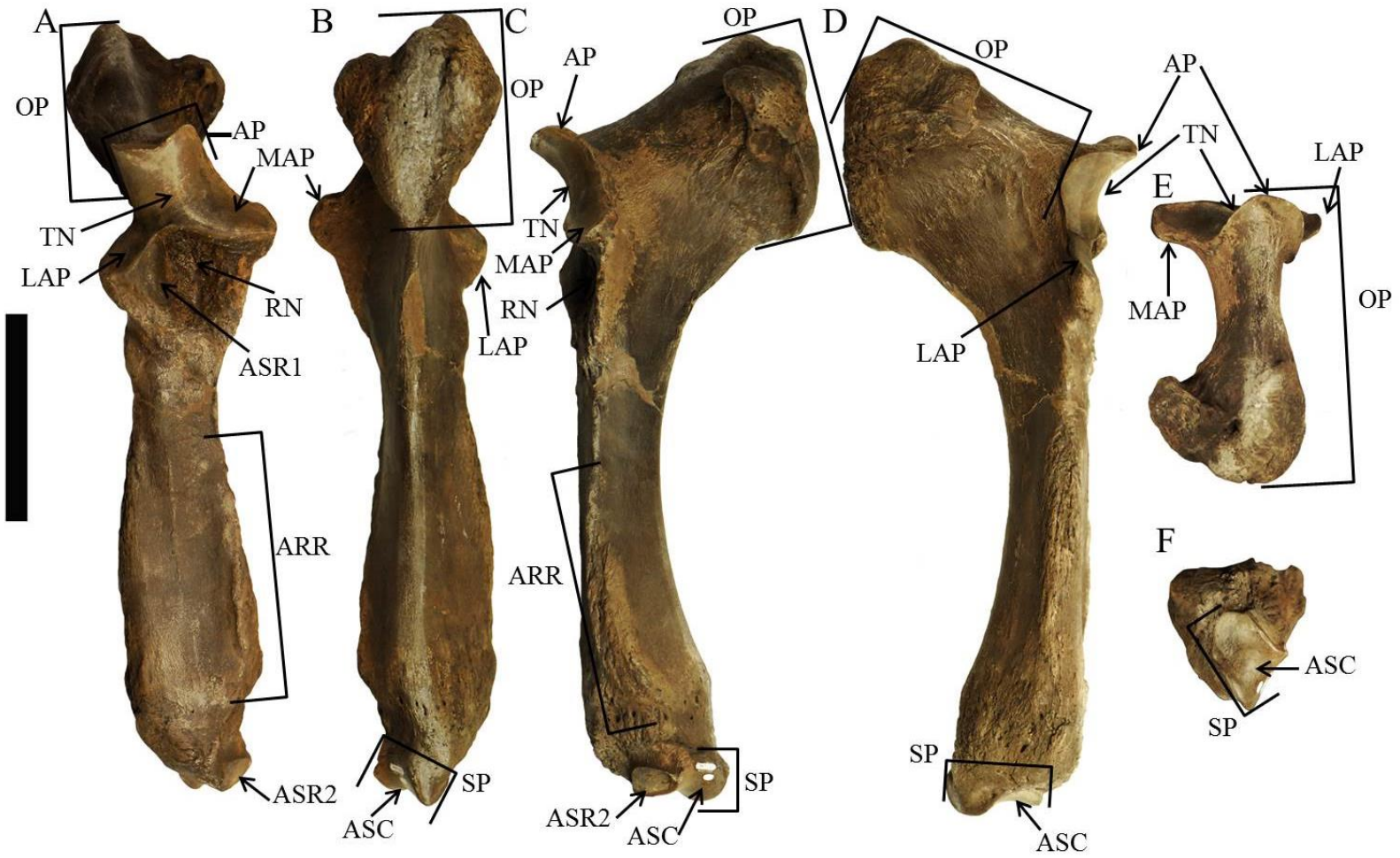

Figure 43. Right ulna of ETMNH 609. Views: A, anterior; B, posterior; C, medial; D, lateral; E, proximal; F, distal. Abbreviations: AP, anconeal process; ARR, articular rugosity for radius; ASC, articular surface for cuneiform; ASR1-2, articular surfaces for radius 1-2; LAP, lateral articular process; MAP, medial articular process; OP, olecranon process; RN, radial notch; SP, styloid process; TN, trochlear notch. Scale bar = 10 cm.

Radius

The radius articulates proximally with the humerus, distally with the scaphoid and lunar, and posterolaterally with the ulna (Fig. 44). At the proximal end, the radius sits in the radial notch of the ulna and curves medially at the distal end so that the radius is directly medial to the styloid process of the ulna. Together, the radius and ulna form a tight articulation with each other and with the humerus to support the graviportal structure of *Teleoceras.* Only the left radius of ETMNH 601 is unbroken; the others have all been repaired. Many foramina are present along the fused epiphyseal regions, especially posteriorly at the proximal end. The neck (NK) of the radius narrows more on the lateral side to form a diaphyseal curve but is only slightly narrowed on the medial side. A radial crest (RCT) extends distomedially along the anterior surface from the proximolateral corner to just distal of midshaft. This crest is more pronounced in ETMNH 601 and possibly becomes more developed through ontogeny

On the proximal end, the coronoid process is a small anteroposterior ridge between the 2 proximal articular surfaces for the capitulum (ASC) and trochlea (AST) of the humerus. This process is offset laterally creating a larger medial articular facet for the trochlea. These 2 proximal facets are slightly depressed but flatten on the medial and lateral edges of the radius. A slight concavity is present along the posterior edges. Also proximally, on the posterior surface, there is a rugose site for attachment to the ulna. A triangular articular surface (ASU1) is on the proximolateral side of the posterior surface and is slightly depressed for articulation with the corresponding facet on the anterior surface of the ulna. On the proximoanterior surface of the radius, there is a radial tuberosity that is rugose but not depressed on the GFS specimens. This feature can form a significant fossa on some *Teleoceras*.

Distally, there is a triangular area of heavy rugosity on the posterolateral surface that fits into the corresponding area of the ulna. No remnant of a styloid process is found on the distal radius. Two small articular facets are along the posterolateral edge for articulation with the ulna. The more posterior of the 2 (ASU2) is ovate and the more lateral (ASU3) is round and posteriorly pinched. Two additional articular surfaces are on the very distal surface and slant from anterolateral to posteromedial. The lateral articular surface (ASL) is smaller and is depressed on the posterior portion for articulation with the lunar and the more rounded medial articular surface (ASS) is depressed on the anterior portion for articulation with the scaphoid. The placement of the depressed areas forms a continuous depression across the slant of the articular surfaces.

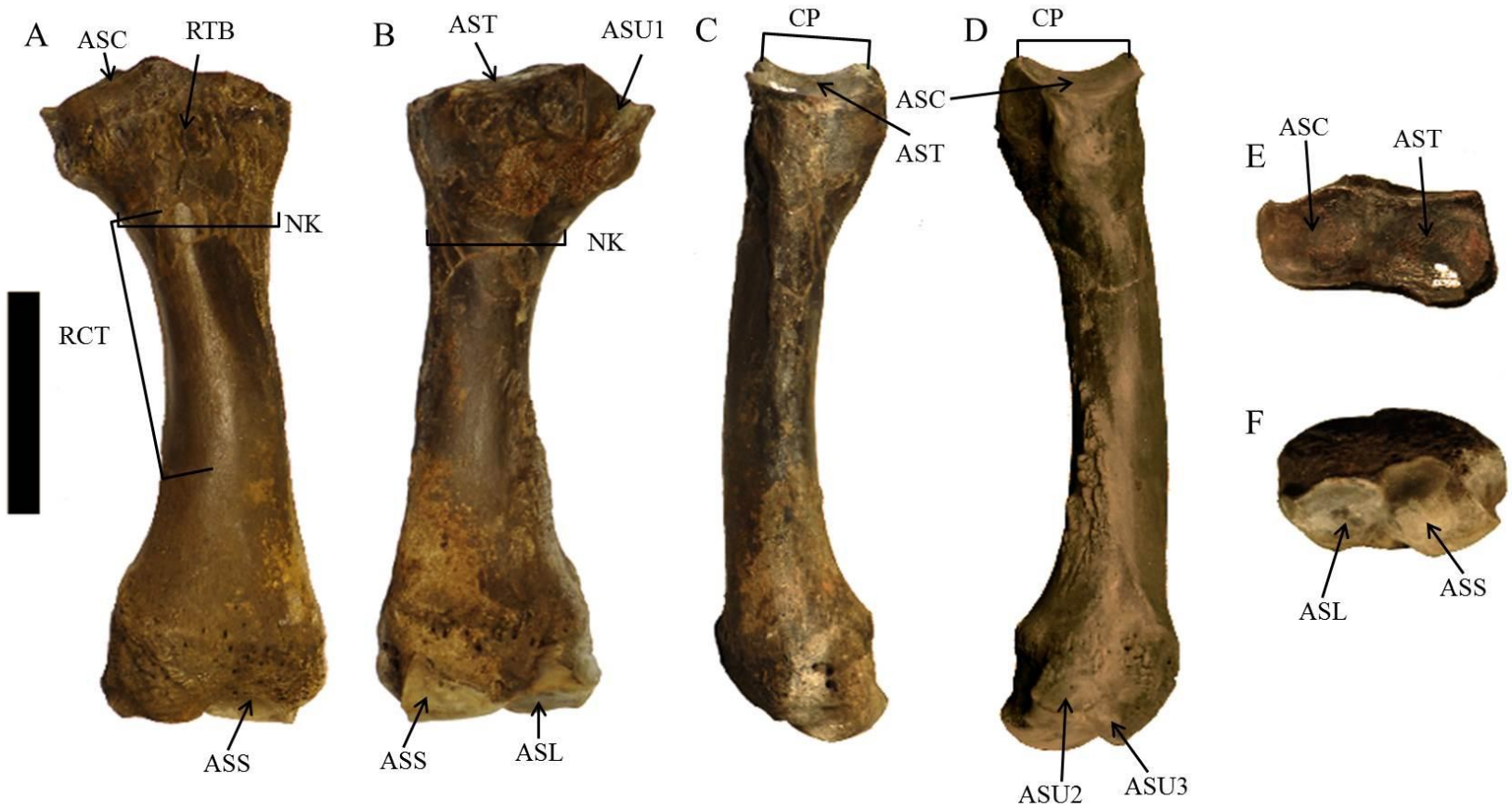

Figure 44. Right radius of ETMNH 609. Views: A, anterior; B, posterior; C, medial; D, lateral; E, proximal; F, distal. Abbreviations: ASU1-3, articular surfaces for the ulna 1-3; ASC, articular surface for the capitulum; ASL, articular surface for the lunar; ASS, articular surface for the scaphoid; AST, articular surface for the trochlea; CP, radial coronoid process; NK, radial neck; RCT, radial crest; RTB, radial tuberosity. Scale bar = 10 cm.

Carpals

Teleoceras has 8 carpals in the manus (Fig. 45). In addition to those from ETMNH 609 and ETMNH 601, there is a carpal fragment (ETMNH 62) that is unassociated with any complete bones. ETMNH 8271 includes elements from an articulated right manus and a few elements from a left manus (Appendix 2). There was nothing else found with these elements and a return to the specific location was unproductive.

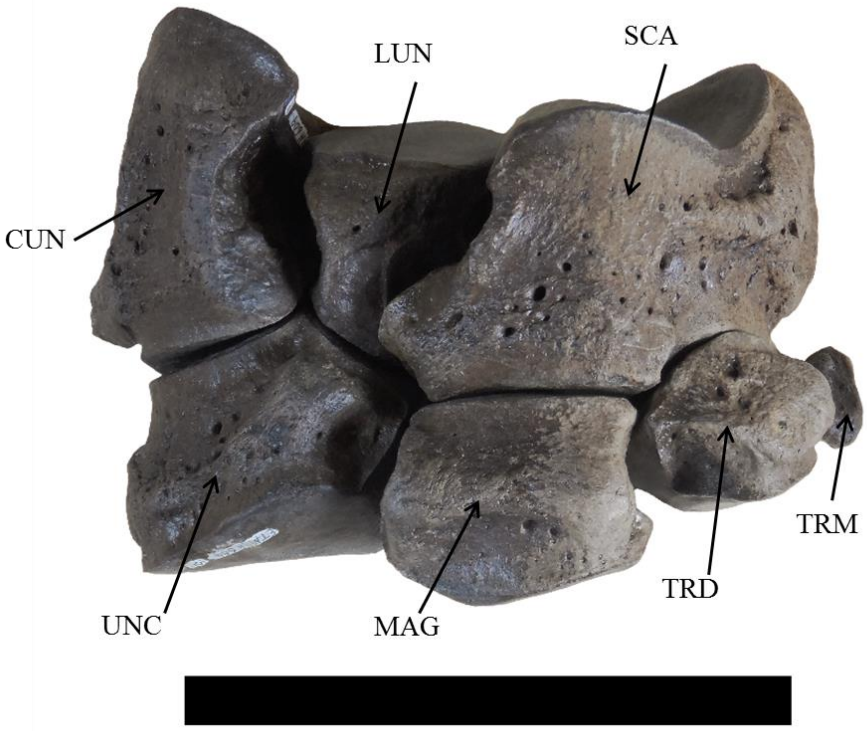

Figure 45. Articulated carpals of ETMNH 609 in anterior view. Abbreviations: CUN, cuneiform; LUN, lunar; MAG, magnum; SCA, scaphoid; TRD, trapezoid; TRM, trapezium; UNC, unciform. The pisiform is not visible in this view. Scale bar = 10 cm.

Scaphoid. The scaphoid articulates proximally with the radius, distally with the magnum and trapezoid, and laterally with the lunar (Fig. 46). This is the largest of the carpal bones. Both scaphoids of both skeletons are present and complete. The scaphoid is longest along the

mediolateral axis and is narrowest along the anteroposterior axis, except for a single posterior process (PP). Foramina are present on each surface that is not articular, especially the anterior and medial, which is also rugose. The proximal articular surface for the radius (ASR) is a concave rounded triangle with the lateral and medial points raised proximally. On ETMNH 601, the medial corner folds over the raised point unlike on ETMNH 609. Where the lateral corner is raised, it forms a lateral edge with an anteroproximal articular surface for the lunar (ASL1) that is anteriorly round and posteriorly pinched.

Posterior to the radial facet is the rugose posterior process with a second, round articular surface for the lunar (ASL2) on the lateral side. On the posterior side of the lateral extension, there is a third, round articular surface for the lunar (ASL3). This facet folds over into the triangular laterodistal articular surface for the magnum (ASM). A raised ridge is formed by this laterodistal facet and the mediodistal facet. The mediodistal articular surface for the trapezoid (AST) is saddled over the distal surface and extends on both the anterior and posterior surfaces.

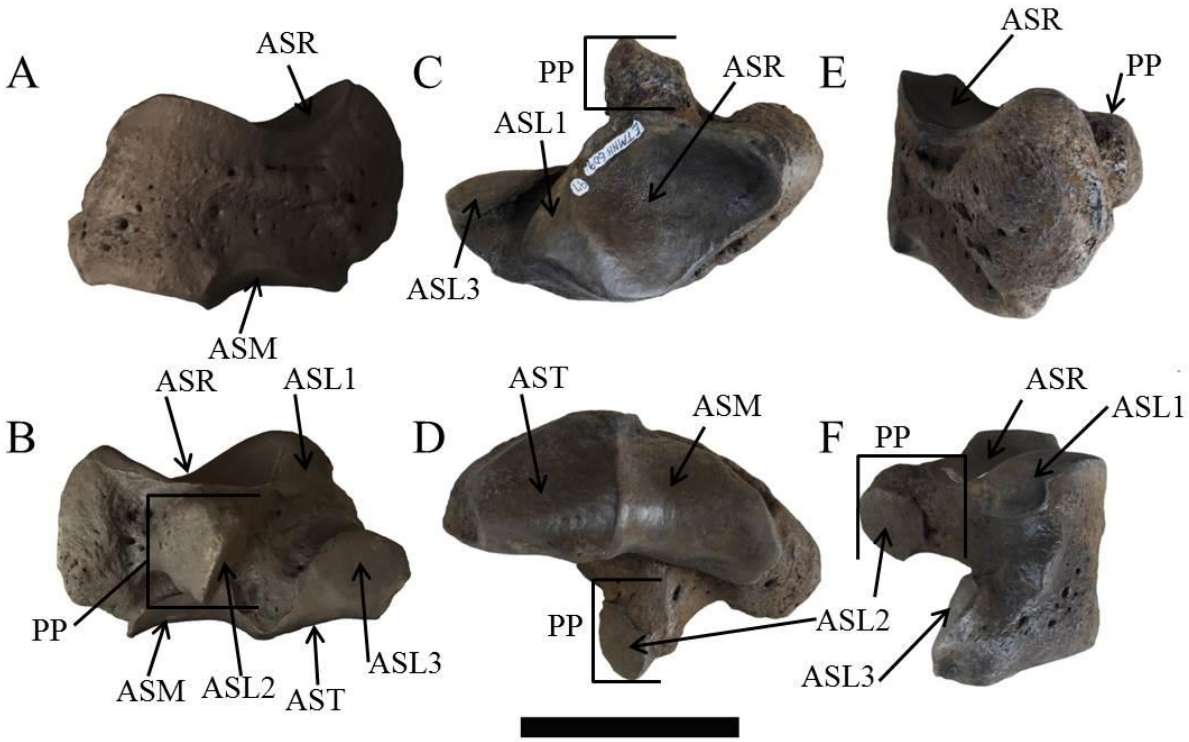

Figure 46. Right scaphoid of ETMNH 609. Views: A, anterior; B, posterior; C, proximal; D, distal; E, medial; F, lateral. Abbreviations: ASL1-3, articular surfaces for lunar 1-3; ASM, articular surface for magnum; ASR, articular surface for radius; AST, articular surface for trapezoid; PP, posterior process. Scale bar = 5 cm.

Lunar. The lunar articulates proximally with the radius, distally with the unciform and magnum, medially with the scaphoid, and laterally with the cuneiform (Fig. 47). Only the right lunar of ETMNH 609 is intact, while the others have been repaired. Overall, the lunar is anteroposteriorly elongate and mediolaterally narrow. Areas between the articular surfaces are rugose and contain foramina. The anterior two-thirds of the lunar contain most of the articular surfaces as the posterior one-third forms a rugose process (LP), which resembles the unciform process. On the proximomedial side of the process, there is an articular surface that is 1 of the

lunar's 3 points of articulation with the scaphoid (ASS1). On ETMNH 601, this proximomedial articular surface is merged with the proximal articular surface.

Proximally, the lunar has a large, hexagonal articular surface for articulation with the radius (ASR). This surface is a saddled facet with the high point positioned just posterior to the anteroposterior midline. The posterior portion of this articular surface slopes distally onto the lunar process while the anterior portion slopes along the anterior edge. Distally, the lunar has 2 concave articular surfaces joined at a slightly elevated ridge. The medial facet is a small tear-drop situated more posteriorly that articulates with the magnum (ASM). The lateral facet is posteriorly square, anteriorly flared, and articulates with the unciform (ASU).

On the medial side, there are 2 articular surfaces, which complete the trio of articular surfaces for the scaphoid. The proximal of these 2 (ASS2) is elongate anteroposteriorly and its proximal edge is adjacent to the proximal articular surface. The distal of these 2 (ASS3) is proximally domed and distally square. On the lateral side, there are also 2 articular surfaces; both of which articulate with the cuneiform. Like on the medial side, the proximal of these 2 (ASC1) is oval and its proximal edge is adjacent to the proximal articular surface. The distal of these 2 (ASC2) is thin and oblong with the distal edge adjacent to the distal articular surface. Because of the position of these articular surfaces, when the carpals are articulated, small gaps are present between the lunar and the cuneiform and between the lunar and the scaphoid.

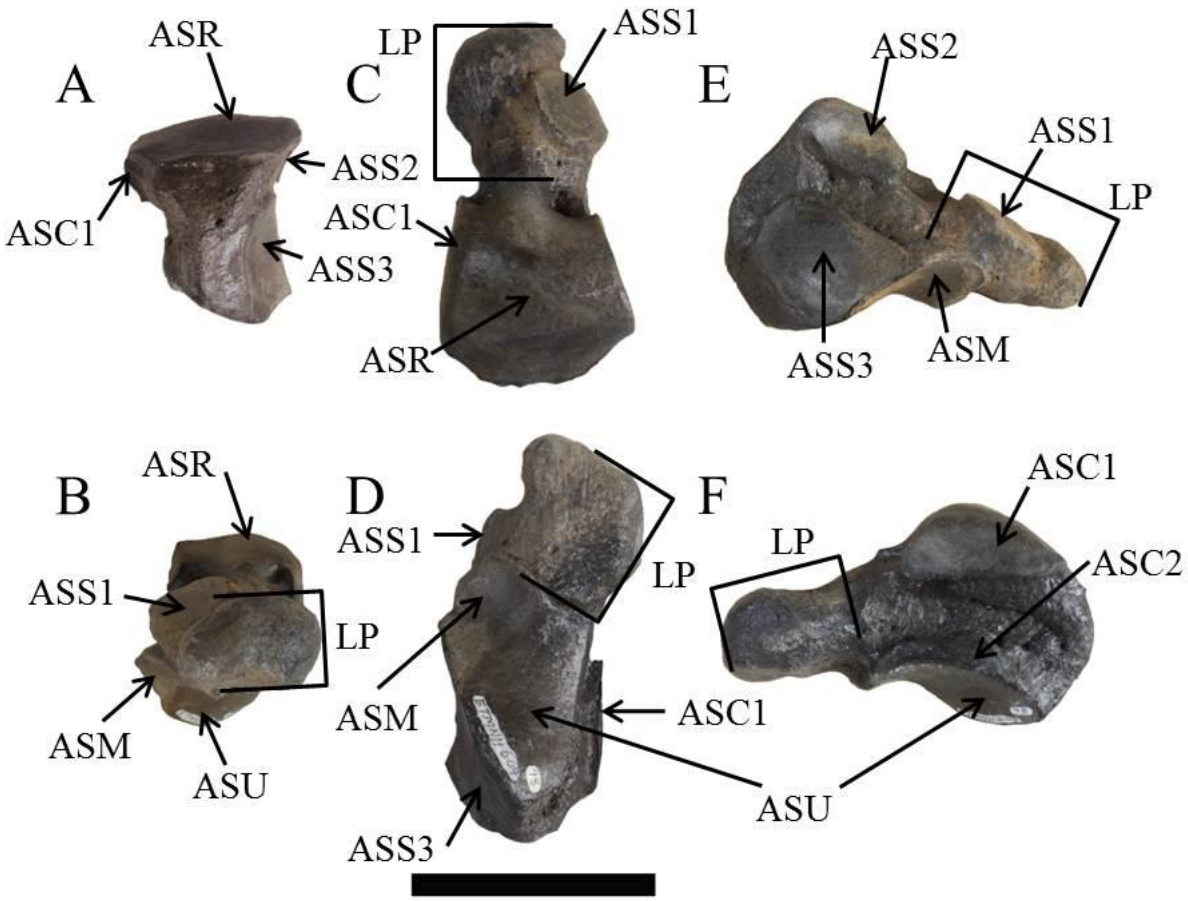

Figure 47. Right lunar of ETMNH 609. Views: A, anterior; B, posterior; C, proximal; D, distal; E, medial; F, lateral. Abbreviations: ASC1-2, articular surfaces for cuneiform 1-2; ASM, articular surface for magnum; ASR, articular surface for radius; ASS1-3, articular surfaces for scaphoid 1-3; ASU, articular surface for unciform; LP, lunar process. Scale bar = 5 cm.

Cuneiform. The cuneiform articulates proximally with the ulna, distally with the unciform, medially with the lunar, and posteriorly with the pisiform (Fig. 48). The proximodistal and anteroposterior axes are long, while the mediolateral axis is short. All surfaces except those for articulation are rugose and foramina are numerous. There is a large rugosity extending anteroposteriorly on the distal portion of the lateral side. Medially, the cuneiform is slightly concave so that there is a gap between the cuneiform and the more medial lunar.

A proximal articular surface is saddle-like for articulation with the styloid process of the ulna (ASUL). This is especially obvious on the lateral side where the articular surface curves distally. The medial side does not continue distally but terminates at a ridge with a rectangular articular surface for the lunar (ASL1) on the medial side of the cuneiform. A square articular surface with a rounded anterolateral corner is present on the distal end of the cuneiform for articulation with the unciform (ASUN). On ETMNH 601, this articular surface is more depressed than is seen on ETMNH 609. Medially, this ulnar articular surface folds proximally onto the medial surface creating a small, domed articulation. This medial articular surface also articulates with the lunar (ASL2). Articulation between the cuneiform and the lunar is loose to allow some degree of mobility within the wrist. On the posterior side, an oblong articular surface is present and forms a lateral ridge as it joins the lateral portion of the proximal articular surface. This posterior surface provides the only articulation site with the pisiform (ASP).

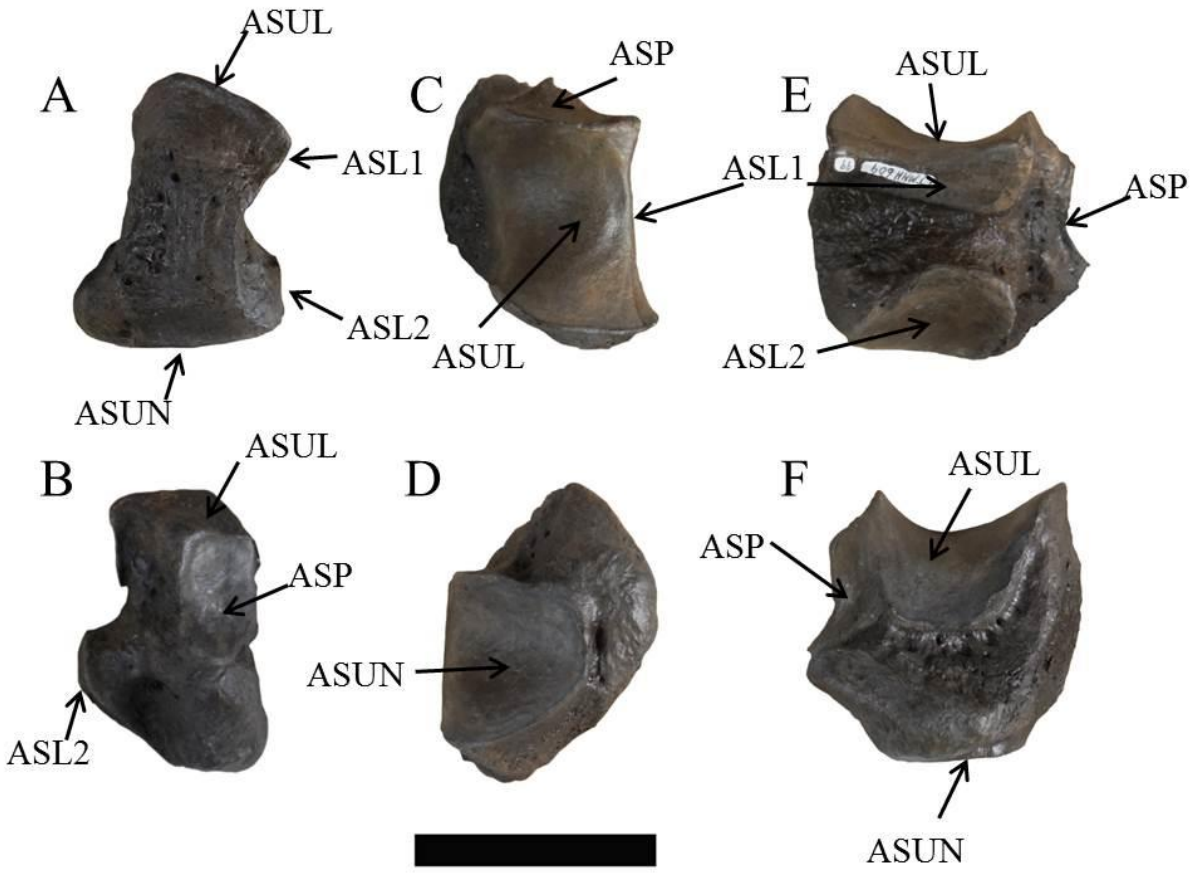

Figure 48. Right cuneiform of ETMNH 609. Views: A, anterior; B, posterior; C, proximal; D, distal; E, medial; F, lateral. Abbreviations: ASL1-2, articular surfaces for lunar 1-2; ASP, articular surface for pisiform; ASUL, articular surface for ulna; ASUN, articular surface for unciform. Scale bar = 5 cm.

Pisiform. The large, rugose pisiform articulates anteriorly with the cuneiform and, on ETMNH 601, proximally with the ulna (Fig. 49). An articular anterior surface for the cuneiform (ASC) is round proximally and square distally. Because the pisiform curves medially and flares at the posterior end, in proximal view, it appears to be pinched mediolaterally. ETMNH 601 has an extra small round anterolateral articular surface for the ulna.

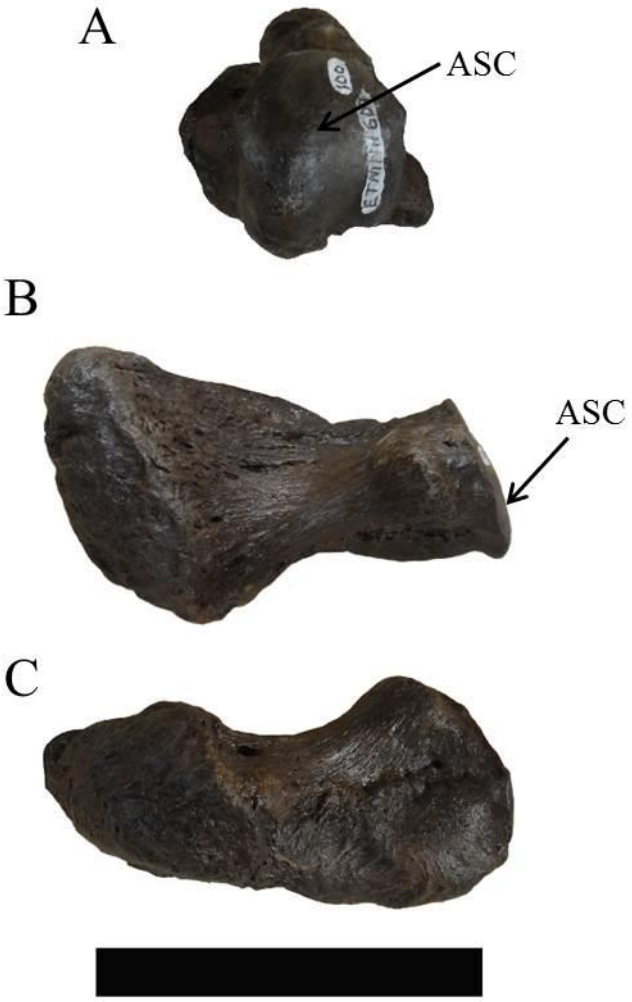

Figure 49. Right pisiform of ETMNH 609. Views: A, anterior; B, dorsal; C, lateral. Abbreviations: ASC, articular surface for cuneiform. Scale bar = 5 cm.

Trapezium. The trapezium articulates laterally with the trapezoid (Fig. 50). Along with those of the 2 skeletons, an isolated trapezium is also in collections (ETMNH 13236). This is a small, rugose bone with a 'V'-shaped rugosity pointed distally. An oval articular surface for the trapezoid (AST) is present on the lateral side.

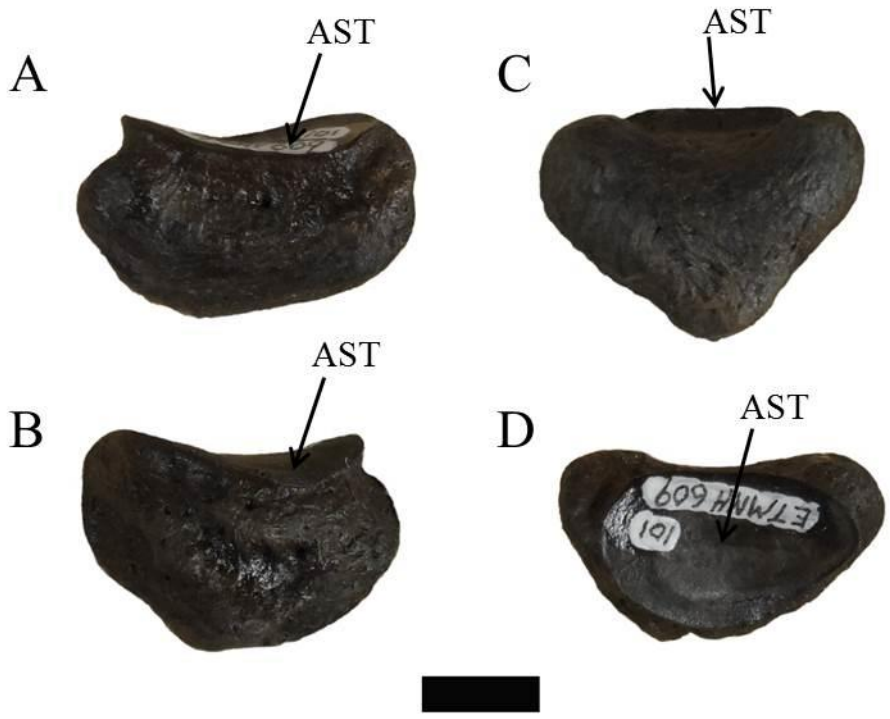

Figure 50. Right trapezium of ETMNH 609. Views: A, proximal; B, distal; C, medial; D, lateral. Abbreviation: AST, articular surface for trapezoid. Scale bar = 1 cm.

Trapezoid. The trapezoid articulates proximally with the scaphoid, distally with the second metacarpal, laterally with the magnum, and medially with the trapezium (Fig. 51). All of the trapezoids are in good condition. This is a cubed bone that is short proximodistally but is of equal length anteroposteriorly and mediolaterally. Foramina are present on the anterior and posterior surfaces and articular surfaces are present on the proximal, distal, medial, and lateral surfaces. On the anterior surface, a rugose prominence is raised but is more pronounced on ETMNH 601. The proximal articular surface for the scaphoid (ASS) is square with a convexly rounded medial edge and is depressed mediolaterally. At the posteromedial corner of this facet, it forms a ridge with a round medial articular surface for the trapezium (AST). Distally, the

trapezium articular surface folds laterally in to the convexly ovate distal articular surface for the second metacarpal (ASMC2). Laterally, this distal articular surface for the magnum (ASM) forms an edge with the lateral kidney-shaped articular surface.

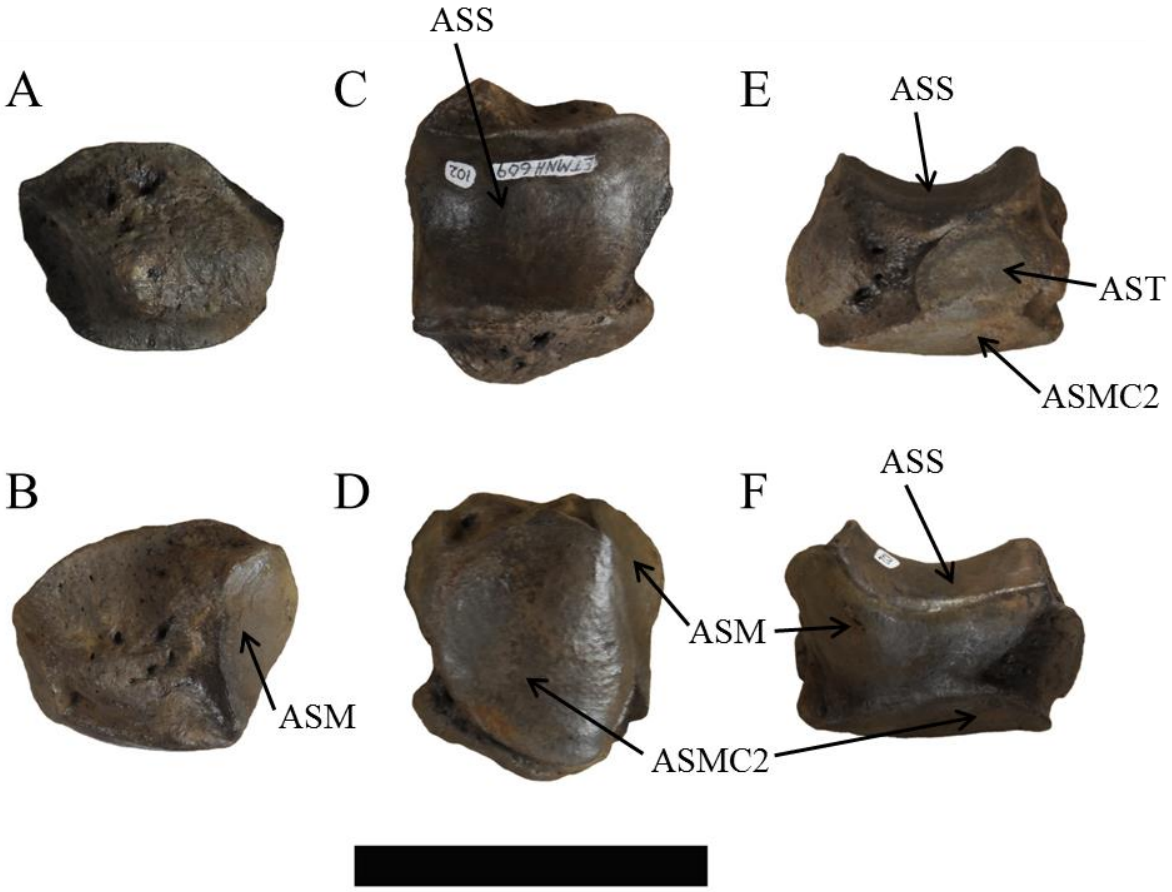

Figure 51. Right trapezoid of ETMNH 609. Views: A, anterior; B, posterior; C, proximal; D, distal; E, medial; F, lateral. Abbreviations: ASM, articular surface for magnum; ASMC2, articular surface for second metacarpal; ASS, articular surface for scaphoid; AST, articular surface for trapezium. Scale bar = 5 cm.

Magnum. The magnum articulates proximally with the lunar and scaphoid, distally with the second and third metacarpals, medially with the unciform, and laterally with the trapezoid. Both magnums are present and complete in both skeletons (Fig. 52) and there is an isolated left

magnum in the collections (ETMNH 8516). None of the magnums have a posterior process resembling those discussed by Harrison and Manning (1983). Anteriorly, the magnum has a transverse rugosity across the surface. Posteriorly, the magnum extends more proximally than the anterior portion because of a raised articular surface. The magnum is narrower mediolaterally than anteroposteriorly. Anteroproximally, there is an articular surface for the scaphoid (ASS) that is triangular with an anterior straight edge and posterior point that is laterally raised. This raised portion forms a ridge with the posteroproximal articular surface. For articulation with the lunar (ASL), this posteroproximal articular surface resembles a tear-drop with the anterior point oriented along the lateral edge of the anteroproximal facet and the posterior portion saddled over a proximally raised process.

On the medial surface, there is a kidney-shaped articular surface that forms an edge with the anteroproximal facet. This articular surface for the trapezoid (AST) is wider at the posterior end and narrows anteriorly. Along its distal edge, this articular surface contacts a small, rectangular articular surface for the second metacarpal (ASMC2). One articular surface for the third metacarpal (ASMC3) covers most of the distal surface of the magnum. Posteriorly, this articular surface extends along a small distal process that mirrors the proximal process. This facet is slightly curved anteriorly and has a straight medial edge that forms an edge with the second metacarpal facet. On the lateral side, there is another kidney-shaped articular surface for the unciform (ASU).

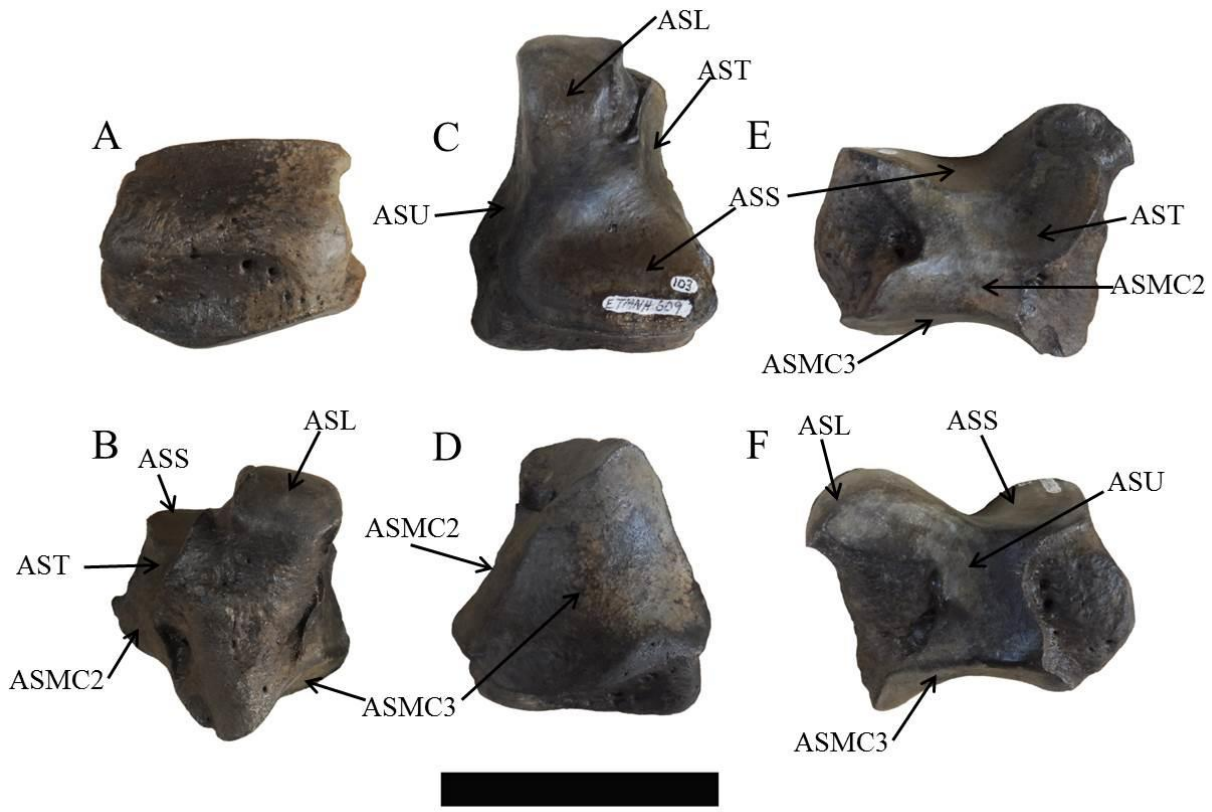

Figure 52. Right magnum of ETMNH 609. Views: A, anterior; B, posterior; c, proximal; D, distal; E, medial; F, lateral. Abbreviations: ASL, articular surface for lunar; ASMC2-3, articular surfaces for second and third metacarpals; ASS, articular surface for scaphoid; AST, articular surface for trapezoid; ASU, articular surface for unciform. Scale bar = 5 cm.

Unciform. The unciform articulates proximally with the cuneiform, distally with the third and fourth metacarpal, and medially with the magnum and lunar (Fig. 53). On ETMNH 601, the unciform also articulates distally with the fifth metacarpal. All of the articular surfaces are on the anterior portion of the unciform and, distolaterally curving; a rugose process makes up the posterior portion of the unciform. This process can be variable within a population as demonstrated by Harrison and Manning (1983) but is consistent within the limited sample from GFS. Two articular surfaces meet at a ridge on the proximal side of the anterior portion. The

proximolateral articular surface for the cuneiform (ASC) is slightly saddled anteroposteriorly and comes to a rounded point on the lateral side. A round articular surface for the lunar (ASL) that is longer anteroposteriorly is present on the proximomedial side. A second medial articular surface (ASM) is distal to the lunar facet and is ‘C’-shaped for articulation with the magnum.

On the distal surface, articular facets for the third, fourth, and, on ETMNH 601, fifth metacarpals are present. The more medial third metacarpal and the lateral fourth metacarpal share the articular surface (ASMC3-4) without a dividing ridge; however, there is an indicative line formed by wear. Overall, the articular surface is triangular with an indentation on the lateral edge and a small convexity along the medial edge near where it contacts the medial articular surface for the magnum (ASM). On ETMNH 609, this lateral indentation articulates with a proximal expansion on the fourth metacarpal; however, on ETMNH 601, it articulates with the reduced fifth metacarpal.

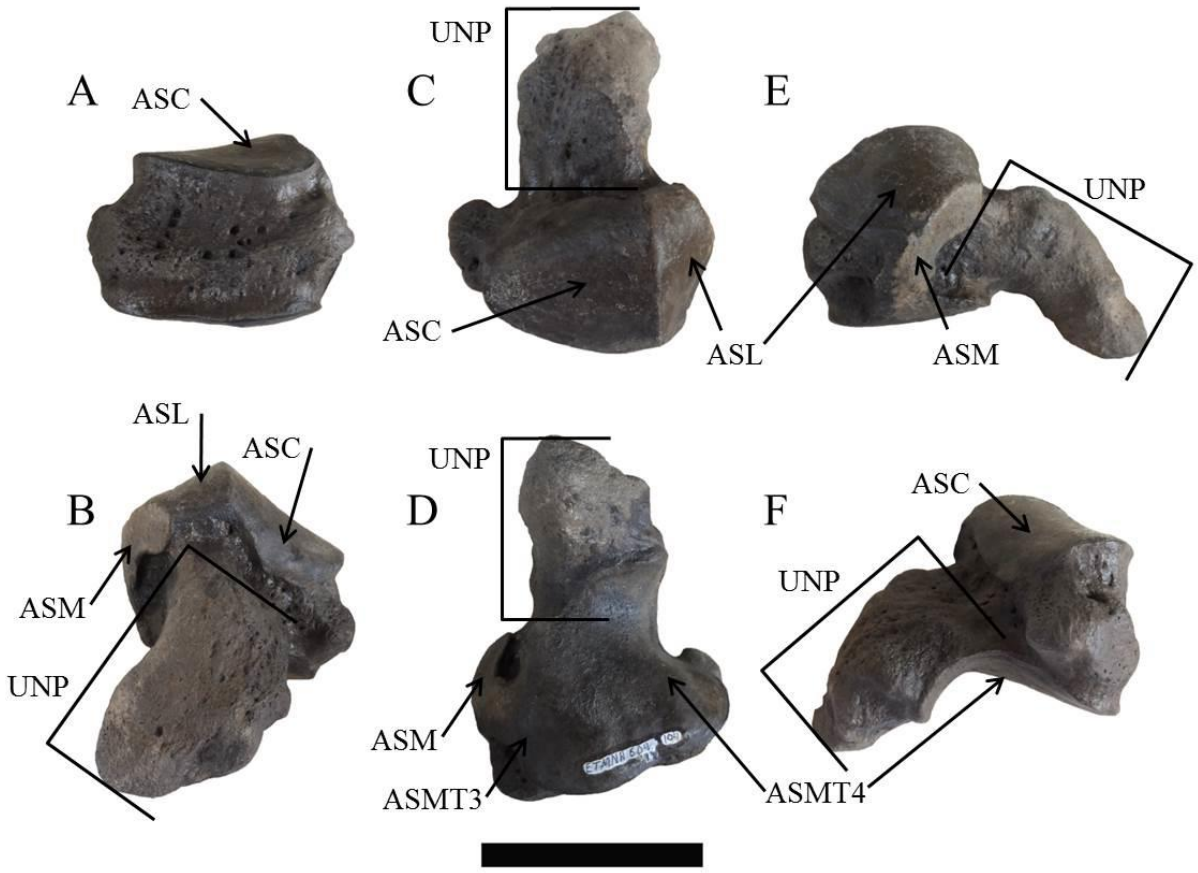

Figure 53. Right unciform of ETMNH 609. Views: A, anterior; B, posterior; C, proximal; D, distal; E, medial; F, lateral. Abbreviations: ASC, articular surface for cuneiform; ASL, articular surface for lunar; ASM, articular surface for magnum; ASMC3-4, articular surfaces for third and fourth metacarpals; UNP, unciform process. Scale bar = 5 cm.

Metacarpals

In each manus, ETMNH 609 has 3 metacarpals—the second, third, and fourth—while ETMNH 601 has 4—the typical 3 and a reduced fifth metacarpal. There is a distal metapodial fragment that may be a metacarpal but that cannot be confidently identified (ETMNH 565). Again, ETMNH 8271 includes metacarpal elements from an articulated right manus and a few elements from a left manus.

Second Metacarpal. The second metacarpal articulates proximally with the magnum and trapezoid, distally with the proximal phalanx of the second digit and 2 sesamoids, and laterally with the third metacarpal (Fig. 54). Most of the second metacarpals are in fairly good condition. Foramina and rugosities are along the epiphyseal areas, though all of the metapodials are completely fused. Both medial and lateral edges are slightly curved inward, the medial side appears as if it was pinched anteroposteriorly, and a large rugosity is on the distal end of the lateral side. There is a slight posterior ridge (PR) just medial to the midline of the bone that extends from proximal to distal and, at the posterodistal facets, matches with the intermediate relief (IR). On ETMNH 601, this ridge is more pronounced and is bordered by deeper depressions.

On the proximal end, there are 3 articular surfaces. A roughly square medial articular surface for the trapezoid (AST) is the largest and has a slight depression in the middle. The lateral edge of this facet is raised to form a ridge with the rectangular proximomedial articular surface for the magnum (ASM), which slopes distally and laterally from the ridge. At the distal edge, this facet folds into the lateral-most articular surface of the proximal end. This lateral articular surface for the third metacarpal (ASMC3) is rectangular. At the distal end, the anterior articular surface for the proximal phalanx (ASPP2) is smooth and, though the lateral edge is parallel to the axis of the bone, the medial edge curves laterally creating a half-dome shape. On the posterior articular surface, 2 facets are separated by the intermediate relief. Both facets are oval with slight depressions along their midlines, are slanted from proximomedial to distolateral, and each articulates with 1 sesamoid (ASS1-2). The outer edges of the condyles are slightly rounded but this is variable.

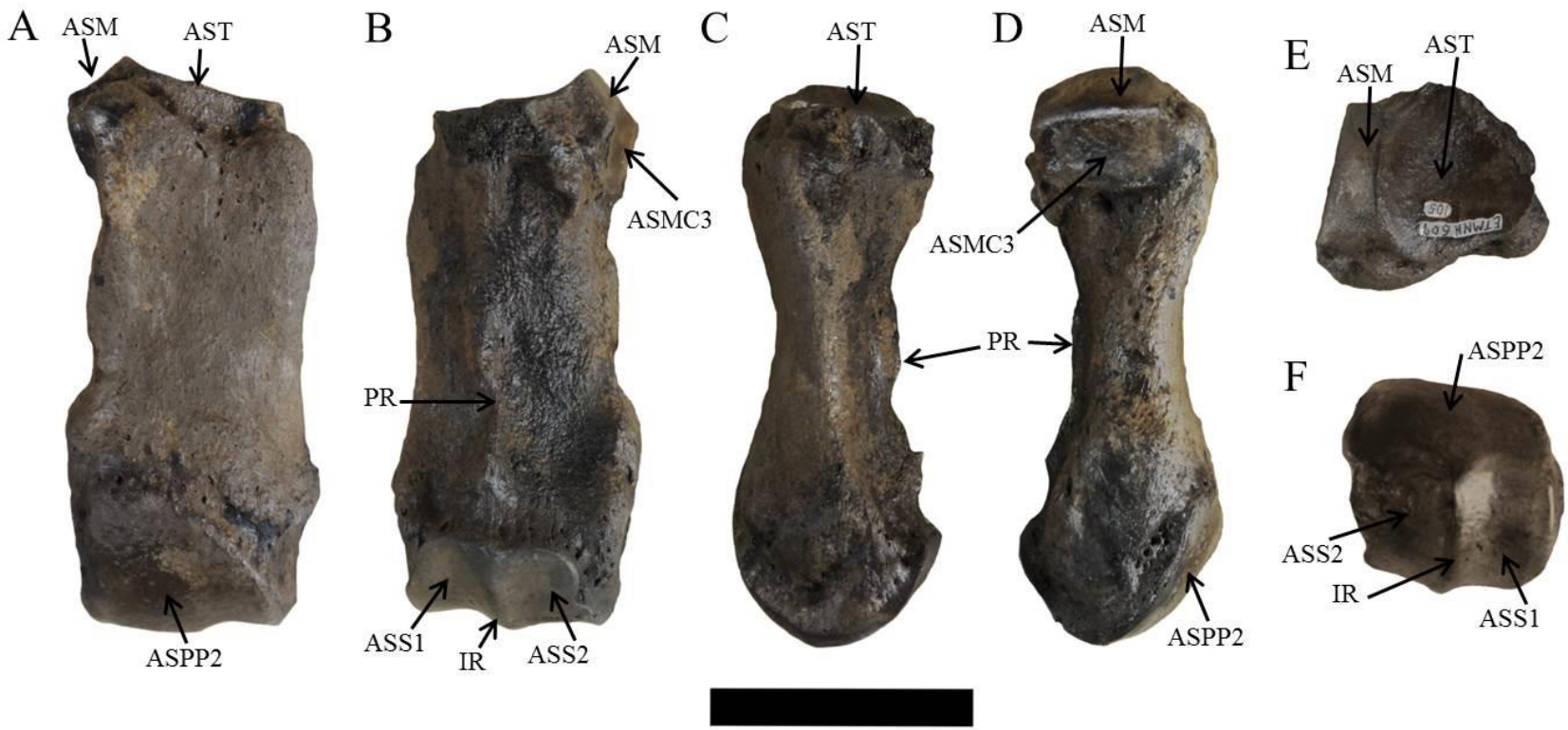

Figure 54. Right second metacarpal of ETMNH 609. Views: A, anterior; B, posterior; C, medial; D, lateral; E, proximal; F, distal. Abbreviations: ASM, articular surface for magnum; ASMC3, articular surface for third metacarpal; ASPP2, articular surface for proximal phalanx of the second digit; ASS1-2, articular surfaces for sesamoids 1-2; AST, articular surface for trapezoid; IR, intermediate relief; PR, posterior ridge. Scale bar = 5 cm.

Third Metacarpal. The third metacarpal articulates proximally with the unciform and magnum, distally with the proximal phalanx of the third metacarpal and 2 sesamoids, medially with the second metacarpal, and laterally with the fourth metacarpal (Fig. 55). Only the left third metacarpal of ETMNH 601 is undamaged and without repair. Foramina are concentrated along the epiphyseal regions, which are completely fused. As with the second metacarpals, the third metacarpals curve slightly inward along the medial side but more so on the lateral side. On the anterior surface of the proximal end, there are 2 rugose knobs that serve as sites of muscle attachment. Similar rugosities are on the posterior surface as well. In posterior view, a nutrient foramen (NF) is present at the midpoint of the diaphysis; though, this is barely visible on ETMNH 601, possibly because of increased ossification due to age. Also on the posterior surface and proximal to the distal articular surfaces, a posterior ridge (PR) similar to that of the second metacarpal separates a pair of depressions.

Proximally, there are 4 articular surfaces. On the medial and lateral sides of the bone, there are rectangular articular surfaces for the second (ASMC2) and fourth (ASMC4) metacarpals, respectively. An articular surface for the (ASM) is on the medial side of the proximal end and has a concavity at the narrow posterior end. This articular surface is squarer in ETMNH 601 than the triangular shape seen in ETMNH 609. The lateral proximal articular surface for the unciform (ASU) is medially domed with a straight lateral edge and a pinched posterior point. Distally, the anterior articular surface for the proximal phalanx of the third digit (ASPP3) is smooth and domed proximally. Posteriorly, an intermediate relief (IR) divides the distal articular surface into 2 facets for articulation with the 2 sesamoids (ASS1-2). Though the facets are anteroposteriorly oval with slight depressions in the middle, the edges are not smooth and can be variable.

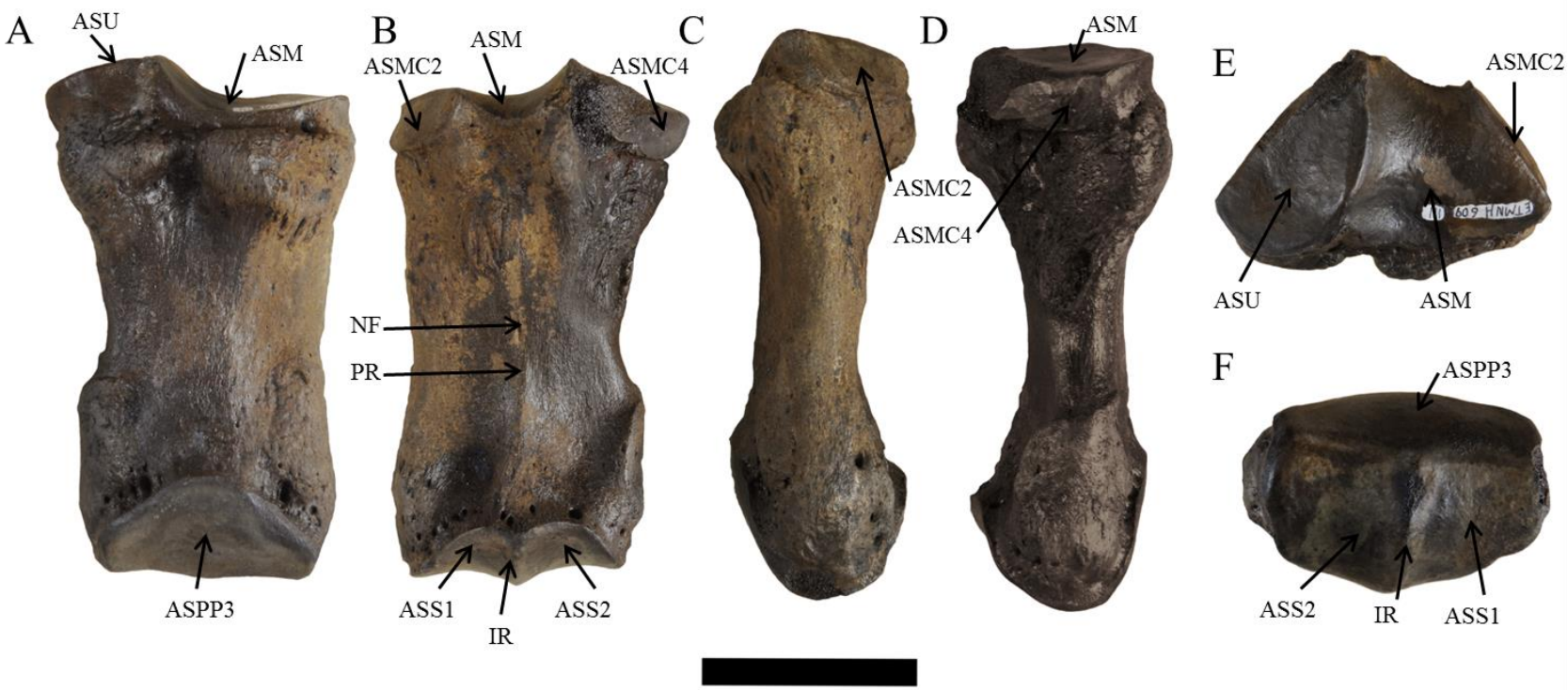

Figure 55. Right third metacarpal of ETMNH 609. Views: A, anterior; B, posterior; C, medial; D, lateral; E, proximal; F, distal. Abbreviations: ASM, articular surface for magnum; ASMC2, articular surface for second metacarpal; ASMC4, articular surface for fourth metacarpal; ASPP3, articular surface for proximal phalanx of third digit; ASS1-2; articular surface for sesamoids 1-2; ASU, articular surface for unciform; IR, intermediate relief; NF, nutrient foramen; PR, posterior ridge. Scale bar = 5 cm.

Fourth Metacarpal. The fourth metacarpal articulates proximally with the unciform, distally with the proximal phalanx and 2 sesamoids, medially with the third metacarpal, and, on ETMNH 601, laterally with the fifth metacarpal (Fig. 56). Only the right fourth metacarpal of ETMNH 609 has damage and it has not been repaired. Along the diaphysis, the narrower lateral side is curved more inward than the rugose medial side. As with all of the metacarpals, foramina and rugosities are along the epiphyseal lines, which are completely fused. However, there are very few foramina on the posterior surface. Both the proximal and the distal ends curve further posteriorly than the diaphyseal area giving the appearance that the midsection is depressed.

Two articular surfaces are on the proximal end of the fourth metacarpal. Medially, there is a rectangular articular surface for the third metacarpal (ASMC3). The proximal edge of this facet forms a ridge with the medial edge of the proximal articular surface. This proximal articular surface for the unciform (ASU) is the larger of the 2 and is indented along the lateral edge. Posteriorly, it folds over a raised portion that forms a tight articulation with the unciform. On ETMNH 601, there is an articular notch lateral to this facet where the fifth metacarpal articulates; however, on ETMNH 609, there is a knob of bone in place of the notch that represents the remnant of the fifth metacarpal (RMC5), which has fused to the fourth metacarpal. At the distal end, the anterior articular surface for the proximal phalanx (ASPP4) is smooth and proximally domed with only a slight lateral curvature. Two facets are on the posterior surface and are separated by an intermediate relief (IR) that slants from proximolateral to distomedial creating slanted facets for articulation with the 2 sesamoids (ASS1-2).

Figure 56. Right fourth metacarpal of ETMNH 609. Views: A, anterior; B, posterior; C, medial; D, lateral; E, proximal; F, distal. Abbreviations: ASMC3, articular surface for third metacarpal; ASPP4, articular surface for proximal phalanx of fourth digit; ASS1-2, articular surfaces for sesamoids 1-2; ASU, articular surface for unciform; IR, intermediate relief; RMC5, remnant of fifth metacarpal. Scale bar = 5 cm.

Fifth Metacarpal. Each manus of ETMNH 601 has a fifth metacarpal that was described as a "small vestigial nubbin" by Wallace (2006) (Fig. 57). A proximal articular surface for the unciform (ASU) has a posterior convex fold. There is a medial rugosity (MR) that articulates with a proximolateral depression on the fourth metacarpal. On ETMNH 609, the fourth metacarpals have expanded lateral knobs, which are believed to be the remnants of the fifth metacarpals. Unfortunately, the GFS sample size is too small to know which the typical condition is.

Figure 57. Right fifth metacarpal of ETMNH 601. Views: A, anterolateral showing articulation with fourth metacarpal; B, dorsal; C, medial; D, lateral. Abbreviations: ASU, articular surface for unciform; MC4, fourth metacarpal; MR, medial rugosity. Scale bar = 5 cm.

Phalanges

Phalanges and sesamoids of the manus and pes are virtually indistinguishable, so only those of the manus will be described here and a short note will be made in the pes section. Typical of *Teleoceras*, the phalanges are compressed so the second and fourth digits are longer than the third to support the digitigrade splay of the manus and pes. The shape of the proximal and distal articular surfaces varies between and within individuals. Additionally, ETMNH 8271 includes elements from an articulated right manus and a few elements from a left manus.

Proximal Phalanges. Proximal phalanges articulate with the anterior facets of the distal metacarpals and the medial phalanges (Fig. 58). Additional proximal phalanges have been found at GFS, including complete (ETMNH 3755, ETMNH 12450) and fragmented (ETMNH 769). The phalanges of the second and fourth digits are nearly mirror images of each other and are blocky with heavy rugosities on the non-articular surfaces. Distally, these phalanges slope anteriorly so that the posterior edge is more proximal. Proximal articular surfaces vary between round and square and distal articular surfaces are ovate with a small concavity in the center. Between these 2 proximal phalanges, the proximal phalanx of the third digit is more compressed anteroposteriorly but is wider mediolaterally. The ovate proximal articular surface has a domed anterior edge and a straight posterior edge. This facet is larger than the distal articular surface, which is also ovate. All non-articular surfaces are covered with rugosities.

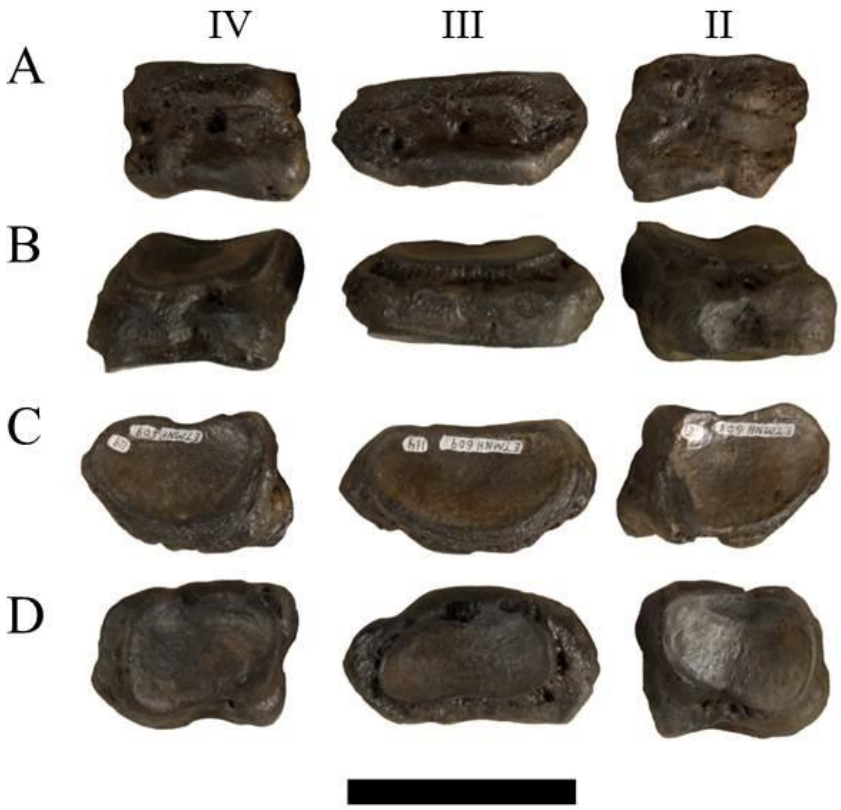

Figure 58. Proximal phalanges of the right manus of ETMNH 609. Views: A, anterior; B, posterior. Abbreviations: II, second digit; III, third digit; IV, fourth digit. Scale bar = 5 cm.

Medial Phalanges. Medial phalanges articulate with the proximal phalanges and the distal phalanges (Fig. 59). In addition to those of the complete skeletons, there is 1 isolated medial phalanx of the third digit (ETMNH 564) and some fragments of a second medial phalanx (ETMNH 269). These are much more compressed than the proximal phalanges. However, like with the proximal phalanges, the medial phalanges of the second and fourth digits are nearly mirror images of each other. In anterior view, these phalanges are domed proximally. Trapezoidal articular surfaces slope from anterolateral to posteromedial on the proximal surfaces. The distal articular surfaces are saddled anterior to posterior and just barely curve over the

anterior edges. The medial phalanx of the third digit is even more compressed than those of the second and fourth digits. The proximal articular surface is ovate with a domed anterior edge and the distal articular surface curves over both anterior and posterior surfaces. All medial phalanges have rugosities present on every non-articular surface.

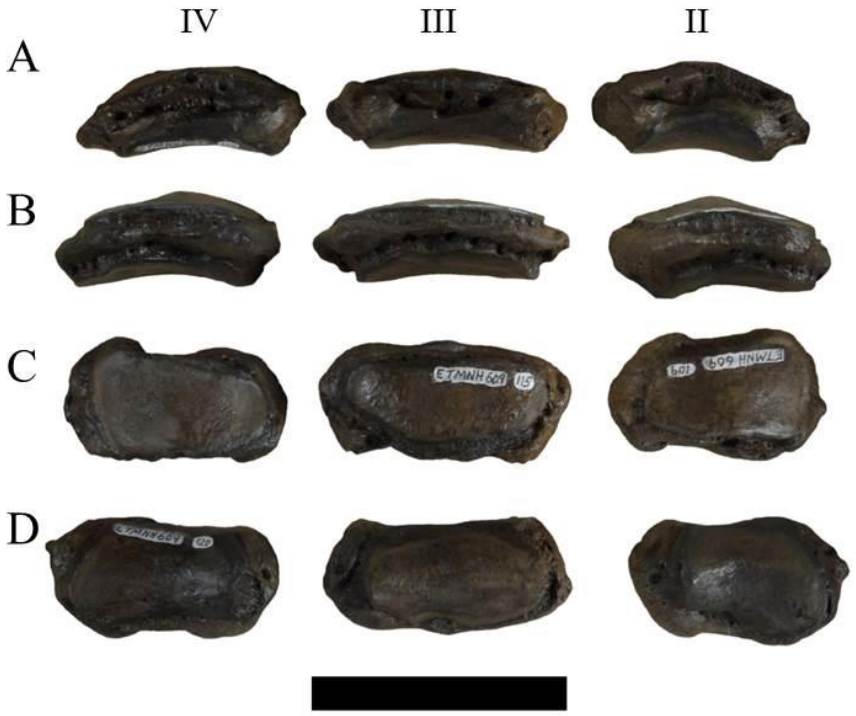

Figure 59. Medial phalanges of the right manus of ETMNH 609. Views: A, anterior; B, posterior. Abbreviations: II, second digit; III, third digit; IV, fourth digit. Scale bar = 5 cm.

Distal Phalanges. Distal phalanges articulate only with the medial phalanges (Fig. 60). Isolated distal phalanges, both complete and fragmentary, are also present in collections (ETMNH 80, ETMNH 107, ETMNH 712, ETMNH 713, ETMNH 743, ETMNH 5233, and ETMNH 11651). All of the phalanges are rugose and porous to allow blood vessels and nerves to reach the hoof structure. On the distal phalanges of the second and fourth digits, the proximal

articular surfaces are round and slightly raised along the anterior edge. These distal phalanges arc medially and laterally, respectively, and narrow to a point giving them a triangular appearance. Between these 2 distal phalanges, the distal phalanx of the third digit has an ovate proximal articular surface. The distal phalanx fans both medially and laterally.

Figure 60. Distal phalanges of the right manus of ETMNH 609. Views: A, anterior; B, proximal. Abbreviations: II, second digit; III, third digit; IV, fourth digit. Scale bar = 5 cm.

Sesamoids

Two sesamoids articulate with the paired posterodistal facets on each metapodial (Fig. 61). There are 6 isolated sesamoids and it is not possible to determine if they belong to a manus or pes. All of these sesamoids are rugose ‘blobs’ of bone that have concave articular surfaces and that assist with muscle attachment.

Figure 61. Posterior view of sesamoids articulated with the fourth metacarpal. Scale bar = 5 cm.

Hind limb

Innominate

The innominate articulates medially with the other innominate and sacrum and laterally with the femur (Fig. 62). Both innominates of ETMNH 609 have been heavily repaired using MagicSculpt and those of ETMNH 601 are in poorly preserved and, thus, have not been reconstructed. It is difficult to differentiate the 3 bones—ilium, ischium, and pubis—that make up each innominate due to the degree of fusion. Thus, the innominate must be described in terms of regions, i.e. the iliac region. The acetabulum is round with the acetabular incision on the edge of the obturator foramen. There is no fossa or semi-lunar surface in the acetabulum but there is some pitting that does not appear to be natural. The obturator foramen is oblong with some slight doming on its ventral edge.

Largest of the innominate bones, the ilium expands into a broad wing. Laterally, the iliac wing is smooth but the medial iliac wing is rugose for articulation with the sacrum. The iliac crest is rounded at the dorsocranial spine, which is turned dorsolaterally, and makes a nearly straight edge to the ventrocranial spine, which is rugose. A sciatic eminence is prominent on the

caudal edge of the ilium and the greater sciatic notch is deep. A thin, smooth ischium forms the symphysis, which is small relative to the overall size of the innominate. Between this symphysis and the rugose ischiatic tuberosity, the ischial arch is straight. There is no evidence of an ilio-pubic eminence between the ilium and the pubis, which has a broad body and slender branches.

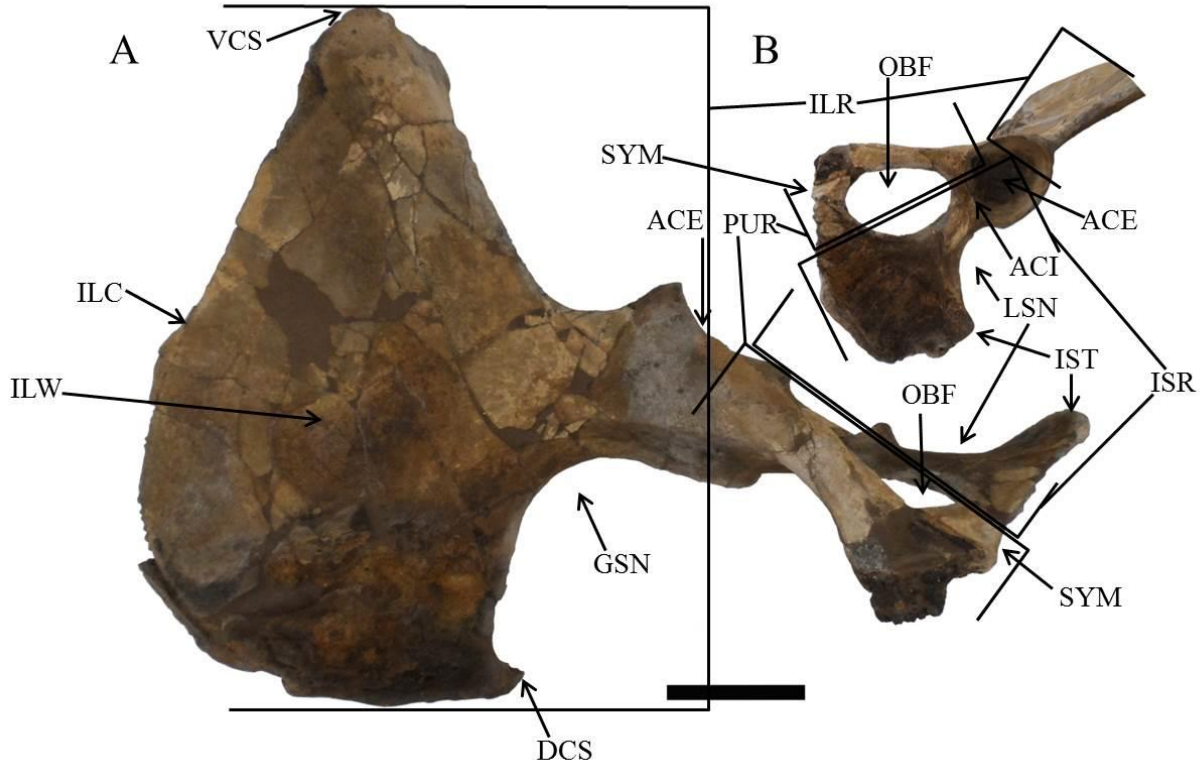

Figure 62. Left innominate of ETMNH 609. Views: A, anterodorsal; B, anteroventral. Abbreviations: ACE, acetabulum; ACI; acetabular incision; DCS, dorsocranial spine; GSN, greater sciatic notch; ILC, iliac crest; ILR, iliac region; ILW, iliac wing; ISR, ischiatic region; IST, ischiatic tuberosity; OBF, obturator foramen; PUR, pubic region; SYM, symphysis; VCS, ventrocranial spine. Scale bar = 10 cm.

Femur

The femur articulates proximally with the acetabulum of the innominate and distally with the tibia and patella (Fig. 63). All of the femora were broken across their diaphyses and have been repaired. Epiphyseal sutures are completely fused but are still visible. Overall, the femur appears depressed in the middle so that, when viewed laterally, the diaphysis loosely forms an arc. Both proximal and distal ends have multiple foramina but no large or distinct foramen. The posterior surface of the femur is nearly flattened but the anterior surface is more rounded. At the proximal end, there is a minimal trochanteric fossa (TF) along the posterior edge of the greater trochanter.

At the proximal end, the round articular head (AH) extends only minimally above the greater trochanter. Along the medial edge, the head forms a lip that overlies the suture line. There is no obvious fovea capitis on the femoral head. A shallow depression is the only evidence of a femoral neck (NK) between the head and the greater trochanter. There is a blunt greater trochanter (GRT) without a definite summit and with only a minimal crest at the laterodistal point of the proximoanterior surface. There is a lesser trochanter (LET) that is merely a bump on the medial surface and it does not extend more medially than the femoral head. An elongate third trochanter (THT) is on the lateral surface but does not extend as far laterally as the greater trochanter.

Distally, there are 2 trochlear tubercles—medial and lateral—on the anterior surface. There is a pronounced femoral ridge (FRD) that extends between the medial trochlear tubercle along the diaphysis to the head. In anterior view, the more prominent medial trochlear tubercle (MTT) is also more rounded compared to the smaller, angular lateral trochlear tubercle (LTT). A

shallow trochlear groove (TG) separates the medial and lateral trochlear tubercles. Like the intermediate tubercle of the humerus, the enlarged medial trochlear ridge (MTR) acts as a passive stay-mechanism in the knee by serving as a 'hook' for the patellar ligaments to enable the animal to stand for long periods of time without the high energy cost (Hermanson and MacFadden 1996). Enlarged MTRs are well-known in horses and, while Hermanson and MacFadden (1996) do not give a definite mechanical function, Kappelman (1988) suggests that, in bovids, this feature represents an open habitat. However, given the forested interpretation of GFS, this seems unlikely for the MTR in *Teleoceras*.

Two condyles are present on the posterior surface of the distal end. The larger medial condyle (MCD) slants slightly compared to the smaller lateral condyle (LCD), which is more aligned with the diaphyseal axis. A deep intercondylar fossa (ICF) is deep and extends medially and laterally beneath the edges of the articular condyles. Both epicondyles are very robust but the medial epicondyle (MEC) is more so than the lateral epicondyle (LEC), and both have large muscle scars on the outer surfaces. Most muscle attachments are well-defined, especially the supracondylar fossa (SCF) on the posterior surface just proximal to the condyles.

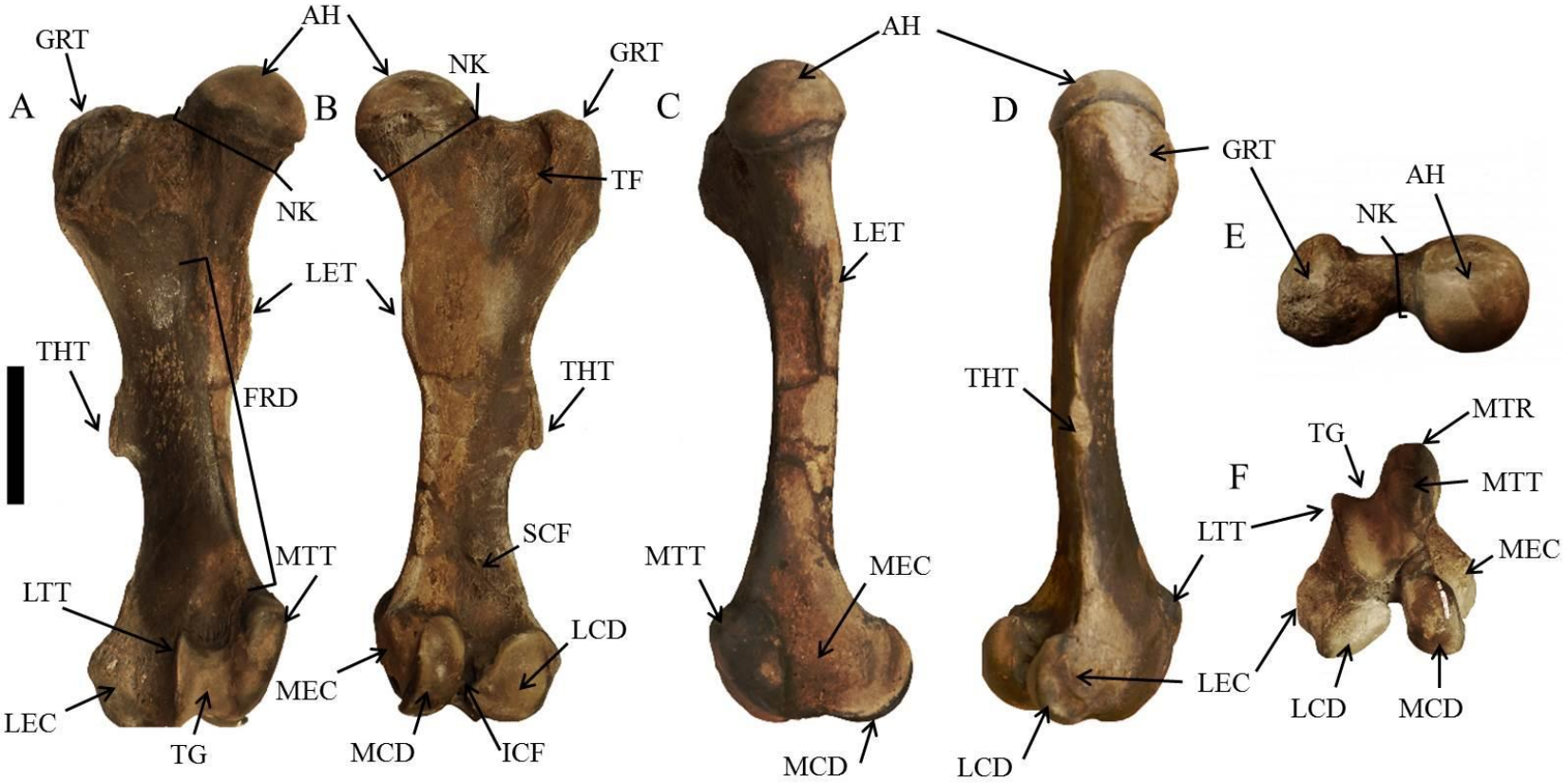

Figure 63. Right femur of ETMNH 609. Views: A, anterior; B, posterior; C, medial; D, lateral; E, proximal; F, distal. Abbreviations: AH, articular head; FRD, femoral ridge; GRT, greater trochanter; ICF, intercondylar fossa; LCD, lateral condyle; LEC; lateral epicondyle; LET, lesser trochanter; LTT, lateral trochlear tubercle; MCD, medial condyle; MEC, medial epicondyle; MTR, medial trochlear ridge; MTT, medial trochlear tubercle; NK, neck; SCF, supracondylar fossa; TF, trochanteric fossa; TG; trochlear groove; THT, third trochanter. Scale bar = 10 cm.

Patella

The patella articulates posteriorly with the distal femur (Fig. 64). Both right patellae have been repaired and both of the left patellae are complete. The patellae are massive, rugose bones that articulate with the femoral trochlear tubercles. A distinct point is formed by the apex (AP) at the proximal end while the base (BA) forms a rounded angle at the distal end. The base does not extend much further proximally than the posterior articular surface (PAS) does. This articular surface covers nearly the entire posterior surface and has a convexity (CV1) that extends from the apex to just lateral of the base. The lateral angle is not obvious but is rounded off. In contrast, the medial angle (MA) is a well-defined prominence that forms a distomedial point. A second concavity (CV2) is present on the posterior articular surface between the medial angle and the apex.

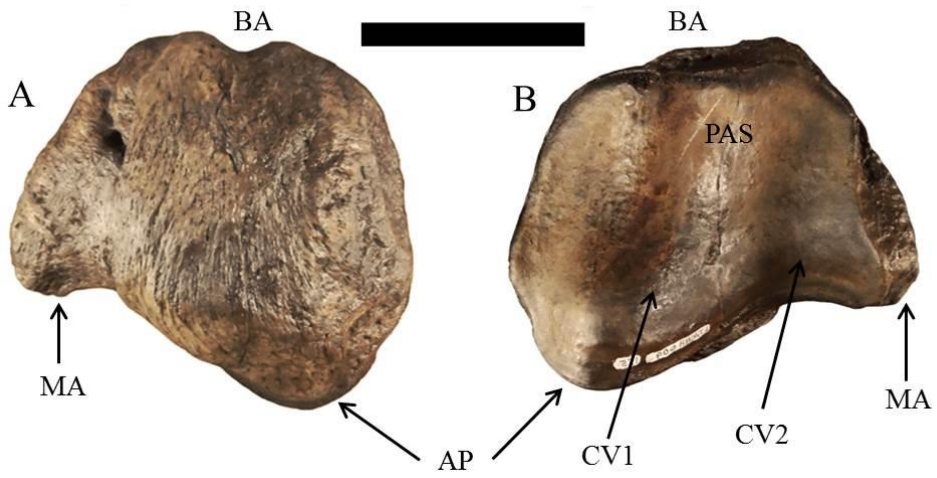

Figure 64. Right patella of ETMNH 609. Views: A, anterior; B, posterior. Abbreviations: AP, apex; BA, base; CV1 and CV2, patellar convexity 1 and 2; MA, medial angle; PAS, posterior articular surface. Scale bar = 5 cm.

Tibia

The tibia articulates proximally with the femur, distally with the astragalus, and laterally with the fibula (Fig. 65). ETMNH 1902 is an associated tibia and fibula that are juvenile and possibly fetal because of the incredibly small size and the lack of epiphyseal plates. All the tibiae from ETMNH 609 and ETMNH 601 were broken across the diaphysis and all except the right of ETMNH 601 have been repaired. This specimen still has some concretion on it and is associated with fragments. Both tibiae of ETMNH 601 have proximally fused to their corresponding fibulae. There are many nutrient foramina around the epiphyseal sutures and articular surfaces of both ends. The proximal end is larger than the distal and has 2 large articular facets for the femur. On the proximal surface, the lateral articular surface (LASF) is a rounded triangle with a minimal popliteal notch (PN) on the posteromedial edge of the lateral articular surface. The 2 articular surfaces barely curve over the proximal portion of this notch. Medially, the lateral articular surface rises proximally to form the lateral intercondylar eminence (LIE). A narrow depression—the central intercondylar area (CTIA)—separates the lateral articular surface from the medial articular surface. The medial articular surface (MASF) is smaller and more rounded with a slight concavity along the medial edge. The medial articular surface is more centrally depressed than the lateral articular surface. Medially, the medial articular surface rises proximally to form the medial intercondylar eminence (MIE), which is more proximal and slightly shorter than the lateral intercondylar eminence.

There is a caudal intercondylar area (CDIA) between the posterior portions of the medial and lateral articular surfaces. This small, flat area extends into a slight prominence posterior to the medial articular surface. A larger cranial intercondylar area (CRIA) is present between the

anterior portions of the medial and lateral articular surfaces. Lateral to the cranial intercondylar area is a small notch between the lateral articular surface and the tibial tuberosity. Between the medial and lateral tibial tuberosities, there is a shallow tuberosity groove (TTG) that forms a 'V.' While the medial tibial tuberosity (MTT) is slightly rugose and aligned with the diaphysis, the lateral tibial tuberosity (LTT) is more prominent, more rugose, and protrudes laterally from the diaphysis. Proximolaterally, there is a fibular articular surface (ASF1) that is shaped like an upside-down teardrop. Rather than being smooth as most articular surfaces are, this 1 is rugose for a tight articulation that becomes fused with age.

In cross-section, the diaphysis is triangular as the tibial crest (TCT) extends for nearly the entire length of the bone to the anterodistal process (ADP). The medial diaphysis is nearly straight but the lateral diaphysis is concavely curved with a slight projection near the midpoint of the diaphysis. Distally, there is a parallelogram-shaped articular surface for the astragalus (ASA). Depressions for the astragalar trochlea are slanted from anterolateral to posteromedial and are separated by a raised ridge that appears to be pinched anteroposteriorly. This feature is consistent within the GFS population but the degree of pinching seems to vary between *Teleoceras* populations. Posteromedially to this articular surface is the medial malleolus (MM) that is the distal-most point of the tibia. On the lateral surface of the distal end, there is a small, domed articular surface for the fibula (ASF2). This surface is in contact with the distal astragalar facet. A triangle of rugosity extends proximal to the fibular facet to form a tighter articulation with the fibula. The proximal and distal fibular facets are connected by a ridge that runs the length of the diaphysis.

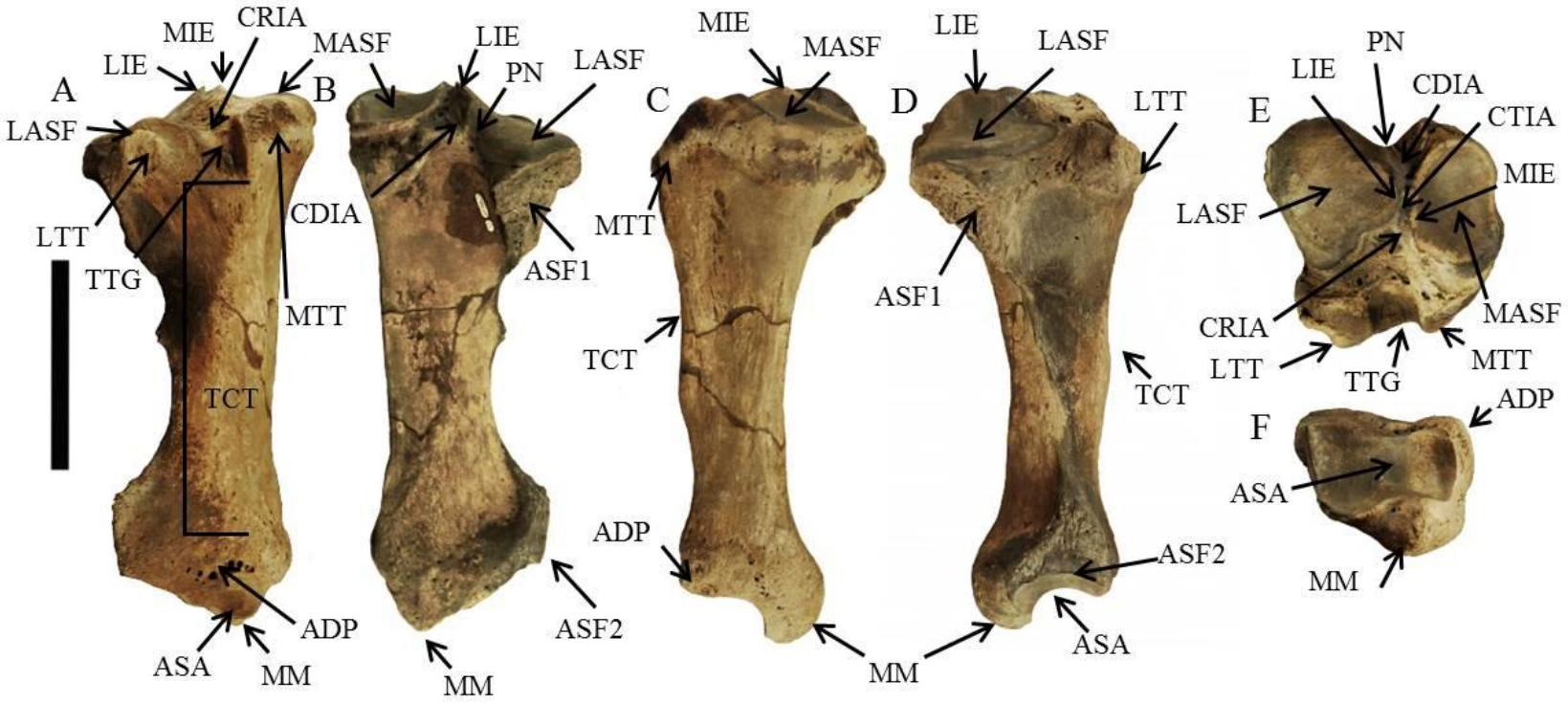

Figure 65. Right tibia of ETMNH 609. Views: A, anterior; B, posterior; C, medial; D, lateral; E, proximal; F, distal. Abbreviations: ADP, anterodistal process; ASA; articular surface for astragalus; ASF1-2, articular surfaces for fibula 1-2; CDIA, caudal intercondylar area; CRIA, cranial intercondylar area; CTIA, central intercondylar area; LASF, lateral articular surface for femur; LIE, lateral intercondylar eminence; LTT, lateral tibial tuberosity; MASF, medial articular surface for femur; MIE, medial intercondylar eminence; MM, medial malleolus; MTT, medial tibial tuberosity; PN, popliteal notch; TCT, tibial crest; TTG, tibial tuberosity groove. Scale bar = 10 cm.

Fibula

The fibula articulates proximomedially with the tibia and distomedially with the astragalus (Fig. 66). Again, ETMNH 1902 is an associated tibia and fibula that are juvenile and possibly fetal because of the incredibly small size and lack of epiphyseal plates. All of the adult fibulae were broken across their diaphyses but only the left of ETMNH 609 and the right of ETMNH 601 have been repaired. Both left fibulae are more weathered than the corresponding right fibulae. On ETMNH 601, both fibulae are fused to the tibiae at the proximal end but there is no evidence of fusion at the distal end. All 4 fibulae have rugose proximal and distal ends. The proximal diaphysis is anteroposteriorly compressed and the distal diaphysis is triangular with rounded angles.

The proximal articulation site for the tibia (AST) is shaped like an upside-down teardrop. There is also a distal articulation site for the tibia (AST2) that is shaped like a half-circle. The distal lateral malleolus (LML) has a small, round articular surface for the astragalus (ASA) that is continuous with the corresponding distolateral articular facet on the tibia. A muscle attachment line curves from proximal posterolateral articulation site to distolateral articulation site. Along this line, there is a bump that, when articulated with the tibia, is only slightly distal to the corresponding projection on the lateral tibial diaphysis.

Figure 66. Left fibula of ETMNH 609. Views: A, medial; B, lateral. Abbreviations: ASA, articular surface for astragalus; AST1-2, articular surfaces for tibia 1-2; LML, lateral malleolus. Scale bar = 10 cm.

Tarsals

Teleoceras has 7 tarsals in the pes (Fig. 67).

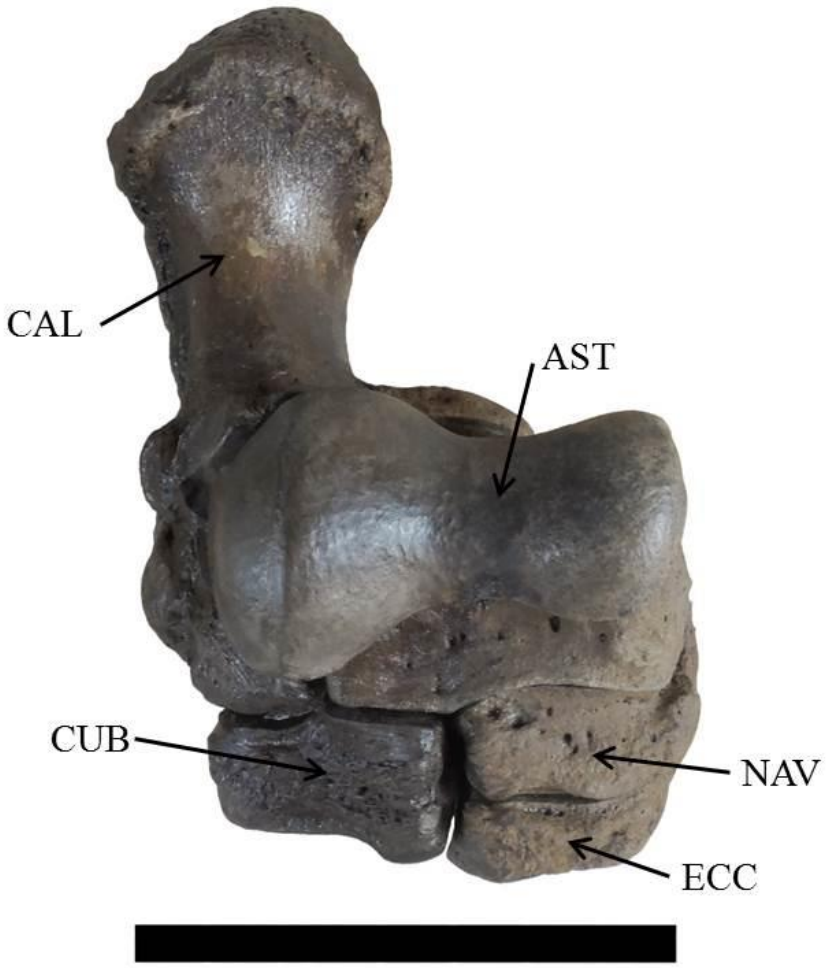

Figure 67. Articulated tarsals of ETMNH 609 in anterior view. Abbreviations: AST, astragalus; CAL, calcaneum; CUB, cuboid; ECC, ectocuneiform; NAV, navicular. The mesocuneiform and entocuneiform are not visible in this view. Scale bar = 10 cm.

Calcaneum. The calcaneum articulates anteroproximally with the astragalus and laterally with the fibula (Fig. 68). All 4 calcanea of ETMNH 609 and ETMNH 601 are either complete or nearly so. Heavy rugosity is present on the calcaneal tuber (CTB) and forms a ridge along the lateral surface of the diaphysis, which appears to be pinched mediolaterally. On the medial surface, the sustentaculum (SUS) is prominent and rugose and there is only a slight tendon

groove (TG) along the sustentaculum. A dorsal, roughly rounded articular surface for the astragalus (ASA1) is present on the sustentaculum. Lateral to the sustentaculum is a second articular surface for the astragalus (ASA2). This facet is ovate, slants toward the sustentaculum, and is depressed along a mediolateral fold. The lateral edge of this articular surface folds over into a domed fibular articular surface (ASF). There is a small knob of rugosity lateral to the fibular facet. An anterior process (AP) has 2 articular surfaces and forms the furthest extent opposite the calcaneal tuber. On the medial side of the process, there is a small, domed facet that articulates with the astragalus (ASA3). This facet folds into the oval articular surface for the cuboid (ASC) on the plantar side of the calcaneum. It is important to note that the articular surfaces of the calcanea display a large amount of variation in their size and shape.

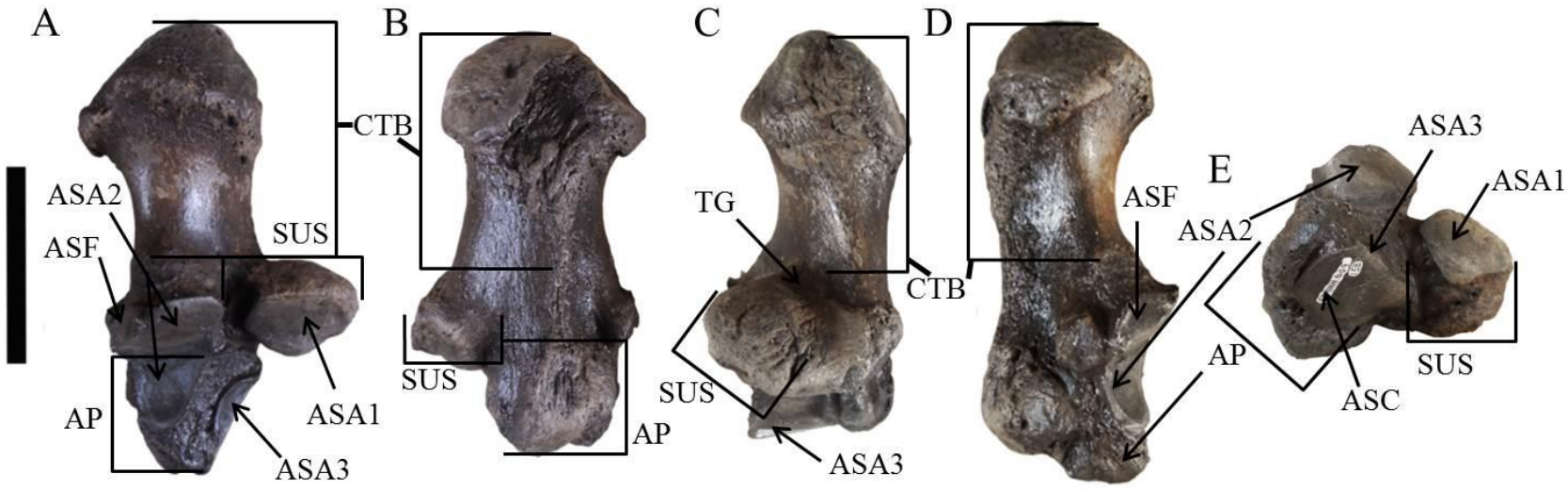

Figure 68. Right calcaneum of ETMNH 609. Views: A, dorsal; B, plantar; C, medial; D, lateral; E, anterior. Abbreviations: AP, anterior process; ASA1-3, articular surfaces for astragalus 1-3; ASC, articular surface for cuboid; ASF, articular surface for fibula; CTB, calcaneal tuber; SUS, sustentaculum; TG, tendon groove. Scale bar = 5 cm.

Astragalus. The astragalus articulates proximally with the tibia, posterodistally with the calcaneum, proximolaterally with the fibula, and distally with the cuboid and navicular (Fig. 69). With those of the 2 complete skeletons, there is also a right astragalus (ETMNH 14175) and 2 left astragali (ETMNH 6647, ETMNH 1901). Both astragali of ETMNH 609 are complete but both astragali of ETMNH 601 have been repaired. Proximally, a trochlea (TRO) provides the articular surface for the tibia (AST). The lateral portion of the trochlea is larger and extends more proximally than the smaller medial portion. Between the lateral and medial portions of the trochlea, a wide trochlear groove (TRG) is nearly centered. The articular surface of the lateral trochlea folds posterolaterally to form a second proximal articular surface. This surface matches with the small lateral articular surface on the calcaneum to create the site of fibular articulation (ASF). Distal to the trochlea is the 'base' of the astragalus (BAS), which extends from the medial edge of the trochlea almost to the lateral edge of the trochlea. This portion of the astragalus has little rugosity but does have many foramina.

Two articular surfaces are present on the distal surface of the astragalus 'base.' Medially, there is a square surface with rounded medial corners for articulation with the navicular (ASN). The lateral-most edge is raised to form a ridge (DR) with the lateral articular surface. The lateral articular surface for the cuboid (ASCB) is rectangular with the long axis oriented anterior to posterior. This articular surface is nearly flat at the level of the ridge formed with the medial articular surface. The posterior portion of the ridge between the 2 distal articular surfaces extends more distally.

On the posterior surface of the astragalus, there is an oval articular surface that is in contact with the ridge between the distal articular surfaces. This articular surface for the sustentaculum of the calcaneum (ASS) is near the midpoint of the 'base' and distal to the

trochlear groove on the proximal surface. Laterally, there is a large articular surface for the calcaneum on the posterior side and proximolateral to the astragalar ‘base.’ This articular surface is oblong with the long axis oriented proximomedial to distolateral. There is a depression in the middle of the proximal portion of this articular surface (PASCL) and a fold between the proximal and distal portions (DASCL) of this articular surface for the calcaneum.

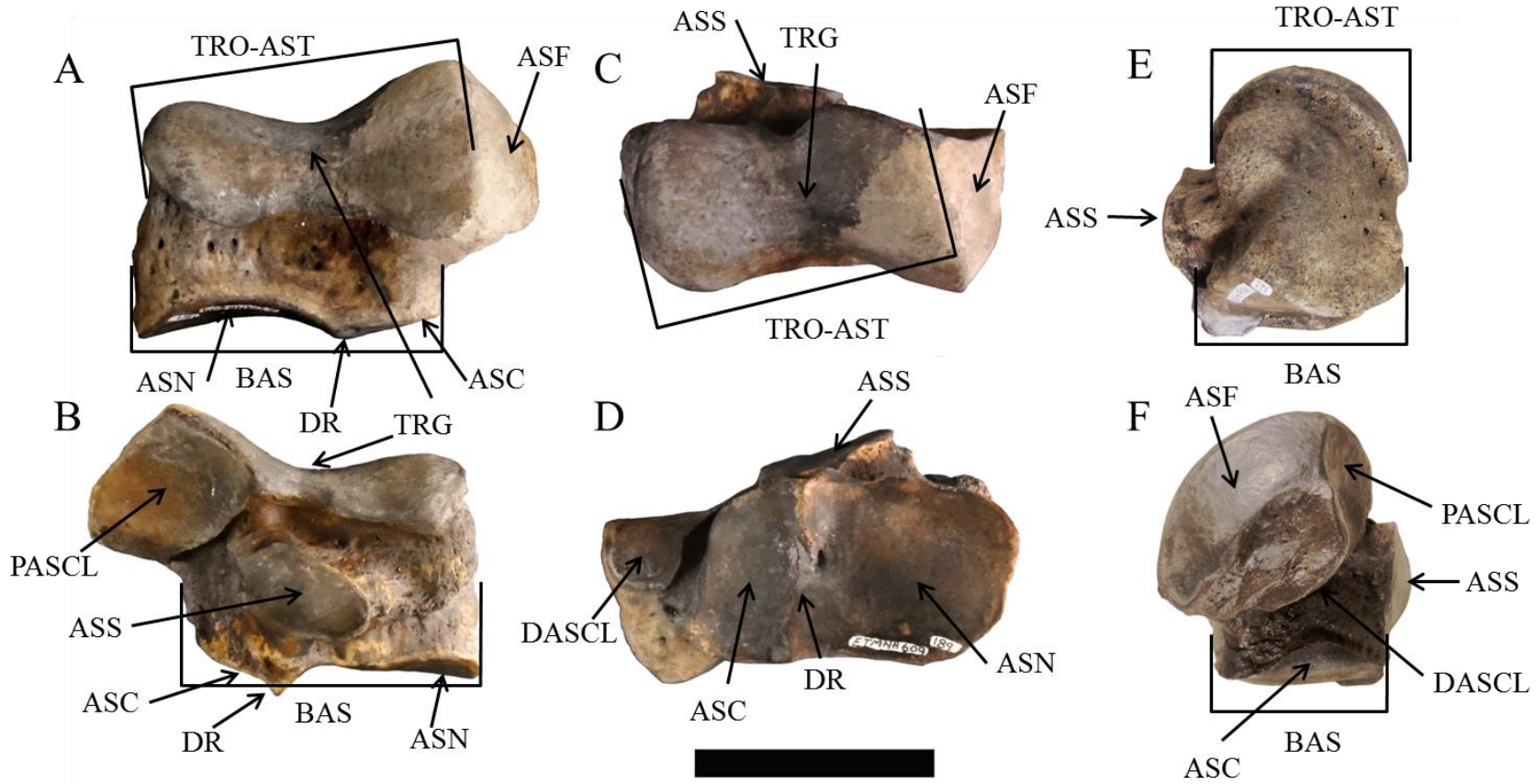

Figure 69. Left astragalus of ETMNH 609. E and F are flipped images of the right astragalus of the same specimen. Views: A, anterior; B, posterior; C, proximal; D, distal; E, medial; F, lateral. Abbreviations: ASCB, articular surface for cuboid; ASF, articular surface for fibula; ASN, articular surface for navicular; ASS, articular surface for sustentaculum; AST, articular surface for tibia; BAS, base; DASCL, distal articular surface for calcaneum; DR, distal ridge; PASCL, proximal articular surface for calcaneum; TRG, trochlear groove; TRO, trochlea. Scale bar = 5 cm.

Navicular. The navicular articulates proximally with astragalus, distally with the ectocuneiform, mesocuneiform, and entocuneiform, and laterally with the cuboid (Fig. 70). Both naviculars of ETMNH 609 are complete but both naviculars of ETMNH 601 have been repaired. In general, the navicular is a square bone and is compressed proximodistally. Proximally, there is 1 articular surface for the astragalus (ASA) that covers nearly the entire surface of the bone. This surface slants from the proximal-most posteromedial corner to the distal-most anterolateral corner. At its anterolateral corner, there is a small articular surface for the cuboid (ASC1). There is another small, round articular surface on the posterolateral surface. This articular surface (ASC2) is slanted proximolaterally to distomedially and it forms a second articulation with the cuboid. The 2 lateral articular surfaces are separated by a depression but both form an edge with the distal articular surface.

Rugosity covers the anterior, medial, and most of the posterior surfaces. There is a small medial protuberance (MPT) on the posterior surface with a small, round, distal articular surface for the entocuneiform (ASEN). Distally, there are 2 articular surfaces for the mesocuneiform and the ectocuneiform. The smaller, round, medial articular surface for the mesocuneiform (ASM) separated from the larger, triangular, lateral articular surface for the ectocuneiform (ASEC) by a slight ridge. There is a concavity on the lateral edge of the ectocuneiform articular surface that corresponds to the depression between the lateral cuboid articular surfaces.

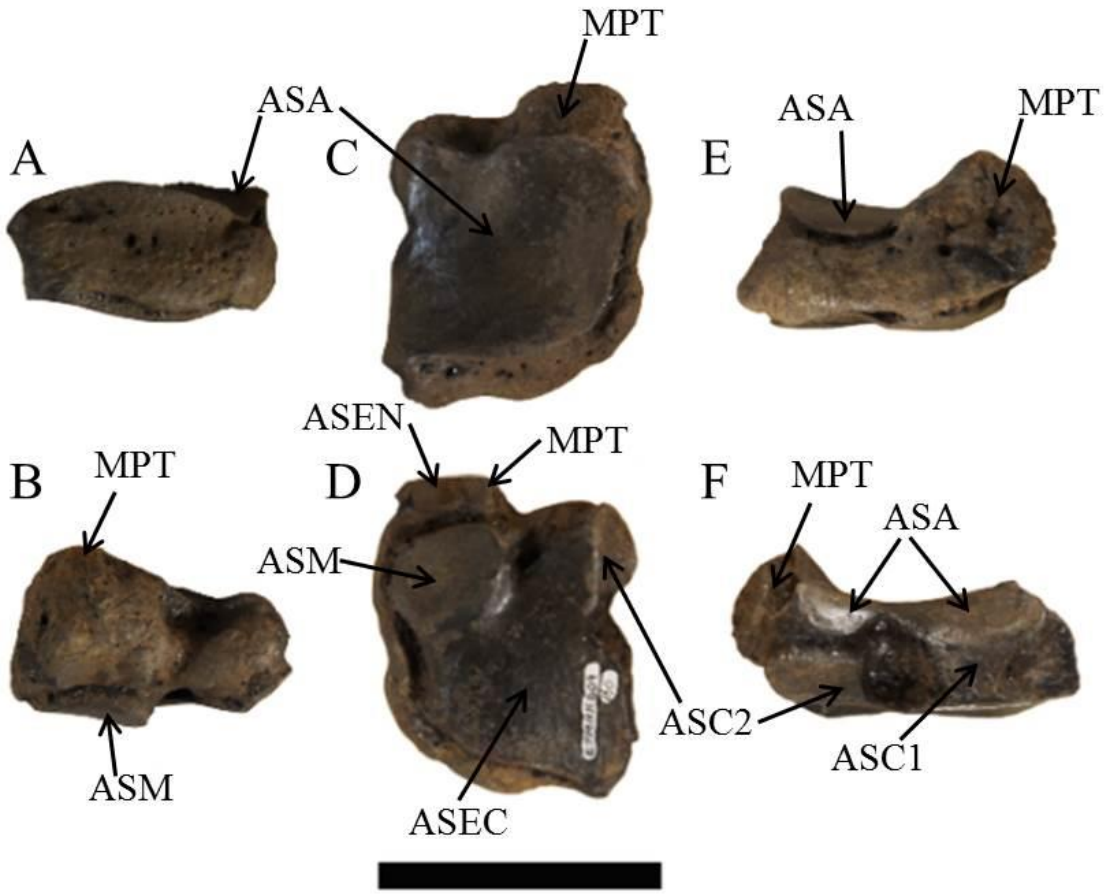

Figure 70. Right navicular of ETMNH 609. Views: A, anterior; B, posterior; C, proximal; D, distal; E, medial; F, lateral. Abbreviations: ASA, articular surface for astragalus; ASC1-2, articular surfaces for cuboid 1-2; ASEC, articular surface for ectocuneiform; ASEN, articular surface for entocuneiform; ASM, articular surface for mesocuneiform; MPT, medial process. Scale bar = 5 cm.

Cuboid. The cuboid articulates proximally with the astragalus and calcaneum, distally with the fourth and third metatarsals, and medially with the navicular and ectocuneiform (Fig. 71). Only the right cuboid of ETMNH 609 was broken and repaired. This bone is compressed proximodistally but is elongated anteroposteriorly. A nearly triangular portion extends into a posterior process. Two articular surfaces are present on the proximal surface of the anterior

portion; both are triangular and are divided by a ridge. The medioproximal articular surface articulates with the astragalus and the lateroproximal articular surface articulates with the calcaneum. On the medial surface of the anterior portion, there is a small, proximal articular surface for the navicular. Distal to this facet is a domed articular surface for articulation with the ectocuneiform. This facet folds onto the distal surface into 2 articular surfaces that are separated by a slight ridge. The smaller medial articular surface for the third metatarsal is a slender rectangle with the long axis oriented anterolateral to posteromedial. Laterally, a larger, triangular articular surface is present for articulation with the fourth metatarsal. Both the anterior and lateral surfaces lack articular surfaces but do have slight rugosities. Posteriorly, there is a rugose process with a distal curvature. There is a single anteromedial articular surface that is divided into 2 half-circle facets by a ridge on the side on the process. The proximal surface articulates with the navicular and the distal articulates with the ectocuneiform.

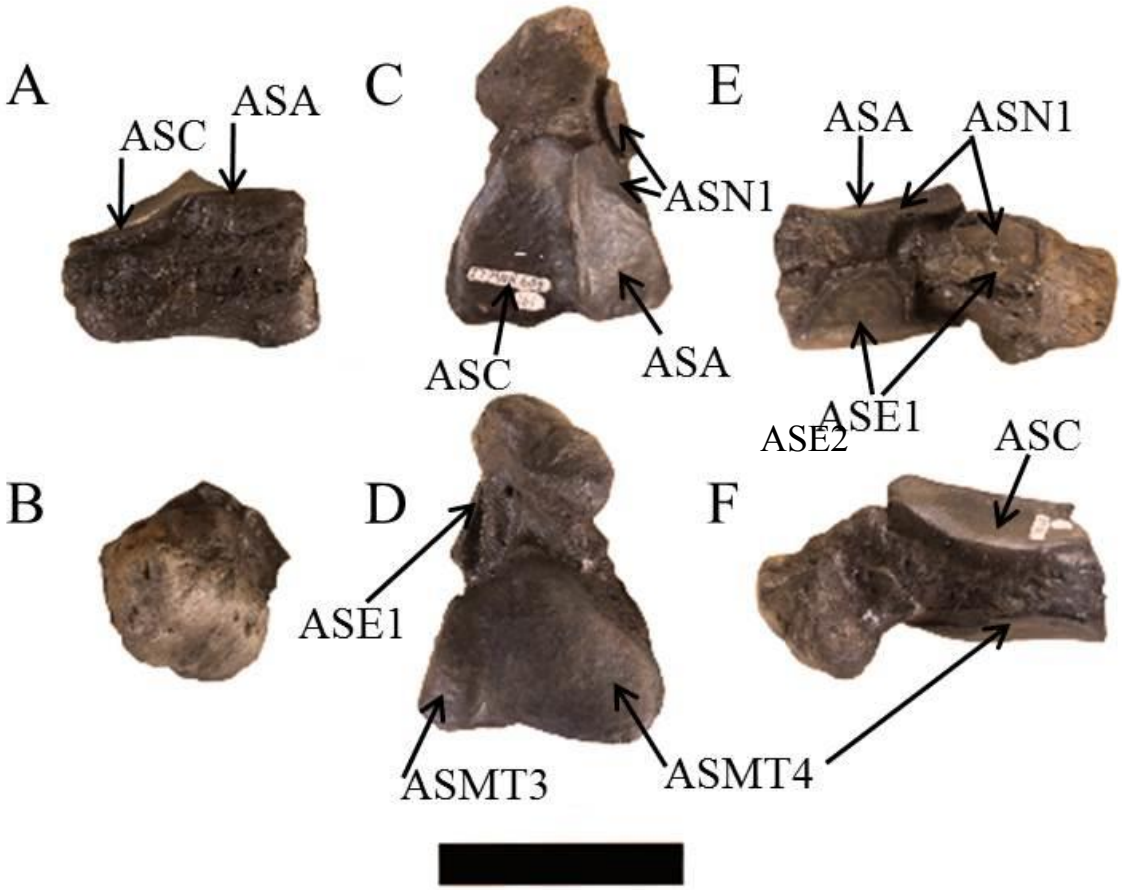

Figure 71. Right cuboid of ETMNH 609. Views: A, anterior; B, posterior; C, proximal; D, distal; E, medial; F, lateral. Abbreviations: ASA, articular surface for astragalus; ASC, articular surface for cuboid; ASN1-2, articular surfaces for navicular 1-2; ASE1-2, articular surface for ectocuneiform 1-2; ASMT3, articular surface for third metacarpal; ASMT4, articular surface for fourth metacarpal. Scale bar = 5 cm.

Entocuneiform. The entocuneiform articulates proximally with the navicular and anterolaterally with the mesocuneiform (Fig. 72). This is a small bone with a rugosity that curves distolaterally. An oval anterolateral surface articulates with the mesocuneiform (ASM) and a small round proximal surface articulates with the navicular (ASN).

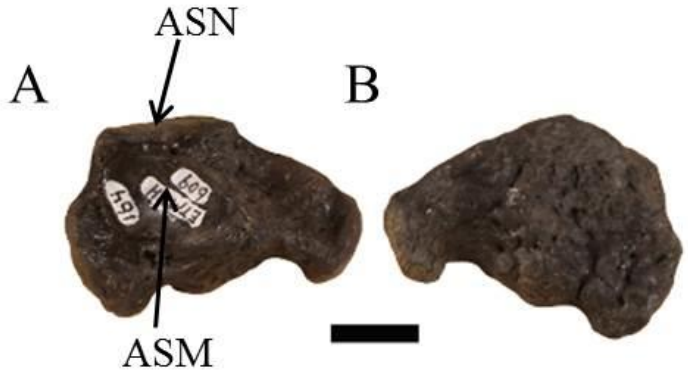

Figure 72. Right entocuneiform of ETMNH 609. Views: A, anterolateral; B, posteromedial. Abbreviations: ASM, articular surface for mesocuneiform; ASN, articular surface for navicular. Scale bar = 1 cm.

Mesocuneiform. The mesocuneiform articulates proximally with the navicular, distally with the second metatarsal, medially with the entocuneiform, and laterally with the ectocuneiform (Fig. 73). An isolated right mesocuneiform is also in collections (ETMNH 3749). Only the right mesocuneiform of ETMNH 601 is damaged with a small piece of the rugosity broken. A rugose knob is present on the anteromedial face of the mesocuneiform. Proximally, the mesocuneiform has an oval surface for articulation with the navicular (ASN). Distally, there is a diamond-shaped surface for articulation with the second metatarsal (ASMT2). From the distal articular surface, the lateral edge folds proximally into a half-circle articular surface for the ectocuneiform (ASEC). Also from the distal articular surface, the posteromedial edge folds proximally into an oval articular surface for articulation with the entocuneiform (ASEN).

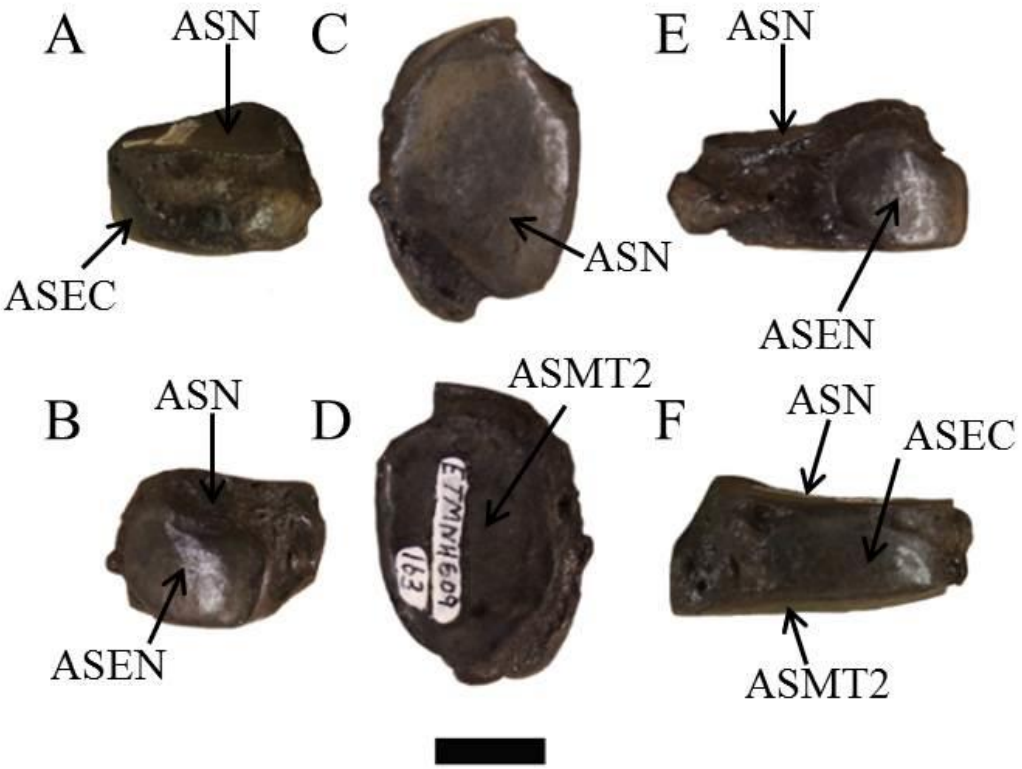

Figure 73. Right mesocuneiform of ETMNH 609. Views: A, anterior; B, posterior; C, proximal; D, distal; E, medial; F, lateral. Abbreviations: ASEC, articular surface for ectocuneiform; ASEN, articular surface for entocuneiform; ASMT2, articular surface for second metatarsal; ASN, articular surface for navicular. Scale bar = 1 cm.

Ectocuneiform. The ectocuneiform articulates proximally with the navicular, distally with the third metatarsal, medially with the second metatarsal and mesocuneiform, and laterally with the cuboid (Fig. 74). Both ETMNH 609 and ETMNH 601 have complete ectocuneiform, which are, in general, triangular. A raised knob of rugosity is present on the anterior surface of the ectocuneiform. There is a concavity (CV) just posterior to the midpoint on the lateral edge that corresponds to the concavity on the lateral edge of the navicular. Proximally, there is 1 articular surface for the navicular (ASN) that covers nearly the entire surface and has both the

posterior and medial corners turned proximally. On the posterior portion of the proximal surface, an edge is formed with the slender, elongate articular surface for the cuboid (ASC1) on the lateral surface of the ectocuneiform.

There is a small, half-circle articular surface on the posteromedial edge of the ectocuneiform for articulation with the mesocuneiform (ASM). This articular surface folds distally into a rectangular articular surface, with the long axis oriented laterally to posteromedially, for articulation with the second metatarsal (ASMT2). The articular surface for the second metatarsal forms a lateral edge with the distal, triangular articular surface that articulates with the third metatarsal (ASMT3). On the lateral edge, this distal articular surface forms an anterolateral edge with a second cuboid articular surface (ASC2) that is round. This anterior cuboid articulation site is separated from the posterior cuboid articulation site by a depressed area. On the ectocuneiforms of ETMNH 601, the more anterior of the 2 cuboid articulations is also in contact with the proximal navicular articular surface.

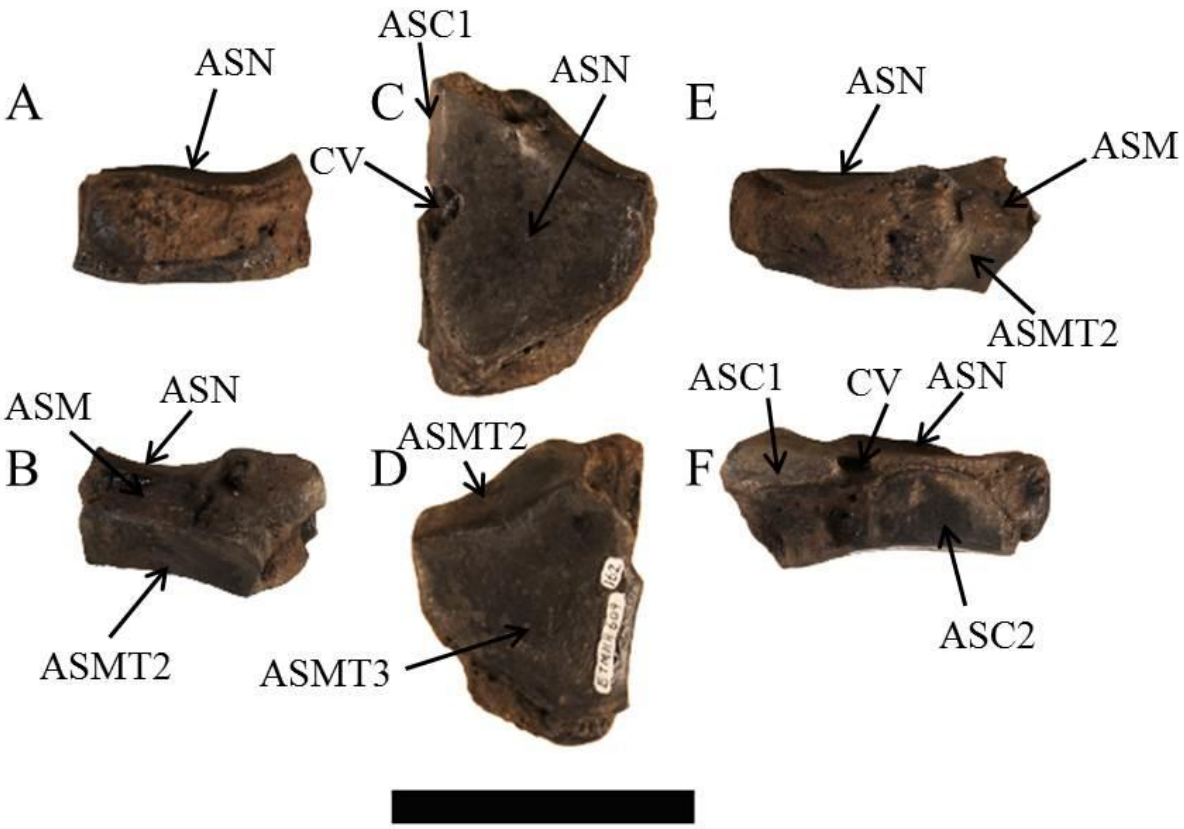

Figure 74. Right ectocuneiform of ETMNH 609. Views: A, anterior; B, posteromedial; C, proximal; D, distal; E, medial; F, lateral. Abbreviations: ASC1-2, articular surfaces for cuboid 1-2; ASM, articular surface for mesocuneiform; ASMT2, articular surface for second metatarsal; ASMT3, articular surface for third metatarsal; ASN, articular surface for navicular; CV, concavity. Scale bar = 5 cm.

Metatarsals

In each pes, *Teleoceras* has 3 metatarsals—the second, third, and fourth. The metatarsals articulate more tightly than the metacarpals do and exhibit less splay.

Second Metatarsal. The second metatarsal articulates proximally with the mesocuneiform and the ectocuneiform, distally with the proximal phalanx, and laterally with the third metatarsal (Fig. 75). ETMNH 601 has a pathological left second metatarsal that articulates

with the pathological phalanges discussed in Gilmore and Wallace (in prep.).Unlike the second metacarpal, the medial and lateral edges of the second metatarsal do not curve; though on some, the medial edge looks as though it has been pinched. Foramina and rugosities are present along the epiphyseal regions and on the non-articular surfaces, especially the anterior. There is a small rugose prominence on the anterolateral side (ALP) of the distal end and a second rugose knob on the posterior surface.

Three articular surfaces are present on the proximal end of the second metatarsal. Medially, there is a round articular surface for the mesocuneiform (ASM). This facet forms a medial edge with the rectangular proximolateral articular surface for the ectocuneiform (ASEC), which has a rounded, convex posterior portion. On the lateral side of the proximal end, the ectocuneiform facet forms an edge with a small, triangularly elongate articular surface for the third metatarsal (ASMT3). Distally, the anterior articular surface for the proximal phalanx of the second digit (ASPP2) is smooth and angled distomedially from the anterolateral prominence. On the posterior surface the distal articular surface is divided into 2 facets by the intermediate relief (IMR), which is aligned with the medial rugosity along the posterior surface. The facets (ASS1-2) slant proximomedially and each articulates with a sesamoid.

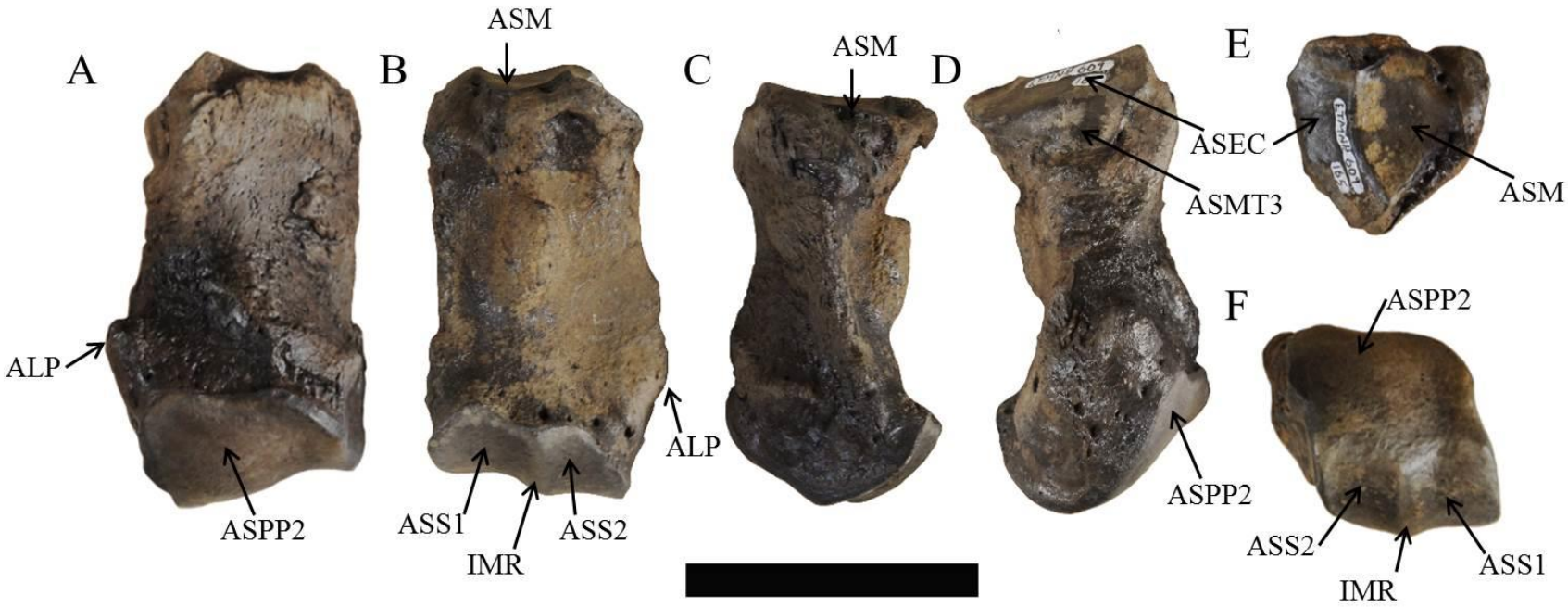

Figure 75. Right second metatarsal of ETMNH 609. Views: A, anterior; B, posterior; C, medial; D, lateral; E, proximal; F; distal. Abbreviations: ALP, anterolateral process; ASEC, articular surface for ectocuneiform; ASM, articular surface for mesocuneiform; ASMT3, articular surface for third metatarsal; ASPP2, articular surface for proximal phalanx of second digit; ASS1-2, articular surfaces for sesamoids 1-2; IMR, intermediate relief;. Scale bar = 5 cm.

Third Metatarsal. The third metatarsal articulates proximally with the ectocuneiform, distally with the proximal phalanx, laterally with the fourth metatarsal, and medially with the second metatarsal (Fig. 76). ETMNH 609 has a complete right third metatarsal and ETMNH 601 has a complete left third metatarsal; the others have been damaged. While both medial and lateral edges curve inward, the medial does more so, which positions the proximal end more medial than the distal. The proximal end is also positioned slightly posterior to the distal creating the slant seen in the articulated pes. Foramina are present along the epiphyseal lines, which are completely fused in both skeletons. Nutrient foramina (NF) are near the anterior and posterior midpoints on the third metatarsals of ETMNH 609 but are missing from the left third metatarsal of ETMNH 601 and are nearly closed on the right. This could be due to advanced age and ossification. Rugosity is present along the epiphyseal lines, which are all completely fused. Paired, round rugosities are on the anterodistal surface, 1 medially and 1 laterally, and both extend distally around their respective edges forming distal rugosities on either side.

Four articular surfaces are found at the proximal end of the third metatarsal. On the medial surface, a slender articular surface extends anteroposteriorly for the second metatarsal (ASMT2). The proximal edge of this surface contacts the medial articular facet on the proximal surface. This proximomedial articular surface for the ectocuneiform (ASEC) is large with a broad, round anterior edge and a narrow, square posterior edge. A raised lateral edge forms a ridge between the medioproximal articular surface and the larger, rectangular proximolateral articular surface for the cuboid (ASC). On the lateral side of the proximal end, there is an articular surface for the fourth metatarsal (ASMT4) that has 2 rounded portions—anterior and posterior—with an indentation between them. A straight proximal edge contacts the lateral edge of the proximal cuboid articular facet. On the posterior side, there is a gap between the posterior

portion of the fourth metatarsal facet and the ectocuneiform facet. This gap is consistent within the GFS population but is variable in size and shape within *Teleoceras*.

At the distal end of the third metatarsal, the anterior articular surface is smooth and domed proximally with edges that are variable in shape. This articular surface is for the proximal phalanx of the third digit (ASPP3). Posteriorly, an intermediate relief that is slanted slightly laterally as it extends proximally separates the distal articular surface into 2 facets (ASS1-2) that each articulate with 1 sesamoid. There is no distinct corresponding ridge or rugosity along the midline of the diaphysis as in some other metapodials but only a raised area that creates paired depressions proximal to the distal facets.

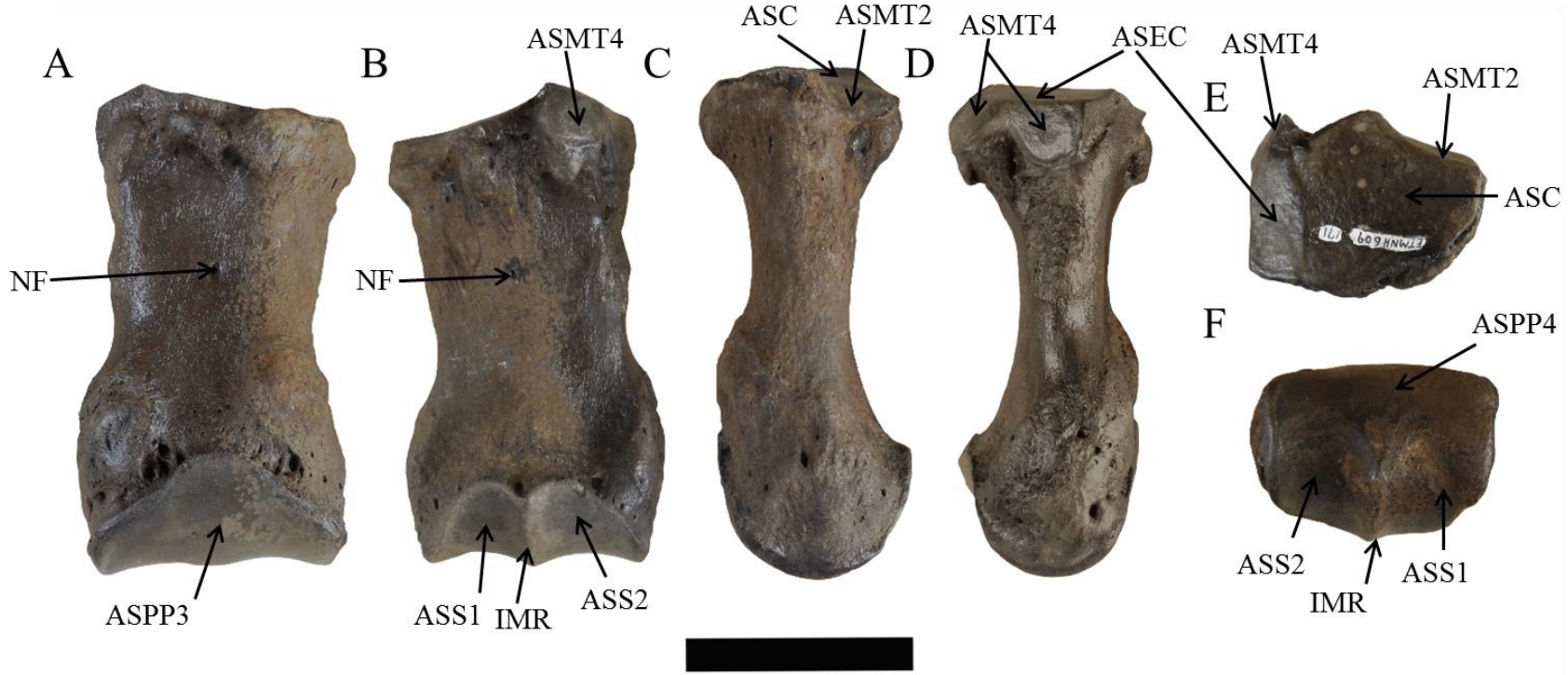

Figure 76. Right third metatarsal of ETMNH 609. Views: A, anterior; B, posterior; C, medial; D, lateral; E, proximal; F, distal. Abbreviations: ASC, articular surface for cuboid; ASEC, articular surface for ectocuneiform; ASMT2, articular surface for second metatarsal; ASMT4, articular surface for fourth metatarsal; ASPP3, articular surface for proximal phalanx of the third digit; ASS1-2, articular surfaces for sesamoids 1-2; IMR, intermediate relief; NF, nutrient foramen. Scale bar = 5 cm.

Fourth Metatarsal. The fourth metatarsal articulates proximally with the cuboid, distally with the proximal phalanx, and medially with the third metatarsal (Fig. 77). Only the left fourth metatarsal of ETMNH 609 has been damaged. Some foramina are present along the epiphyseal lines but most of the non-articular surfaces, especially the anterior, are heavily rugose. ETMNH 609 has a slight inward curvature along the lateral edge that is more pronounced than that of ETMNH 601. In both specimens, the lateral edge appears pinched anteroposteriorly. On the posterior surface, there is a rugose bump at the proximal end along the midline of the diaphysis.

Only 2 articular surfaces are on the proximal end of the fourth metatarsal. A slightly depressed triangular facet covers the proximal surface and for articulation with the cuboid (ASC). The straight medial edge of this facet forms an edge with the medial articular surface for the third metatarsal (ASMT3). This facet consists of 2 rounded portions—anterior and posterior—that are connected in the middle. The posterior portion forms a process that extends posteriorly from the body of the fourth metatarsal to form a site of muscle attachment. At the distal end, the anterior articular surface (ASPP4), which articulates with the proximal phalanx of the fourth metatarsal, is smooth and domed proximally with a slant from proximomedial to distolateral. An intermediate relief, divides the posterior articular surface of the distal end into 2 facets that each articulate with 1 sesamoid (ASS1-2). The sesamoid facets are slanted from proximolateral to distomedial with smooth outer edges but are squarer than the typically round condyles of other metapodials.

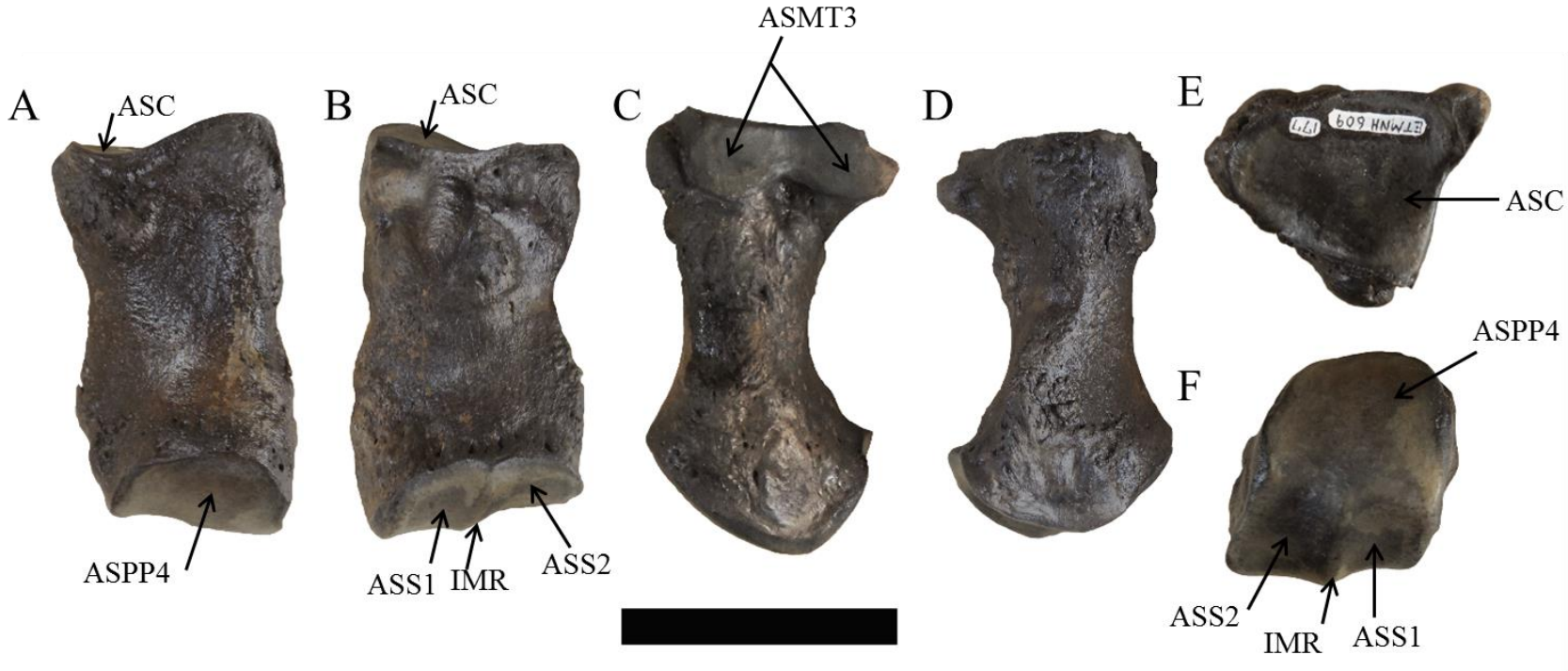

Figure 77. Right fourth metatarsal of ETMNH 609. Views: A, anterior; B, posterior; C, medial; D, lateral; E, proximal; F, distal. Abbreviations: ASC, articular surface for cuboid; ASMT3, articular surface for third metatarsal; ASPP4, articular surface for proximal phalanx of digit four; ASS1-2, articular surfaces for sesamoids 1-2; IMR, intermediate relief. Scale bar = 5 cm.

Phalanges

As in the manus, the second and fourth digits of the pes are longer to accommodate the splayed posture of the pes. Also like in the manus, the third digit is the most compressed. Because the phalanges of the pes are so similar to those of the manus, the descriptions will not be repeated here. However, it is important to note that, on the second digit of the left pes of ETMNH 601, the phalanges are pathological so that the proximal and medial phalanges are completely fused and the distal phalanx is remodeled as discussed by Gilmore and Wallace (in prep.) (Fig. 78).

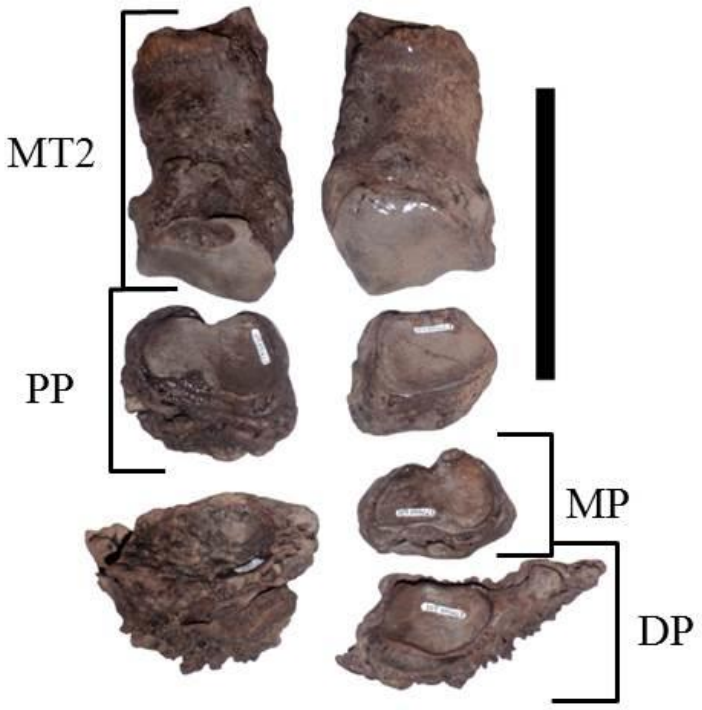

Figure 78. Pathological phalanges of the left hind second digit of ETMNH 601 with healthy phalanges of the right hind second digit. Notice that the left medial and distal phalanges are fused together. Abbreviations: DP, distal phalanx; MP, medial phalanx; MT2, second metatarsal; PP, proximal phalanx. Scale bar = 10 cm.

Proximal Phalanges. Proximal phalanges articulate with the anterior facets of the distal metatarsals and with the medial phalanges. Those of the second and fourth digits are like those of the manus but smaller. Those of the third digits are nearly identical, including in size, to those of the manus.

Medial Phalanges. Medial phalanges articulate with the proximal phalanges and the distal phalanges. Those of the second and fourth digits are like those in the manus but smaller. Those of the third digits are nearly identical to those of the manus, except the anterior edge of the proximal surface is concave rather than convex but this could be normal variation.

Distal Phalanges. Distal phalanges articulate with the medial phalanges. Those of the second and fourth digits are like those in the manus but slightly smaller. Those of the third digits are nearly the same size as those of the manus.

Sesamoids

Like in the manus, the sesamoids of the pes articulate with the distal facets of the metatarsals. On the second and fourth digits, the external sesamoids are larger than those in the manus to account for the greater curvature of distal articular surfaces on the metatarsals. Other than that, the sesamoids of the manus and pes are nearly indistinguishable.

CHAPTER 4

RESULTS

For the GFS population, the generic determination of *Teleoceras* follows the descriptions of Hatcher (1894a, 1894b) and Prothero (2005). Of the 6 Teleoceratini synapomorphies and 11 *Teleoceras* characteristics given by Prothero (2005), the GFS population has 5 and 8, respectively (Table 2). One Teleoceratini synapomorphy described by Prothero (2005) addresses the nasal incision but is believed to be poorly defined. Most, if not all, *Teleoceras* skulls, including those from GFS, have a nasal incision that extends beyond the upper third premolar.

Table 2. Synapomorphies of Teleoceratini and characters of *Teleoceras* from Prothero (2005:94) that are present in the GFS population. Those present are marked with '*,' those missing are marked with 'X,' and those that are a questionably synapomorphy or character are marked with '?.'

A. Synapomorphies of Teleoceratini	**GFS**
1. short, stumpy limbs with robust, flattened carpals, tarsals, and metapodials	*
2. a very brachycephalic skull with a flaring lambdoid crest and broad zygomatic arches	*
3. nasals that are U-shaped in cross-section, with or without a small terminal horn	*
4. a nasal incision retracted to anterior P3 (not as far as in aceratheriines)	?
5. a strong, lobal antecrochet on the upper molars	*
6. an elongate calcaneal tuber	*
B. Characters of *Teleoceras*	**GFS**
1. hypsodont teeth	X
2. strong antecrochets	*
3. greatly reduced premolars with deciduous first premolars lost and occasional loss of second premolars	*
4. thick cement on teeth	*
5. narrow nasals with strongly downturned lateral edges	*
6. enlarged premaxilla and upper first incisor	*
7. broad zygomatic arches	*
8. flaring lambdoid crests (skull semicircular in posterior view)	*
9. small terminal nasal horn and fused nasals	X
10. lower second incisor (tusk) shaped like a teardrop in cross-section	*
11. teleoceratine body proportions of a barrel-shaped trunk and short, robust limbs	X

Despite not having all synapomorphies and characters, this population is *Teleoceras* based on the large number of obviously teleoceratine features. Moreover, during the Hemphillian, *Aphelops* was the only other rhinocerotid genus in North America (Prothero 2005) and, given the morphological features already discussed, the GFS population is most certainly not *Aphelops* (Fig. 79). However, while there is no doubt that this population is of the genus *Teleoceras*, species determination is more difficult.

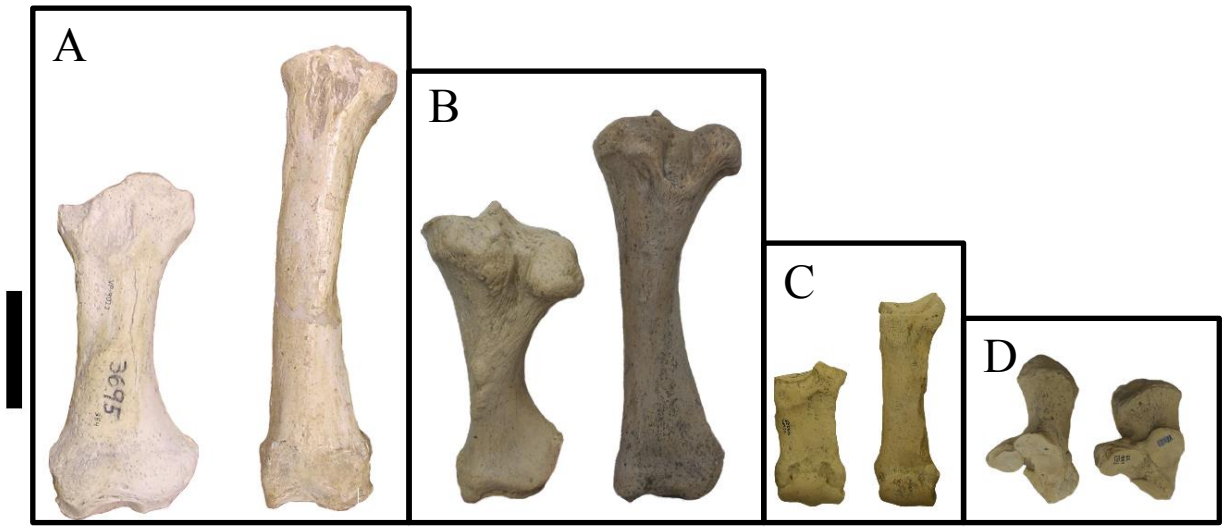

Figure 79. *Teleoceras* compared to *Aphelops*. *Teleoceras* is on the left and *Aphelops* is on the right. A; radius; B, tibia; C, third metacarpal; D, calcaneum. All specimens are from Long Island Quarry. Photo A is courtesy of Steven Wallace. Scale bar = 10 cm.

Data from GFS and Prothero (2005)

Prothero (2005) provides the most recent review of North American rhinos and documents cranial, post-cranial, and dental measurements of each species. Here, these data are graphed with data from the GFS specimens.

Skull Comparisons

Five of the 7 cranial measurements given by Prothero (2005) were reproduced on the GFS specimens. These measurements included: (1) distance between the upper second premolar to the occiput; (2) distance between the lambdoid crest and the nasals; (3) width at the zygomatic arches; (4) width of the occiput; and (5) height of the occiput. There is little to no variation between the average measurements of *Teleoceras* spp. given by Prothero (2005) and those from GFS (Fig. 80).

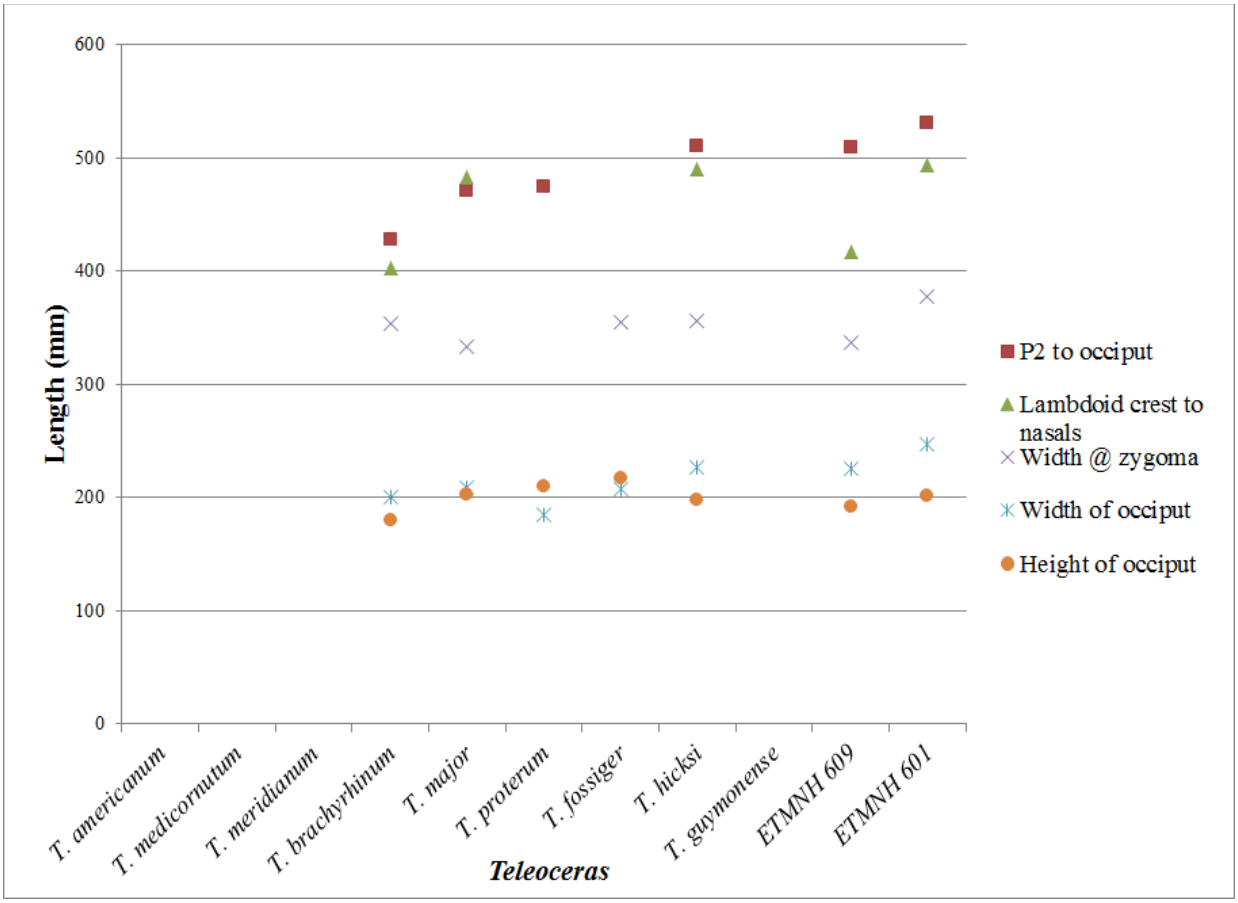

Figure 80. Skull measurements of *Teleoceras* species and the GFS specimens. All measurements and data are from Prothero (2005) except those of the GFS specimens. Lack of a data point indicates a missing measurement.

Similarly, there is little to no variation in the tooth row length measurements of *Teleoceras* spp. given by Prothero (2005) and those measured on the GFS specimens (Fig. 81). Only the upper complete row lengths of *T. fossiger* and *T. proterum* fall outside of the range created by the other species.

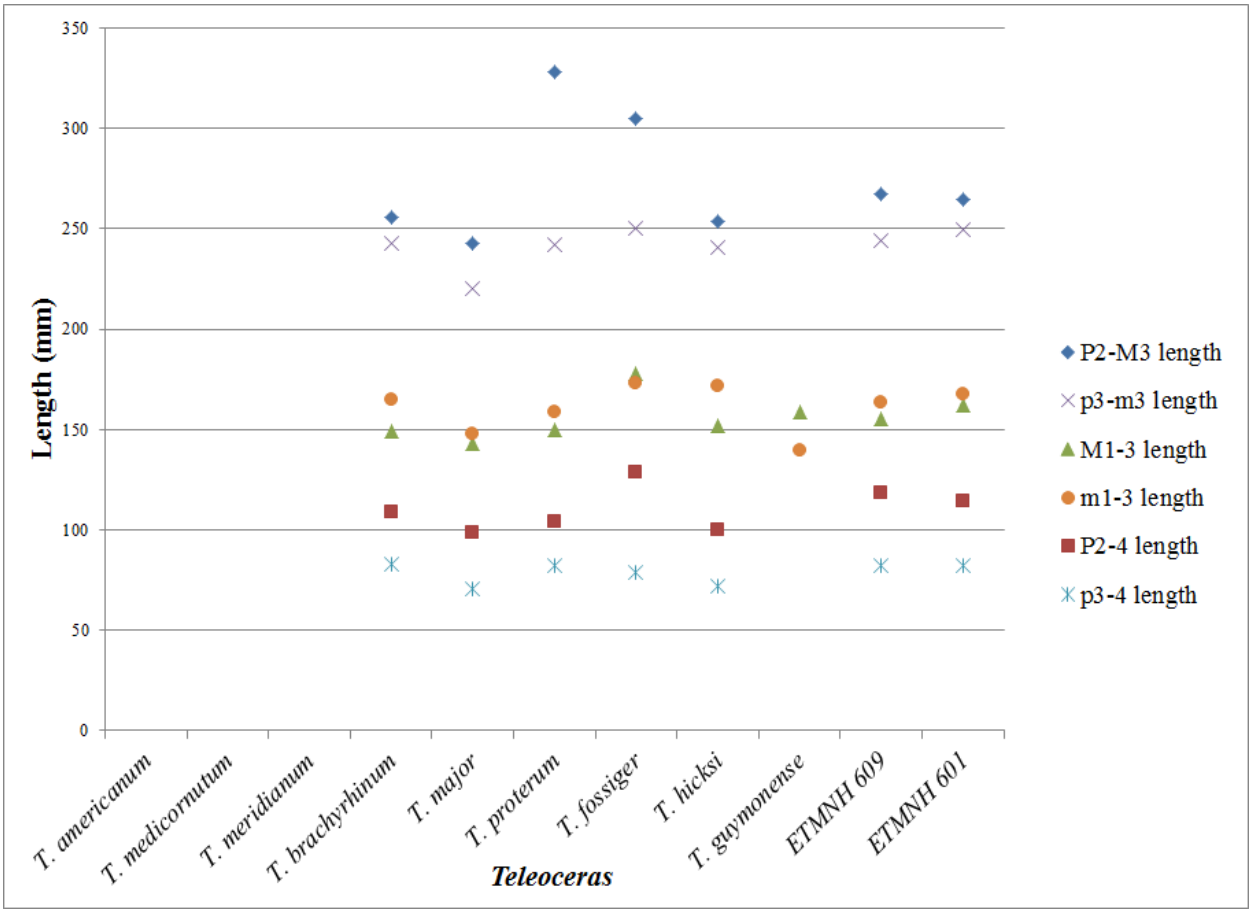

Figure 81. Dental measurements of *Teleoceras* species and the GFS specimens. All measurements and data are from Prothero (2005) except that of the GFS specimens. Lack of a data point indicates a missing measurement.

If the molar row length ranges given as size determinants in the diagnoses by Prothero (2005) are considered, there is considerable overlap among the 3 Hemphillian *Teleoceras* species

of interest (Fig. 82). Based on these measurements, Prothero (2005) describes *T. fossiger* as the largest species and *T. proterum* as the smallest. Upper molar row length indicates that the GFS rhino is within the range of both *T. fossiger* and *T. hicksi*. Lower molar row length indicates that the GFS rhino is within the range of both *T. proterum* and *T. hicksi*.

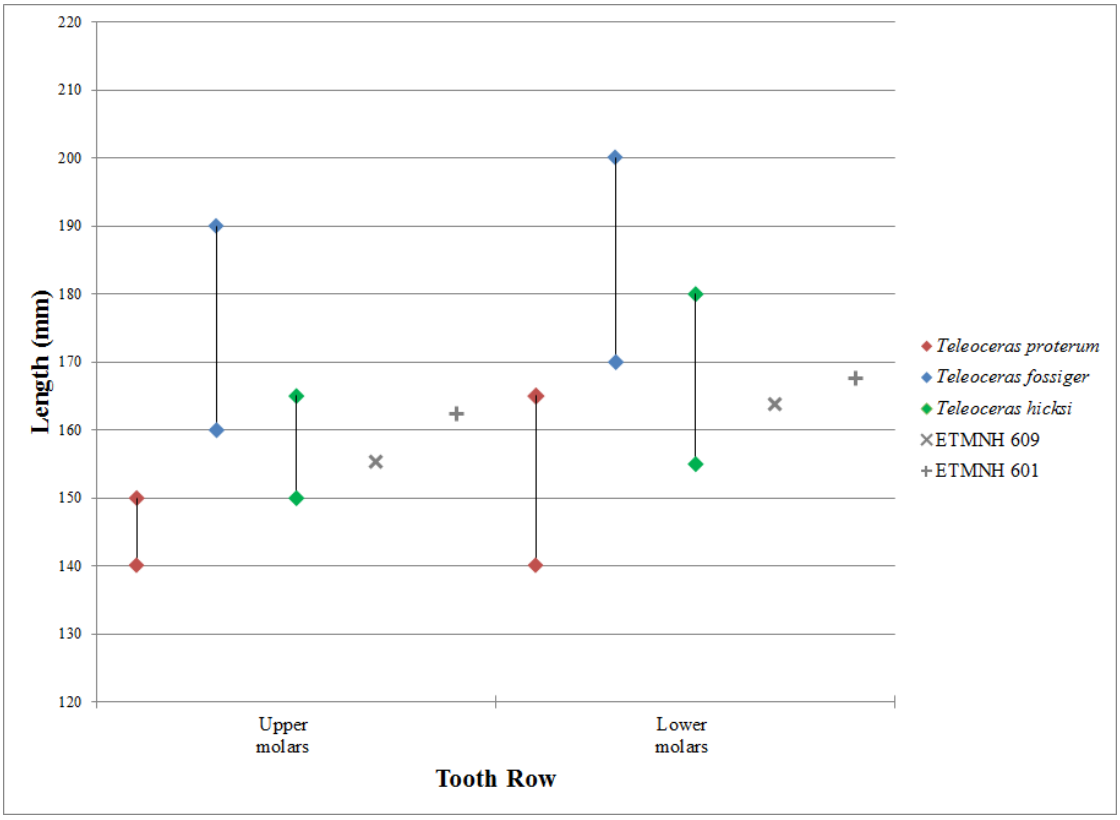

Figure 82. Molar row length measurements of the Hemphillian species of *Teleoceras* and the GFS population. Data are from Prothero (2005) except those of the GFS specimens.

Limb Comparisons

Length measurements of the post-cranial elements indicate that the GFS specimens are considerably larger than all of the *Teleoceras* species measured in Prothero (2005) (Fig. 83). The lengths of all long bones (humerus, radius, ulna, femur, and tibia) are outside of the size

ranges created by the 9 species. Interestingly, *Teleoceras meridianum* and *T. guymonense*, the 2 dwarf species according to Prothero (2005), fall within the length ranges created by all 9 species. Most length differences between GFS and the other *Teleoceras* rhinos are seen in the forelimb elements; there are smaller discrepancies in the lengths of the hind limb elements. In contrast to the long bones, the pedal elements (third metacarpal, calcaneum, and third metatarsal) are conservative and show very little variation between species and the GFS specimens.

In addition to overall length differences within each long bone element, there are relative proportional differences as well. Of the long bones from GFS, the tibiae are the most consistent within the genus and also display the greatest proportional differences when compared to the other elements (humerus, radius, ulna, and femur) from GFS. Compared to the data from Prothero (2005), *Teleoceras* from GFS also display a greater difference in length between the ulna and radius and humerus and radius. There is a smaller difference in length between the femur and ulna and humerus and ulna. These combinations suggest that the humerus, radius, and ulna are primarily responsible for the proportional differences seen in the GFS population.

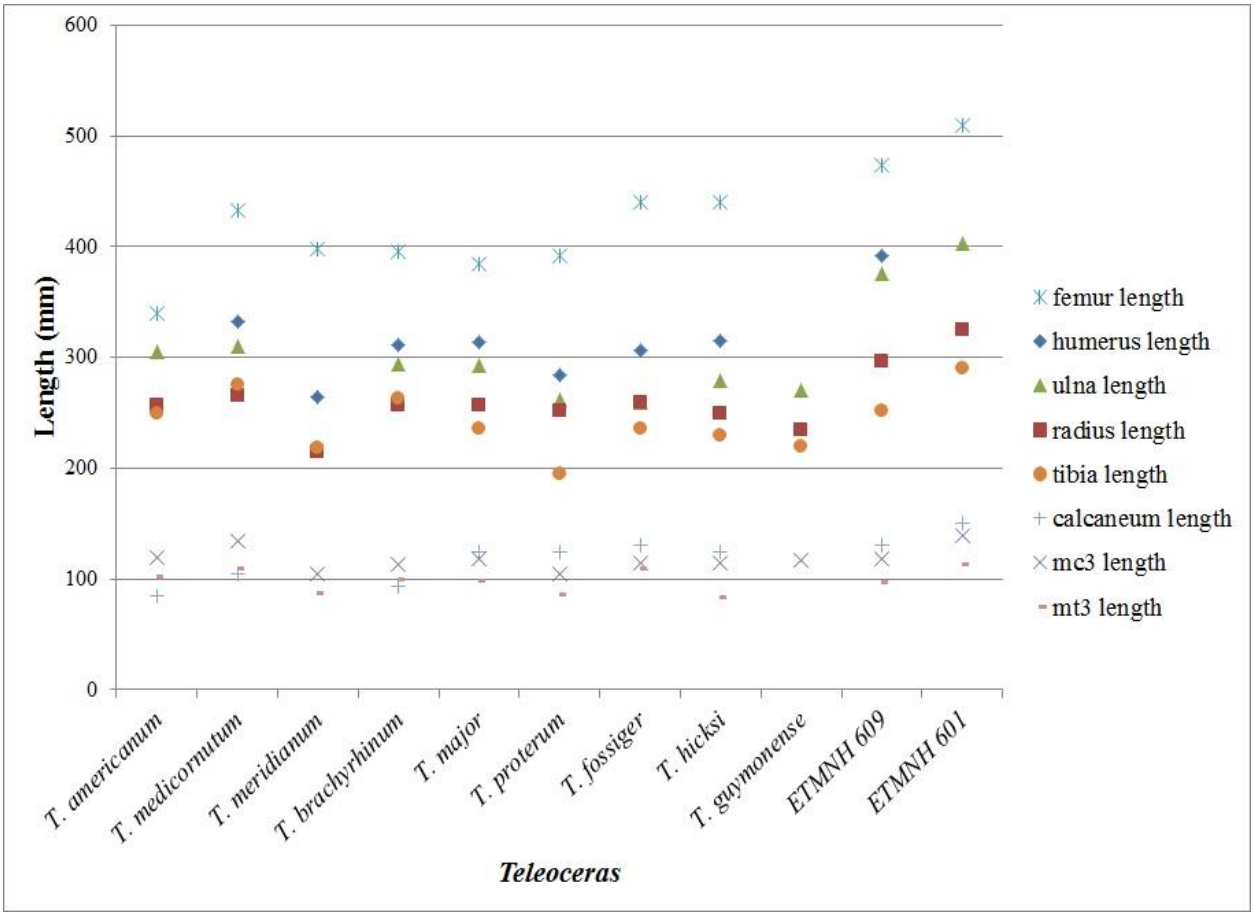

Figure 83. Lengths of limb elements from the *Teleoceras* species and the GFS specimens. All measurements and data are from Prothero (2005) except that of the GFS specimens. Lack of a data point indicates a missing measurement.

Data from GFS, Museum Visits, and Prothero (2005)

Once data from the museum visits are included with the data from Prothero (2005), it is possible to see the linear size trend within Hemphillian *Teleoceras*. This trend is shown in bivariate plots; however, there is a large amount of overlap amongst the species.

Humerus

Only 1 graph was produced for the humerus with the overall length plotted against the distal width (Fig. 84). Though Prothero (2005) gives a third measurement, midshaft width, it was not reproduced with enough confidence to be included here. In the single graph produced, there is a definite linear trend with the *Teleoceras proterum* of MF and LBB at the bottom and both *T. fossiger* of BTR and LIQ and the GFS specimens at the top. Interestingly, the data from Prothero (2005) do not fall within the range produced by the museum data.

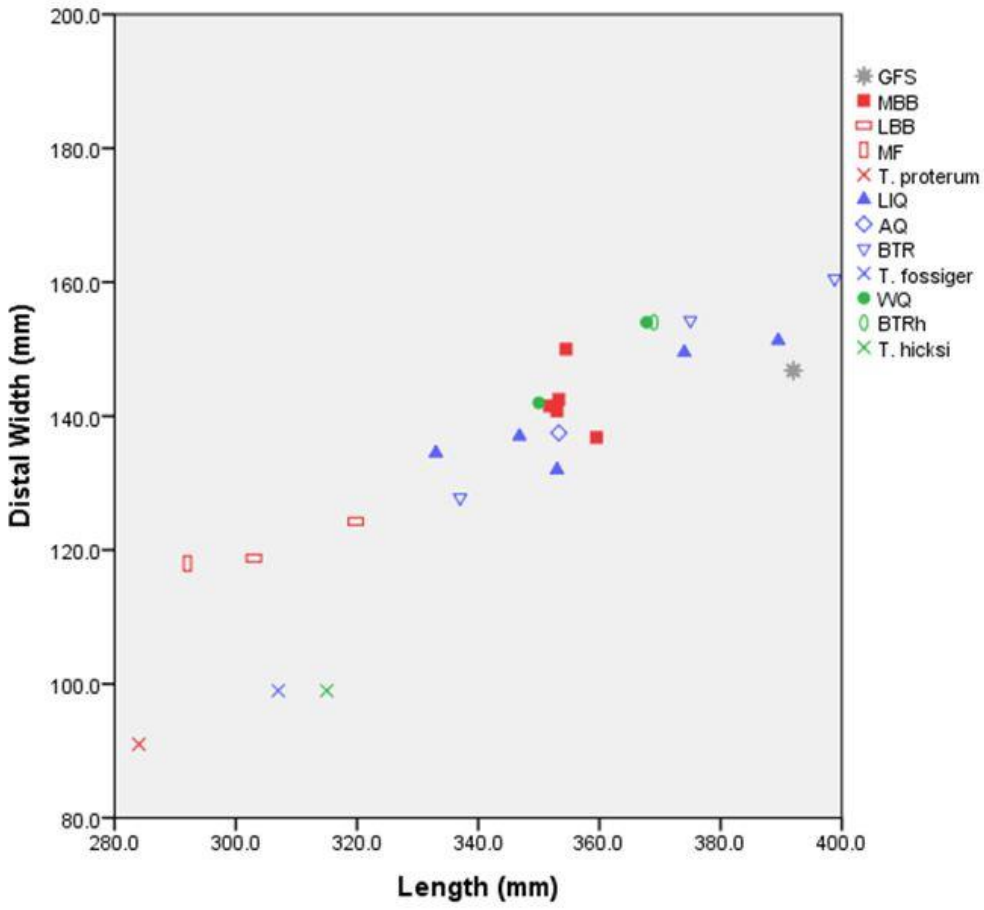

Figure 84. Bivariate graph showing length and distal width of humerus (mm). Data from Prothero (2005) are indicated by 'X's. Abbreviations are provided in Chapter 2.

Ulna

Only 1 graph was produced for the ulna with the length plotted against the midshaft width (Fig. 85). Again, the specimens form a group with a somewhat linear trend. The average measurements given by Prothero (2005) are plotted as the shortest and narrowest. Length is the greatest source of variation in this graph and, along that axis, the GFS specimens are the longest. However, the GFS specimens are within the normal range of midshaft width.

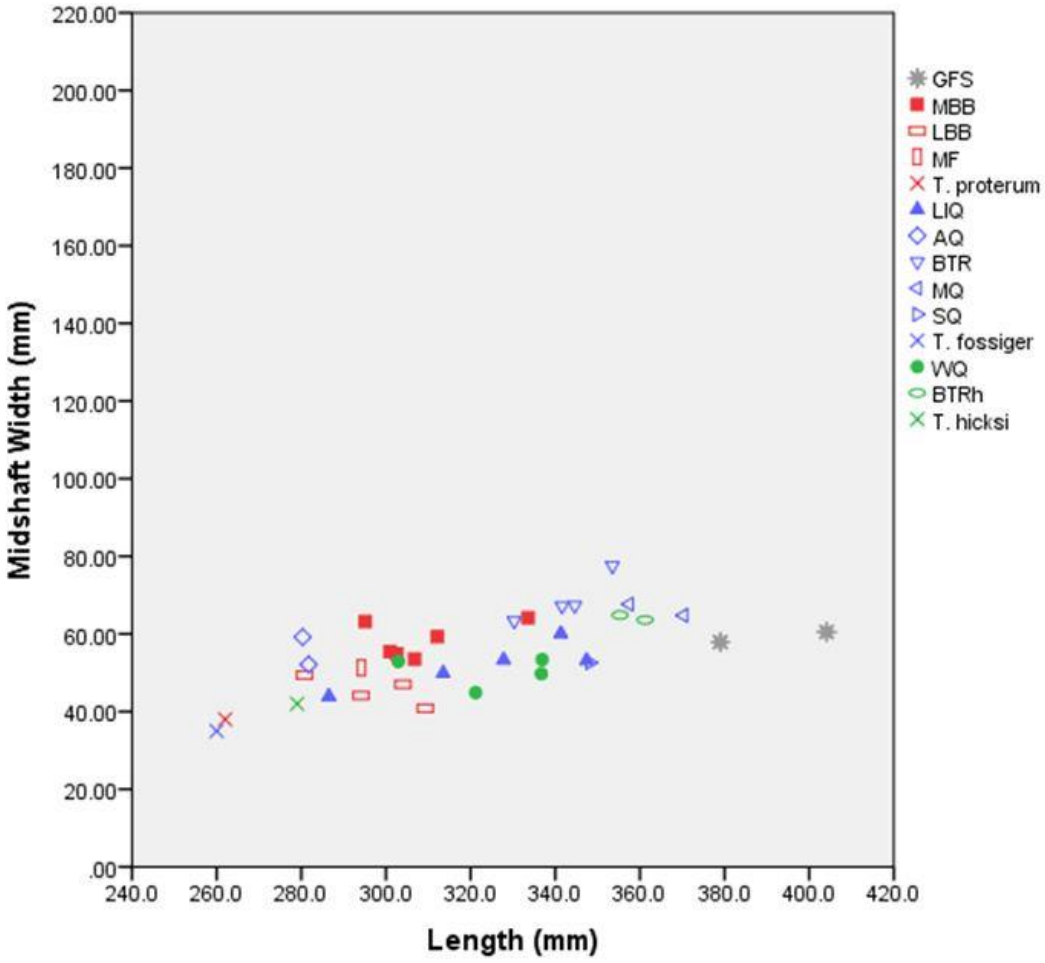

Figure 85. Bivariate graph showing length and midshaft width of the ulna (mm). Data from Prothero (2005) are indicated by 'X's. Abbreviations are provided in Chapter 2.

Radius

Four graphs were produced for the radius using measurements of the length, distal width, and midshaft width. When length was plotted against the distal width, the specimens formed a linear cluster with the averages from Prothero (2005) in the middle but with the GFS specimens separated from the group along the length axis (Fig. 86). For the most part, the distal width remained fairly consistent and most of the variation was seen in the length.

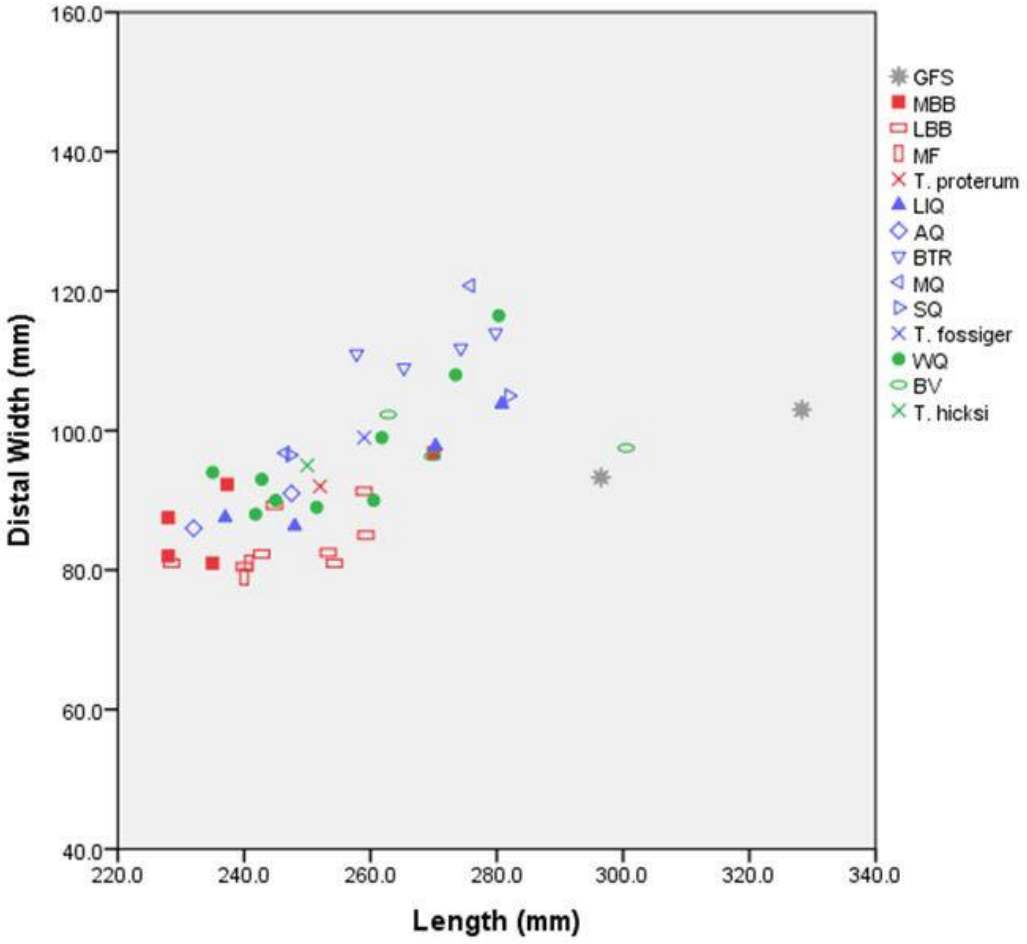

Figure 86. Bivariate graph of length and distal width of the radius (mm). Data from Prothero (2005) are indicated by 'X's. Abbreviations are provided in Chapter 2.

Also for the radius, length was plotted with the midshaft width (Fig. 87). In this case, as in the previous, the comparative specimens form a group with an obvious trend. The GFS specimens fall outside of this trend because the midshaft widths show little variation while the lengths are quite different.

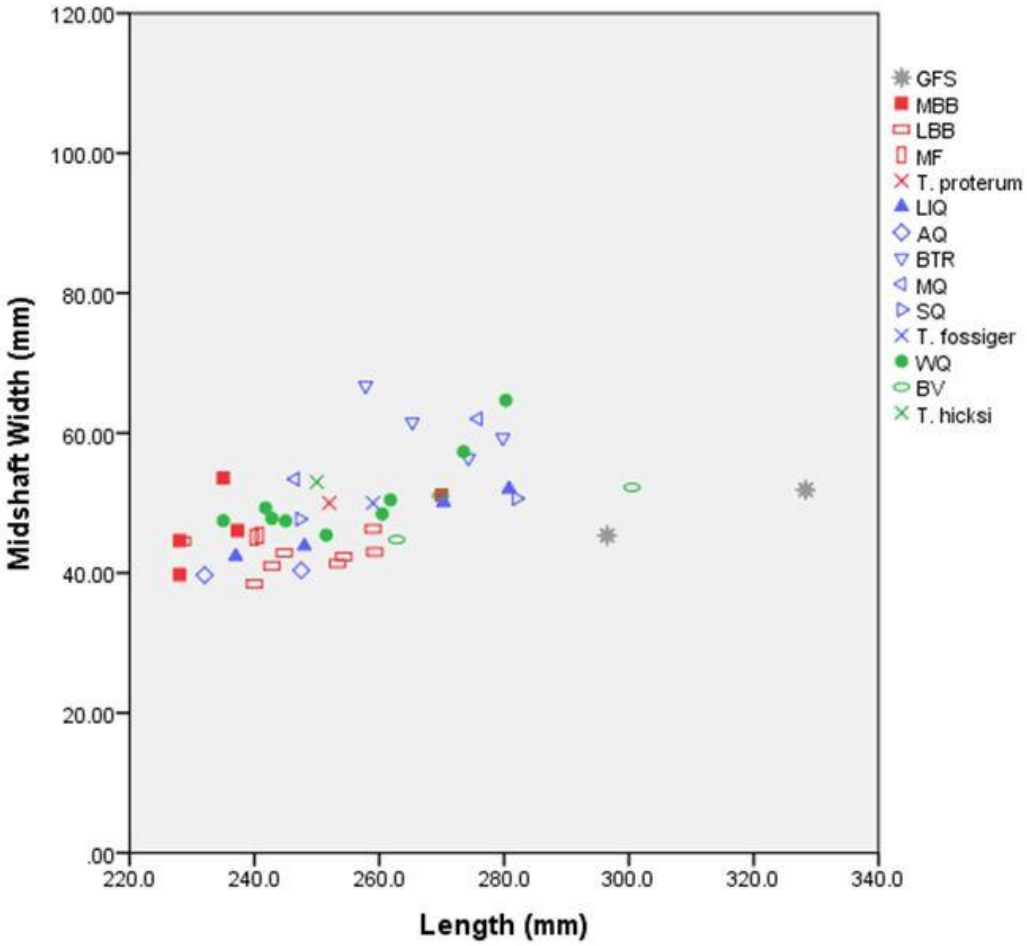

Figure 87. Bivariate graph of length and midshaft width of the radius (mm). Data from Prothero (2005) are indicated by 'X's. Abbreviations are provided in Chapter 2.

Finally, the midshaft and distal widths of the radii were plotted and formed a linear trend with the data from Prothero (2005) and GFS in the middle (Fig. 88). For the most part, localities

containing *Teleoceras proterum* are at the bottom and those containing *T. hicksi* and *T. fossiger* are at the top. Because the GFS specimens are localized within the cluster, it can be concluded that width proportions do not vary from the other *Teleoceras*. But, combined with the previous graphs, this suggests that the proportional differences are seen primarily in the length.

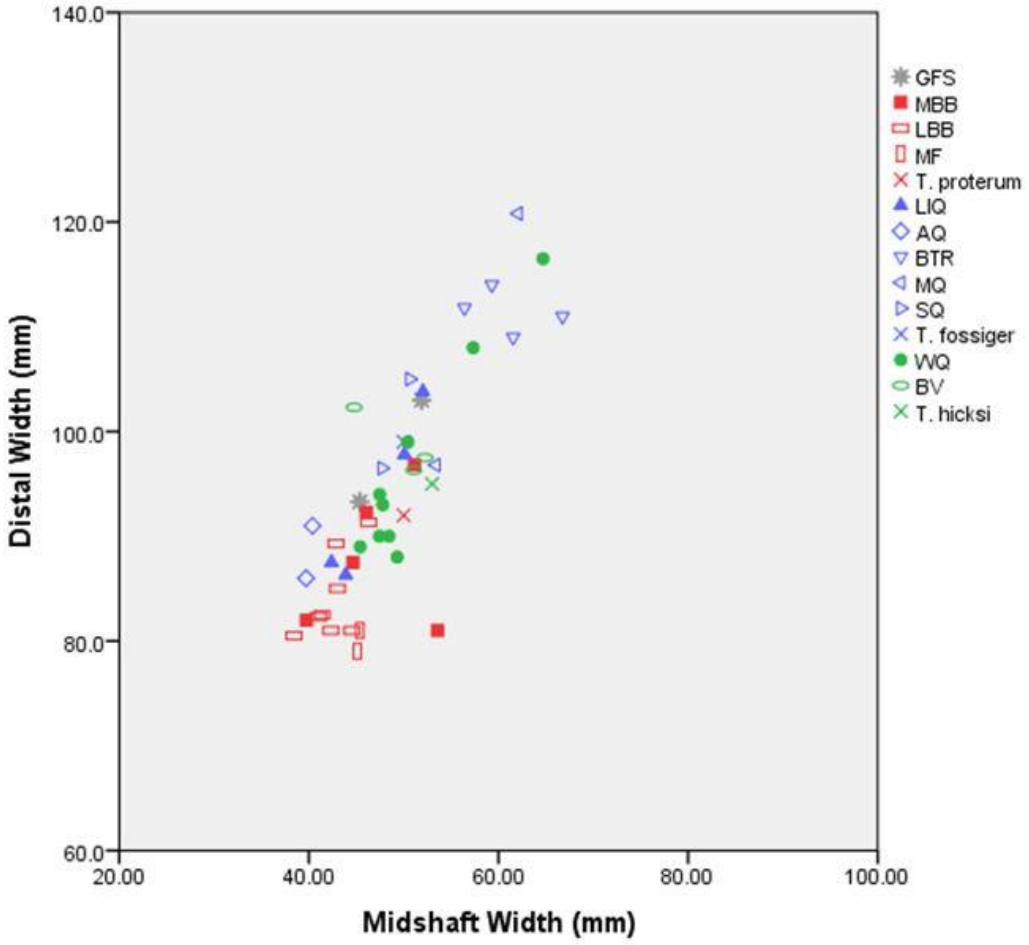

Figure 88. Bivariate graph of midshaft width and distal width of the radius (mm). Data from Prothero (2005) are indicated by 'X's. Abbreviations are provided in Chapter 2.

These radial measurements can also be graphed in 3 dimensions (Fig. 89). This graph emphasizes the large differences in length but also the consistency of the midshaft and distal widths seen in the GFS specimens.

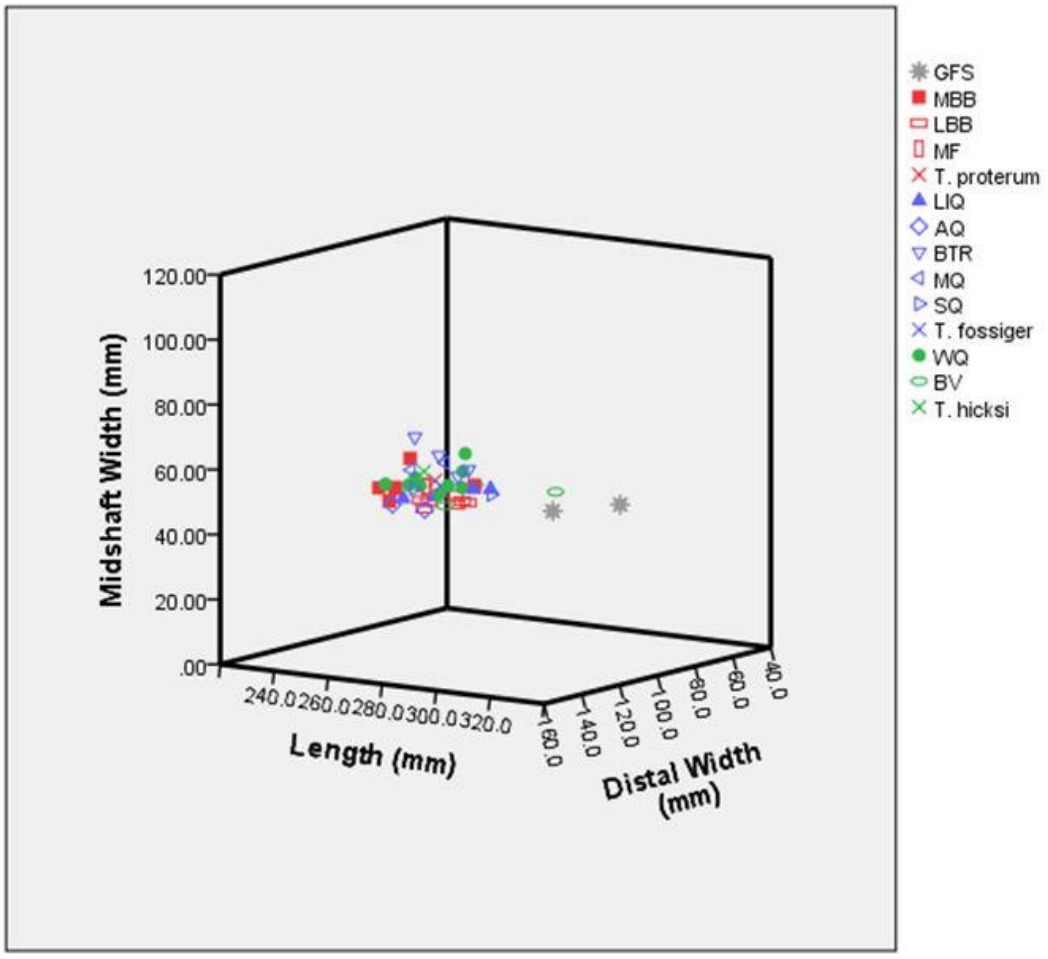

Figure 89. Three-dimensional graph of length, midshaft width, and distal width of the radius (mm). Data from Prothero (2005) are indicated by 'X's. Abbreviations are provided in Chapter 2.

Third Metacarpal

One graph was produced for the third metacarpal using the length and proximal width (Fig. 90). The third metacarpals produce less overlap amongst the species with *Teleoceras*

proterum at the small end and *T. fossiger* and *T. hicksi* overlapping at the large end. Again, though, the proximal width of the GFS specimens stays fairly consistent so that most of the change is seen in the length. However, only ETMNH 601 is outside the cluster but is still within the linear trend formed by the comparative specimens.

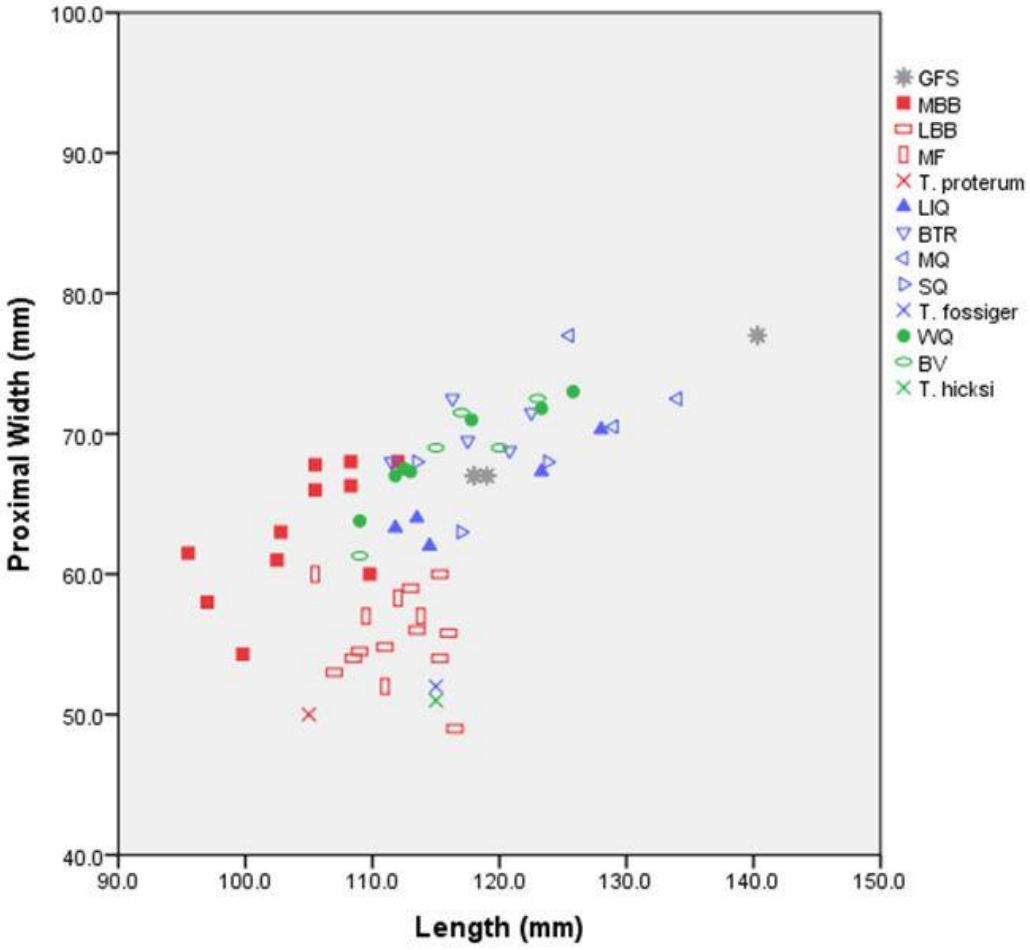

Figure 90. Bivariate graph of length and proximal width of the third metacarpal (mm). Data from Prothero (2005) are indicated by 'X's. Abbreviations are provided in Chapter 2.

Femur

Four graphs were produced for the femur using measurements of length, distal width, and midshaft width. When length and distal width were plotted, there was a linear trend with the GFS specimens at the larger end of the length axis amongst primarily *Teleoceras fossiger* specimens (Fig. 91). In this case, neither distal width nor length are particularly distinct from the other specimens.

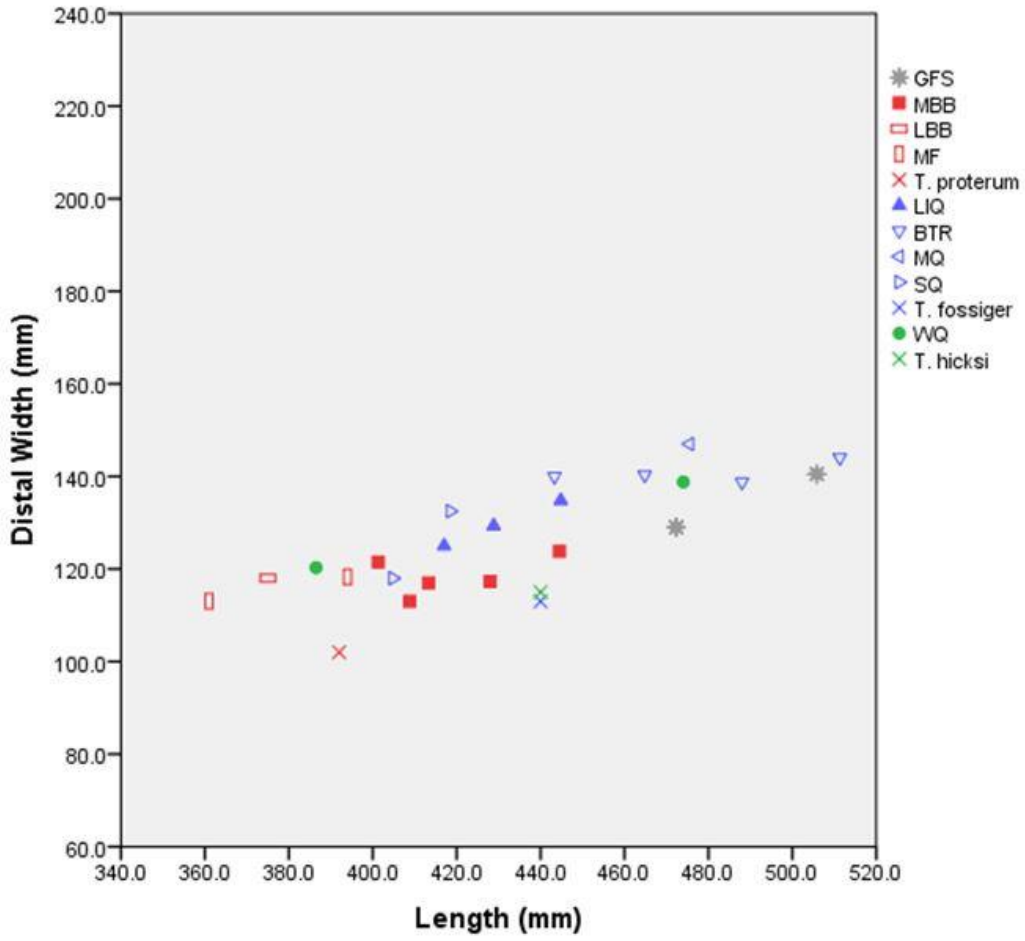

Figure 91. Bivariate graph of length and distal width of the femur (mm). Data from Prothero (2005) are indicated by 'X's. Abbreviations are provided in Chapter 2.

Length and midshaft width produced a graph very similar to that of length and distal width (Fig. 92). In this case, midshaft width is constant and length is the primary source of variation; however, though, the GFS specimens are at the larger end, they are in no way distinct.

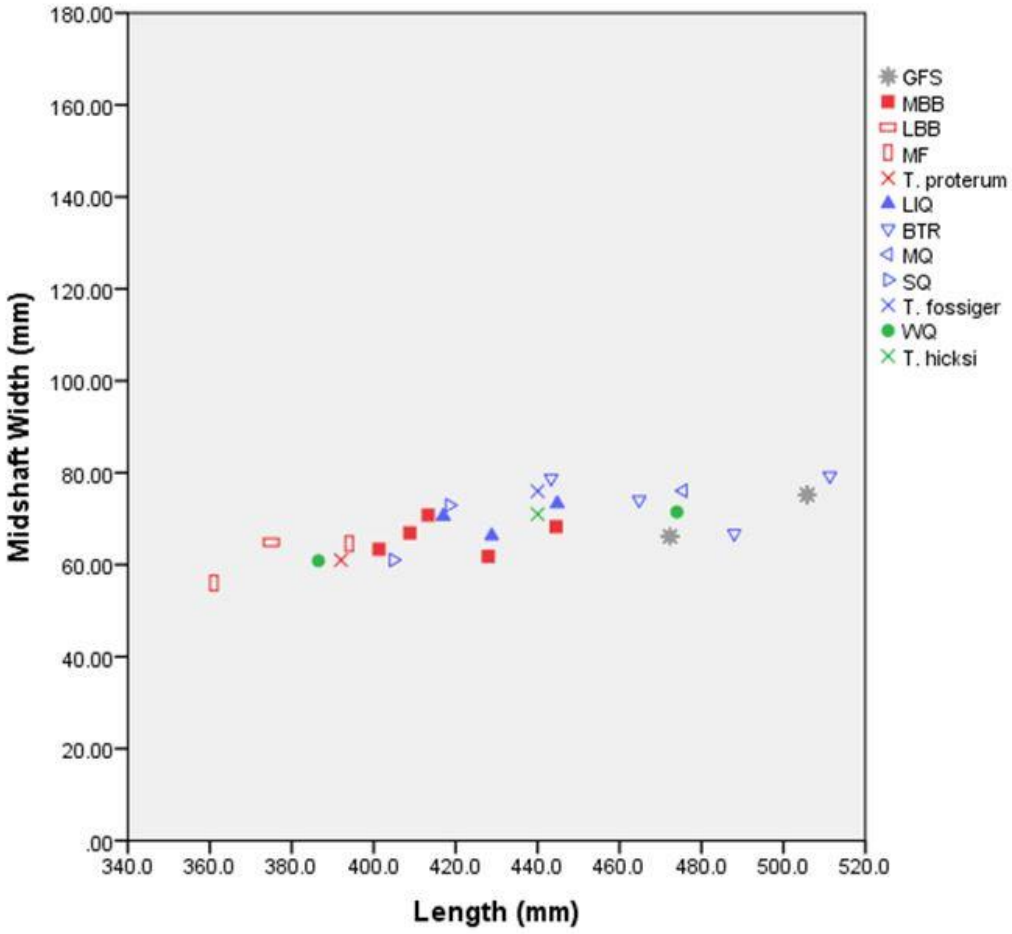

Figure 92. Bivariate graph of length and midshaft width of the femur (mm). Data from Prothero (2005) are indicated by 'X's. Abbreviations are provided in Chapter 2.

Midshaft width and distal width generated a graph with GFS amidst the cluster of comparative specimens (Fig. 93). In this case, midshaft width stays relatively constant and distal

width is the primary source of variation. Like in previous femora graphs, the GFS specimens are not proportionally remarkable.

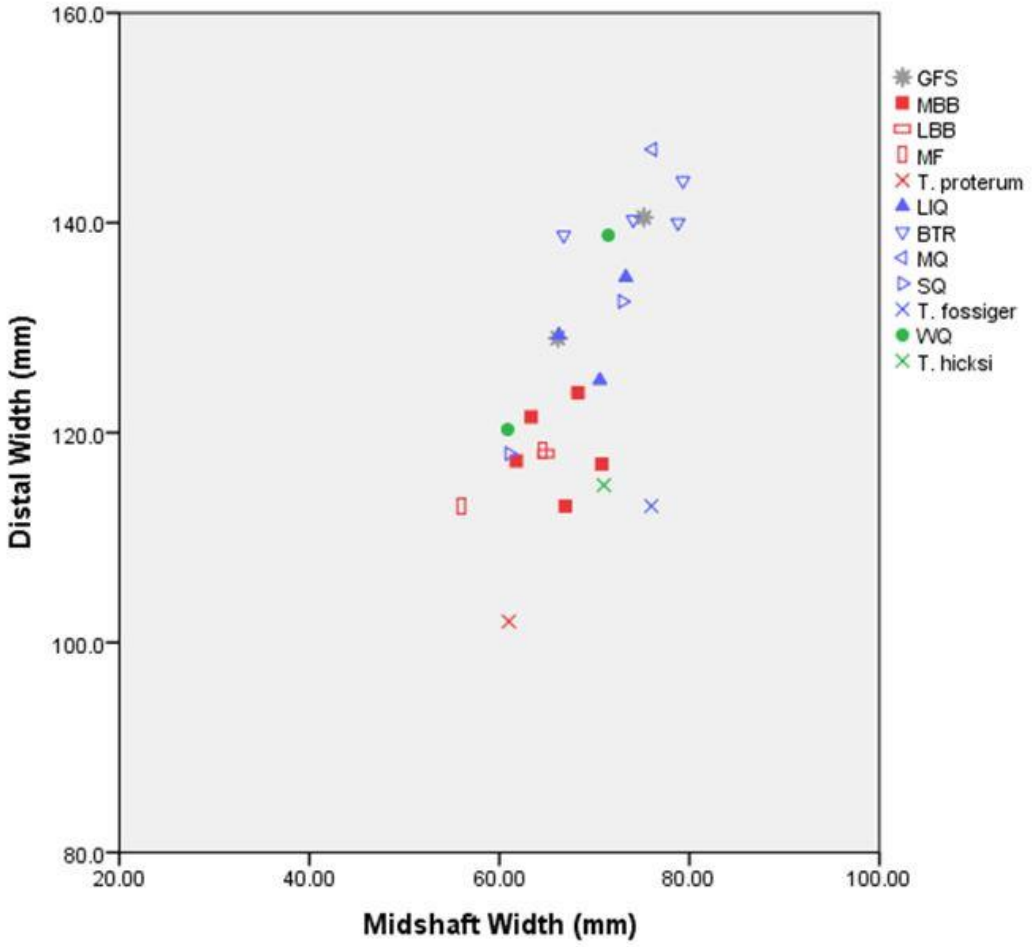

Figure 93. Bivariate graph of midshaft and distal widths of the femur (mm). Data from Prothero (2005) are indicated by 'X's. Abbreviations are provided in Chapter 2.

These femoral measurements can also be graphed in 3 dimensions (Fig. 94). Obviously, the femur is long for *Teleoceras* but it is not distinct as with some other elements, and both the midshaft and distal widths are well within the normal range.

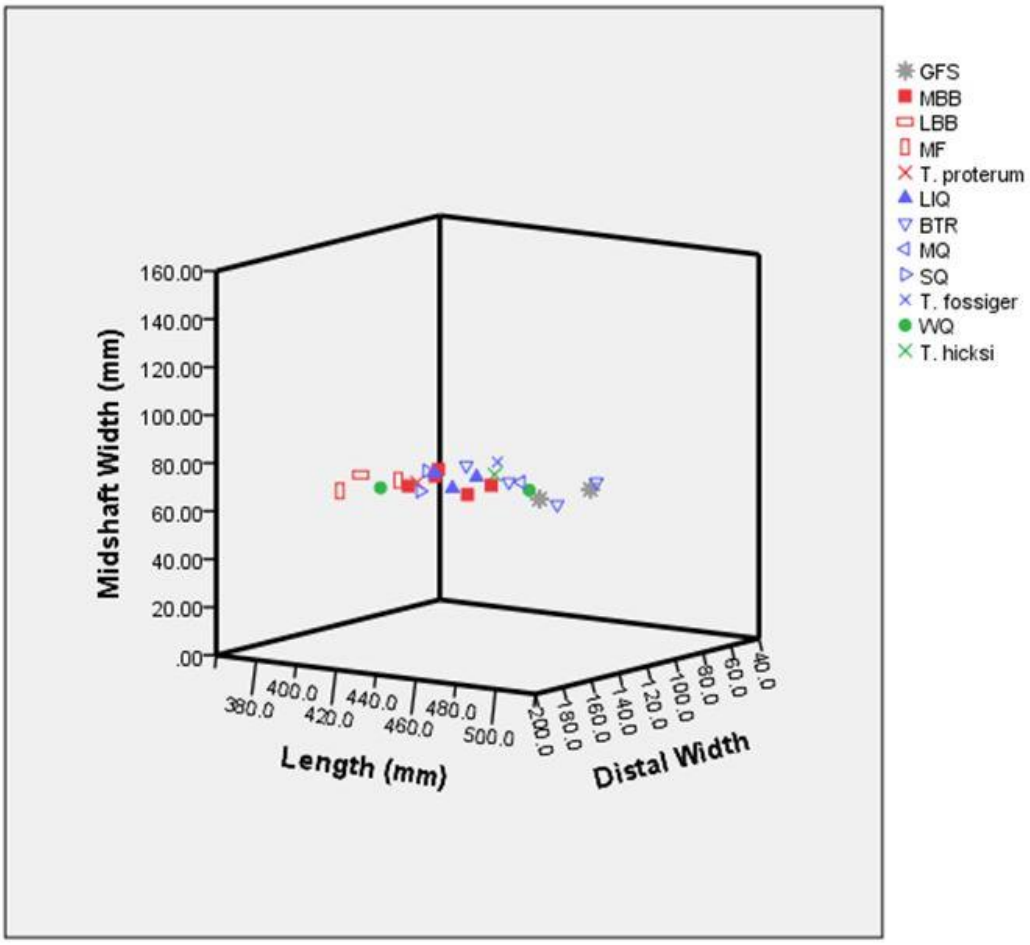

Figure 94. Three-dimensional graph of the length, midshaft width, and distal width of the femur (mm). Data from Prothero (2005) are indicated by 'X's. Abbreviations are provided in Chapter 2.

Tibia

Four graphs were generated for the tibia using measurements of length, distal width, and midshaft width. Again, a linear trend was produced in the graph of length and distal width (Fig. 95). For the most part, the GFS specimens fall within this trend; although, ETMNH 601 lies outside of the cluster because of its long length.

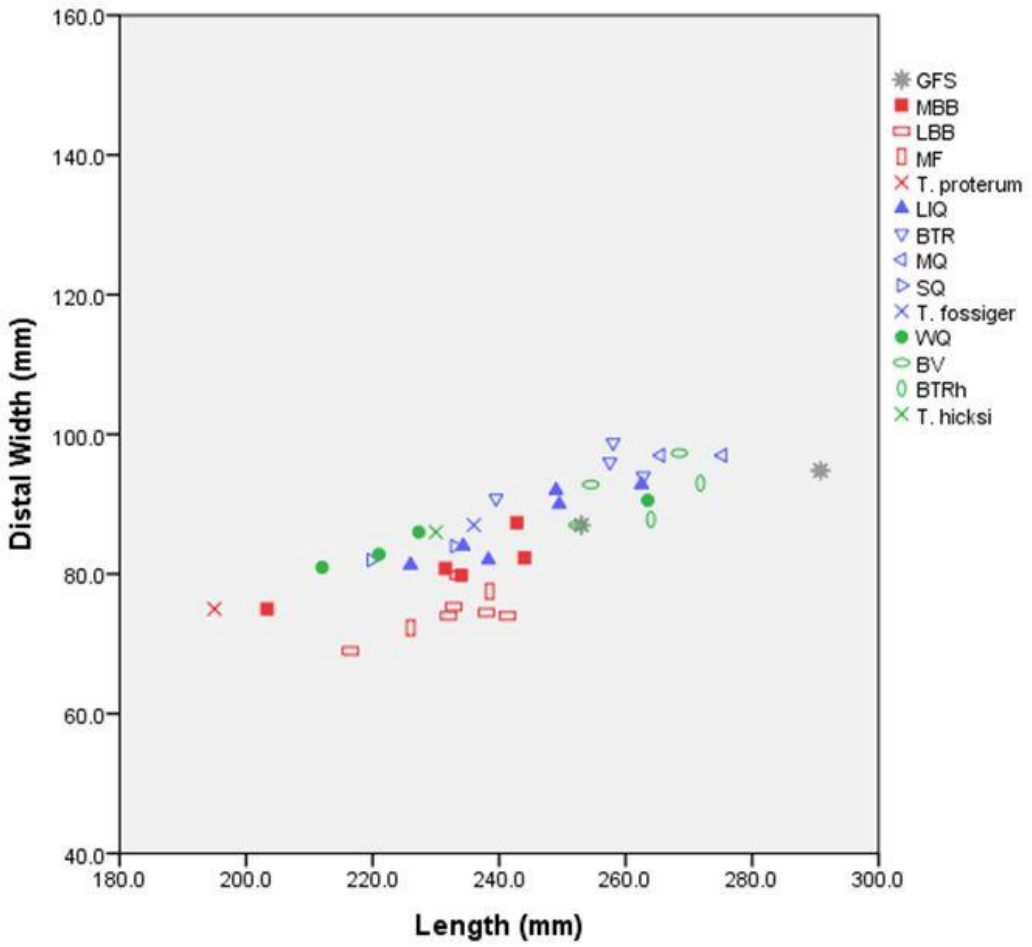

Figure 95. Bivariate graph of length and distal width of the tibia (mm). Data from Prothero (2005) are indicated by 'X's. Abbreviations are provided in Chapter 2.

As with length and distal width, length and midshaft width created a linear cluster (Fig. 96). Also as before, the midshaft width varies little so most of the differences are seen in the length. While ETMNH 609 is within the cluster, ETMNH 601 is outside of the cluster and, thus, is longer than the other specimens but still falls along the trend formed by the comparative specimens.

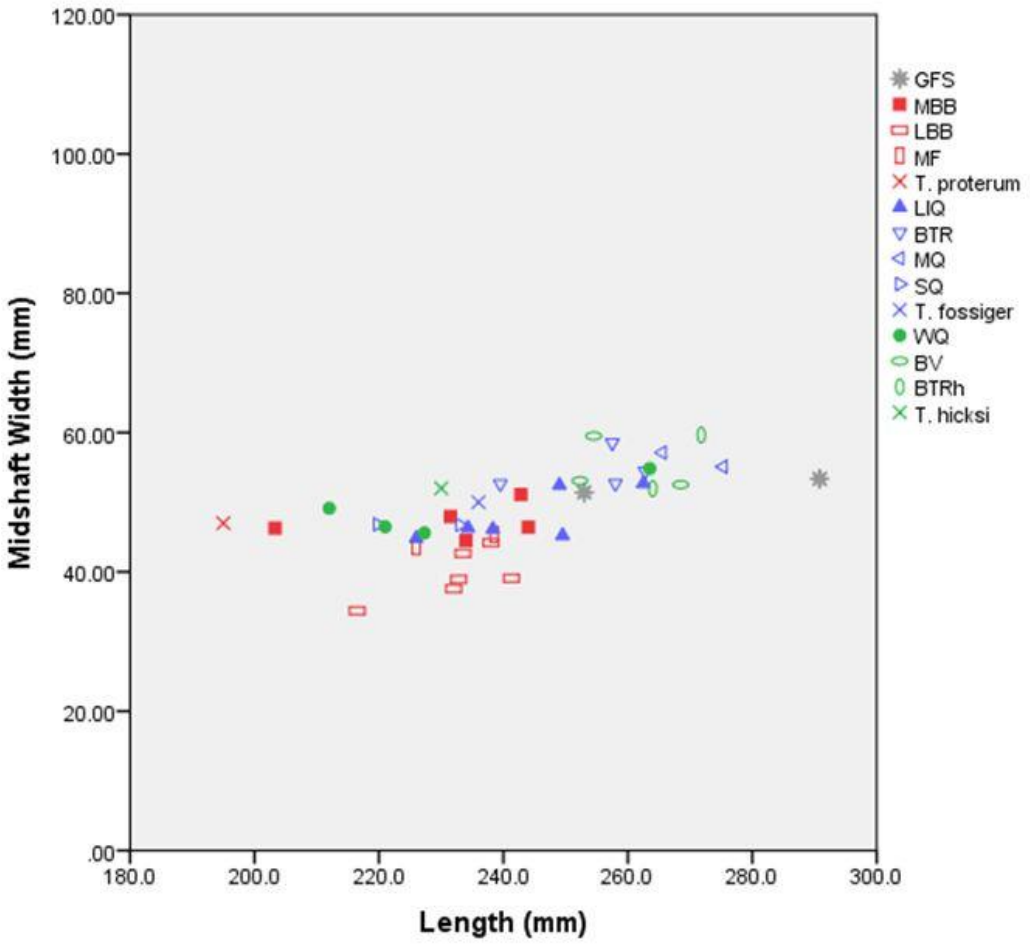

Figure 96. Bivariate graph of length and midshaft width of tibia (mm). Data from Prothero (2005) are indicated by 'X's. Abbreviations are provided in Chapter 2.

A typically linear trend was generated by the midshaft width and distal width of the tibiae (Fig. 97). Also, as is typical, the localities containing *Teleoceras proterum* are at the small end and localities containing *T. hicksi*, *T. fossiger*, and the GFS specimens are at the large end; although, there is overlap among all. When addressing only the widths, the GFS specimens are in the middle of the linear cluster, suggesting, again, that length is the source of most variation.

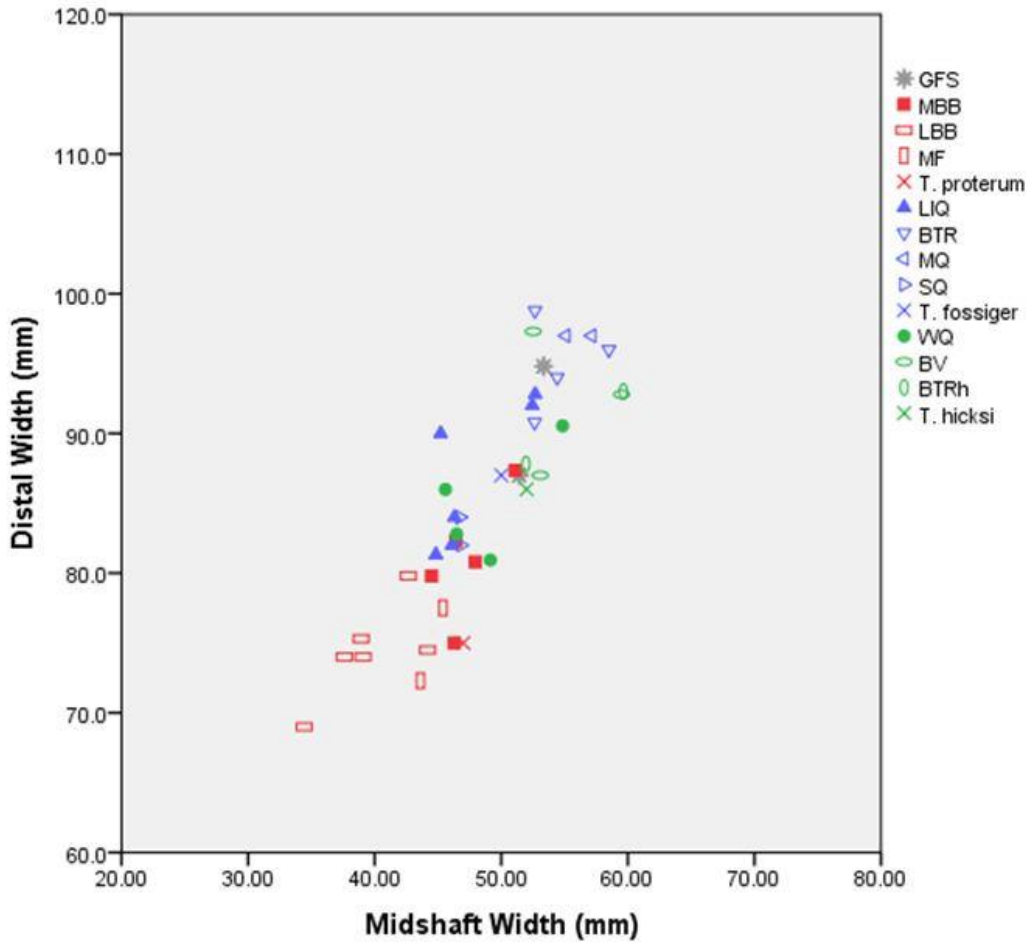

Figure 97. Bivariate graph of midshaft width and distal width of the tibia (mm). Data from Prothero (2005) are indicated by 'X's. Abbreviations are provided in Chapter 2.

These tibial measurements can also be graphed in 3 dimensions (Fig. 98). In this case, ETMNH 609 is amidst the linear cluster of specimens and ETMNH 601 stands out as longer than the others.

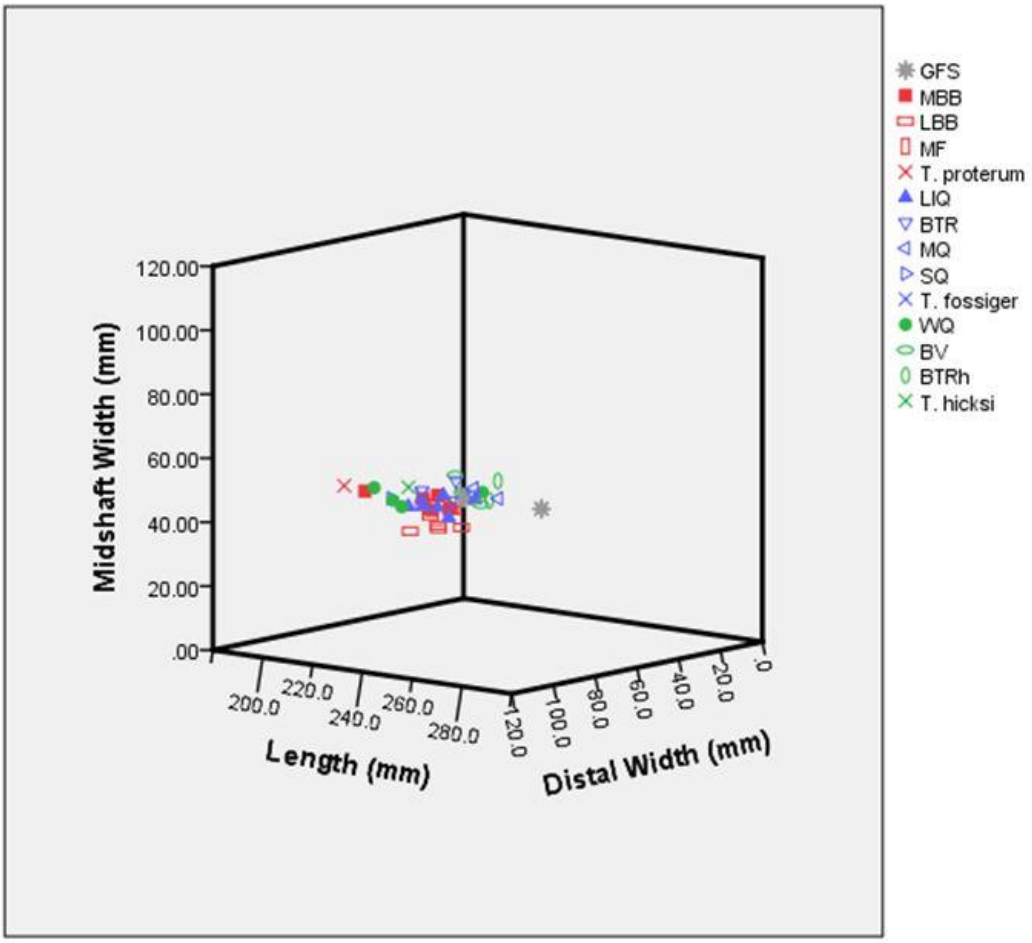

Figure 98. Three-dimensional graph of length, midshaft width, and distal width of the tibia (mm). Data from Prothero (2005) are indicated by 'X's. Abbreviations are provided in Chapter 2.

Calcaneum

One graph was produced for the calcaneum using the length and the sustentacular width (Fig. 99). There is a linear trend from *Teleoceras proterum* of Mixson's Bone Bed to *T. fossiger* of Minium Quarry. Calcanea of the GFS specimens are not remarkably different from the other *Teleoceras* calcanea and are plotted within the cluster but they are on the larger side of the graph.

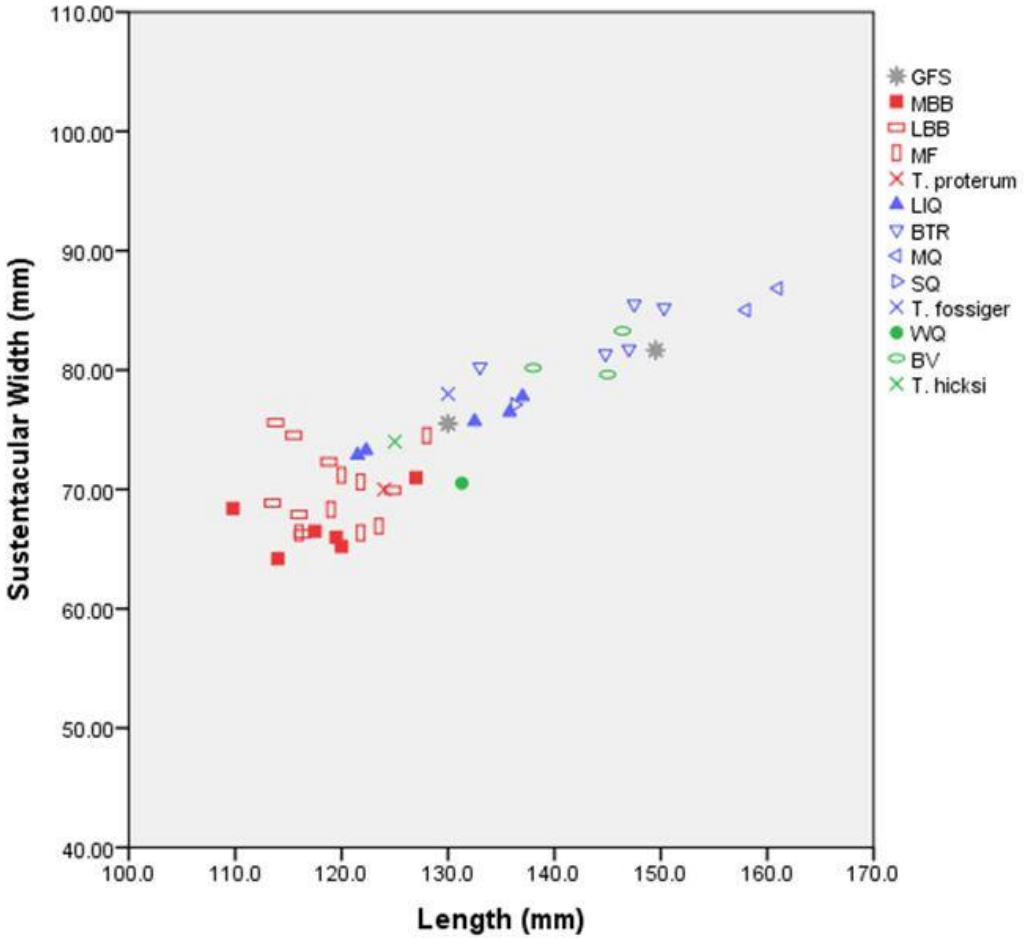

Figure 99. Bivariate plot of length and sustentacular width of the calcaneum (mm). Data from Prothero (2005) are indicated by 'X's. Abbreviations are provided in Chapter 2.

Third Metatarsal

One graph was produced for the third metatarsal using length and proximal width (Fig. 100). This graph does not have the tightly constricted linear cluster as seen in previous graphs but a slight trend is still present. As is typical, the localities considered to have *Teleoceras proterum* tend to plot at the bottom and those with *T. fossiger* are near the top; however, there is a good amount of overlap amongst the 3 species.

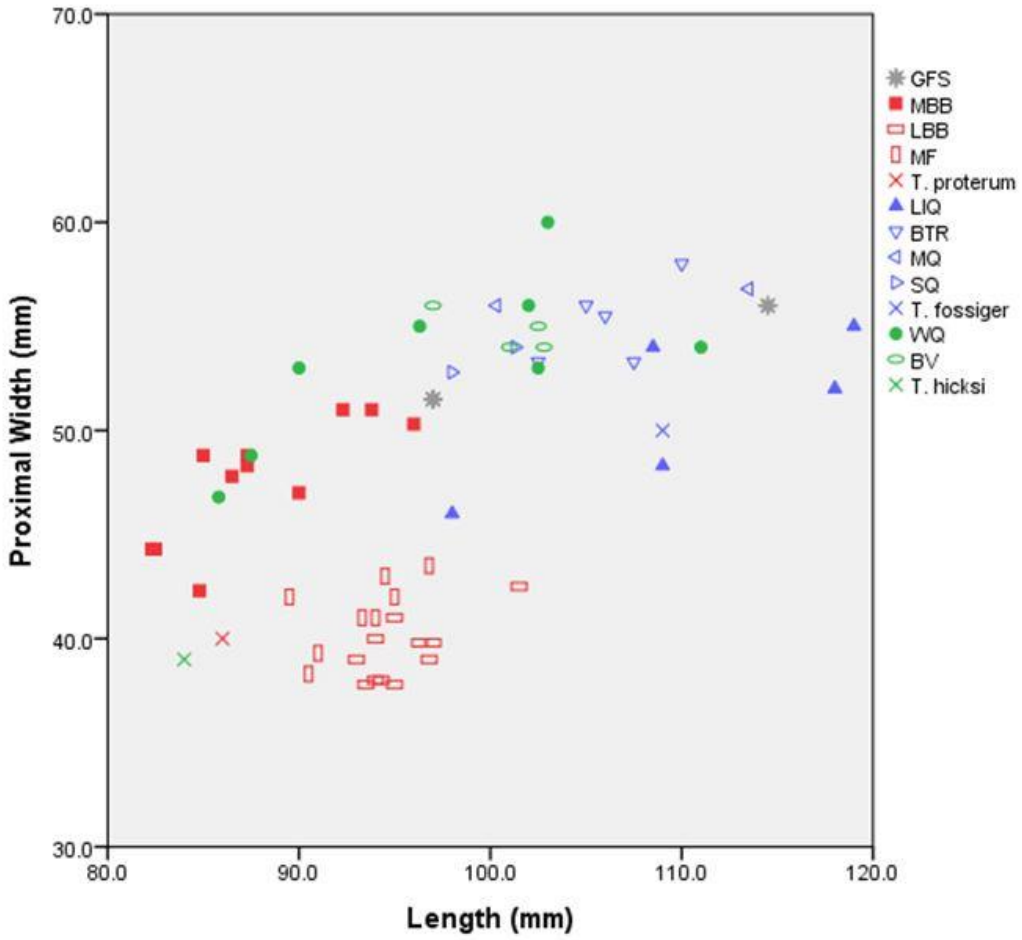

Figure 100. Bivariate graph of length and proximal width of the third metatarsal (mm). Data from Prothero (2005) are indicated by 'X's. Abbreviations are provided in Chapter 2.

Statistical Analyses

Gray Fossil Site

Like with the bivariate graphs, statistical analyses generated better separation in analyses of the forelimb elements than of the hind limb elements. While some PCAs produced separation, DAs were unable to consistently assign the GFS specimens with only 1 type locality (Appendix 5).

Unstandardized Principal Components Analyses. Frequently, PCAs of unstandardized data were not able to produce good separation between species. Typically, localities with *Teleoceras proterum* plot toward 1 extreme and those with *T. hicksi* and *T. fossiger* plot toward the other extreme; however, in the middle, there is a large amount of overlap between all of the localities and the 3 species. Because these data are unstandardized, this separation is caused primarily by overall size rather than morphology or proportional relationships. In most cases, the GFS specimens plot near the larger extreme with *T. hicksi* and *T. fossiger*.

Analyses including all of the comparative localities and only a partial set of measurements produced 1 component for every element except the ulna and tibia. In each, the specimens formed a bell curve with a high degree of overlap. Even with 2 components, neither the ulna nor the tibia produced good separation between the species.

With only specimens from the type localities and GFS, the radius, femur, calcaneum, and third metatarsal all produced only 1 component, and all graphed as a bell curve with a large amount of overlap. Even with 2 components each, the humerus, third metacarpal, and tibia produced very little separation between the species as did the ulna, which had 3 components.

With only the type localities and GFS included and all of the measurements used, the radius, femur, calcaneum, and third metatarsal produced 1 component that each graphed as a bell curve with overlap between the localities. Again, the humerus, third metacarpal, and tibia each produced 2 components and only the humerus formed separate groups (Fig. 101). However, this could be caused by the unfortunately small sample sizes, which was necessary to include all of the measurements. The ulna, with 3 components, has somewhat distinct groupings but very little separation between the groups.

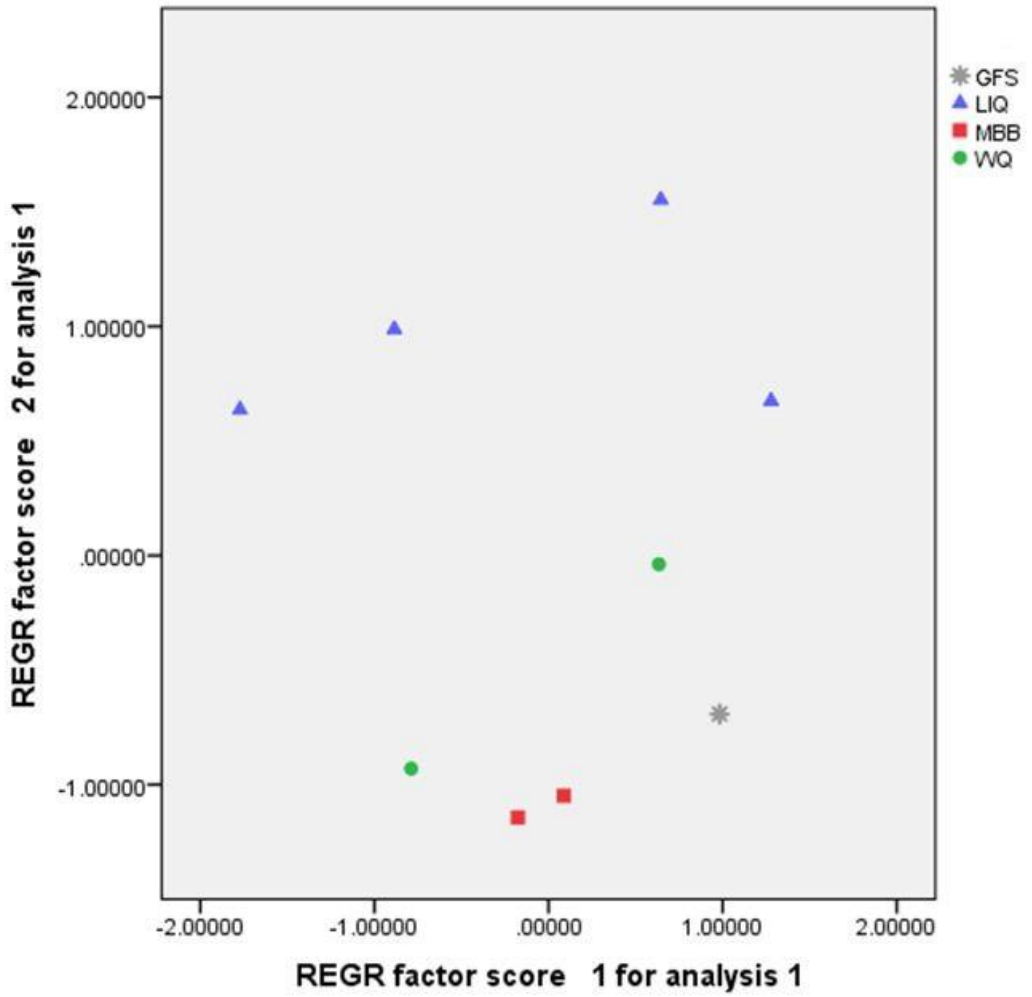

Figure 101. Principal components analysis of humeri from the type localities and GFS using the full set of unstandardized measurements. Abbreviations are provided in Chapter 2.

Standardized Principal Components Analyses. PCAs of standardized data were also typically not able to produce good separation between the species. With standardized data, the overall size of the specimens is no longer a factor, so the results are based on proportional relationships. In most of these analyses, there was even less separation between the localities and

the species than was seen in the previous analyses and there is no consistent pattern to describe where the GFS specimens plot in these analyses.

Analyses including all of the comparative localities and only a partial set of measurements produced 1 component for the radius, third metacarpal, calcaneum, and third metatarsal. In each of these, the specimens formed a bell curve with a high degree of overlap and no obvious separation. Even with 2 components, the humerus, femur, and tibia lacked separation of any kind. Finally, even with 3 components, the ulna also could not separate into clear groupings.

With only the type localities included, the third metacarpal, tibia, calcaneum, and third metatarsal each produced 1 component and all graphed as bell curves with large amounts of overlap. Only the third metatarsal graphed the GFS specimens in the middle rather than at an extreme, which is consistent with the morphological conservativeness of *Teleoceras* foot elements. Interestingly, the analysis of the radius produced only 1 component and the GFS specimens plotted separately from all of the other specimens (Fig. 102). With 2 components, the analysis of the humerus graphed with very little separation between species. Both the ulna and the femur produced graphs with 3 components, though the ulnae were able to produce better separation (Fig. 103).

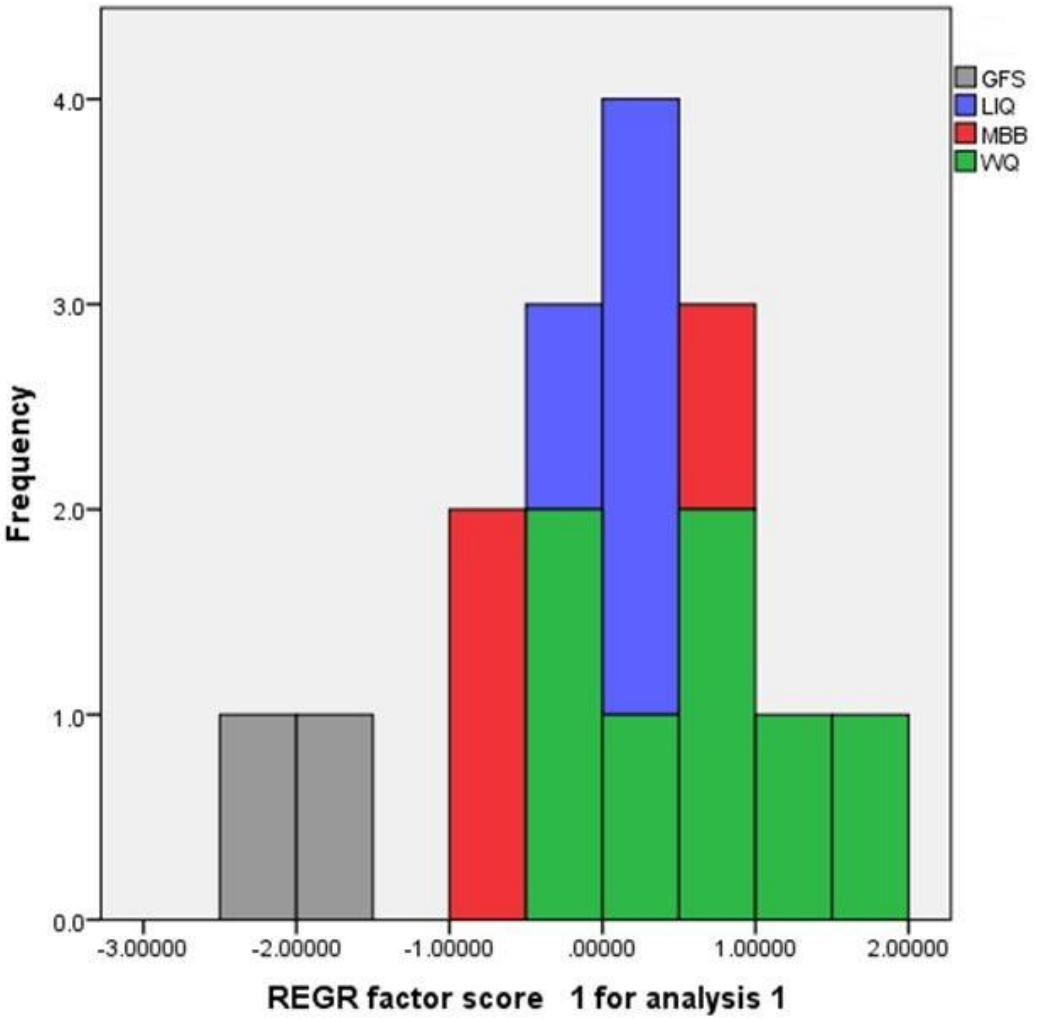

Figure 102. Principal components analysis of radii from the type localities and GFS using the partial set of standardized measurements. Abbreviations are provided in Chapter 2.

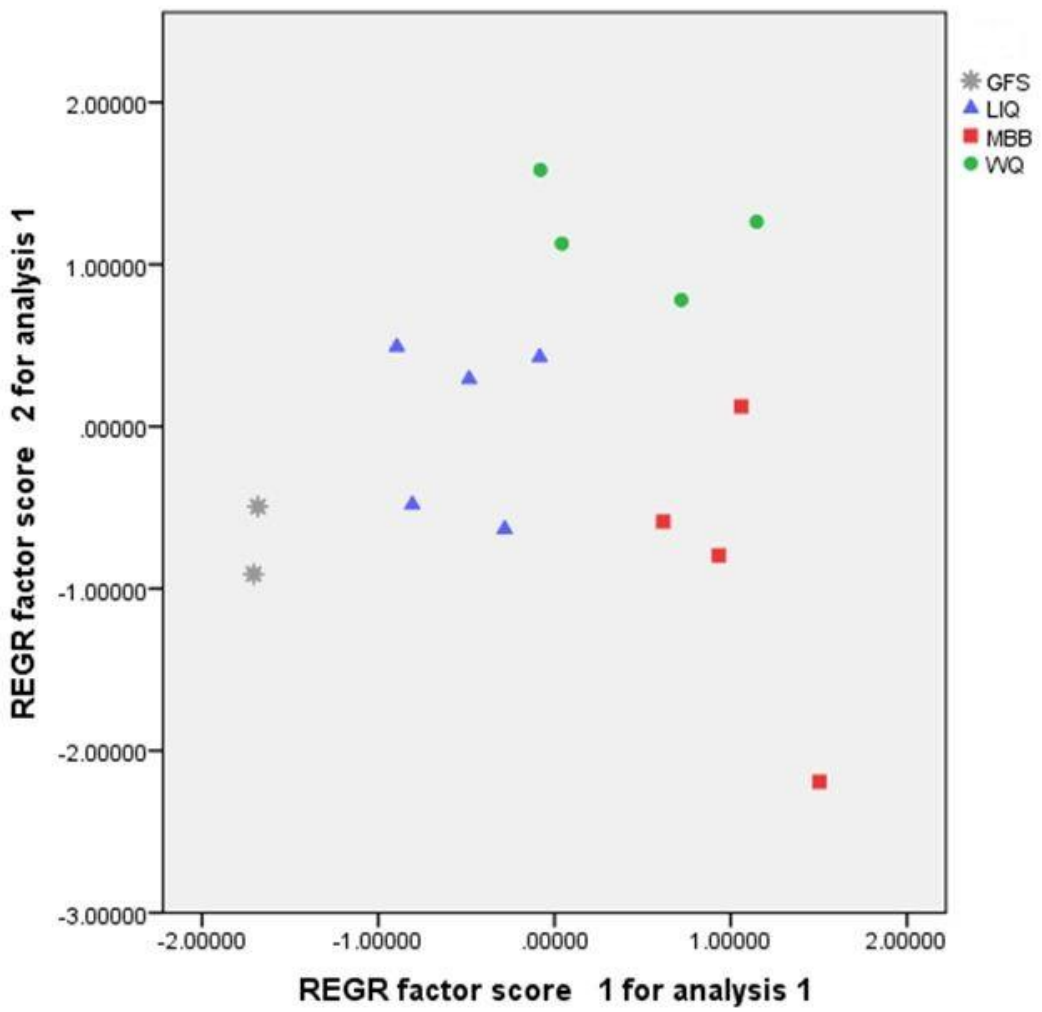

Figure 103. Principal components analysis of ulnae from the type localities and GFS using the partial set of standardized measurements. Abbreviations are provided in Chapter 2.

With only the type localities and GFS included and all of the measurements used, the radius, third metacarpal, calcaneum, and third metatarsal produced 1 component that each graphed as a bell curve with overlap between the localities. Again, the GFS radii are separated from the other 3 localities, which form 1 large group. Because all of the measurements were able to be included in the 'partial' set, this analysis here produces the same graph (Fig. 102). Only the

tibiae produced 2 components and, when graphed, there was very little separation. With 3 components, the humerus, ulna, and femur were able to form groupings that are most apparent when the humeri are graphed in 3 dimensions (Fig. 104).

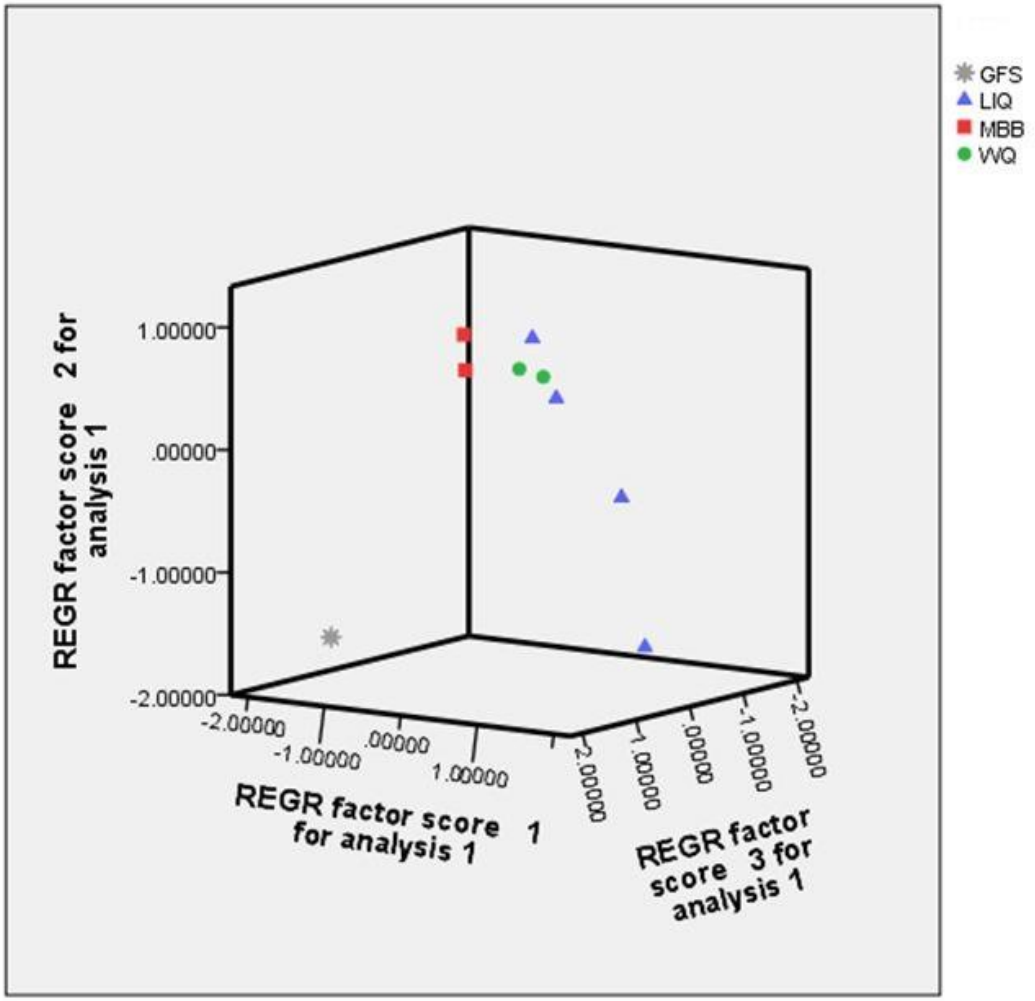

Figure 104. Principal components analysis of humeri from the type localities and GFS using the full set of standardized measurements. Abbreviations are provided in Chapter 2.

Unstandardized Discriminant Function Analyses. There was little agreement amongst the unstandardized DAs as to which species the GFS *Teleoceras* should be assigned. Some DAs

demonstrated difficulty even assigning the GFS specimens to a known group, such as in the case of the humerus (Fig. 105). A discriminant assignment was given but is only weakly supported by the morphospace relationships.

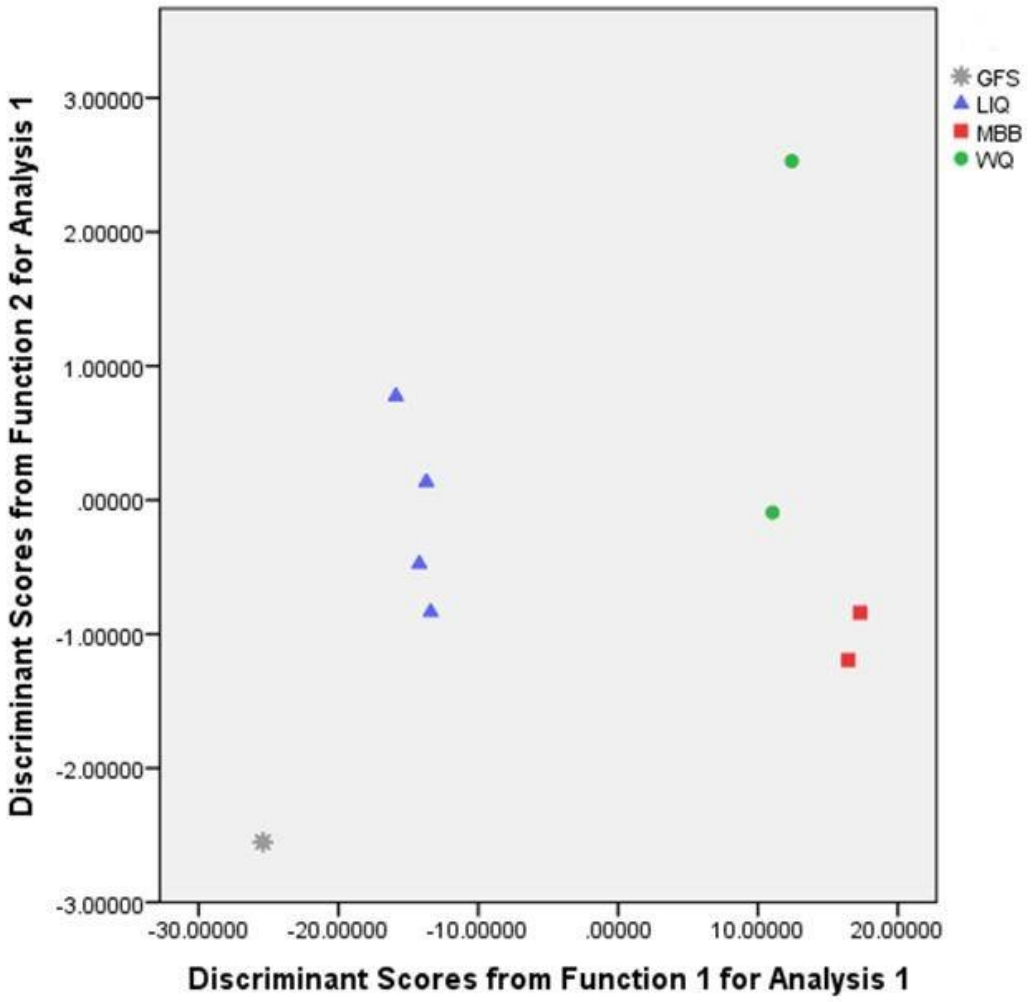

Figure 105. Discriminant function analysis of humeri from the type localities and GFS using the full set of unstandardized measurements. Abbreviations are provided in Chapter 2.

When all of the comparative localities were included, the GFS *Teleoceras* was evenly distributed amongst the 3 species with all 3 falling between 29.41% (*T. fossiger*) and 35.29%

(both *T. fossiger* and *T. hicksi*) (Fig. 106). However, when only the type localities were included as knowns and analyzed with the partial set of measurements, the GFS *Teleoceras* was assigned to *T. fossiger* most often at 64.71%. With only the type localities, the assignment distribution varied little depending on whether the partial set of measurements was used or only the full set, which assigned GFS to *T. fossiger* 56.25% of the time.

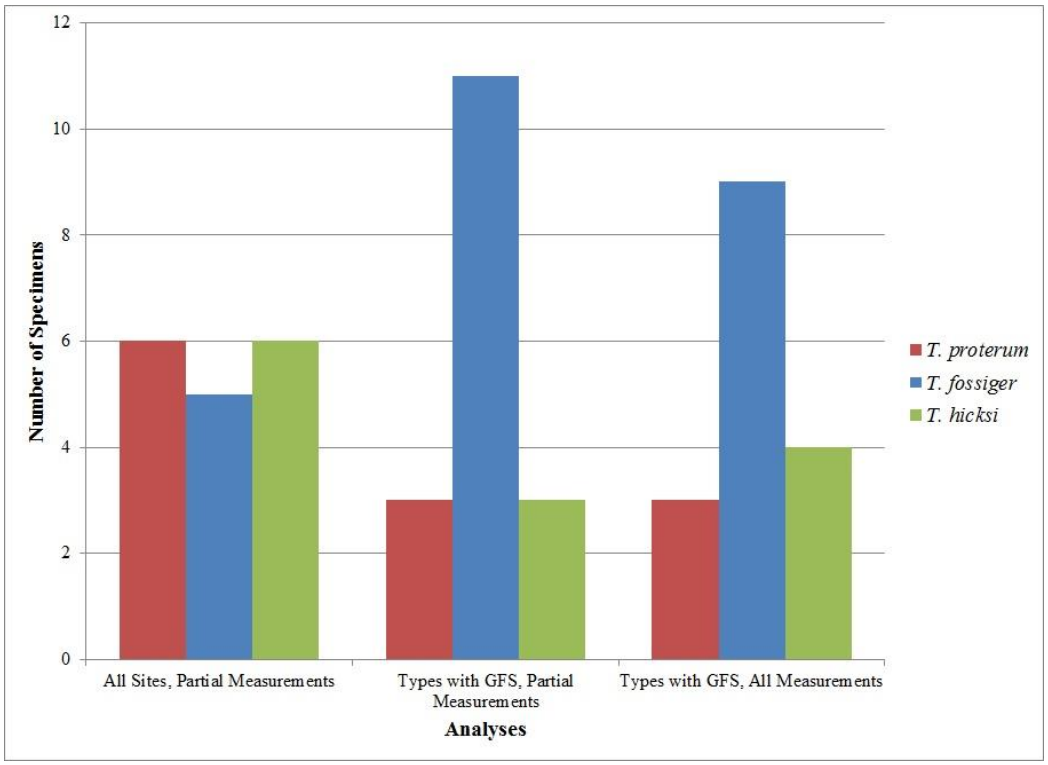

Figure 106. Bar graph showing species assignment of the GFS *Teleoceras* in the 3 discriminant function analyses using unstandardized data

In all unstandardized DAs, 5 of the 8 elements were most frequently assigned to *Teleoceras fossiger* (Fig. 107). Only the third metacarpal and the femur were most often assigned to *T. hicksi* and only the third metatarsal was most often assigned to *T. proterum.*

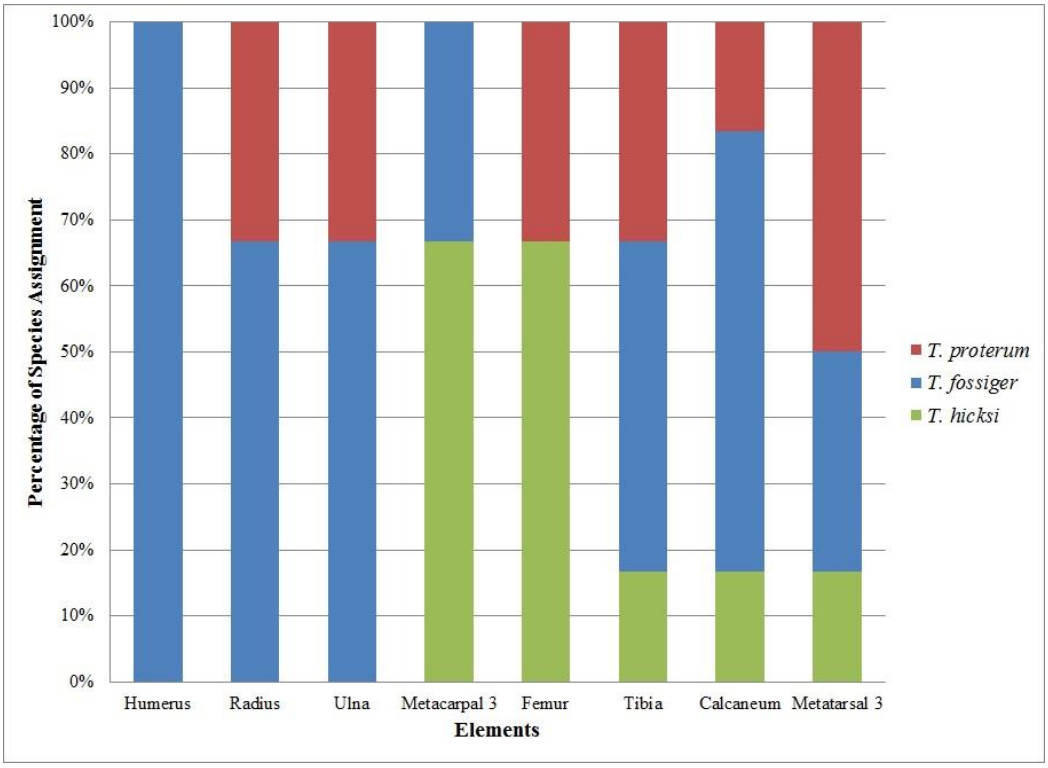

Figure 107. Frequency of GFS specific assignments by element in discriminant function analyses using unstandardized data

Standardized Discriminant Function Analyses. Like with the unstandardized DAs, there was little agreement amongst the standardized DAs as to which species the GFS *Teleoceras* should be assigned. Again, some DAs demonstrated difficulty even assigning the GFS specimens to a known group and, again, the humerus is a good example (Fig. 108).

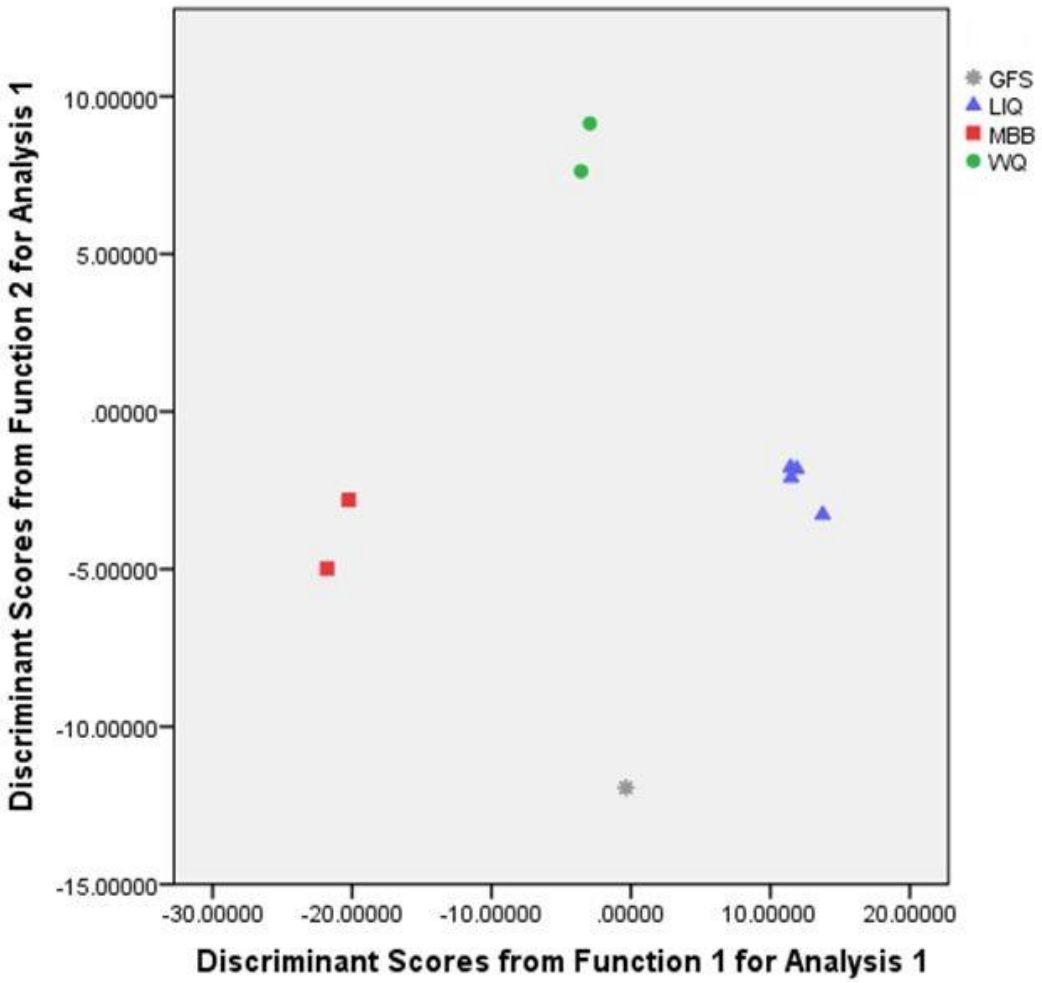

Figure 108. Discriminant function analysis of humeri from the type localities and GFS using the full set of standardized measurements. Abbreviations are provided in Chapter 2.

In all 3 analyses with standardized data, the GFS *Teleoceras* was most often assigned to *T. proterum* (Fig. 109). In the analysis including all of the comparative localities and only the partial sets of measurements, the GFS specimens were assigned to the 3 type localities at similar rates with all 3 falling between 23.53% (*T. hicksi*) and 41.18% (*T. proterum*). When the comparative localities were removed so that only the type localities were analyzed with the partial set of measurements, GFS was assigned to *T. proterum* most often at 64.71%. GFS was

also assigned to *T. proterum* 56.25% of the time when the type localities were analyzed using the full sets of measurements.

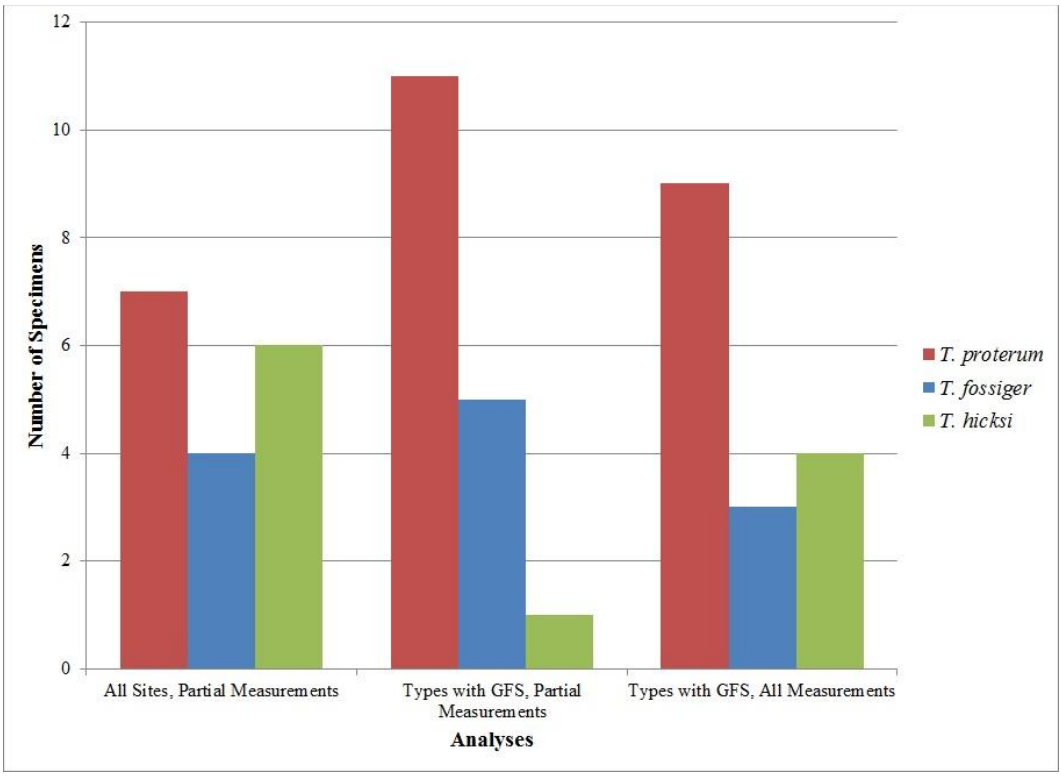

Figure 109. Bar graph showing species assignment of the GFS *Teleoceras* in 3 discriminant analyses using standardized data

Unlike in the analyses with unstandardized data, most elements were assigned to *Teleoceras proterum* when standardized data were used (Fig. 110). Only the ulna was most frequently assigned to *T. fossiger* and the third metacarpal was assigned to *T. fossiger* and *T. proterum* at an equal rate.

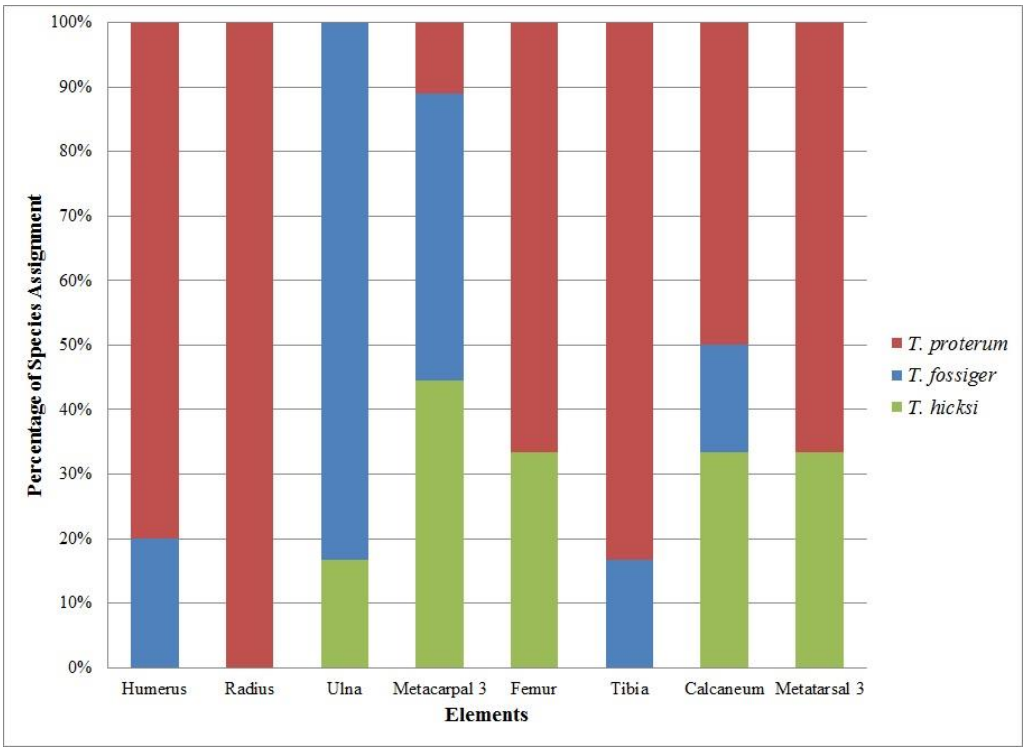

Figure 110. Frequency of GFS specific assignments by element in discriminant analyses using standardized data

Comparative Localities

In all, 12 fossil localities were used in this study, including GFS, the 3 type localities (MBB, *Teleoceras proterum*; LIQ, *T. fossiger*; and WQ, *T. hicksi*), and 8 additional localities (AQ, BTR, BTRh, BV, LBB, MF, MQ, SQ) that were used as comparisons. Some separation occurred when elements from the 3 type localities were analyzed with PCA but there was even less when the comparative localities were individually treated as unknowns (Appendix 6)

Unstandardized Principal Components Analyses. Unstandardized PCAs were typically able to form clusters of the 3 type localities but with a large amount of morphospace overlap. Typically, *Teleoceras hicksi* and *T. fossiger* show more overlap than either do with *T. proterum*.

The femur, particularly along the second axis, shows more separation than the other 7 elements (Fig. 111). Axis 1 corresponds to an increase in the medial trochlea width and an increase in the trochlear tubercle height. Axis 2 corresponds to a decrease in the minimum diaphyseal width and an increase in the trochlear tubercle width. However, this separation could also be due to the low number of femora included; elements with larger numbers tend to show more overlap.

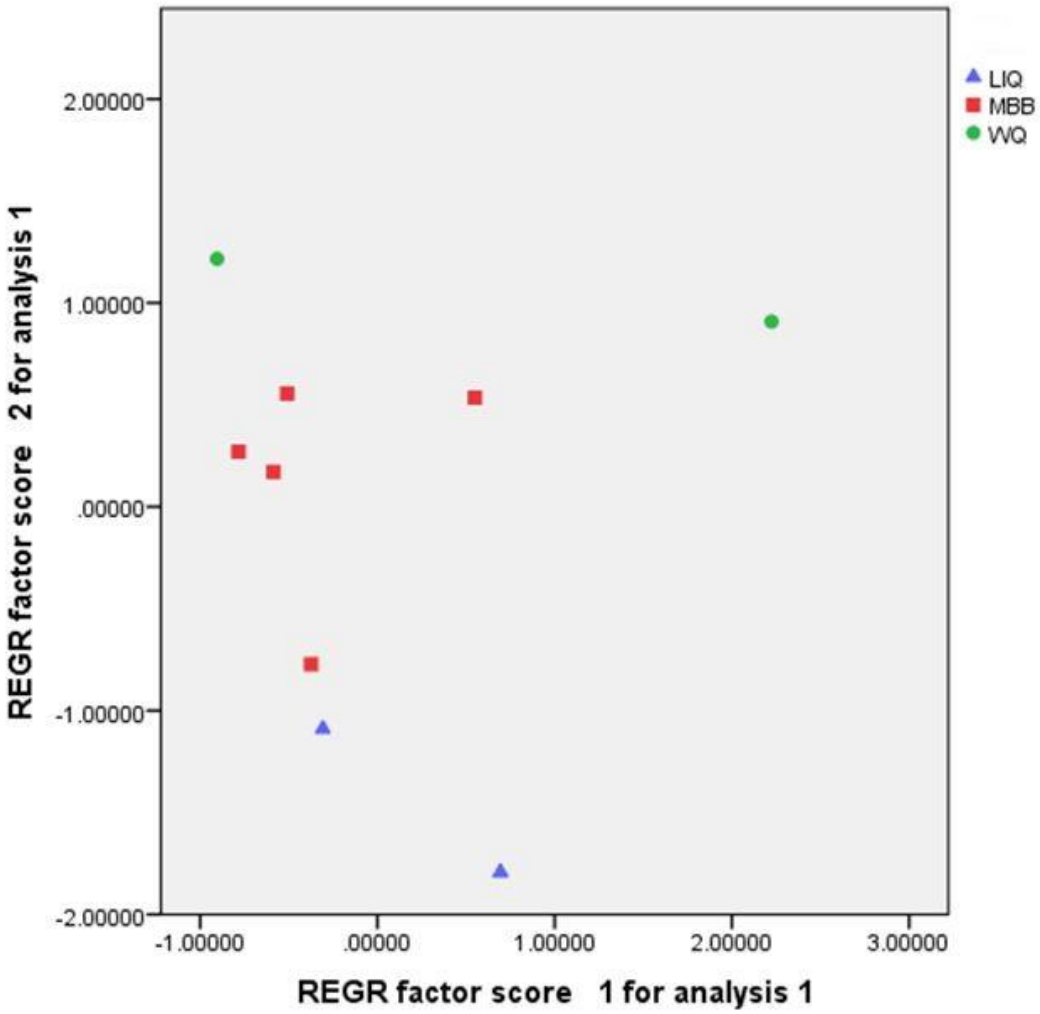

Figure 111. Principal components analysis of femora from the 3 type localities using unstandardized measurements. Abbreviations are provided in Chapter 2.

Standardized Principal Components Analyses. As in the previous set of analyses, standardized PCAs were typically able to form clusters of the 3 type localities but with a large amount of morphospace overlap; however, unlike in the previous set of analyses, the overlap does not always follow the same pattern. The ulnae show more complete separation than the other 7 elements (Fig. 112). Axis 1 corresponds to an increase in the midway depth of the olecranon process and the medial midshaft width and axis 2 corresponds to an increase in the length of the olecranon process and the length of the olecranon process including the semilunar notch.

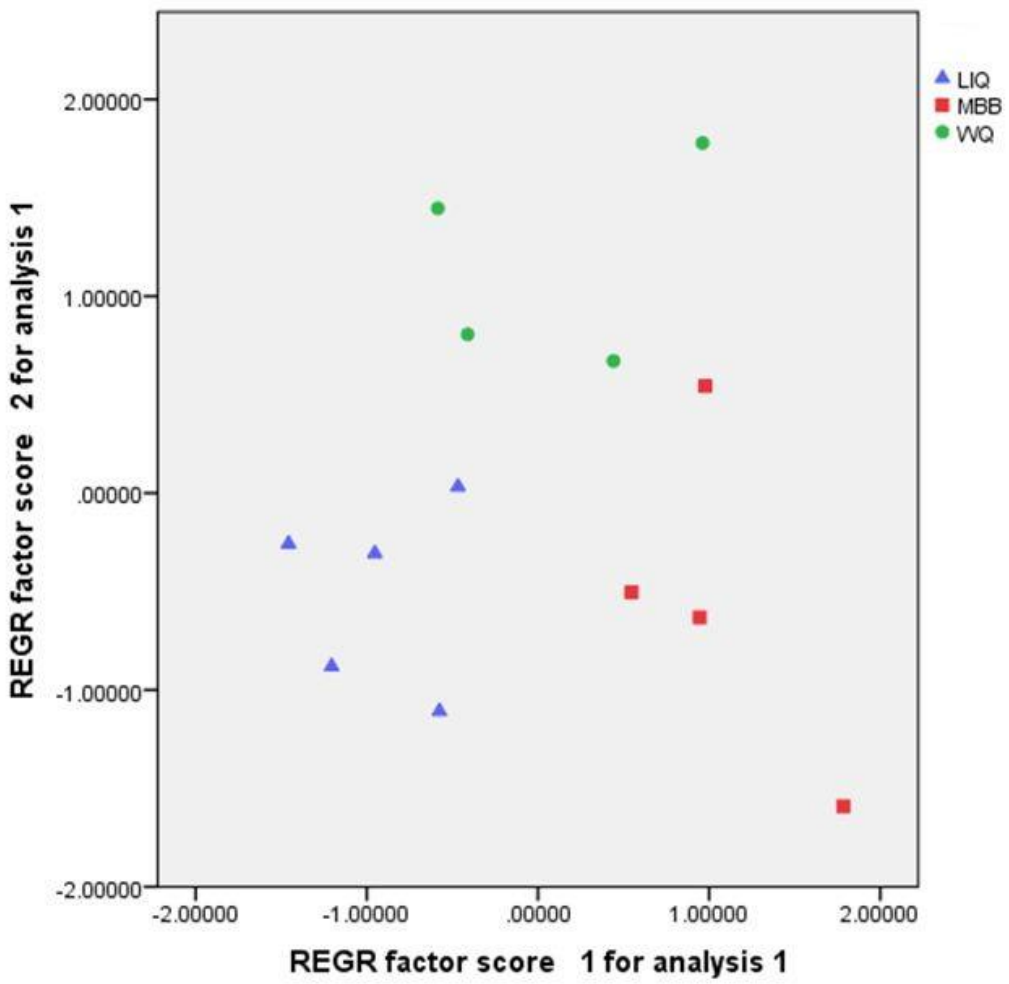

Figure 112. Principal components analysis of ulnae from the 3 type localities using standardized measurements. Abbreviations are provided in Chapter 2.

Unstandardized Discriminant Function Analyses. These analyses assigned the comparative specimens to the incorrect species more often than to the correct. From the 2 *Teleoceras proterum* localities (LBB and MF), only 31.88% of the 69 elements were assigned to MBB (*T. proterum*). From the 4 *T. fossiger* localities (AQ, BTR, MQ, and SQ), only 35.48% of the 62 elements were assigned to LIQ (*T. fossiger*). From the 2 *T. hicksi* localities (BTRh and BV), only 31.82% of the 22 elements were assigned to WQ (*T. hicksi*). In all, only 33.33% of the

153 specimens were assigned to their respective species' type locality (Fig. 113). The calcaneum had the highest success rate with 64.00% correctly classified, while the third metatarsal was the least successful with only 3.33% correctly classified (Fig. 114).

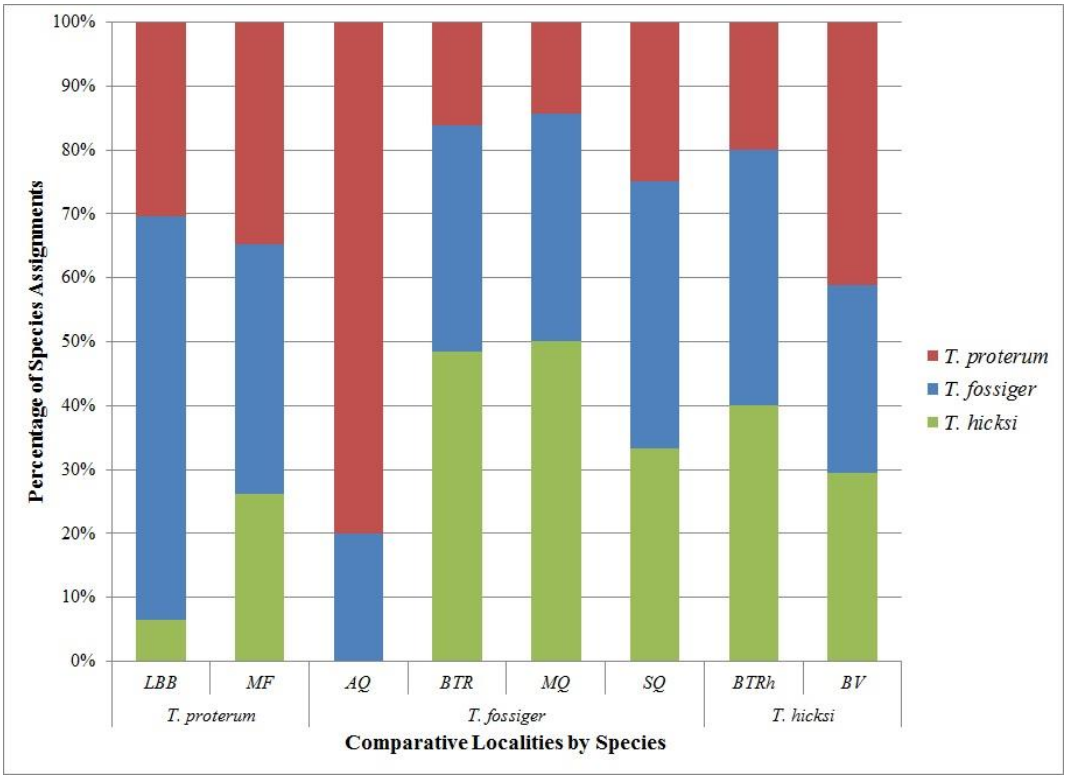

Figure 113. Unstandardized discriminant assignments of comparative specimens by locality. Names of species below the locality abbreviations refer to the current classifications. Abbreviations are provided in Chapter 2.

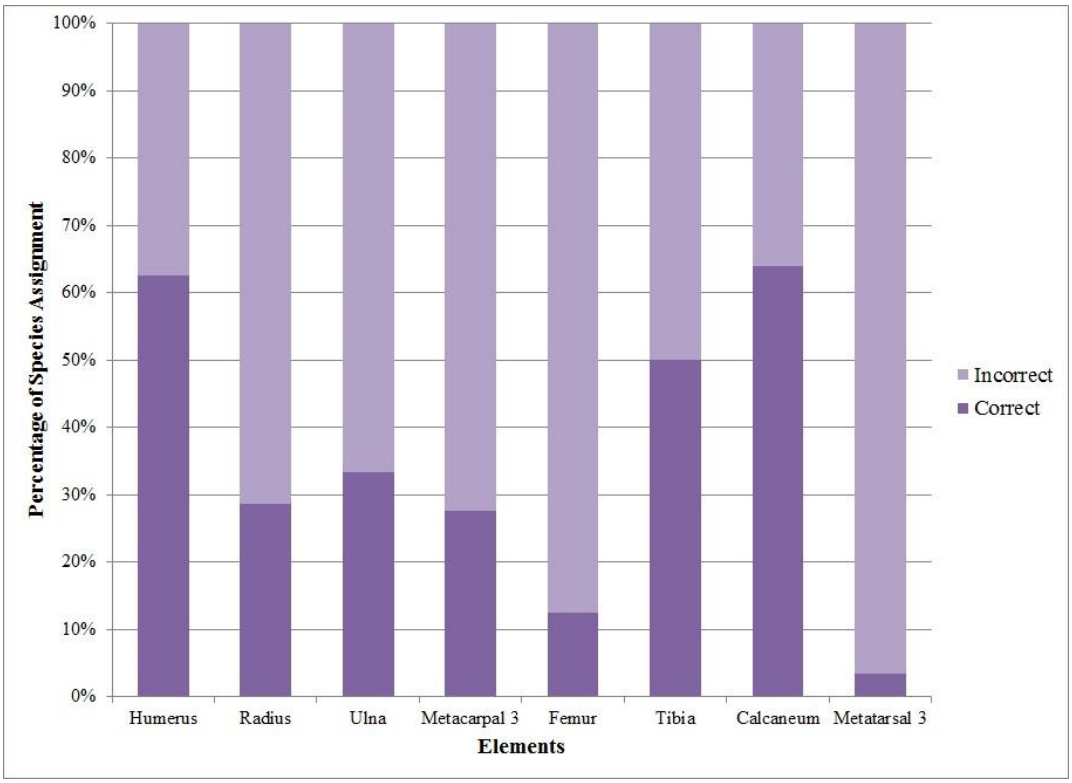

Figure 114. Unstandardized discriminant assignments of comparative specimens by element. 'Correct' refers to an assignment that matches the current species classification.

Standardized Discriminant Function Analyses. Once the measurements were standardized, the analyses assigned the specimens to the correct species even less frequently than with the unstandardized measurements. From the 2 *Teleoceras proterum* localities (LBB and MF), 20.29% of the 69 elements were assigned to MBB (*T. proterum*). From the 4 *T. fossiger* localities (AQ, BTR, MQ, and SQ), 22.58% of the 62 elements were assigned to LIQ (*T. fossiger*). From the 2 *T. hicksi* localities (BTRh and BV), 22.73% of the 22 elements were assigned to WQ (*T. hicksi*). In all, only 20.92% of the 153 specimens were assigned to their respective species' type locality (Fig. 115). In this case, the radius had the highest success rate

with 38.10% correctly classified, while the third metatarsal again was the least successful with 0.00% correctly classified (Fig. 116).

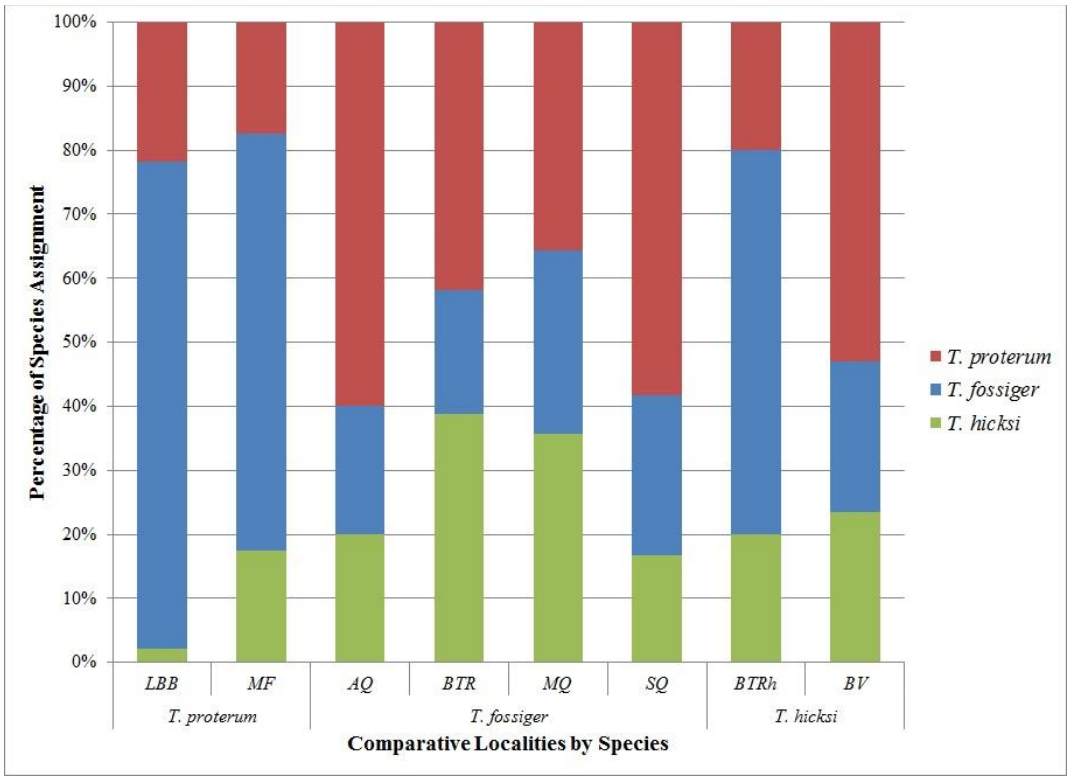

Figure 115. Standardized discriminant assignments of comparative specimens by locality. Names of species below the locality abbreviations refer to the current classifications. Abbreviations are provided in Chapter 2.

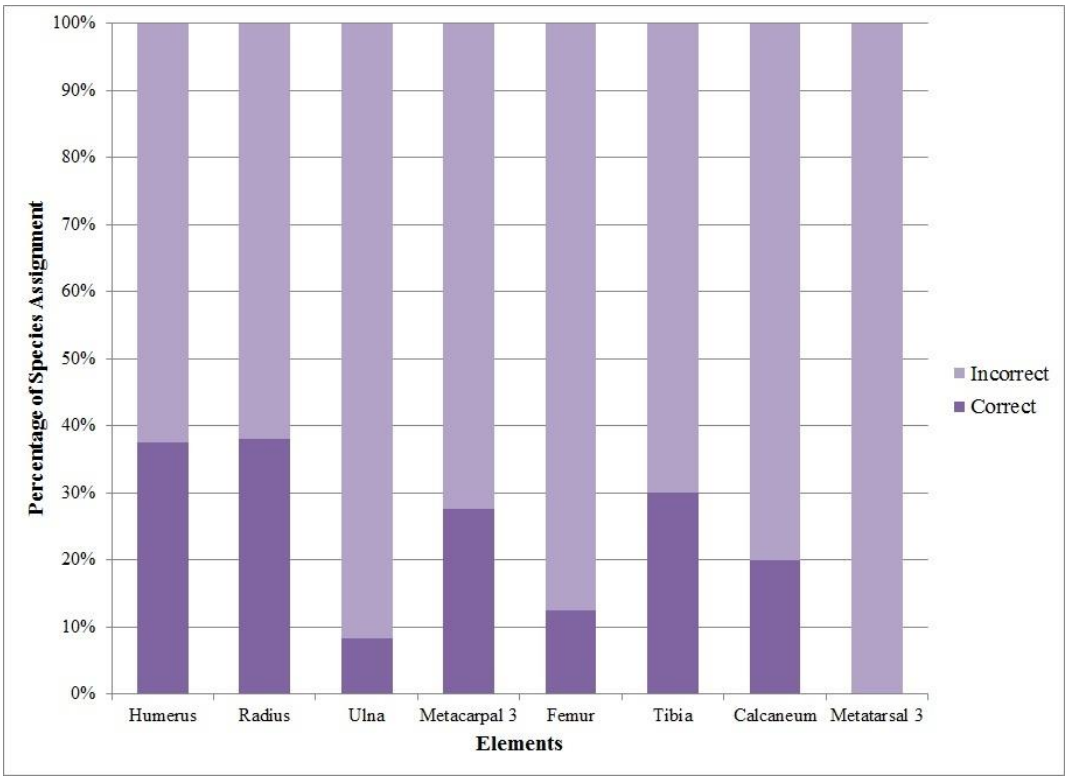

Figure 116. Standardized discriminant assignments of comparative specimens by element. 'Correct' refers to an assignment that matches the current species classification.

Holotype Morphology

In addition to these statistical analyses, morphological comparisons were made between the GFS *Teleoceras* specimens and the 3 primary Hemphillian *Teleoceras* species—*T. proterum*, *T. fossiger*, and *T. hicksi*. Again, *Teleoceras guymonense* was not included in this analysis because it is considered to be a dwarf species, which the GFS rhino is clearly not. Also, the *T. guymonense* material is in very poor condition and most is not readily accessible.

Teleoceras proterum

The holotype of *Teleoceras proterum* (USNM 3190) is an isolated upper left third molar from Mixson's Bone Bed, Levy County, Florida. Compared to the GFS specimens, *T. proterum*

is relatively simple with no evidence of an antecrochet or a crista (Fig. 117). *Teleoceras proterum* has a crochet on this third molar but it does not extend within an antecrochet or the protocone. This shape of the crochet creates a round fossette. Unfortunately, the preservation at MBB is too poor to produce intact skulls that are suitable for morphological comparisons.

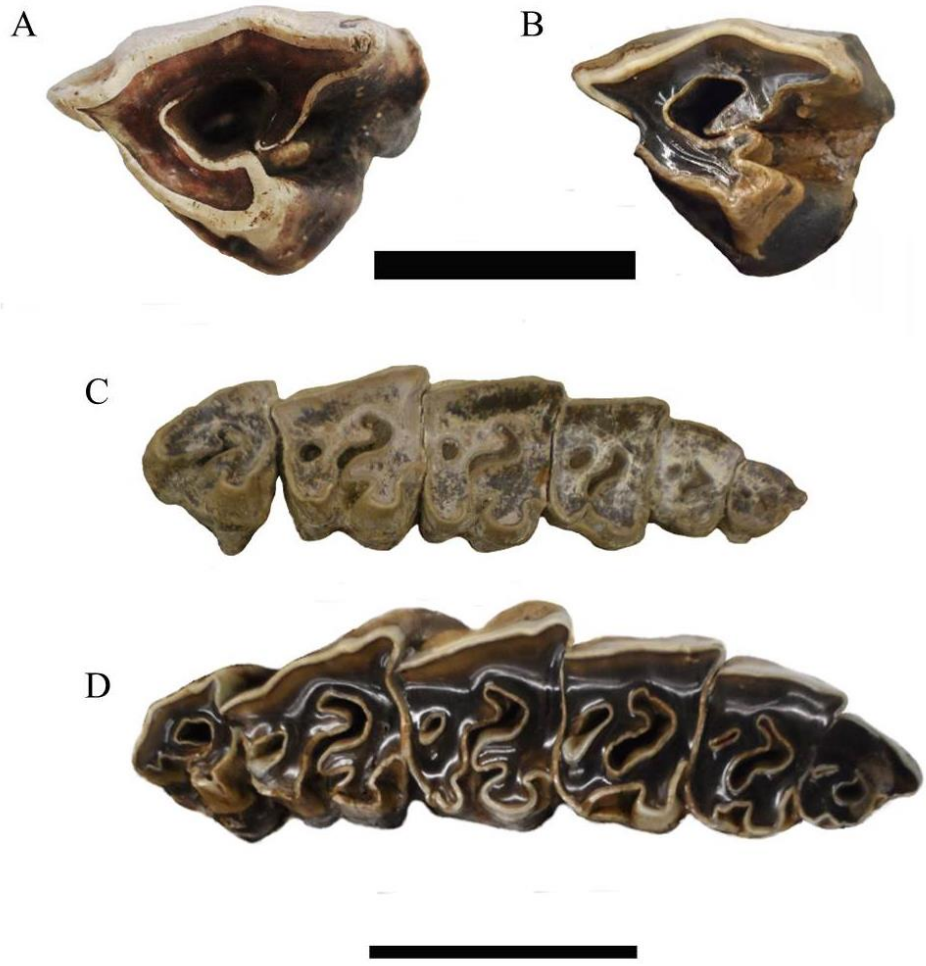

Figure 117. Dentition of *Teleoceras proterum* and the GFS specimen in occlusal view. A, Left upper third molar of *T. proterum* holotype, USNM 3190; B, Left upper third molar of ETMNH 601; C, Upper right dentition of *T. proterum* from LBB, UF 40058; D, Upper right dentition of ETMNH 601. Anterior is to the right. In A and B, scale bar = 5 cm. In C and D, scale bar = 10 cm. Refer to text for dental terminology (Fig. 5).

Teleoceras proterum skulls from LBB can be used for morphological comparisons with the GFS rhino (FIG. 118). Along the whole tooth row, *Teleoceras proterum* has relatively simple teeth that are anteroposteriorly compressed. The crochet is smaller than the antecrochet, in contrast to the equally sized features of the GFS *Teleoceras*. The dorsal surface of *T. proterum* is more concave and the nasals are more upturned. There are slight dorsal orbit knobs *T. proterum* but they typically are not as pronounced as those on the GFS skulls.

Figure 118. Skulls of *Teleoceras proterum* and the GFS specimen in right lateral view. A, *T. proterum*, UF 40058; B, ETMNH 601. Anterior is to the right. Scale bar = 10 cm.

Teleoceras fossiger

The holotype of *Teleoceras fossiger* (F:AM 8390) is a partial skull from the Beaver Creek area, Decatur County, Kansas. Unfortunately, F:AM 8390 has the palate broken mesial to the right third premolar and the left fourth premolar. Though the teeth on both sides have been damaged, the right side is in better condition than the left and is used as the primary comparison (Fig. 119). However, both upper third molars are too damaged to make any comparisons. On the upper second molars, the antecrochet is smaller than is seen in the GFS specimens. *Teleoceras fossiger* has more well-developed, though still not significant, cingula along the lingual surface of the upper first and second molars. The molars are more anteroposteriorly compressed than those of the GFS *Teleoceras*. On the upper teeth, the fossettes have more open curves than those seen in the GFS specimens.

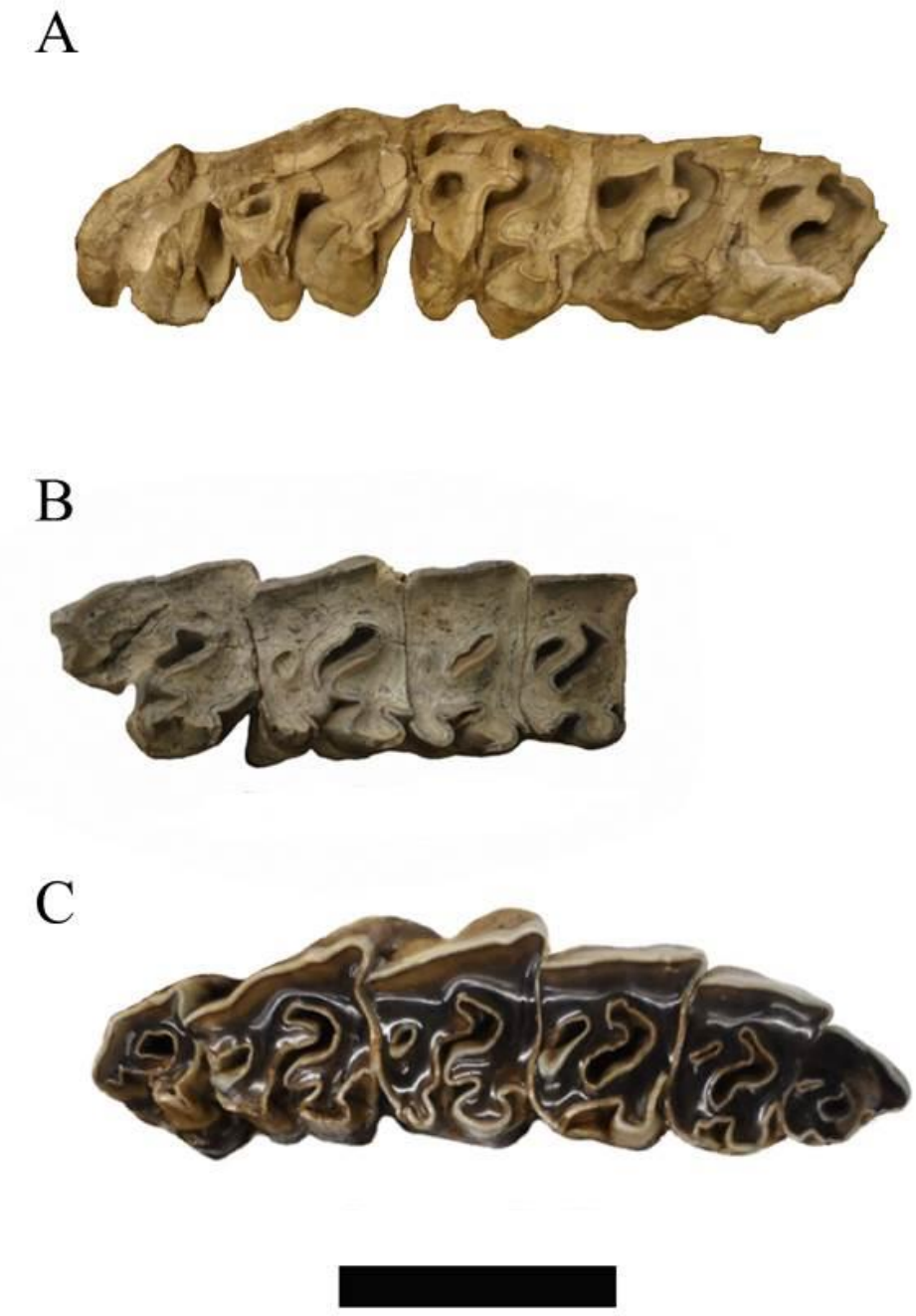

Figure 119. Right upper dentition of *Teleoceras fossiger* and the GFS specimen in occlusal view. A, *T. fossiger* holotype, F:AM 8390; B, *T. fossiger* from LIQ, USNM 415871; C, ETMNH 601. Anterior is to the right in all. Scale bar = 10 cm. Refer to text for dental terminology (Fig. 5).

When compared to the GFS *Teleoceras*, *T. fossiger* also displays cranial differences that are evident in other specimens from LIQ (Fig. 120). Along the dorsal surface, *T. fossiger* has a greater concave curvature from the upturned nasal bones to the occiput, which makes the skull appear shorter anteroposteriorly. There is very little evidence of rugosity dorsal to the orbit. The less robust zygomatic arch has a narrower transverse breadth and inserts more proximally on the occiput simply because there is less occiput available in *T. fossiger*. Though the palates of both ETMNH 609 and ETMNH 601 have been partially reconstructed, the remnants of the bone suggest a wide U-shaped palatal incisure. This is in contrast to the narrow incisure seen in *T. fossiger*.

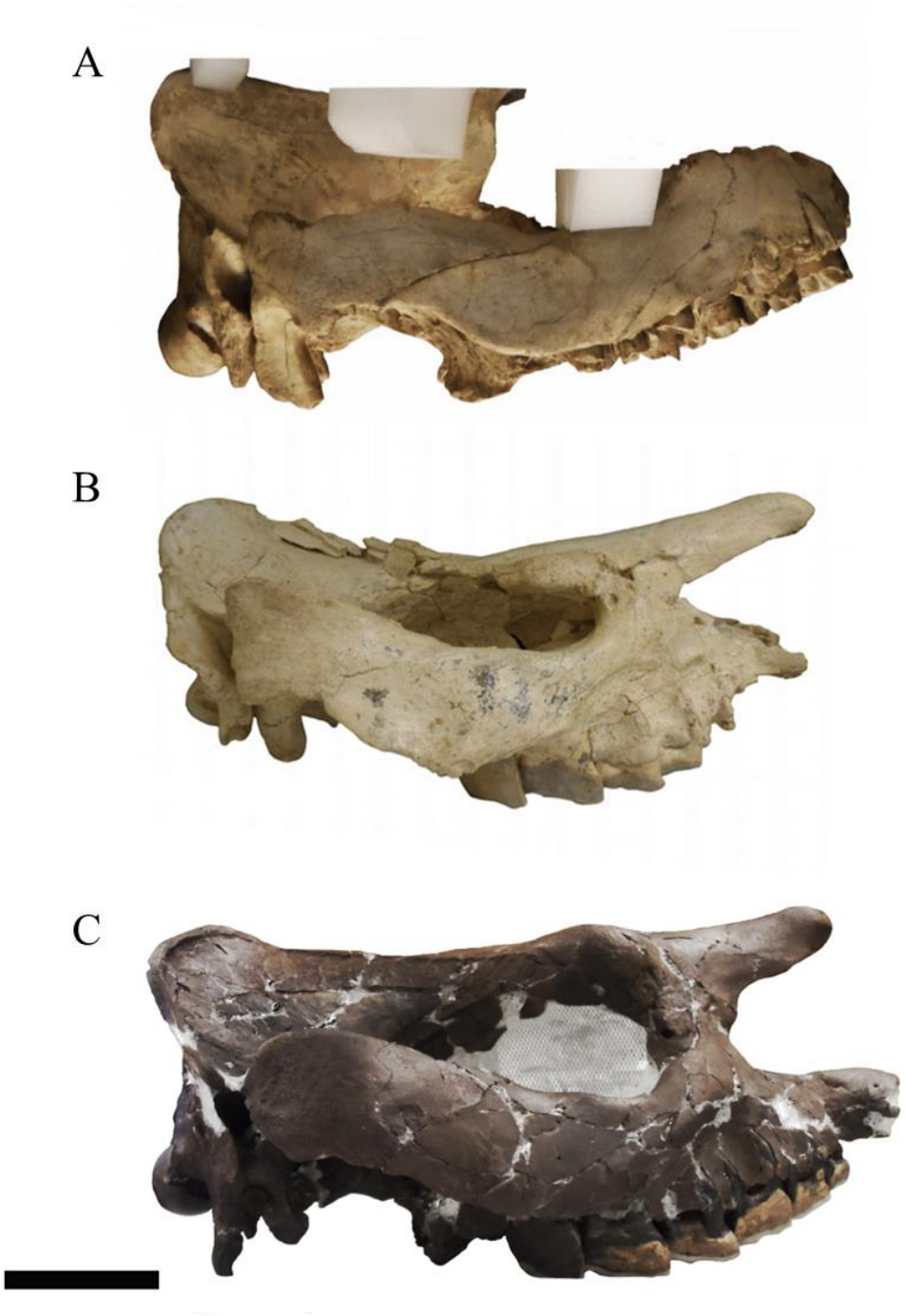

Figure 120. Skulls of *Teleoceras fossiger* and the GFS specimen in lateral view. A, *T. fossiger* holotype, F:AM 8390; B, *T. fossiger* from LIQ, USNM 256531; C, ETMNH 601. B has been flipped horizontally for comparison, so that anterior is to the right in all. Scale bar = 10 cm.

Teleoceras hicksi

The holotype of *Teleoceras hicksi* (DMNH 304) is a nearly complete skull from the Wray Local Fauna, Yuma County, Colorado that has been mounted on a composite skeleton. For this comparison, the paratype skull (DMNH 309) was used in place of the holotype. This skull is missing the anterior portion of the palate including the right second and third premolars and both incisors. Overall, the teeth are labiolingually longer but more anteroposteriorly compressed than the GFS specimens (Fig. 121). There are very minimal crochets and, thus, very simple fossettes are on the upper molars. A cingulum with a slight basin is present on the third molar's anterior edge of the protocone. Compared to the elongate parastyles seen on the GFS specimens, the second molars of *T. hicksi* have relatively small parastyles. The first molars and fourth premolars do not have styles that extend mesial or distal to the lophs but form a rectangle with them.

Figure 121. Right upper dentition of *Teleoceras hicksi* and the GFS specimen in occlusal view. A, *T. hicksi* paratype, DMNH 309; B, ETMNH 601. Anterior is to the right. Scale bar = 10 cm. Refer to text for dental terminology (Fig. 5).

Teleoceras hicksi also displays cranial differences when compared to the GFS specimens (Fig. 122). The nasals of *T. hicksi* are more upturned as in *T. fossiger* and the zygomatic arches have a narrow transverse breadth more reminiscent of *T. fossiger* than the GFS *Teleoceras*. Also like *T. fossiger*, the dorsal surface of *T. hicksi* is concave creating a dorsoventrally short appearance. Neither the paratype nor the holotype has the enlarged knobs above the orbits.

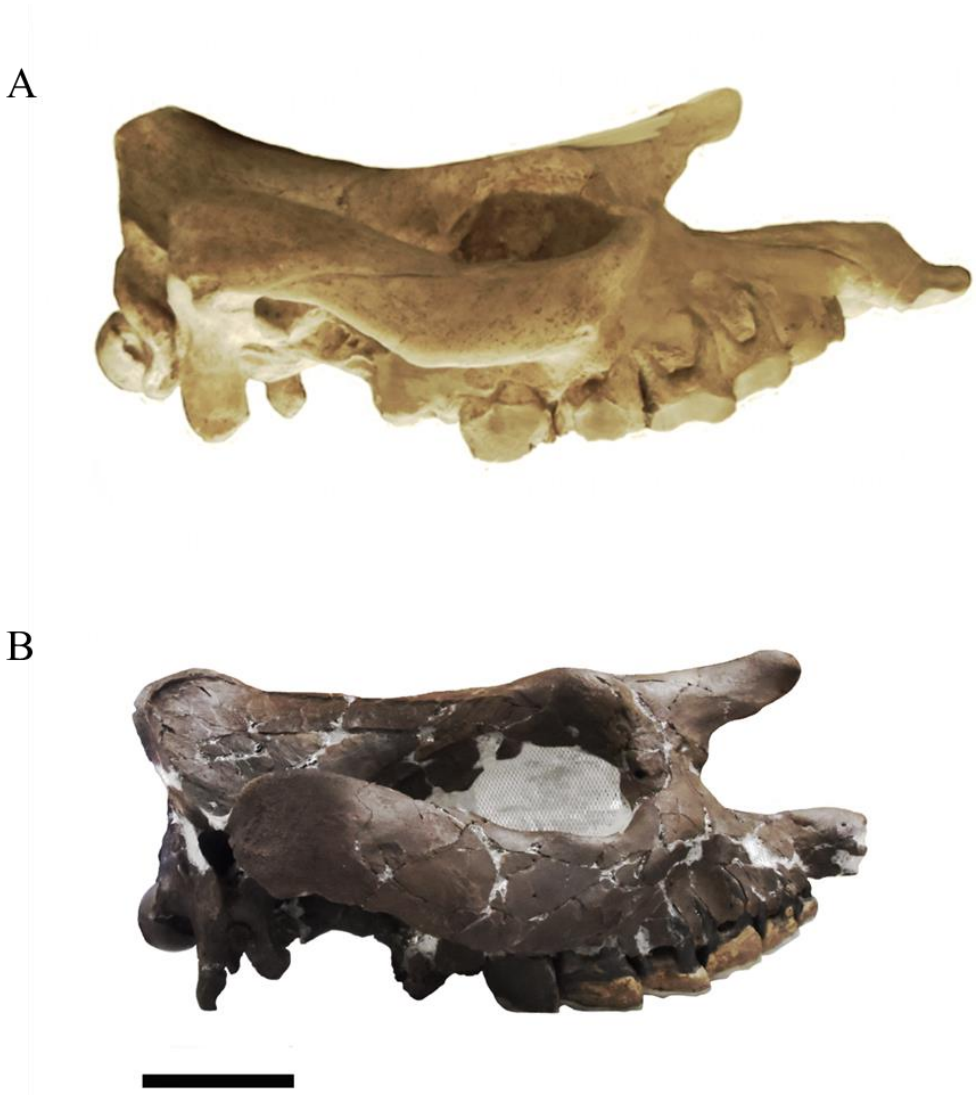

Figure 122. Skull of *Teleoceras hicksi* and the GFS specimen in right lateral view. A, *T. hicksi* paratype, DMNH 309; B, ETMNH 601. A has been flipped horizontally for comparison, so that anterior is to the right in both. Scale bar = 10 cm.

CHAPTER 5

DISCUSSION & CONCLUSIONS

Morphological Description

Morphology of the GFS rhino is undoubtedly that of *Teleoceras*; however, it appears taller with more gracile limbs than most *Teleoceras.* These specimens also have morphological features, both skeletal and dental, that differ from the current Hemphillian species.

Post-Cranial Analysis

Using post-cranial elements, statistical analyses were able to neither confidently differentiate the species of *Teleoceras* nor successfully classify the GFS *Teleoceras*. Any analyses using unstandardized data show a trend that separates by size, especially by the overall length measurement. Typically, *T. proterum* tends to be the smallest and *T. fossiger* tends to be the largest but there are not discrete enough groupings to make a species determination on this feature alone. Any separation seen in these graphs is diminished once the data are standardized by length. There is very little distinction between the species until the comparative localities are removed leaving only the type localities but, even then, there is little separation. Furthermore, where there is separation between the type species, the GFS *Teleoceras* does not consistently plot within the morphospace of 1 species but varies depending on the element being analyzed.

Although the analyses were unable to group by species, they could frequently group by locality. This suggests that the individuals from a given locality are more proportionally similar to each other than to those of the same species at another locality. This is supported by morphological observations made during data collection and could be described as population variance. Furthermore, in some graphs, the localities are split along an axis, which indicates that

there is some difference that divides the specimens from a single locality into 2 groups. This could be sexual dimorphism, which is known to be present in some populations of *Teleoceras* (Mead 2000). Unfortunately, more often than not, discriminant function analyses were unable to correctly assign all 8 post-cranial elements to the 'correct' species using both unstandardized and standardized data. Moreover, in both unstandardized and standardized DAs, only the calcaneum and humerus were able to assign the correct species in more than half of the cases (64.00% and 62.50%, respectively). Even still, the results produced here contribute to our understanding of the Hemphillian rhinos and demonstrate the problems that can come from making specific assignments based on post-cranial measurements.

Morphological Comparisons

Based on the analyses in this study and comparisons with the 3 Hemphillian *Teleoceras* species, the GFS rhino appears to be a new species, *Teleoceras* sp. nov. (Fig. 123). Dental morphology indicates that the Palmetto Fauna (Bone Valley Formation) *Teleoceras hicksi* can be included with the GFS rhino. *Teleoceras* sp. nov. is characterized by: (1) more complex upper molars than *T. proterum*, *T. fossiger*, and *T. hicksi*; (2) an ectoloph on the upper second molar that is longer than the metaloph and protoloph, which creates a rectangular tooth with the long axis oriented anteroposteriorly; (3) an upper first molar that is nearly square rather than anteroposteriorly compressed to a rectangle; (4) upper molars with crochets and antecrochets that are of equal size and that are larger than those seen in the other species; (5) a crochet on the upper third molar that folds well within the antecrochet; (6) a fossette on the upper molars that is more complex with more curvature; and (7) longer, more gracile limbs, especially the radius and other forelimb bones, that create proportions unique within the genus.

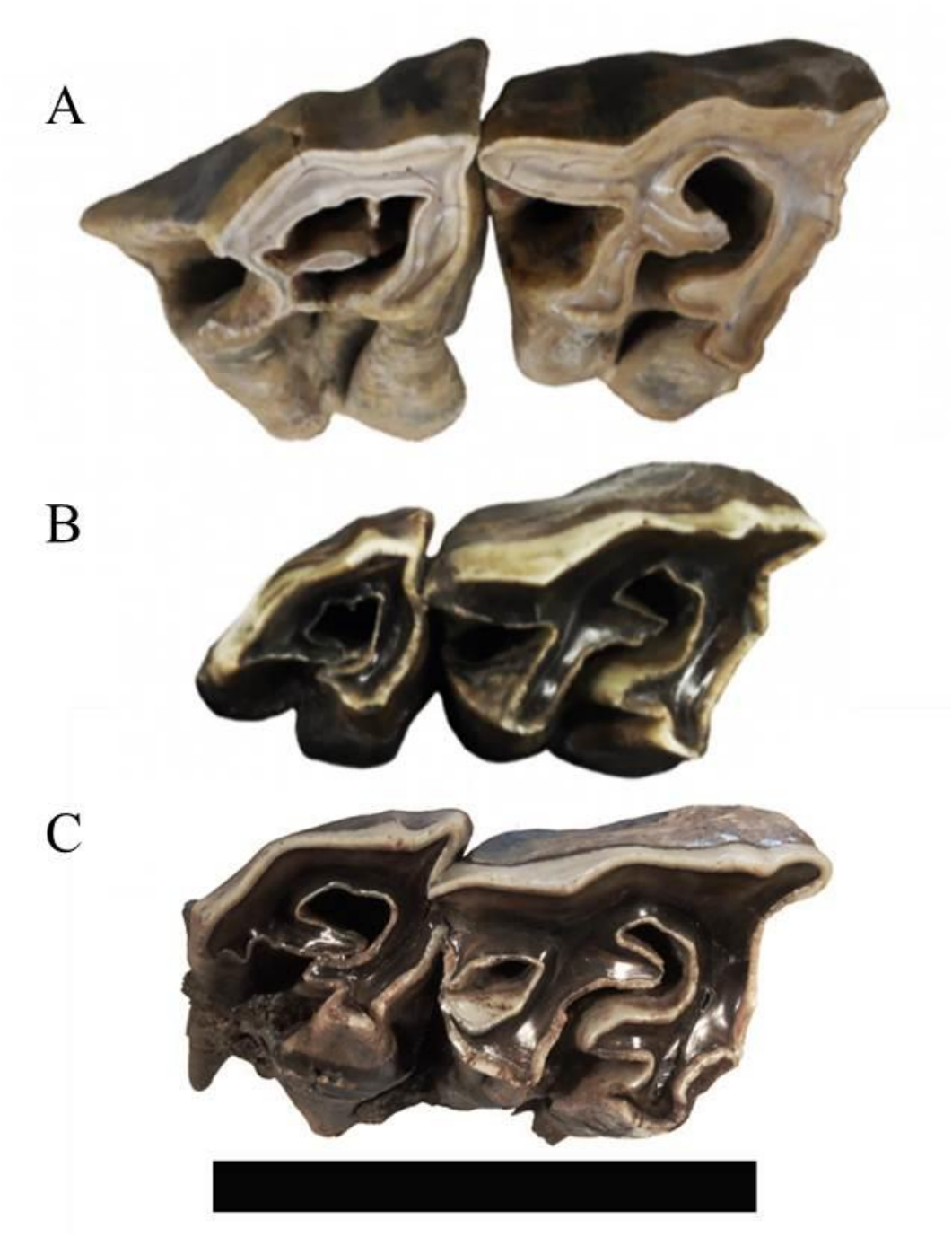

Figure 123. Upper second and third molars of *Teleoceras* sp. nov. in occlusal view with the scale bar on the lingual side and anterior to the right. A, UF 14483; B, ETMNH 609; C, ETMNH 601. Refer to text for dental terminology (Fig. 5). Scale bar = 10 cm.

Comments on Paleobiology

Because GFS only has skeletons of adult males, it is impossible, at this time, to comment on the ontogeny or sexual dimorphism of this population.

Diet

It is important to note that, contrary to most other *Teleoceras*, the GFS population consists of browsers based on isotope analyses (DeSantis and Wallace 2008) . MacFadden (1998) showed that, following the expansion of grasslands at approximately 7 Ma, *Teleoceras* of Florida shifted from mixed feeders or browsers to grazers. It is possible that *Teleoceras* sp. nov. of GFS represents a holdover of the browsers from before the expansion of C_4 grasses. Because GFS was a forested refugium with little to no grass (Wallace and Wang 2004; DeSantis and Wallace 2008), this *Teleoceras* did not have to adapt to a changing food source as its grassland contemporaries did. It is also possible that the long limbs seen in the GFS *Teleoceras* evolved in response to the browsing ecology. Because most of the length differences are seen in the forelimb elements, the head is more elevated than in other species. This would allow for easier browsing of the trees at GFS while those species with shorter forelimbs and lower heads could more easily graze. While the Palmetto Fauna *Teleoceras* sp. nov. has been shown to be a grazer (MacFadden 1998), the environment was a low-elevation floodplain with forests and grasslands (MacFadden 1999) suggesting that perhaps this rhino took on the grazer role.

Ecology

Many, including Cope (1879), Osborn (1898), Voorhies (1985, 1992), Prothero et al. (1986, 1989), Prothero and Manning (1987), and Prothero (1998, 2005), have noted that the

morphology of *Teleoceras* is comparable to the modern *Hippopotamus* and have described *Teleoceras* as semi-aquatic to aquatic. Conversely, Matthew (1932) described *Teleoceras* as living on flat, open prairies as a grazer and, thus, the short, compact limbs were sufficient. More recently, oxygen isotopes indicate that Florida *Teleoceras* were most likely not aquatic (MacFadden 1998). Mihlbachler (2001, 2003) studied the population structure at Love Bone Bed and Mixson's Bone Bed (both in Florida) and described the *Teleoceras* populations as more similar to modern rhinos than to modern herding ungulates or to *Hippopotamus*.

Unfortunately, because of the small sample from GFS, it is not possible to make interpretations of population structure. However, given the post-cranial features, such as the passive stay-apparati in the shoulder and knee (Hermanson and MacFadden 1992, 1996), it is possible that *Teleoceras* was spending a large amount of time on land. Longer limb elements in the GFS *Teleoceras* sp. nov. may be better suited for the woodland environment than the open prairies. This is not to say that these rhinos never entered the water but only that they may not be the hippo-ecomorph that many have believed them to be.

Size Trends

Prothero (2005) describes an increase in size through the *Teleoceras* lineage until the largest *T. fossiger* and then a reduction in size to *T. hicksi*. If *Teleoceras* sp. nov. is considered, this is no longer true because it is larger than most *T. fossiger* specimens examined and, yet occurs at a later time. Furthermore, there is such a size overlap between *T. fossiger* and *T. hicksi* that it is unwise to determine 1 to be larger than the other. It has also been suggested that the "shortening and stumpiness of the limbs" increases through the lineage (Prothero 2005:207). Yet,

the *Teleoceras* sp. nov. has relatively long and thin limb elements when compared to other Hemphillian individuals.

Implications for *Teleoceras*

Teleoceras sp. nov. requires that the definition of the genus *Teleoceras* be revised. While the GFS population has many of the characters previously described as typical of *Teleoceras*, it is missing some features that can now no longer be used to adequately describe the genus as a whole. *Teleoceras* sp. nov. has: 1. mesodont teeth, rather than hypsodont; 2. as adults, unfused nasals without a nasal horn; and 3. a less rotund body with longer, more gracile limbs. The presence of the GFS population illustrates the degree of generic variation and brings attention to the possibility of more populations with variable character states.

If the Palmetto Fauna *Teleoceras* is included with *Teleoceras* sp. nov., it can be described as a southeastern endemic species, which may be comparable to *T. proterum* in the early Hemphillian. Further west, *T. fossiger* tends to be found at early Hemphillian localities and *T. hicksi* tends to be found at late Hemphillian localities. However, until more work is done, the age of a fossil locality should not be the sole factor in identifying these rhino species and, likewise, rhino fossils should not be the sole factor in identifying the age of a fossil locality. This creates circular reasoning that has, in large part, contributed to the current phylogenetic problems within the genus.

Furthermore, although Madden and Dalquest (1990:266) discuss "the last rhinoceros in North America" from Blancan sediments in Texas, this is only a small, isolated tooth fragment that is identified as *Teleoceras* based purely on size and, until more material is found, this should not extend the temporal range of *Teleoceras* beyond the end of the Hemphillian. Therefore, GFS

can be added to the latest Hemphillian localities, represented by the Mount Eden Fauna, the Yepómera Fauna, the Rancho El Ocote Fauna, and the Palmetto Fauna (Richard Hulbert, pers. comm.; Tedford et al. 2004; Webb et al. 2008), that contain the last of the North American rhinos.

Future Work

Because the post-cranial morphology does seem to be so conservative, statistical analyses should be expanded to include cranial and dental morphology. In addition to including more skeletal material, the advanced methods should be used. Landmark morphometrics, in both 2 and 3 dimensions, might aid in elucidating phylogenetic relationships with more success than is seen when linear measurements are used. This would greatly increase the amount of shape differences captured and, thus, available to be analyzed.

Perhaps most importantly, all of the *Teleoceras* species should be included in a large scale statistical analysis of phylogeny. By including all *Teleoceras* specimens, morphological groupings may become more obvious because it is possible that the Hemphillian species were sharing a morphotype that differs from that of the Hemingfordian, Barstovian, and Clarendonian morphotypes. Aspects of the paleobiology of *Teleoceras* should also be analyzed to form a more well-rounded interpretation of morphology. Without understanding the effects of sexual dimorphism and ontogeny within the genus as a whole, it becomes difficult to understand the overall morphology.

REFERENCES

Barone R. 1999. Anatomie Comparée des Mammifères Domestiques, Tome 1: Osteologie. Vigot Freres, Paris, 761 pp.

Cerdeño E. 1995. Cladistic analysis of the family Rhinocerotidae (Perissodactyla). American Museum Novitates 3143:1-25.

Churchill JM. 1992. Depositional environment of the Ogallala Group (Miocene), Minium Quarry, Graham County, Kansas. Master's thesis, Fort Hays State University, Fort Hays, Kansas.

Cook HJ. 1922. A Pliocene fauna from Yuma County, Colorado, with notes on the closely related Snake Creek Beds from Nebraska. Proceedings of the Colorado Museum of Natural History 4(2):3-29.

Cook HJ. 1927. A new rhinoceros of the genus *Teleoceras* from Colorado. Proceedings of the Colorado Museum of Natural History 7:1-5.

Cope ED. 1878. Descriptions of new extinct Vertebrata from the upper Tertiary and Dakota Formations. Bulletin of the United States Geological and Geographical Survey of the Territories 4(2):379-396.

Cope ED. 1879. On the extinct American rhinoceroses and their allies. The American Naturalist 13(12): 771a-771j.

DeSantis LRG, Wallace SC. 2008. Neogene forests from the Appalachians of Tennessee, USA: geochemical evidence from fossil mammal teeth. Palaeogeography, Palaeoclimatology, Palaeoecology 266:59-68.

Farlow JO, Sunderman JA, Havens JJ, Swinehart AL, Holman JA, Richards RL, Miller NG,

Martin RA, Hunt RM Jr., Storrs GW, Curry BB, Fluegeman RH, Dawson MR, Flint, MET. 2001. The Pipe Creek Sinkhole biota, a diverse late Tertiary continental fossil assemblage from Grant County, Indiana. American Midland Naturalist 145:367-378.

Flower WH. 1896. On some cranial and dental characters of the existing species of rhinoceroses Proceedings of the Scientific Meetings of the Zoological Society of London. 44(1):443-457.

Gilmore LS, Wallace SC. In prep. Potential mating related pathologies in the fossil rhinoceros, *Teleoceras* cf. *T. hicksi*, from the Gray Fossil Site.

Hagge MD. 2010. A functional and ontogenetic skull analysis of the extant rhinoceroses and *Teleoceras major*, an extinct Miocene North American rhinoceros. Master's thesis, Louisiana State University, Baton Rouge, Louisiana.

Harrison JA, Manning EM. 1983. Extreme Carpal Variability in *Teleoceras* (Rhinocerotidae, Mammalia). Journal of Vertebrate Paleontology 3(1):58-64.

Hatcher JB. 1894a. A median horned rhinoceros from the Loup Fork Beds of Nebraska. The American Geologist 13(3):149-150.

Hatcher JB. 1894b. On a small collection of vertebrate fossils from the Loup Fork Beds of northwestern Nebraska: with note on the geology of the region. The American Naturalist 28(327):236-248.

Hermanson JW, MacFadden BJ. 1992. Evolutionary and functional morphology of the shoulder region and stay-apparatus in fossil and extant horses (Equidae). Journal of Vertebrate Paleontology 12(3):377-386.

Hermanson JW, MacFadden BJ. 1996. Evolutionary and functional morphology of the knee in

fossil and extant horses (Equidae). Journal of Vertebrate Paleontology 16(2):349-357.

Hitchins PM. 1978. Age determination of the black rhinoceros (*Diceros bicornis* Linn.) in Zululand. South African Journal of Wildlife Research 8(2):71-80.

Kappelman J. 1988. Morphology and locomotor adaptations of the bovid femur in relation to habitat. Journal of Morphology 198:113-130.

Leidy J. 1865. [Descriptions of *Rhinoceros meridianus* and *R. hesperius*]. Proceedings of the Academy of Natural Sciences 17(4):176-177.

Leidy J. 1885. *Rhinoceros* and *Hippotherium* from Florida. Proceedings of the Academy of Natural Sciences of Philadelphia 37:32-33.

Leidy J. 1896. Fossil vertebrates of the Alachua Clays of Florida. Transactions of the Wagner Free Institute of Science of Philadelphia 4:9-61.

Liggett GA. 1994. The Beckerdite Local Biota, (Miocene: early Hemphillian) Clark County, southwestern Kansas. Master's thesis, Fort Hays State University, Fort Hays, Kansas.

MacFadden BJ. 1998. Tale of two rhinos: isotopic ecology, paleodiet, and niche differentiation of *Aphelops* and *Teleoceras* from the Florida Neogene. Paleobiology 24:274-286.

Madden CT, Dalquest WW. 1990. The last rhinoceros in North America. Journal of Vertebrate Paleontology 10:266-267.

Matthew WD. 1932. A review of the rhinoceroses with a description of *Aphelops* material from the Pliocene of Texas. University of California Publications Bulletin of the Department of Geological Sciences 20:411-482.

McFadyean J. 1908. The Comparative Anatomy of the Domesticated Animals, Part 1: Osteology and Arthrology. William R. Jenkins Co., New York, 208 pp.

Mead AJ. 2000. Sexual dimorphism and paleoecology in *Teleoceras*, a North American Miocene rhinoceros. Paleobiology 26:689-706.

Mead JI, Schubert BW, Wallace SC, Swift SL. 2012. Helodermatid lizard from the Mio-Pliocene oak-hickory forest of Tennessee, eastern USA, and a review of monstersaurian osteoderms. Acta Palaeontologica Polonica 57(1):111-121.

Mihlbachler MC. 2001. Aspects of the paleobiology of the Neogene rhinoceroses of Florida. Master's thesis, University of Florida, Gainesville, Florida.

Mihlbachler MC. 2003. Demography of late Miocene rhinoceroses (*Teleoceras proterum* and *Aphelops malacorhinus*) from Florida: linking mortality and sociality in fossil assemblages. Paleobiology 29(3):412-428.

Mullin TC. 2006. Systematics, osteology, sexual dimorphism, age classes, and population dynamics of *Teleoceras fossiger* from Jack Swayze Quarry, Clark County, Kansas, and Minium Quarry, Graham County, Kansas. Master's thesis, Fort Hays State University, Fort Hays, Kansas.

Ochoa D, Whitelaw M, Liu Yu-Sheng (Christopher), Zavada M. 2012. Palynology of Neogene sediments at the Gray Fossil Site, Tennessee, USA: floristic implications. Review of Palaeobotany and Palynology 184:36-48.

Osborn HF. 1898a. The extinct rhinoceroses. Memoirs of the American Museum of Natural History 2(3): 75-164.

Osborn HF. 1898b. A complete skeleton of *Teleoceras*, the true rhinoceros from the upper Miocene of Kansas. Science 7:554-557.

Osborn HF. 1904. New Miocene rhinoceroses with revision of known species. Bulletin of the American Museum of Natural History 20:307-326.

Prothero DR. 1998. Rhinocerotidae; pp. 595-605 in Janis CM, Scott KM, Jacobs LL (eds.), Evolution of Tertiary Mammals of North America, Volume 1: Terrestrial Carnivores, Ungulates, and Ungulatelike Mammals. Cambridge University Press, Cambridge, United Kingdom.

Prothero DR. 2005. The Evolution of North American Rhinoceroses. Cambridge University Press, Cambridge, United Kingdom, 218 pp.

Prothero DR, Guérin C, Manning E. 1989. The History of the Rhinocerotoidea; pp. 321–340 in Prothero DR, Schoch RM (eds.), The Evolution of Perissodactyls. Oxford University Press, New York.

Prothero DR, Manning E. 1987. Miocene rhinoceroses from the Texas Gulf Coastal Plain. Journal of Paleontology 61(2):388-423.

Prothero DR, Manning E, Hanson CB. 1986. The phylogeny of the Rhinocerotoidea (Mammalia, Perissodactyla). Zoological Journal of the Linnean Society 87:341-366.

Radinsky LB. 1966. The families of the Rhinocerotoidea (Mammalia, Perissodactyla). Journal of Mammalogy 47(4):631-639.

Schubert BW. 2011. History of the Gray Fossil Site and the Don Sundquist Center of Excellence in Paleontology; pp.1-6 in Schubert BW, Mead JI (eds.). 2011. Gray Fossil Site: 10 Years of Research.

Shunk AJ, Driese SG, Clark GM. 2006. Latest Miocene to earliest Pliocene sedimentation and

climate record derived from paleosinkhole fill deposits, Gray Fossil Site, northeastern Tennessee, U.S.A. Palaeogeography, Palaeoclimatology, Palaeoecology 231:265-278.

Shunk AJ, Driese SG, Dunbar JA. 2009. Late Tertiary paleoclimatic interpretation from lacustrine rhythmites in the Gray Fossil Site, northeastern Tennessee, USA. Journal of Paleolimnology 42:11-24.

Sternberg CH. 1905. The Loup Fork Miocene of western Kansas. Transactions of the Kansas Academy of Science 20: 71-74.

Strömberg CAE, McInerney FA. 2011. The Neogene transition from C_3 to C_4 grasslands in North America: assemblage analysis of fossil phytoliths. Paleobiology 37(1):50-71.

Tedford RH, Albright III LB, Barnosky AD, Ferrusquia-Villafranca I, Hunt RM Jr., Storer JE, Swisher III CC, Voorhies MR, Webb SD, Whistler DP. 2004. Mammalian biochronology of the Arikareean through Hemphillian interval (late Oligocene through early Pliocene epochs); pp. 169-231 in Woodburne MO (ed.), Late Cretaceous and Cenozoic Mammals of North America: Biostratigraphy and Geochronology. Columbia University Press, New York.

Thomasson JR, Zakrzewski RJ, LaGarry HE, Mergen DE. 1990. A late Miocene (late early Hemphillian) biota from northwestern Kansas. National Geographic Research 6:231-244.

Voorhies MR. 1985. A Miocene rhinoceros herd buried in volcanic ash. National Geographic Society, Research Report 19:671-688.

Voorhies MR. 1992. Ashfall: life and death at a Nebraska waterhole ten million years ago. University of Nebraska State Museum, Museum Notes 81:1-4.

Voorhies MR, Stover SG. 1978. An articulated fossil skeleton of a pregnant rhinoceros,

Teleoceras major Hatcher. Proceedings of the Nebraska Academy of Sciences 88:47-48.

Wallace SC. 2006. A new population of *Teleoceras* (Mammalia: Rhinocerotidae) from the Southern Appalachians (Gray, Tennessee). Geological Society of America Abstracts with Programs 38:85.

Wallace SC. 2011. The short-legged rhinoceros, *Teleoceras*; pp. 75-77 in Schubert BW, Mead JI (eds.), Gray Fossil Site: 10 Years of Research.

Wallace SC, Hulbert RC Jr. 2009. First record of *Cormohipparion* (*Notiocradohipparion*) outside the Gulf Coastal Plain. Southeastern Association of Vertebrate Paleontologists, 2nd Annual Meeting.

Wallace SC, Nave JW, Burdick KM. 2002. Preliminary report on the recently discovered Gray Fossil Site (Miocene), Washington Co., Tennessee: with comments on observed paleopathologies—the advantages of a large sample. Journal of Vertebrate Paleontology 22(3, supplement):117A.

Wallace SC, Wang X. 2004. Two new carnivores from an unusual late Tertiary forest biota in eastern North America. Nature 431:556-559.

Webb SD, MacFadden BJ, Baskin JA. 1981. Geology and paleontology of the Love Bone Bed from the late Miocene of Florida. American Journal of Science 281:513-544.

Webb SD, Hulbert RC Jr., Morgan GS, Evans HF. 2008. Terrestrial mammals of the Palmetto Fauna (early Pliocene, latest Hemphillian) from the Central Florida Phosphate District; pp. 93-312 in Wang X, Barnes LG (eds.), Geology and Vertebrate Paleontology of Western and Southern North America: Contributions in Honor of David P. Whistler. Natural History Museum of Los Angeles County, Science Series 41.

Yatkola D, Tanner LG. 1979. *Brachypotherium* from the Tertiary of North America. Occasional Papers of the Museum of Natural History, University of Kansas 77:1-11.

Zobaa MK, Zavada MS, Whitelaw MJ, Shunk AJ, Oboh-Ikuenobe FE. 2011. Palynology and palynofacies analyses of the Gray Fossil Site, eastern Tennessee: their role in understanding the basin-fill history. Palaeogeography, Palaeoclimatology, Palaeoecology 308:433-444.

APPENDIX A

Map of Excavation of ETMNH 601 and 609

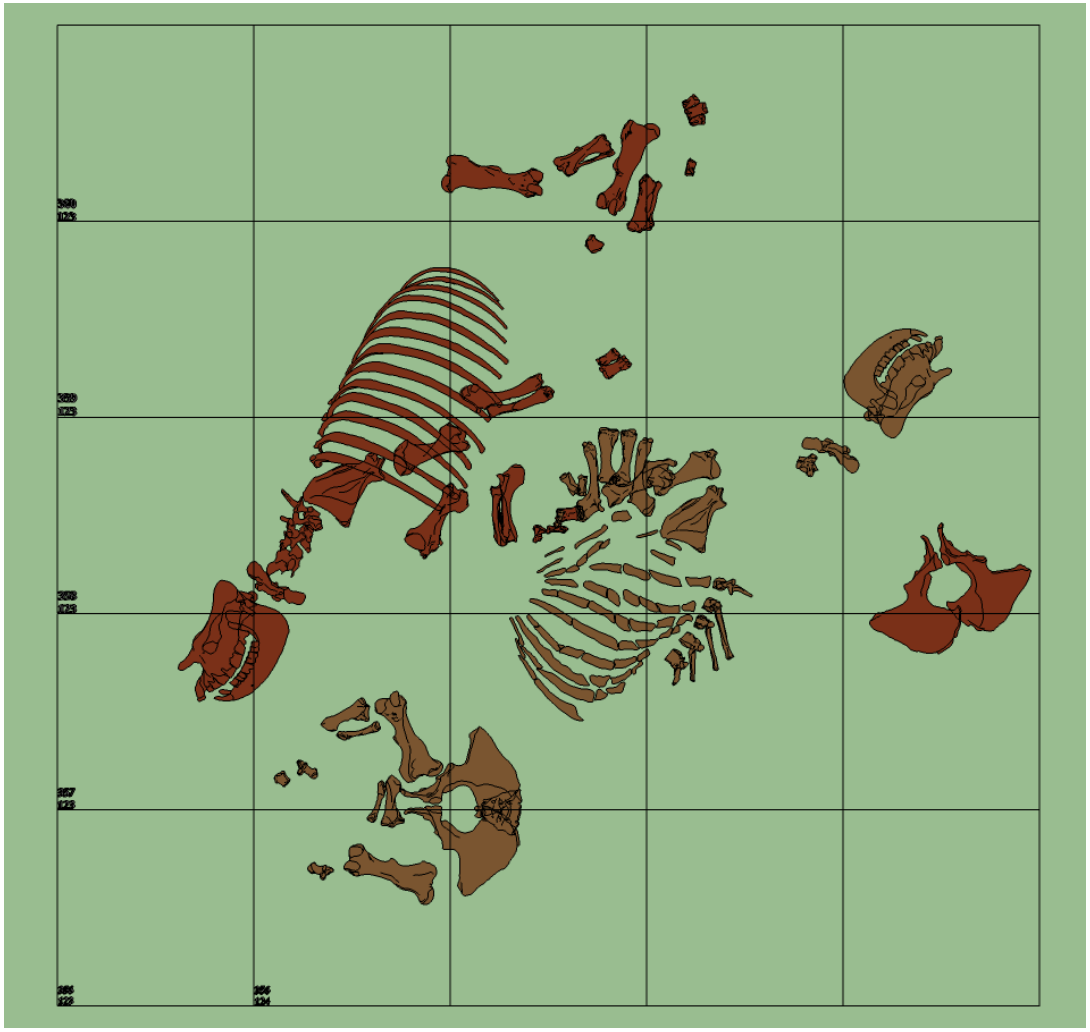

APPENDIX B

Specimens of *Teleoceras* from the Gray Fossil Site

ETMNH #	Specimen
62	carpal fragment
80	distal phalanx of second or fourth digit
107	distal phalanx
502	right ulna
559	caudal vertebra
564	medial phalanx of third digit
565	distal metapodial fragment
566	upper premolar fragment
573	caudal vertebra
601	mostly complete skeleton
609	complete skeleton
712	distal phalanx of second or fourth digit (donated from Gray Library, Gray, TN)
713	distal phalanx of second or fourth digit
743	partial distal phalanx
769	2 medial and proximal phalanges fragments
780	partial upper right molar, possibly first
781	upper left first molar fragment, partial upper left first molar
1901	left astragalus
1902	tibia and fibula, possibly fetal
3747	rib fragments
3749	right mesocuneiform
3751	neural spine epiphysis
3752	rib, possibly of ETMNH 601
3752	rib fragment, thoracic vertebra, sesamoid, 2 pieces of ossified cartilage
3754	3 rib fragments, associated
3755	proximal phalanx
3763	tusk fragment
4286	2 rib fragments
4381	sesamoid
5057	right humerus epiphyseal plate and fragments
5233	distal phalanx fragment
5235	lower tusk fragments, possibly female
6037	rib head fragment
6207	bone fragments
6647	left astragalus

6648	right proximal humerus
6649	rib fragment
6749	rib fragment
7291	rib head
7294	rib fragment
7894	tooth fragment
8173	rib fragments, frothing present
8182	rib fragment
8271	left unciform, right unciform, trapezium, right trapezoid, broken right cuneiform, right pisiform, 8 sesamoids, right second metacarpal, right third metacarpal, right fourth metacarpal, left fourth metacarpal, right second proximal phalanges, right third proximal phalanx, right fourth proximal phalanx, proximal phalanges, 2 third medial phalanges, 2 medial phalanges, right second distal phalanx, right third distal phalanx, partial distal phalanx, fragment of a carpal or tarsal
8516	left magnum
8636	partial rib
8762	left ulna fragment
10959	rib fragment
11651	distal phalanx
12175	nasal fragment, possibly female, thoracic vertebra, sesamoid
12242	rib fragment
12450	proximal phalanx of second or fourth digit
12487	right upper first molar
12776	sesamoid
12777	sesamoid
13031	bone fragment
13236	trapezium
13510	neural spine fragment
13914	right maxilla fragment with upper first molar (from Annex construction)
13968	sesamoid
14174	rib fragment
14175	right astragalus
14701	partial rib
14710	partial rib
14894	rib fragment

APPENDIX C

Linear Measurements

Humerus (Fig. 1)

1) In posterior view: Maximum width of proximal end. Measure in measuring box with the diaphysis perpendicular to the bottom and measure just distal to the articular surfaces so that both the medial side of articular head and the lateral extent of the deltoid tuberosity are included.
2) In posterior view: Maximum width of distal end. Measure in measuring box with the diaphysis perpendicular to the bottom and measure just proximal to the articular surfaces so that both medial and lateral epicondyles are included.
3) In posterior view: Greatest length. Measure in measuring box with the distal-most point of the capitulum against the end plate, align the diaphysis parallel to the bottom of the measuring box, and measure to the proximal-most point of the greater trochanter.
4) In anterior view: Greatest length 2. Measure in measuring box but adjust the movable base to avoid the greater trochanter. Place the capitulum against the end plate, align the diaphysis parallel to the bottom of the measuring box and measure to the proximal-most point of head.
5) In anterior view: Minimum width of diaphysis. Measure perpendicular to axis of diaphysis and across the humeral crest, keep calipers perpendicular to table, and measurement should not include the humeral crest.
6) In anterior view: Midshaft width. Measure perpendicular to axis of diaphysis and across the humeral crest, keep the calipers perpendicular to table, and the measurement will incorporate the humeral crest.

7) In lateral view (illustrated in anterior view): Distance between proximal-most point of lesser tuberosity and the distal-most point of the deltoid tuberosity along lateral side. At lesser tuberosity, measure from proximal-most point of medial projection and, at deltoid tuberosity, measure from the distal-most and lateral-most point on lateral edge near confluence with humeral crest. Do not measure to posterior extent of deltoid tuberosity as this is highly variable with muscle attachment.
8) In lateral view: Greatest length of greater tuberosity. Measure from proximal-most point of tuberosity to distal-most point of deltoid tuberosity along lateral side. At greater tuberosity, measure from proximal most point and, at deltoid tuberosity, measure from the distal-most and lateral-most point on lateral edge near confluence with humeral crest. Do not measure to posterior extent of deltoid tuberosity as this is highly variable with muscle attachment.
9) In lateral view (illustrated in posterior view): Distance between distal deltoid tuberosity and lateral epicondyle. Measure from the distal extent of deltoid tuberosity spot to the proximolateral most point of the lateral epicondyle
10) In anterior view: Width of trochlea and capitulum. Align calipers with the medial edge of the trochlea, the proximal edges of the capitulum and trochlea, and measure to the lateral edge of the capitulum.
11) In medial view: Greatest width of trochlea. Measure from posterior point of trochlea, perpendicular to axis of diaphysis, and keep calipers perpendicular to table surface.
12) In posterior view: Width of olecranon fossa. Measure with calipers between lateral and medial epicondyles and just below the posterior surfaces of the epicondyles.

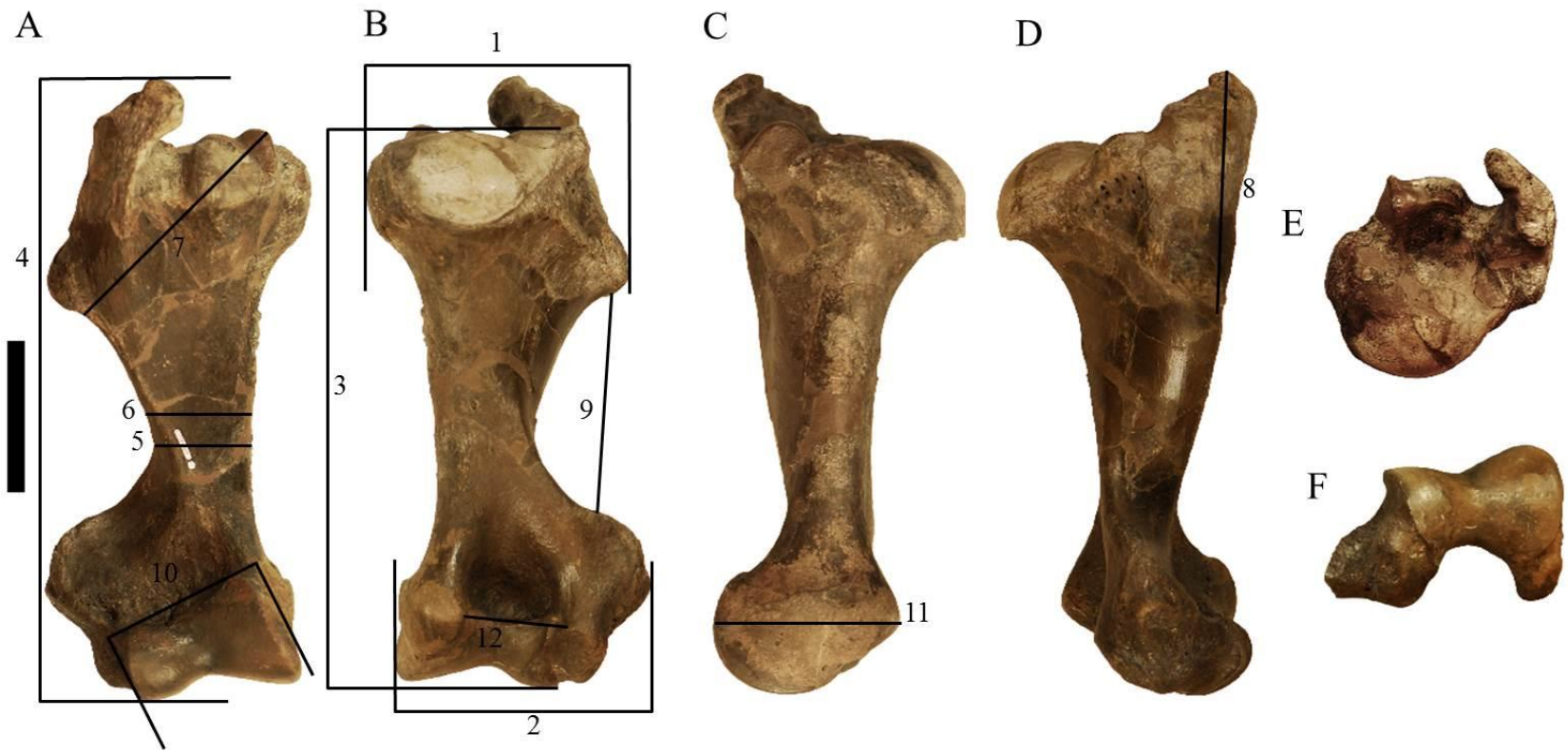

Figure 1. Humerus measurements used in this study. Views: A, anterior; B, posterior; C, medial; D, lateral; E, proximal; F, distal. See corresponding numbers in appendix for descriptions of the measurements. Scale bar = 10 cm.

Ulna (Fig. 2)

1) In medial view: Medial length. Measure in measuring box with the olecranon process against the end plate of the box, the diaphysis parallel to the bottom of the box, and measure to the end of the styloid process.
2) In lateral view: Lateral length. Measure in measuring box with the olecranon process against the end plate of the box, the diaphysis parallel to the bottom of the box, and measure to the end of the styloid process.
3) In anterior view: Dorsal length. Measure in measuring box with the olecranon process against the end plate of the box, the diaphysis parallel to the bottom of the box, and measure to the end of the styloid process.
4) Average length. Average of #1, #2, and #3. This reduces any biases caused by the presence, absence (i.e. broken off), or degree of expansion of the medial and lateral articular processes.
5) In anterior view: Maximum mediolateral width at the proximal end of the diaphysis. Measure across the bone just distal to the trochlear notch so that the calipers are perpendicular to the axis of the ulna but not necessarily to the curvature of the bone. This measurement may include the rugosity distal to the site of radial articulation but should still be proximal to the narrowing at the proximal end of the diaphysis.
6) In anterior view: Maximum mediolateral width at the distal end of the diaphysis. Measure across the bone just proximal to the styloid process so that the calipers are perpendicular to the axis of the bone but not necessarily to the curvature of the bone.
7) In anterior view: Minimum diaphyseal width. Measure across the bone so that the calipers are perpendicular to the axis of the bone but not necessarily to the curvature of the bone. This measurement should be taken between #5 and #8.

8) In anterior view: Midshaft diaphyseal width. Measure across the bone so that the calipers are perpendicular to the axis of the bone but not necessarily to the curvature of the bone. This measurement should be midway between measurements #5 and #6.
9) In medial view: Length of olecranon process. Measure from the anconeal process, at the groove between the articular surfaces for the trochlea and capitulum, to the proximal-most point of the olecranon process so that the calipers are parallel to the angle of the olecranon process.
10) In lateral view: Midway depth of olecranon process. Measure from the midpoint of the anterior surface of the olecranon process to the corresponding point on the posterior surface so that the calipers are perpendicular to the anterior surface of the olecranon process.
11) In anterior view: Length of olecranon process and the semilunar notch. Measure from the radial notch between the medial and lateral articular processes to the proximal-most point of the olecranon process so that the calipers are parallel to the angle of the olecranon process.
12) In anterior view: Length of trochlear notch. Measure from the starting point of #11 to the starting point of #9. Both caliper tips should be just outside the edges of the articular surface.
13) In anterior view: Width of articular processes. Measure from the lateral-most point to the medial-most point so that calipers follow the slant of the processes.
14) In anterior view: Midsection width of trochlear notch. Measure from the lateral edge to the medial edge of the facet so that the calipers are parallel to the plane of #13.
15) In distal view: Length of styloid process. Measure from the anterior-most (dorsal when viewed distally) point to the posterior-most (ventral when viewed distally) point. The calipers should be perpendicular to the axis of the diaphysis.

16) In medial view: Anterolateral midshaft diaphyseal width. Measure from anterior to posterior at the same location as #8 so that the calipers are perpendicular to the axis of the ulna but not necessarily to the curvature of the bone.

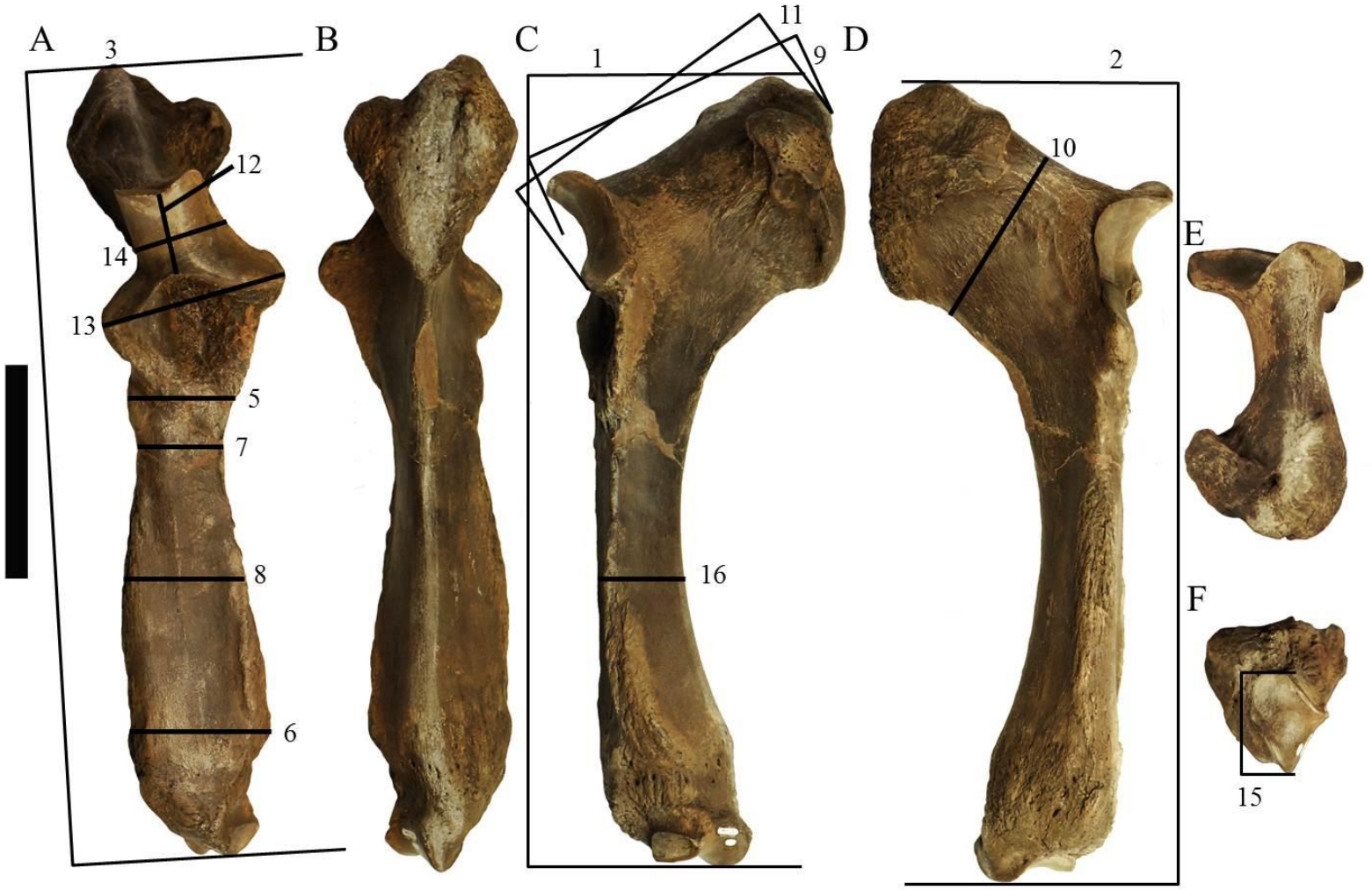

Figure 2. Ulna measurements used in this study. Views: A, anterior; B, posterior; C, medial; D, lateral; E, proximal; F, distal. See corresponding numbers in appendix for descriptions of the measurements. Measurement #4 is not shown because it is an average. Scale bar = 10 cm.

Radius (Fig. 3)

1) In anterior view: Greatest length. Measure in measuring box with mediodistal articular surface against the base, axis parallel to the bottom of the box, and measure to the proximal-most point of the coronoid process.
2) In anterior view: Maximum width of proximal end. Measure in measuring box, with the diaphysis perpendicular to the bottom and measure just distal to the articular surfaces. The radius may have to be rotated slightly so that both proximal articular surfaces rest on the bottom of the measuring box.
3) In anterior view: Maximum width of distal end. Measure in measuring box, with the diaphysis perpendicular to the bottom and measure just proximal to the articular surfaces. The radius may have to be rotated slightly so that both distal articular surfaces rest on the bottom of the measuring box.
4) In anterior view: Minimum diaphyseal width. Measure mediolaterally and perpendicular to the axis at the narrowest point of the diaphysis.
5) In anterior view: Midshaft width 1. Measure mediolaterally and perpendicular to the axis at the proximodistal midpoint.
6) In medial view: Midshaft width 2. Measure anteroposteriorly and perpendicular to the axis at the proximodistal midpoint.
7) In distal view: Width of distal articular facets. Align calipers with the medial and anterior edges of the medial articular surface and measure to the lateral-most point of the lateral articular surface.
8) In proximal view: Depth of proximal articular surface. Measure with calipers at anterior and posterior ends of the coronoid process between the medial and lateral articular surfaces.

Figure 3. Radius measurements used in this study. Views: A, anterior; B, posterior; C, medial; D, lateral; E, proximal; F, distal. See corresponding numbers in appendix for descriptions of the measurements. Scale bar = 10 cm.

Metapodials (Fig. 4)

1) In posterior view: Length of metapodial. Measure in measuring box with distal end against the end plate of the box, the axis parallel to the bottom of the box, and measure to the proximal-most point. To keep the metapodial parallel to the box, only 1 distal articular surface may rest against the end plate.
2) In posterior view: Maximum width of proximal end. Measure in measuring box with the metapodial axis perpendicular to the box. This measurement may include the proximal articular expansion.
3) In posterior view: Maximum width of distal end. Measure in measuring box with the metapodial axis perpendicular to the box. This measurement may include the distal articular expansion.
4) In anterior view: Minimum width of diaphysis. Measure the narrowest mediolateral point with the calipers perpendicular to the axis of the diaphysis. Rotate the metapodial so that the anterior surface is leveled rather than sloped.
5) In anterior view: Midshaft width. Measure mediolaterally at the midpoints and perpendicular to the axis of the metapodial.
6) In medial view: Midshaft width. Measure anteroposteriorly at the midpoints and perpendicular to the axis of the metapodial.

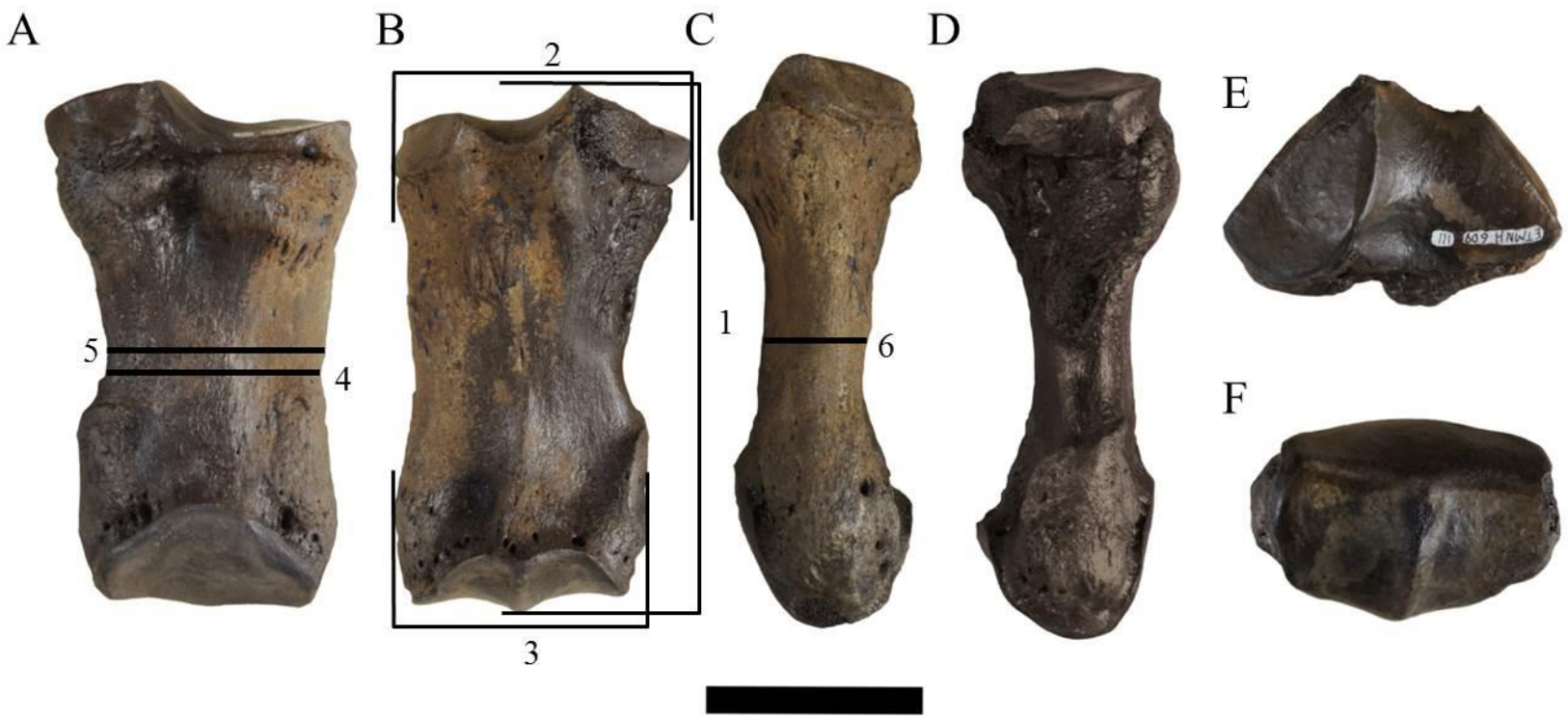

Figure 4. Third metapodial measurements used in this study. Views: A, anterior; B, posterior; C, medial; D, lateral; E, proximal; F, distal. The third metacarpal is illustrated but the same measurements apply to the third metatarsal . See corresponding numbers in appendix for descriptions of the measurements. Scale bar = 10 cm.

Femur (Fig. 5)

1) In anterior view: Length of femur. Measure in measuring box with the lateral condyle flush with the end of box, align the axis parallel to the bottom of the box, and measure to the proximal-most point of the femur. In *Teleoceras*, this proximal-most point should be the articular head rather than the greater trochanter.
2) In anterior view: Length of femur excluding head. Measure in measuring box with the lateral condyle flush with the end of the box, align the axis parallel to the bottom of the box, and measure to the proximal-most point of the greater trochanter. This may require shifting the end plate so that the head does not interfere.
3) In anterior view: Maximum proximal width. Measure in measuring box with the articular head and the greater trochanter laying flush on the bottom of the box and the axis of the diaphysis perpendicular to the box.
4) In anterior view (illustrated in distal view): Maximum distal width. Measure in measuring box with both condyles flush on the bottom of the box and with the axis of the diaphysis perpendicular to the box.
5) In anterior view: Minimum width of the diaphysis. With both condyles resting on the table, measure perpendicular to the axis just distal of the third trochanter and keep the calipers upright and level.
6) In posterior view: Furthest lateral expansion of third trochanter. Measure as the mediolateral width with calipers perpendicular and as flush as possible with the posterior surface of the diaphysis.
7) In anterior view: Expanse of third trochanter. Measure in measuring box from the proximal-most point of greater trochanter to the distal-most point of the third trochanter. The end plates

of the measuring box may have to be adjusted to allow the measurement to be taken parallel to the diaphysis.

8) In anterior view: Width of trochlear tubercles. Measure with calipers flush along the proximal and medial surfaces of the trochlear tubercle and measure to the lateral surface so that the calipers are parallel with the slant of the tubercle.
9) In proximal view: Depth of femoral head. Measure with calipers along the epiphyseal suture lines of the medial and posterior surfaces, which may have to be estimated, and perpendicular to the head-greater trochanter axis. Measure to the anterior surface of the head but not necessarily to the lip. The calipers may have to be tilted downward slightly to reach these landmarks.
10) In distal view: Height of trochlear tubercles. Measure with calipers flush with the anterior-most point of tubercle and the posterior-most point of the medial condyle. The calipers should be parallel to the axis of measurement.
11) In lateral view: Width of lateral condyle. Measure at the maximum width of the lateral condyle and perpendicular to the axis of the femur.
12) In medial view: Width of medial condyle. Measure at maximum width of the medial condyle and perpendicular to the axis of the femur.

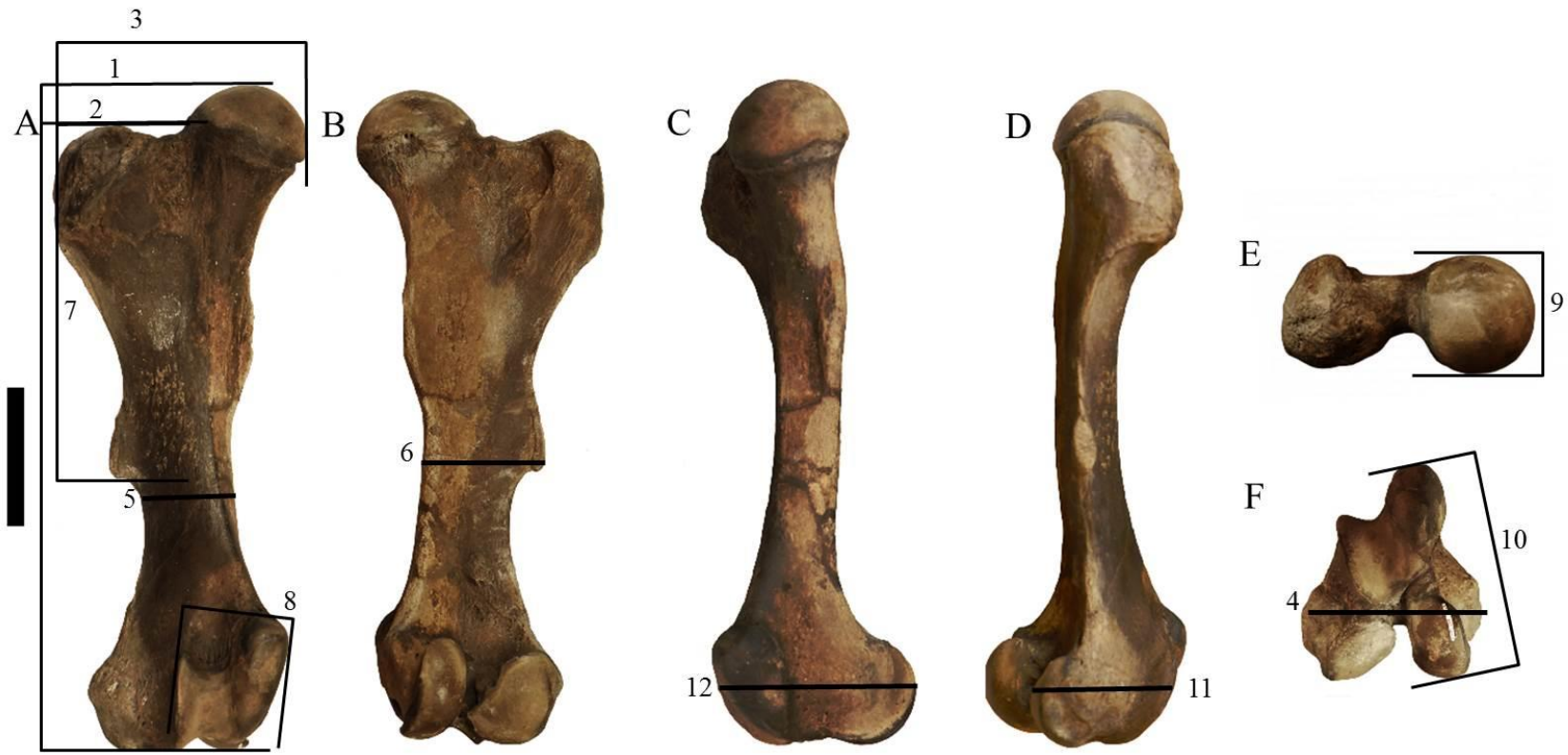

Figure 5. Femur measurements used in this study. Views: A, anterior; B, posterior; C, medial; D, lateral; E, proximal; F, distal. See corresponding numbers in appendix for descriptions of the measurements. Scale bar = 10 cm.

Tibia (Fig. 6)

1) In posterior view: Length of tibia. Measure in measuring box with the proximal end against the end of the box and the diaphyseal axis parallel to the bottom of the box. Measuring in the posterior view removes any possible bias caused by a fusion or lack of fusion of the fibula.
2) In posterior view: Width of proximal articular surfaces. Measure in measuring box with both the medial and lateral articular surfaces of the proximal end on the bottom of the box and the axis perpendicular to the box. If the fibula is fused, it may be necessary to take, and possibly estimate, the measurement with calipers.
3) In posterior view: Width of distal end. Measure in measuring box with the medial surface against end of the box and the diaphyseal axis perpendicular to the scale of the box. The tibia may have to be slightly rotated mediolaterally so that the anterior edges of both the lateral and medial articular surfaces are resting on the bottom of the box. If the fibula is fused, it may be necessary to take, and possibly estimate, the measurement with calipers.
4) In anterior view: Minimum diaphyseal width. Measure mediolaterally across the diaphysis at the least width with the calipers perpendicular to the axis.
5) In anterior view: Midshaft width. Measure mediolaterally at the proximodistal midpoint of the diaphysis with the calipers perpendicular to the axis.
6) In proximal view: Expansion of tibial tuberosity. Measure from the posteromedial-most point of the intercondylar area, across the intercondylar eminence, and to the anterolateral-most point of the tibial tuberosity.
7) In distal view: Depth of distal articular surface. Measure across the midline ridge of the articular surface for the astragalus posterior edge to the anterior edge. The calipers should be just outside of the lips of the articular surface.

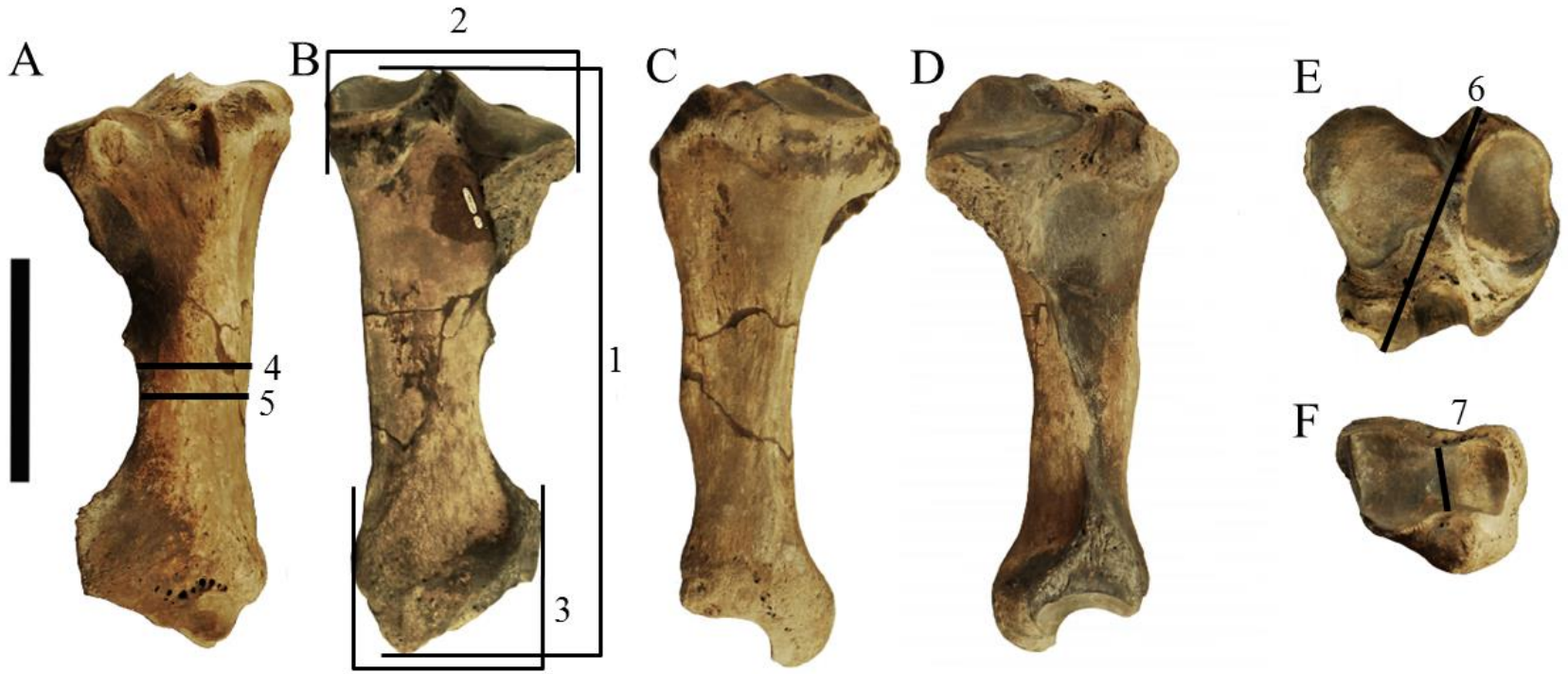

Figure 6. Tibia measurements used in this study. Views: A, anterior; B, posterior; C, medial; D, lateral; E, proximal; F, distal. See corresponding numbers in appendix for descriptions of the measurements. Scale bar = 10 cm.

Calcaneum (Fig. 7)

1) In plantar view: Length of calcaneum. Measure in measuring box with the axis parallel to the box and the sustentaculum extending outward.
2) In medial view: Distance between calcaneal tuber end and sustentaculum. Measure from the midpoint of the medial attachment site on the posterior-most calcaneal tuber to the medial-most point of sustentaculum.
3) In dorsal view: Midshaft width of diaphysis. Measure mediolaterally with calipers perpendicular to the diaphyseal axis (ignoring the sustentaculum). Rotate the calcaneum just slightly so that the sustentaculum and the flat mediodorsal surface of the calcaneal tuber are pointed upward but not completely medially (not rotated in illustration).
4) In dorsal view: Length of sustentaculum. Measure mediolaterally from the medial-most point of the sustentaculum to the lateral-most point of the lateral process. The calipers should parallel the slant of the processes and any bone beyond the articular surfaces should be included in the measurement.

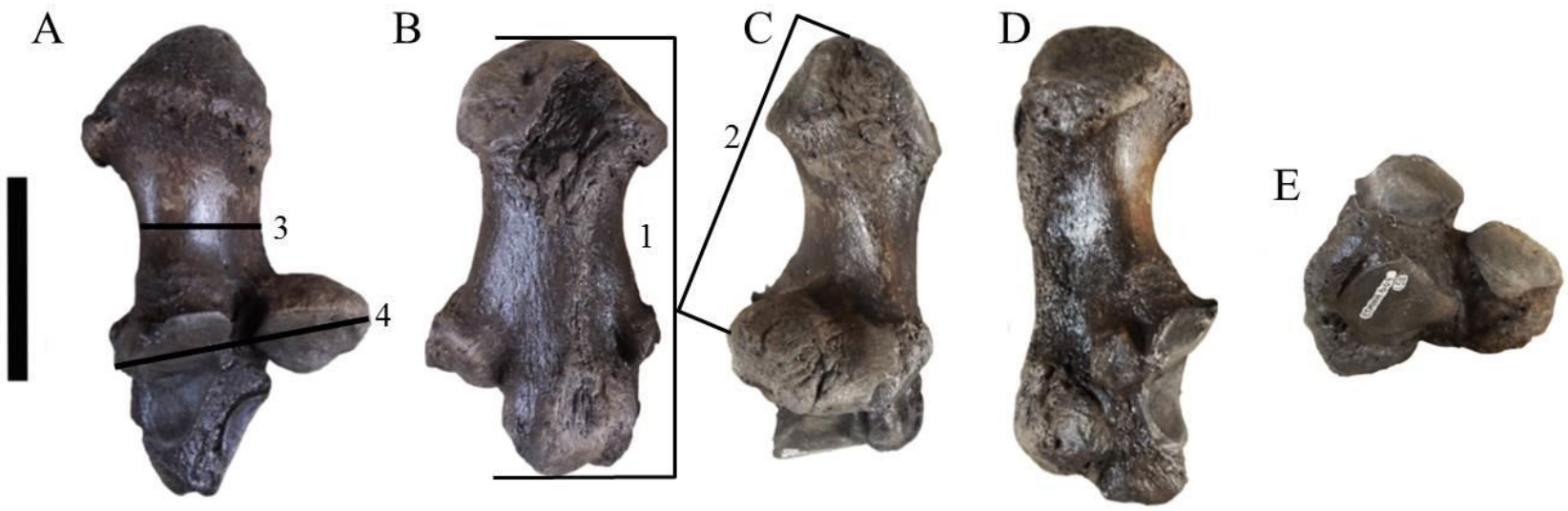

Figure 7. Calcaneum measurements used in this study. Views: A, dorsal; B, plantar; C, medial; D, lateral; E, anterior. See corresponding numbers in appendix for descriptions of the measurements. Scale bar = 5 cm.

APPENDIX F

Data

Asterisks indicate least measurements or questionable data, e.g. damaged or repaired specimens that might influence the measurement. Blank spaces indicate that the measurement could not be taken reliably.

Humerus

Locality	Number	Side	1	2	3	4	5	6	7	8
AQ	F:AM 104007	R	112.3	137.5	353.3	303.8	54.52	60.45		171.73*
AQ	F:AM 104008	L		128.5		282.3	54.67	65.32	144.19	
BTR	F:AM 115752b	R	149.5	160.5	398.8*		73.37	80.50		172.48
BTR	F:AM 115752c	L	119.5	127.8	337.0	291.8*	65.09	74.01	128.96*	139.65*
BTR	F:AM 115754c	L	150.5	154.3	375.0*		63.08	70.56		
BTR	F:AM 115815	R	155.5		394.3	353.3	65.51	76.50		173.10
BTRh	F:AM 115821	L	138.0	154.0	369.0	326.0	62.99	81.67		148.10*
BV	UF 200908	R					56.96			
BV	UF 200937	L		136.0						
BV	UF/TRO 3894	R								
BV	UF/TRO 3895	R								
GFS	ETMNH 601	L		161.5		388.5	66.32	75.58		
GFS	ETMNH 601	R	161.0	161.5*		389.3*	66.56	77.27		
GFS	ETMNH 609	L	158.5	146.8	393.0	360.5	53.86	77.44	161.49	150.88
GFS	ETMNH 609	R	150.0	146.8	392.0	356.8	56.14	74.02	156.03	149.93
LBB	UF 26351	L	103.3	124.3	319.8	283.00	47.45	60.10		
LBB	UF 27394	L	117.3							128.42
LBB	UF 27395	L		130.5		291.57	53.84	65.56		
LBB	UF 39838	L		127.5		294.19	56.44			

LBB	UF 39839	L	118.5				50.23	67.17		
LBB	UF 39840	L	114.0	118.8	303.0	274.95	50.51	65.74	129.81	133.59
LBB	UF 39842	L				273.31	52.79	66.48		
LIQ	AMNH 2643; F:AM 104056	L	125.3	137.0	346.8	298.8	54.76	71.00	150.23	165.54
LIQ	AMNH 2665	R	115.0	134.5	333.0	293.5	49.56	64.18	137.51	162.02
LIQ	USNM PAL 419090	R	118.0	132.0	353.0	295.8	50.62	60.48*		160.91*
LIQ	USNM V 7875	R	135.0	149.5	374.0	311.3	55.62	66.74	167.93	184.08
LIQ	USNM V 7902	L	150.8	151.3	389.5	337.5	66.99	94.60	167.19	185.45
MBB	F:AM 104197	R	150.0	141.5	351.8	331.5	66.42	78.05	151.11	127.35*
MBB	F:AM 144170	R	146.5	150.0	354.5	320.5	62.86	69.99		138.58
MBB	F:AM 144171	L	151.5	140.8	353.0	327.5	63.31	71.19	146.76	130.56
MBB	F:AM 144172	L	151.8	136.8*	359.5	330.0	66.69	77.49	135.17	
MBB	F:AM 144173	L	144.8	142.5	353.3	326.5	61.52	74.01		128.75
MBB	USNM PAL 416320	L		125.3						
MBB	USNM PAL 416322	L		129.3						
MBB	USNM PAL 416324	L		127.0						
MBB	USNM PAL 416325 (1)	R								
MBB	USNM PAL 416325(2)	R		127.8						
MBB	USNM PAL 416326	L								
MBB	USNM V 3594	R	127.5	136.8		322.5	55.96	56.87		
MBB	USNM V 3595	R		135.0						
MBB	USNM V 3596	R		138.5						
MBB	USNM V 3597	L		133.0						
MF	UF 10956a	L	106.5	118.0	292.0	255.50	53.19	62.38	128.33	135.19
MF	UF 10956b	L		126.5		275.25	55.92			
MF	UF 16844	R		134.0			57.61			

MF	UF 17085	L		133.3						
MF	UF 3075	L	138.5							
MF	UF 59618	L				285.31				
MF	UF 59620	R	128.5							151.25
MF	UF 59622	R		136.5						
MF	UF 59624	L	121.5	119.0			56.68	68.50		122.90
MQ	FHSM VP-8091	R	155.0	169.3		356.5	63.65			
MQ	FHSM VP-8267	R		134.5						
MQ	FHSM VP-8318	R		150.0		312.5	61.13			
SQ	FHSM VP-1058	R	151.8	163.0		335.5	69.45	85.49		
SQ	FHSM VP-2046	L	159.3	144.3		344.5	68.02	89.06	163.46	
WQ	DMNH 1180	R		152.3						
WQ	DMNH 22321	L		152.0						
WQ	DMNH 23190	L		137.3						
WQ	DMNH 23920	R		139.5			62.05			
WQ	DMNH 304	R					60.74	76.40		
WQ	DMNH 307	R	145.0*	154.0	367.8	331.5	66.41	80.46*	146.86*	147.91*
WQ	DMNH 308	R	137.5	139.3		330.3	60.20	71.87		
WQ	F:AM 115886b	L	142.3	142.0	350.0	306.3	58.35	63.34	139.99	132.46

Locality	Number	Side	9	10	11	12
AQ	F:AM 104007	R	70.34	90.25	90.70	46.98
AQ	F:AM 104008	L	79.40	78.62	91.89	36.85
BTR	F:AM 115752b	R	115.48	106.50	110.91	42.68
BTR	F:AM 115752c	L	98.03	90.04*	101.25	23.13
BTR	F:AM 115754c	L		103.59	112.58	43.75
BTR	F:AM 115815	R		101.65		

BTRh	F:AM 115821	L	127.54	99.08	115.18	48.84
BV	UF 200908	R			87.03	
BV	UF 200937	L		96.65		
BV	UF/TRO 3894	R		88.76		
BV	UF/TRO 3895	R		94.58	106.71	
GFS	ETMNH 60	L		100.20	108.31	46.09
GFS	ETMNH 601	R	166.07	99.35*		
GFS	ETMNH 609	L	159.72	95.28	103.33	
GFS	ETMNH 609	R	156.12	92.63	103.44	58.73
LBB	UF 26351	L	87.08	76.94	89.51	33.37
LBB	UF 27394	L			90.33	
LBB	UF 27395	L	75.63	88.20	86.55	
LBB	UF 39838	L		81.57	88.51	30.30
LBB	UF 39839	L	81.75			
LBB	UF 39840	L	87.34	76.24	83.00	
LBB	UF 39842	L		74.26	81.75	
LIQ	AMNH 2643; F:AM 104056	L	99.77	100.03	99.43	46.09
LIQ	AMNH 2665	R	83.76	92.20	97.88	35.90
LIQ	USNM PAL 419090	R	90.44*	86.66	95.85	65.90
LIQ	USNM V 7875	R	104.95	96.95	104.13	68.56
LIQ	USNM V 7902	L	99.76	92.94	106.73	59.44
MBB	F:AM 104197	R	109.90	89.19	101.72	54.71
MBB	F:AM 144170	R	111.73	95.62	101.00	51.54
MBB	F:AM 144171	L	120.93	91.04*	100.08	46.83
MBB	F:AM 144172	L	107.00	89.13*	100.50	54.65
MBB	F:AM 144173	L	118.66	84.88*	101.05	43.93

MBB	USNM PAL 416320	L		87.99		
MBB	USNM PAL 416322	L		82.66	94.63	46.44
MBB	USNM PAL 416324	L				
MBB	USNM PAL 416325 (1)	R			96.74	
MBB	USNM PAL 416325 (2)	R		86.79	90.55	
MBB	USNM PAL 416326	L		87.86		
MBB	USNM V 3594	R	153.08	86.75	103.63	
MBB	USNM V 3595	R		90.59	103.63	57.72
MBB	USNM V 3596	R		87.91		
MBB	USNM V 3597	L		84.74	94.04	41.37
MF	UF 10956a	L	72.56	76.23	81.12	29.67
MF	UF 10956b	L		77.77	88.43	
MF	UF 16844	R		85.49	86.62	40.50
MF	UF 17085	L		79.68	85.58	34.36
MF	UF 3075	L		86.69		
MF	UF 59618	L		76.67		
MF	UF 59620	R			83.96	
MF	UF 59622	R		87.07	95.72	37.05
MF	UF 59624	L	94.34			
MQ	FHSM VP-8091	R	97.02	108.51	115.23	36.87
MQ	FHSM VP-8267	R		96.34		
MQ	FHSM VP-8318	R		92.97	102.74	55.98*
SQ	FHSM VP-1058	R	105.27	94.79	110.81	
SQ	FHSM VP-2046	L		96.32	103.61	
WQ	DMNH 1180	R		102.47		
WQ	DMNH 22321	L		98.84		

WQ	DMNH 23190	L		94.28	103.80	
WQ	DMNH 23920	R		91.84		
WQ	DMNH 304	R	129.50	96.71		48.28
WQ	DMNH 307	R	122.22	101.00	104.28	53.00
WQ	DMNH 308	R	132.56	94.88		
WQ	F:AM 115886b	L	124.15	91.59	96.58	42.56

Ulna

Locality	Number	Side	1	2	3	4	5	6	7	8
AQ	F:AM 104010	R	279.0	279.5	282.3	280.3	48.74	69.19	43.31*	59.20*
AQ	F:AM 104011	R	280.8	279.8	284.5	281.7	42.30	55.22*	38.59	52.14
BTR	F:AM 115756a	L	331.0	329.0	330.8	330.3	62.01	73.89	50.25	63.38*
BTR	F:AM 115756b	R	342.3	339.5	343.0*	341.6	56.05	68.29	48.29	67.23
BTR	F:AM 115756c	R	344.5	343.5	345.8	344.6	55.54	72.60	48.87	67.35
BTR	F:AM 115756f	R	354.0	352.0	354.5	353.5	54.72	72.47	53.28	77.51
BTRh	F:AM 115822a	L	360.3	359.3	364.0	361.2	60.51	66.61	43.25	63.63
BTRh	F:AM 115822b	R	354.8	351.8	359.3	355.3	49.14	61.82	44.34*	64.85*
BV	UF 200919	L								
BV	UF 212466	R					41.89			
BV	UF 212467	R					48.77			
BV	UF/TRO 3879	L								
BV	UF/TRO 3880	L								
BV	UF/TRO 3881	R								
GFS	ETMNH 601	L	402.5	401.0	403.0	402.2	58.45	67.54*	45.70*	59.80*
GFS	ETMNH 601	R	402.8	403.5	406.0*	403.1	57.78	68.59*	47.57*	60.50*
GFS	ETMNH 609	L	379.3	378.5	379.3	379.0	50.74*	63.78	41.49*	57.91

GFS	ETMNH 609	R	370.3	372.0	374.0	372.1	45.88	66.97	40.39*	58.57
LBB	UF 39944	R	293.0	293.0	296.3*	293.0	39.22	49.11	33.87	44.13
LBB	UF 39945	R					32.12	49.90		44.56
LBB	UF 39946	R	310.8	306.8	310.5	309.3	40.14	45.81	37.55	40.88
LBB	UF 39947	R					40.44	46.45		48.39
LBB	UF 39949	R					46.36		42.90	
LBB	UF 39950	R					36.15		36.74	
LBB	UF 39954	L	303.3	304.0	304.8	304.0		50.08		47.05
LBB	UF 39955	L	279.8	280.0	282.5	280.8	46.58	49.76	39.57	49.46
LIQ	USNM PAL 419048 (1)	R	283.0	286.5	290.0	286.5	45.75	53.27	36.16	43.90
LIQ	USNM PAL 419048 (2)	L	326.0	326.0	331.3	327.8	47.97	58.49	38.57	53.25
LIQ	USNM V 1445	R	346.3	347.3	348.8	347.4	43.37	64.51	39.59	53.12
LIQ	USNM V 1446	L	313.5	312.8	314.3	313.5	46.83	59.68	39.80	49.86
LIQ	USNM V 7881	L	339.3	340.3	344.5	341.3	52.14	55.13	43.40	60.07
MBB	F:AM 104200	R	294.5	293.0	297.8	295.1	44.71	59.37	40.05	63.20
MBB	F:AM 144174	R	311.8	310.5	314.0	312.1	42.68	64.06	38.89	59.29
MBB	F:AM 144175	R	301.0	301.3	305.5	302.6	42.63	61.82	39.99	54.86
MBB	F:AM 144176	R	334.3	332.8	333.8	333.6	47.70	61.08	45.07	64.17
MBB	F:AM 144177	R	304.8	305.8	309.8	306.8	40.33	56.94	39.69	53.55
MBB	USNM PAL 416325	R								
MBB	USNM V 3410	L								
MBB	USNM V 3411	R	300.0	298.5*	304.3	300.92	47.75	58.67	43.00	55.46
MBB	USNM V 3412	R						61.19		
MBB	USNM V 3413	R						61.19		
MBB	USNM V 3414	L								
MBB	USNM V 3733	R						68.82		

MF	UF 10961	L	296.5	293.0	293.0	294.2	45.24	51.17	39.64	51.28
MF	UF 59635	R						52.27		
MF	UF 59636	L								
MF	UF 59637	L						52.81		
MF	UF 59638	L								
MF	UF 59641	L								
MQ	FHSM VP-8269	R	355.5	355.0	362.0	357.5	52.89	83.01	45.41	67.66*
MQ	FHSM VP-8919	R	369.3	369.3	372.5	370.3	60.65	63.42	48.11	64.80
SQ	FHSM VP-1079	R	346.5	345.0	353.0	348.2	49.27	62.88	44.30	52.63*
WQ	DMNH 23183	L	302.0	300.0	306.8	302.9	48.16	64.89	39.71	52.90
WQ	DMNH 297	L	318.0	319.5	326.0	321.2	49.42	61.44	39.86	44.89
WQ	DMNH 298	L	336.8	335.0	339.0	336.9	60.74*	63.00	45.51*	53.41
WQ	DMNH 304	R					47.80	55.12	40.41	53.64
WQ	F:AM 115888b	L	335.8	334.0	340.3	336.7	48.88	57.46	44.07	49.77
Locality	Number	Side	9	10	11	12	13	14	15	16
AQ	F:AM 104010	R	122.72	73.26	118.88	45.53	76.12	37.90	40.39	37.06
AQ	F:AM 104011	R	111.19*	68.27	113.44*	48.01	68.02	27.81	37.48	32.23
BTR	F:AM 115756a	L	125.44	94.64	140.50	46.62	90.86	42.72	45.76	40.43
BTR	F:AM 115756b	R	135.76	91.59	145.30	56.21	87.78	39.83	46.88	39.44
BTR	F:AM 115756c	R	140.89	99.36	145.63	53.13	85.50	44.17	50.17	37.44
BTR	F:AM 115756f	R	140.57	96.13	147.66	55.77	95.96	42.08	48.53	43.73
BTRh	F:AM 115822a	L	141.66	89.29	150.99	52.92	89.61	39.51	52.93	46.42
BTRh	F:AM 115822b	R	142.12	95.39	149.57	51.92	89.07	43.84*	49.36	47.32
BV	UF 200919	L	131.46	85.13	129.30	42.02	86.53			
BV	UF 212466	R								
BV	UF 212467	R					80.44			

BV	UF/TRO 3879	L				48.44	80.99	39.55		
BV	UF/TRO 3880	L				45.49		38.89		
BV	UF/TRO 3881	R				43.41	87.41	42.45		
GFS	ETMNH 601	L	144.32	102.77*	150.03	49.37	90.26	37.08	53.06	45.75*
GFS	ETMNH 601	R	148.28*	101.09*	149.14*	51.39	92.61	37.36	54.30	47.75*
GFS	ETMNH 609	L	129.91	86.33	139.10	38.72	85.61*	37.72	48.72	38.08
GFS	ETMNH 609	R	140.58	86.82	142.39	42.80	86.70	40.59	48.24	39.84
LBB	UF 39944	R	104.77	69.56					39.76	33.04
LBB	UF 39945	R					65.05		43.57	33.71
LBB	UF 39946	R	110.43	67.95	118.52	44.35	71.53	32.20	36.62	33.59
LBB	UF 39947	R				46.90	74.30	32.57	40.88	36.70
LBB	UF 39949	R		77.59*						
LBB	UF 39950	R	103.77	65.64	120.56	46.46	73.73	32.91		
LBB	UF 39954	L	108.97	67.70	115.88	47.68		29.05	45.30	33.85
LBB	UF 39955	L	102.80	64.20	106.63	42.74		32.26	38.88	36.28
LIQ	USNM PAL 419048 (1)	R	111.31*	70.88	121.73	44.90*	77.65	32.58	42.43	31.18
LIQ	USNM PAL 419048 (2)	L	129.38	77.47	132.95	50.44	81.82	41.73	40.66	39.54
LIQ	USNM V 1445	R	137.23	87.07	141.54	43.55	78.53	39.21	54.56	36.93
LIQ	USNM V 1446	L	112.77	76.81	126.20	47.31	76.99	34.98	46.44	38.32
LIQ	USNM V 7881	L	133.58	83.00	136.89	46.62	82.46	36.96	40.95	37.15
MBB	F:AM 104200	R	126.63	77.34	125.52	41.65	83.62	38.11	42.80	37.49
MBB	F:AM 144174	R	124.60*	98.57	131.46*	54.59	87.37	38.77	53.40	46.41
MBB	F:AM 144175	R	118.61	83.80	125.04	46.99	78.86	38.24	44.62	36.57
MBB	F:AM 144176	R	137.39*	103.39	139.37	57.92*	90.01	40.28	47.31	41.98
MBB	F:AM 144177	R		77.29	126.58		78.32	37.93	40.83	33.12
MBB	USNM PAL 416325	R	127.47*	77.94	129.81	33.06*				

MBB	USNM V 3410	L	123.34	80.12	127.43	46.33		35.87		
MBB	USNM V 3411	R	124.13*	85.46	126.95	43.46*			41.61	38.87
MBB	USNM V 3412	R							45.36	
MBB	USNM V 3413	R								
MBB	USNM V 3414	L			122.30					
MBB	USNM V 3733	R								
MF	UF 10961	L				47.08			40.10	37.60
MF	UF 59635	R							36.47*	
MF	UF 59636	L	105.99*	72.58	113.99	50.26*		31.67		
MF	UF 59637	L							42.74	
MF	UF 59638	L	116.02	78.55	121.96	50.74		27.63		
MF	UF 59641	L	108.37	67.19	117.56	44.64		32.31		
MQ	FHSM VP-8269	R	142.81	89.97	152.61	52.64	87.95	42.87	50.49	44.08*
MQ	FHSM VP-8919	R	152.72	88.89		58.85	88.47	47.49	46.83	47.54
SQ	FHSM VP-1079	R	136.62	76.66	139.44	53.02		43.95	45.99	35.16
WQ	DMNH 23183	L	135.51	79.35	136.14	42.15	85.44	41.66*	45.21	34.50
WQ	DMNH 297	L	134.94	82.28	134.58	49.19	74.15	43.99	43.87	34.12
WQ	DMNH 298	L	141.79	88.57	145.89*	56.88	80.87	37.10	46.37	43.26
WQ	DMNH 304	R		82.51						39.03
WQ	F:AM 115888b	L	152.03	78.12	144.90	43.18	78.83	43.21	47.72	38.58

Radius

Locality	Number	Side	1	2	3	4	5	6	7	8
AQ	F:AM 104003	R	232.0	79.5	86.0	38.09	39.70	34.23	81.29*	37.04
AQ	F:AM 104004	L	247.5	86.0	91.0	40.09	40.38	35.28	84.79	32.89
BTR	F:AM 115758b	R	274.3	105.0	111.8	56.32	56.41	41.59	99.05	45.42

BTR	F:AM 115758f	L	257.8	99.0	111.0	66.59	66.76	36.79*	93.65	44.02
BTR	F:AM 115758g	L	279.8	103.0	114.0	56.50	59.30	35.14	94.38	41.12
BTR	F:AM 115759b	R	265.3	110.0	109.0	60.29	61.55	36.74	94.49	42.31
BV	UF 18754	L			100.0				82.11	
BV	UF 19356	R		87.0						38.61
BV	UF 19357	L		98.5						39.22
BV	UF 200945	L	300.5	95.3	97.5	47.89	52.24	34.61	86.74	
BV	UF 200946	L		97.0						44.88
BV	UF 200948	L		83.0						37.56
BV	UF 200952	R		89.2						36.48
BV	UF 200953	R		89.4						41.87
BV	UF 202823	R	262.8	90.3	102.3	44.29	44.77	31.11	89.34	42.40
BV	UF 202827	R		97.0						47.72
BV	UF/TRO 3882	L	269.8	89.0	96.3	42.85	51.06	31.84	83.82	39.70
BV	UF/TRO 3883	L		90.0						41.84
BV	UF/TRO 3884	R		88.6						47.46*
BV	UF/TRO 3885	R		96.0						47.51
BV	UF/TRO 3886	L		83.7						40.51
BV	UF/TRO 3891	L		90.0						42.44
BV	UF/TRO 3892	L		95.5						40.30
BV	UF/TRO 3893	R			108.8				92.90	
GFS	ETMNH 601	R	328.3	101.8	103.0	51.75	51.89	41.03	95.83	43.85
GFS	ETMNH 601	L	321.8	103.0	103.5	51.82	52.22	39.37	95.52	44.07
GFS	ETMNH 609	L	295.8	98.0	91.8	42.45	45.89	33.67	89.64	39.70
GFS	ETMNH 609	R	296.5	99.0	93.3	44.03	45.36	35.26	90.17	38.59
LBB	UF 27389	L	259.3	80.5	85.0	42.19	43.02	33.00	79.10	36.44

LBB	UF 39917	R	259.0	82.5	91.3	45.68	46.31	34.44	78.71	42.74
LBB	UF 39918	R	254.3	81.3	81.0	41.62	42.34	31.62	77.12	41.47
LBB	UF 39921	R	244.8	82.0	89.3	42.89	42.87	29.88	73.90	38.66
LBB	UF 39922	R	242.8	77.3	82.3	39.56	41.02	30.84	76.51	36.32
LBB	UF 39923	R	228.5	79.5	81.0	44.21	44.56	28.75	73.96	37.34
LBB	UF 39924	R		83.0	84.5	44.81	44.86	31.85	77.53	42.77
LBB	UF 39925	R		86.3	86.5	44.93	45.04	33.53		35.29
LBB	UF 39926	R		80.5	85.0	43.07	43.57	29.20	80.63	37.12
LBB	UF 41381	R	240.0	77.5	80.5	38.43	38.44	29.25	75.32	37.03
LBB	UF 41382	R	253.3	82.8	82.5	41.50	41.38	33.01	77.79	38.49
LIQ	USNM V 1443	R	270.3	100.0	97.8	49.43	50.08	39.52	93.65	40.44
LIQ	USNM V 1500	R	248.0	87.0	86.3	43.43	43.88	34.21	81.85	40.11*
LIQ	USNM V 7881	R	237.0	84.3	87.5	42.30	42.38	33.25	81.31	44.38
LIQ	USNM V 7884	R	280.8	109.0	103.8	50.71	52.02	38.79	95.43	44.58*
MBB	F:AM 104199	R	237.3	89.0	92.3	45.91	46.06	34.63	86.24	42.11
MBB	USNM PAL 416325 (1)	R		90.0						34.61
MBB	USNM PAL 416325 (2)	L		82.8						28.44
MBB	USNM PAL 416325 (3)	L			94.5				88.80	
MBB	USNM PAL 416328	R			94.0				83.81	
MBB	USNM V 3371	R	228.0	86.3	82.0	39.29	39.75	29.33	75.28	27.32
MBB	USNM V 3406	R	235.0	76.5	81.0	49.19	53.57	32.59		38.48*
MBB	USNM V 3407	L	228.0*	79.8	87.5	44.49	44.64	34.02		
MBB	USNM V 3408	R			100.8				93.0	
MBB	USNM V 3415	R	270.0	88.8	96.8	48.78	51.13	35.24	88.31	42.48
MF	UF 10965	L	240.8	83.3	81.0	45.31	45.38	34.41	78.63	36.69
MF	UF 59626	R	267.5	89.5	93.0			32.72	82.80	36.91

MF	UF 59627	L	263.0	89.5		48.87	51.87	36.36		38.90
MF	UF 59629	L		76.3						36.98
MF	UF 59630	R	240.0	83.8	79.0	44.21	45.11	33.62	76.43	37.27
MF	UF 59631	L		75.6						36.10
MF	UF 59632	R			86.8				79.91	
MF	UF 59633	L		83.0						41.62
MQ	FHSM VP-8602	R	246.5	94.5	96.8	53.11	53.42	38.39	89.22	40.63
MQ	FHSM VP-9022	L	275.8	108.0	120.8	60.86	62.05	43.23	100.10	45.48
SQ	FHSM VP-1083	L	247.3	92.0	96.5		47.71		84.88	40.37
SQ	FHSM VP-1088	L	282.0	94.5	105.0	50.43	50.66	39.83	96.04*	41.88
WQ	DMNH 23182	R	235.0	95.0	94.0	47.49	47.47	34.88	91.47	
WQ	DMNH 23184	R	245.0	90.0	90.0	47.14	47.44	37.37	89.42	45.30
WQ	DMNH 23185	L	242.8	83.3	93.0	47.66	47.79	36.02	89.41	
WQ	DMNH 23186	L	251.5	93.8	89.0	45.04	45.41	33.43	85.39	45.50
WQ	DMNH 23187	R		99.0						54.87
WQ	DMNH 23188	R		92.5						43.53*
WQ	DMNH 23189	R		92.0						42.26
WQ	DMNH 23193	R			97.3				89.45	
WQ	DMNH 297	L	260.5	93.0	90.0	48.23	48.45	38.19	84.36	43.66
WQ	DMNH 298	L	241.8	91.0	88.0	48.61	49.31	30.46	84.51	39.53
WQ	DMNH 299	R	280.3	110.0	116.5	63.77	64.69	44.02	101.10	41.92
WQ	DMNH 300	R	273.5	107.5	108.0	56.11	57.33	37.67	98.96	46.84
WQ	DMNH 301	L	261.8	98.5	99.0	49.79	50.45	39.23	88.59	45.32
WQ	DMNH 304	R		99.49						
WQ	DMNH 721	L		89.0						45.14

Metacarpal 3

Locality	Number	Side	1	2	3	4	5	6
BTR	F:AM 144156	R	117.5	69.5	67.0	52.42	52.59	23.69
BTR	F:AM 144157	L	116.3	72.5	69.3	56.85	59.04	23.57
BTR	F:AM 144158	R	111.5	68.0	61.0	53.82	55.19	
BTR	F:AM 144159	L	122.5	71.5	65.0	57.47	58.98	18.38
BTR	F:AM 144160	L	120.8	68.8	67.8	58.00	59.44	24.86
BV	UF 19358	R	109.0	61.3	60.5	47.46	51.79	18.18
BV	UF 200920	L	117.0	71.5	69.8	52.55	57.11	17.17
BV	UF 200921	L	115.0	69.0	67.0	53.81	56.62	17.71
BV	UF/TRO 3900	L	123.0	72.5	70.0	52.63	55.67	22.29
BV	UF/TRO 3901	R	120.0	69.0	66.0	51.37	54.53	19.02
GFS	ETMNH 601	R	140.3	77.0	73.5	56.66	58.03	22.94*
GFS	ETMNH 601	L	139.0	75.0	73.0	56.41	58.55	22.39
GFS	ETMNH 609	L	118.5	66.0	59.5	47.93	48.79	22.40
GFS	ETMNH 609	R	118.0	67.0	60.3	48.25	48.65	21.69
GFS	ETMNH 8271	R	119.0	67.0	61.3	46.98	49.32	20.36
LBB	UF 41016	L	116.5	49.0	51.0	39.72	40.45	16.71
LBB	UF 41017	L	115.3	60.0	54.3	46.70	47.22	15.64
LBB	UF 41018	L	109.0	54.5	50.0	41.29	43.94	15.58
LBB	UF 41019	L	113.5	56.0	52.8	43.54	44.58	16.17
LBB	UF 41021	L	107.0	53.0	50.8	40.39	41.97	15.55
LBB	UF 41031	R	113.0	59.0	52.5	38.49	42.80	16.96
LBB	UF 41033	R	115.3	54.0	56.8	44.29	48.34	16.67
LBB	UF 41035	R	111.0	54.8	54.0	41.80	44.58	15.49
LBB	UF 41036	R	108.5	54.0	51.0	41.35	41.55	14.54

LBB	UF 41038	R	116.0	55.8	53.5	45.52	45.90	15.13
LIQ	USNM PAL 419028 (1)	R	114.5	62.0	59.5	48.54	50.28	16.50
LIQ	USNM PAL 419028 (2)	L	113.5	64.0	63.0	49.80	50.91	23.41
LIQ	USNM PAL 419028 (3)	L	111.8	63.3	60.0	48.22	50.62	18.37
LIQ	USNM V 7884 (1)	L	123.3	67.3	66.3	54.73	55.63	20.36
LIQ	USNM V 7884 (2)	R	128.0	70.3	64.3	55.15	56.62	18.81
MBB	USNM PAL 414809	L	99.8*	54.3*	55.0	43.21	45.01	20.38
MBB	USNM V 3683	L	102.8	63.0	55.0	45.77	46.92	21.16
MBB	USNM V 3689	R	108.3	68.0	62.0	55.44	55.50	23.07
MBB	USNM V 3697 (1)	R	102.5	61.0	60.3	49.57	49.87	21.74
MBB	USNM V 3697 (2)	R	109.8	60.0	56.5	51.14	53.26	22.57
MBB	USNM V 3697 (3)	R	105.5	66.0		54.58	54.57	23.87
MBB	USNM V 3698 (1)	L			57.0	47.00	47.12	20.63
MBB	USNM V 3698 (2)	L	105.5	67.8		54.98	55.33	23.46
MBB	USNM V 3698 (3)	L	112.0	68.0	67.0	56.00	57.09	21.80
MBB	USNM V 3698 (4)	L	108.3	66.3	61.0	52.74	55.47	26.20
MBB	USNM V 3698 (5)	L	111.8		61.0			22.01
MBB	USNM V 3698 (6)	L	97.0	58.0	53.8	45.38	46.34	22.01
MBB	USNM V 3698 (7)	L	95.5	61.5	59.0	48.90	49.62	22.41
MF	UF 10945	L		58.3		42.06	43.63	17.32
MF	UF 59707	L			52.3	39.62		19.12
MF	UF 59709	L	111.0	52.0		43.19	45.82	18.64
MF	UF 59710	R	109.5	57.0	54.0	42.02	43.32	17.61
MF	UF 59711	R	112.0	58.3	53.8	41.16	42.22	18.76
MF	UF 59712	R	105.5	60.0	55.0	45.77	46.87	18.70
MF	UF 59713	L			52.0	38.26	40.96	17.87

MF	UF 59714	R	113.8	57.0	56.0	46.84	48.90	18.43
MQ	FHSM VP-8226	L	125.5	77.0	68.3	60.49	63.30	24.12
MQ	FHSM VP-8677	R	134.0	72.5	75.8	65.92	71.80	24.48
MQ	FHSM VP-8928	L	129.0	70.5	69.0	57.80	60.09	22.84
SQ	FHSM VP-1269	L	123.8	68.0	66.8	58.88	59.50	26.73
SQ	FHSM VP-1270	L	113.5	68.0	64.5	44.41	46.79	18.79
SQ	FHSM VP-1271	L	117.0	63.0	67.0	51.26	52.59	21.21
WQ	DMNH 23180 (1)	L	123.3	71.8	69.0	57.21	60.21	21.97
WQ	DMNH 23180 (2)	L	117.8	71.0		53.33	53.55	24.30
WQ	DMNH 23180 (3)	L	112.5	67.5	60.3	46.74	47.93	20.92
WQ	DMNH 23180 (4)	L	113.0	67.3	58.0	45.14	46.48	19.83
WQ	DMNH 23180 (5)	L	125.8	73.0				22.56
WQ	DMNH 23180 (6)	R	109.0	63.8	55.0	45.73	45.97	16.83
WQ	DMNH 23180 (7)	R	111.8	67.0		53.41	55.06	20.48

Femur

Locality	Number	Side	1	2	3	4	5	6	7	8
BTR	F:AM 115760a	R	443.3	417.5	201.5	140.0	78.80	92.09	255.3	89.26
BTR	F:AM 115760b	R	464.8	442.3	222.0	140.3	74.08	76.89	237.3	87.32
BTR	F:AM 115761b	R	511.3	476.0	208.0	144.0	79.32	89.23	252.0	77.80*
BTR	F:AM 115825b	R	488.0	464.0	211.5	138.8	66.77	73.66	248.3	86.60
GFS	ETMNH 601	R	505.8	490.5	200.0	140.5	75.21	106.53	282.3	87.62
GFS	ETMNH 601	L	513.3*	486.3*	196.8*	139.8	73.13	109.03*	280.5	82.87
GFS	ETMNH 609	L	475.0	446.0	181.5	128.5	65.50	87.31	253.3	75.99
GFS	ETMNH 609	R	472.3	445.8	183.3	129.0	66.15	86.87	251.5	76.46
LBB	UF 26349	L				115.0	60.48	85.58*		72.74

LBB	UF 27975	R	372.5*	363.31*	155.8		56.77*	81.68	198.17	
LBB	UF 40283	R	375.0*	359.50*	158.8	118.0	64.88		193.71	73.39
LBB	UF 40284	R			138.3	108.5				60.69
LBB	UF 40300	L		356.40*			58.21		191.81	68.61
LBB	UF 40301	L			158.0				204.08*	
LBB	UF 40303	L			150.8	117.5	58.56			69.59
LIQ	AMNH 2647	L	444.8	423.5	182.0	134.8	73.30	91.33	242.5	69.54*
LIQ	AMNH 2652	L				122.0	64.03	85.22		
LIQ	AMNH 2665; F:AM 104055	R	417.0	391.0	172.3	125.0	70.57	85.40	238.0	70.31
LIQ	USNM V 6752	R	428.8	405.3	171.8	129.3	66.26	77.61	236.5	
MBB	F:AM 104155	R	408.8	394.3	157.3	113.0	66.93	86.72	233.0	75.04
MBB	F:AM 144166	L	444.5	425.3	178.3	123.8	68.27	84.52	246.0	74.68*
MBB	F:AM 144167	L	401.3	380.5	164.8*	121.5	63.35	79.71	212.0	68.03
MBB	F:AM 144168	L	413.3	387.0	170.5	117.0	70.77	95.74	232.8	70.15
MBB	F:AM 144169	R	428.0	401.5	167.0	117.3	61.79	81.02	240.0	71.85
MBB	USNM V 3599	R								75.58
MBB	USNM V 3601	L						79.24		
MBB	USNM V 3609	L				121.5				76.73
MBB	USNM V 3611	L				112.0				62.33
MBB	USNM V 3612	R								
MBB	USNM V 3613	L								
MBB	USNM V 3614	L								
MBB	USNM V 3615	L					67.33*	94.90		
MBB	USNM V 3616	L						103.04		
MF	UF 10955	R	361.0	335.0	146.3	113.0	56.0	76.5	190.0	71.3
MF	UF 10967	L	394.0	383.81	152.5	118.3	64.56			

MF	UF 59642	R				117.0				74.08
MF	UF 59643	R				115.3				
MF	UF 59645	L				116.0				71.68
MF	UF 59649	L				114.5				
MF	UF 59650	L			153.5					
MF	UF 59651	L			157.3					
MF	UF 59652	L			150.3					
MQ	FHSM VP-8316	L				143.0		99.83		
MQ	FHSM VP-9052	L	475.5	452.0	210.0	147.0	76.11	110.72	244.0	95.27
SQ	FHSM VP-1027	R	404.8	384.5		118.0	61.04	78.53	230.0	72.83
SQ	FHSM VP-1030	R	418.5	389.0	169.5	132.5	72.96	87.56	245.3	82.33
WQ	DMNH 22922	R				121.0				58.87*
WQ	DMNH 23181	R	386.5	366.5	171.3	120.3	60.87	84.48	194.57	75.07
WQ	DMNH 296	L	474.0	448.5	196.8	138.8	71.46	101.36	279.8	81.92
WQ	DMNH 304	R				115.44	69.07	104.43		

Locality	Number	Side	9	10	11	12
BTR	F:AM 115760a	R	92.13	157.47	108.90*	155.44
BTR	F:AM 115760b	R	95.38	168.20	117.99*	158.15
BTR	F:AM 115761b	R	96.55	159.59*	112.79*	157.02*
BTR	F:AM 115825b	R	92.19	164.74	112.55*	156.57
GFS	ETMNH 601	R	91.27	166.43	120.52	164.68
GFS	ETMNH 601	L	90.54*	164.88	120.16	163.51
GFS	ETMNH 609	L	86.00	156.82	111.95	157.16
GFS	ETMNH 609	R	86.56	155.94	113.88	153.34*
LBB	UF 26349	L	74.10	141.28	92.09	135.72
LBB	UF 27975	R	68.34			

LBB	UF 40283	R	70.25	128.03	86.24	126.77
LBB	UF 40284	R	65.42	124.40	91.87	121.54
LBB	UF 40300	L				
LBB	UF 40301	L	67.74			
LBB	UF 40303	L	72.09	131.46	89.26	131.57
LIQ	AMNH 2647	L	86.41	146.73	97.70*	147.87
LIQ	AMNH 2652	L			89.29*	
LIQ	AMNH 2665; F:AM 104055	R	77.62	140.73	94.01	137.86
LIQ	USNM V 6752	R	75.55		98.25	133.75*
MBB	F:AM 104155	R	77.78	136.61	91.18	133.30
MBB	F:AM 144166	L	77.60	150.48	111.90*	148.44
MBB	F:AM 144167	L	77.42	141.82	104.77	138.79
MBB	F:AM 144168	L	78.46	140.65	98.49	140.19
MBB	F:AM 144169	R	78.85	139.36	95.44	135.46
MBB	USNM V 3599	R		134.67		131.43
MBB	USNM V 3601	L				
MBB	USNM V 3609	L		135.52	100.24	134.83
MBB	USNM V 3611	L		125.35	96.23	124.64
MBB	USNM V 3612	R	74.24			
MBB	USNM V 3613	L	71.28			
MBB	USNM V 3614	L	77.68			
MBB	USNM V 3615	L				
MBB	USNM V 3616	L				
MF	UF 10955	R	73.5	126.6	86.5	124.6
MF	UF 10967	L	72.68			
MF	UF 59642	R		134.47	90.21	134.62

MF	UF 59643	R			89.95	113.84*
MF	UF 59645	L		132.86	90.14	131.40
MF	UF 59649	L			95.65	117.50*
MF	UF 59650	L	71.83			
MF	UF 59651	L	70.89			
MF	UF 59652	L	77.22			
MQ	FHSM VP-8316	L			113.30	
MQ	FHSM VP-9052	L	88.11	163.65	115.43*	161.91
SQ	FHSM VP-1027	R	80.11	140.08	100.23	139.59
SQ	FHSM VP-1030	R	81.70	149.79	97.27	146.03
WQ	DMNH 22922	R		138.39*	97.64	137.31*
WQ	DMNH 23181	R	77.75	132.43	95.50	131.46
WQ	DMNH 296	L	93.50	166.54	116.37*	165.46
WQ	DMNH 304	R	81.22			

Tibia

Locality	Number	Side	1	2	3	4	5	6	7
BTR	F:AM 115764a	L	258.0	121.0*	98.8	52.36	52.66	132.20	43.77
BTR	F:AM 115764d	R	257.5	125.0*	96.0	56.71	58.50	127.20	41.16
BTR	F:AM 115764f	R	239.5	110.5	90.8	51.30	52.63	113.19	38.56
BTR	F:AM 115827a	L	262.8	126.5*	94.0	53.45	54.41	137.82	44.28
BTRh	F:AM 115829a	L	264.0	129.8*	87.8	51.01	51.94	125.04*	39.93
BTRh	F:AM 115829b	R	271.8	119.5	93.0	58.54	59.64	126.23	37.58
BV	UF 18756	R			88.8				36.91
BV	UF 200893	R	252.3	110.5	87.0	51.18	53.08		36.26
BV	UF 200894	R	254.5	108.0	92.8	58.92	59.51		38.66

BV	UF 200913	L	268.5	113.5	97.3	52.72	52.52	124.62	39.47
BV	UF 200914	R							37.72
BV	UF 200918	L			95.3				38.75
BV	UF 200934	R			100.0				39.94
BV	UF 200935	R							36.93
BV	UF 200936	R			84.3				39.48
BV	UF 202829	L			91.3				36.91
BV	UF 225797	R			87.3				37.37
BV	UF 57212	R			98.3				42.17
BV	UF/TRO 3887	L			104.0				43.99
BV	UF/TRO 3908	L			93.3	42.74	43.17		34.85
BV	UF/TRO 3909	R		116.8				125.75	
GFS	ETMNH 601	R		122.0*	94.3*			131.39	38.43
GFS	ETMNH 601	L	290.8	117.5	94.8*	49.47	53.35	131.36	35.75
GFS	ETMNH 609	L	251.5	105.8	84.3	45.83	47.67	115.35	33.56
GFS	ETMNH 609	R	253.0	103.3	87.0	47.39	51.41	115.48	33.68
LBB	UF 26347	R	233.5	96.0	79.8	42.13	42.66		39.83
LBB	UF 40351	R	221.5		74.0	40.89	41.62		39.50
LBB	UF 40352	R	238.0	92.3	74.5	43.29	44.18	96.20	36.15
LBB	UF 40353	R	241.3	97.0	74.0	38.77	39.08	102.95	41.24
LBB	UF 40354	R	216.5	89.3	69.0	34.46	34.43	91.89	39.75
LBB	UF 40356	R	232.0	88.3	74.0	37.17	37.60	95.61	36.04
LBB	UF 40357	R	232.8	91.8	75.3	38.74	38.92		
LIQ	USNM PAL 419060 (1)	L	238.3	99.0*	82.0	44.80	46.10	113.20	31.27
LIQ	USNM PAL 419060 (2)	R	234.3	111.3*	84.0	45.58	46.30	120.68	43.57
LIQ	USNM PAL 419060 (3)	R	249.0	106.17*	92.0	51.87	52.44	132.58	37.07

LIQ	USNM PAL 419060 (4)	R	262.5	113.8*	92.8	50.65	52.67	133.14	39.51
LIQ	USNM V 6752	R	226.0	109.8	81.31*	44.54	44.83	112.62*	42.56
LIQ	USNM V 6756	L	249.5	107.0	90.0	44.94	45.21	118.11	43.36
MBB	F:AM 104156	R	242.8	116.8	87.345*	49.99	51.09	123.08	37.52
MBB	USNM PAL 416325 (1)	R			72.0				33.15
MBB	USNM PAL 416325 (2)	R			71.5				36.94*
MBB	USNM PAL 416325 (3)	L			81.3				33.54
MBB	USNM PAL 416325 (4)	L		109.8*				106.61	
MBB	USNM PAL 416325 (5)	L		98.0				97.78	
MBB	USNM PAL 416328	L			81.0	47.87	48.18		
MBB	USNM V 3374	L	234.0	105.0	79.8	42.93	44.50	114.27*	
MBB	USNM V 3399	R		104.0				101.77	
MBB	USNM V 3400	R	244.0	101.5	82.3	46.07	46.40	107.43	41.60
MBB	USNM V 3401	L	219.0		79.0	44.77	45.47	111.76	41.46
MBB	USNM V 3402	L	203.3	98.8	75.0	44.45	46.29		38.95
MBB	USNM V 3403	R	231.5	110.3	80.8	45.42	47.95	118.89	37.94
MBB	USNM V 3627	R		109.0*				107.69	
MBB	USNM V 3628	L		104.5*					
MBB	USNM V 3629	L			79.3*				39.81
MF	UF 59653	L			78.0				42.06
MF	UF 59654	L			83.8				39.55*
MF	UF 59656	R			81.5				38.58
MF	UF 59657	L			76.0	44.51			45.82
MF	UF 59659	R		100.0				104.42	
MF	UF 59660	L			74.8				39.42
MF	UF 59661	L	238.5	99.5	77.5	45.17	45.40	103.32	38.42

MF	UF 59662	R	226.0	93.3	72.3	43.24	43.61	102.88	40.19
MQ	FHSM VP-8268	R	265.5	131.70*	97.0	57.17	57.14	130.21	45.87
MQ	FHSM VP-8971	R	275.3	124.39*	97.0	52.78	55.11	126.70	51.55
SQ	FHSM VP-1034	L	233.0	105.0*	84.0	46.16	46.75	111.58	37.70
SQ	FHSM VP-1039	L	219.8	107.3*	82.0	44.89	46.82	106.32	44.89
WQ	DMNH 296	L	263.5	127.5*	90.54*	54.48	54.84	126.71	44.21
WQ	DMNH 302	R	212.0	103.3	80.94*	49.02	49.13	110.73	36.51
WQ	DMNH 303	R	221.0	115.0*	82.8	45.97	46.47	112.19	47.64
WQ	DMNH 304	R	227.3	104.0*	86.0	45.46	45.59	104.04	43.52

Calcaneum

Locality	Site	Side	1	2	3	4
BTR	F:AM 144151	L	144.8	118.54	52.02	81.36
BTR	F:AM 144152	R	147.5	117.51	53.46	85.50
BTR	F:AM 144153	R	147.0	121.19	58.27	81.76
BTR	F:AM 144154	R	150.3	116.38	55.04	85.19
BTR	F:AM 144155	R	133.0	110.72	50.33	80.24
BV	UF 200925	L	138.0	101.10	46.29	80.19
BV	UF 202822	R	145.0	118.10	46.50	79.63
BV	UF 212491	R		106.19	48.53	79.84
BV	UF/TRO 3878	L	146.4	117.59	47.50	83.28
GFS	ETMNH 601	R	149.5	105.70	48.20	81.67
GFS	ETMNH 601	L	151.0	110.02	44.56	79.56*
GFS	ETMNH 609	L	130.3	94.81	42.91	71.50
GFS	ETMNH 609	R	130.0	97.35	41.54	75.52
LBB	UF 40823	R	115.5	93.13	44.71	74.53

LBB	UF 40824	R	124.8	109.06	43.79	69.93
LBB	UF 40825	R	113.8	96.13	46.89	75.60
LBB	UF 40828	R	118.8	96.53	41.16	72.31
LBB	UF 40833	R	116.0	91.40	40.21	67.90
LBB	UF 40836	R	113.5	100.45	48.71	68.86
LBB	UF 40849	R	116.3	100.50	39.65	66.27
LIQ	USNM PAL 419037 (1)	R	135.8	110.47	44.38	76.48
LIQ	USNM PAL 419037 (2)	R	122.3	102.84	43.85	73.28
LIQ	USNM PAL 419037 (3)	R	121.5	104.82	42.02	72.86
LIQ	USNM PAL 419037 (4)	R	137.0	114.70	48.29	77.79
LIQ	USNM V 6752	R	132.5	104.3	46.9	75.7
MBB	USNM V 3693 (1)	R	114.0	96.53	40.53	64.19
MBB	USNM V 3693 (2)	R	118.3*		39.56	
MBB	USNM V 3694 (1)	L	109.8		38.32	68.41
MBB	USNM V 3694 (2)	L	128.0*		39.59	
MBB	USNM V 3694 (3)	L	125.5		39.83	
MBB	USNM V 3694 (4)	L	127.0	100.82	46.48	70.99
MBB	USNM V 3694 (5)	L	119.5	94.44	40.71	65.99
MBB	USNM V 3694 (6)	L	117.5	92.02	37.56	66.50
MBB	USNM V 3694 (7)	L	120.0		38.98	65.23
MBB	USNM V 3694 (8)	L	122.8		45.91	
MF	UF 10947	L	120.0	92.74	42.88	71.18
MF	UF 59663	R	128.0	102.42	43.91	74.51
MF	UF 59665	R	121.8	96.12	39.79	66.36
MF	UF 5966	R	116.0	96.87	42.47	66.36
MF	UF 59667	L	123.5	94.03	36.80	66.92

MF	UF 59668	L	119.0	97.95	41.93	68.31
MF	UF 59669	L	121.8	95.43	41.84	70.62
MQ	FHSM VP-8042	R	158.0	135.25	50.04	85.03
MQ	FHSM VP-8043	R	161.0	133.94	55.38	86.85
SQ	FHSM VP-1234	R	136.3	111.47	46.94	77.11
WQ	DMNH 1180	L	131.3	113.42	39.76	70.53
WQ	DMNH 16136	R			43.80	71.91
WQ	DMNH 16137	R			45.83	72.03
WQ	DMNH 304	R			46.82	

Metatarsal 3

Locality	Number	Side	1	2	3	4	5	6
BTR	F:AM 144161	L	105.0	56.0	63.5	48.15	49.67	18.51
BTR	F:AM 144162	L	106.0	55.5	67.0	50.79	52.03	25.52
BTR	F:AM 144163	L	102.5	53.3	59.0	48.78	52.70	17.87
BTR	F:AM 144164	R	107.5	53.3	59.5	47.28	48.03	23.01
BTR	F:AM 144165	R	110.0	58.0	63.0	48.94	50.91	21.01
BV	UF 200915	L	101.0	54.0	58.0	45.31	46.23	20.02
BV	UF 200916	L	97.0	56.0	63.8	46.59	48.47	17.68
BV	UF 200917	L	102.5	55.0	66.3	46.37	47.10	18.64
BV	UF 212505	?			64.0			
BV	UF/TRO 3889	R	102.8	54.0	60.0	46.44	47.61	14.72
GFS	ETMNH 601	L	113.0	57.5	66.5	50.05	50.11	18.69
GFS	ETMNH 601	R	114.5	56.0	64.3	49.48	49.73	19.04
GFS	ETMNH 609	L	97.0	51.5	54.5	41.07	41.41	18.41
GFS	ETMNH 609	R	96.3	52.0	53.8	40.17	40.89	17.82

LBB	UF 40865	R	93.5	37.8	48.0	35.67	35.84	17.12
LBB	UF 40866	R	95.0	37.8	47.5	33.75	33.63	14.79
LBB	UF 40868	R	94.3	38.0	45.0	33.76	33.73	15.46
LBB	UF 40869	R	101.5	42.5	49.5	34.61	34.81	15.35
LBB	UF 40870	R	94.0	38.0	50.0	36.74	37.63	19.32
LBB	UF 40871	R	93.0	39.0	46.0	34.49	34.61	16.27
LBB	UF 40872	R	96.3	39.8	49.0	36.74	37.05	18.64
LBB	UF 40873	R	94.0	40.0	49.0	33.80	34.41	15.59
LBB	UF 40875	R	97.0	39.8	49.5	36.24	36.33	15.63
LBB	UF 40878	R	96.8	39.0	48.8	36.37	36.61	17.39
LBB	UF 40885	R	95.0	41.0	47.3	33.55	33.54	14.02
LIQ	AMNH 2630	L	98.0	46.0	53.3	42.66	43.48	18.89
LIQ	AMNH 2636	L	118.0	52.0	52.3	41.41	43.45	19.15
LIQ	AMNH 2671a	L	119.0	55.0	63.3	48.06	50.07	19.22
LIQ	AMNH 2671a; F:AM 104063	L	109.0	48.3	56.5	44.18	46.14	18.65
LIQ	USNM V 6752	R	108.5	54.0	60.0	48.28	48.28	20.59
MBB	USNM PAL 414809	R	82.5	44.3	51.5	39.42	40.16	17.62
MBB	USNM V 3593	R	92.3	51.0	57.0	44.20	44.46	19.78
MBB	USNM V 3745 (1)	R	87.3	48.3	49.0	40.60	40.87	18.22
MBB	USNM V 3745 (2)	R	84.8	42.3	49.0	40.63	41.25	15.79
MBB	USNM V 3745 (3)	R	86.5	47.8	52.5	39.59	41.82	18.37
MBB	USNM V 3745 (4)	R	82.3	44.3	49.0	40.18	41.27	16.94
MBB	USNM V 3745 (5)	R	90.0	47.0	54.0	40.15	42.51	21.34
MBB	USNM V 3745 (6)	R	87.3	48.8	50.0	42.36	43.28	19.24
MBB	USNM V 3745 (7)	R	93.8	51.0		42.95	42.98	21.44
MBB	USNM V 3745 (8)	L	85.0	48.8	51.0	42.72	42.98	19.25

MBB	USNM V 3745 (9)	R	96.0	50.3	56.0	42.69	45.43	20.16
MF	UF 16636	R	96.8	43.5	51.5	37.44	38.21	21.75
MF	UF 59720	R	95.0	42.0	48.3	34.85	34.90	17.97
MF	UF 59721	R	93.3	41.0	49.3	36.70	36.79	
MF	UF 59722	R	90.5	38.3	50.0	36.12	37.14	16.51
MF	UF 59723	R	94.0	41.0	48.0	35.52	35.99	17.79
MF	UF 59724	R	89.5	42.0	50.0	36.62	36.58	17.78
MF	UF 59725	R	94.5	43.0	51.0	38.40	39.28	16.68
MF	UF 59726	R	91.0	39.3		34.84	34.93	17.80
MQ	FHSM VP-8244	R	113.5	56.8	64.0	48.33	48.65	26.29
MQ	FHSM VP-8828	L	100.3	56.0	64.0	48.90	50.24	23.48
SQ	FHSM VP-1311	R	98.0	52.8	62.0	50.28	50.39	21.48
SQ	FHSM VP-1326	R	101.3	54.0	60.0	50.36	51.78	21.41
WQ	DMNH 1180	R	102.5	53.0	57.5	42.90	42.93	20.51
WQ	DMNH 23180 (1)	R	111.0	54.0	60.0	48.33	48.48	21.83
WQ	DMNH 23180 (2)	R	87.5	48.8	54.5	41.79	43.62	21.57
WQ	DMNH 23180 (3)	R	85.8	46.8	49.0	38.28	38.30	
WQ	DMNH 23180 (4)	R	96.3	55.0	53.0	45.88	46.28	25.62
WQ	DMNH 23180 (5)	L	90.0	53.0	55.0	41.19	41.65	22.26
WQ	DMNH 23180 (6)	L	102.0	56.0	61.0	50.96	52.75	
WQ	DMNH 23180 (7)	L	103.0	60.0	62.0	46.09	46.09	22.37
WQ	DMNH 304	R						22.01

APPENDIX E

Statistical Results

PCA: Unstandardized	Humerus	Radius	Ulna	Metacarpal 3	Femur	Tibia	Calcaneum	Metatarsal 3
All Sites, Partial Measurements								
# of Components*	6--1	8--1	12--2	6--1	10--1	6--2	4--1	6--1
Axis 1	72.600%	77.311%	63.083%	77.814%	84.565%	71.175%	86.852%	77.356%
Axis 2	---	---	9.647%	---	---	17.406%	---	---
Axis 3	---	---	---	---	---	---	---	---
Types with Gray								
# of Components*	6--2	8--1	12--3	6--2	10--1	6--2	4--1	6--1
Axis 1	61.397%	76.500%	48.404%	67.847%	82.785%	61.777%	78.023%	72.591%
Axis 2	18.330%	---	15.443%	20.528%	---	22.024%	---	---
Axis 3	---	---	13.316%	---	---	---	---	---
Types with Gray, All Measurements								
# of Components*	11--2	8--1	15--4	6--2	12--1	7--2	4--1	6--1
Axis 1	53.128%	76.494%	51.515%	67.996%	81.398%	62.281%	77.327%	72.624%
Axis 2	24.719%	---	14.422%	20.582%	---	19.511%	---	---
Axis 3	---	---	10.744%	---	---	---	---	---
Types Only								
# of Components*	6--2	8--1	12--3	6--2	10--2	6--2	4--1	6--1
Axis 1	56.620%	80.842%	43.176%	66.231%	75.096%	61.525%	81.788%	73.389%
Axis 2	23.433%	---	19.615%	22.228%	10.395%	21.326%	---	---
Axis 3	---	---	14.142%	---	---	---	---	---

* The first number refers to the number of components produced and the second number refers to the number of components saved.

PCA: Standardized	Humerus	Radius	Ulna	Metacarpal 3	Femur	Tibia	Calcaneum	Metatarsal 3
All Sites, Partial Measurements								
# of Components*	5--2	7--1	11--3	5--1	9--2	5--2	3--1	5--1
Axis 1	42.818%	70.103%	45.873%	81.844%	52.730%	66.703%	60.436%	82.435%
Axis 2	29.415%	---	14.408%	---	15.765%	22.623%	---	---
Axis 3	---	---	12.806%	---	---	---	---	---
Types with Gray								
# of Components*	5--2	7--1	11--3	5--1	9--3	5--1	3--1	5--1
Axis 1	46.482%	73.352%	45.793%	79.405%	48.071%	72.132%	54.903%	79.718%
Axis 2	34.310%	---	19.769%	---	17.822%	---	---	---
Axis 3	---	---	13.173%	---	13.584%	---	---	---
Types with Gray, All Measurements								
# of Components*	10--3	7--1	14--4	5--1	11--4	6--2	3--1	5--1
Axis 1	54.184%	73.352%	41.425%	76.732%	43.192%	66.828%	53.688%	79.718%
Axis 2	18.096%	---	20.302%	---	17.207%	17.339%	---	---
Axis 3	14.046%	---	11.573%	---	12.362%	---	---	---
Types Only								
# of Components*	5--2	7--2	11--3	5--1	9--3	5--2	3--2	5--1
Axis 1	45.052%	59.015%	34.759%	77.799%	44.352%	63.814%	50.480%	81.610%
Axis 2	31.980%	17.795%	23.515%	---	17.908%	21.679%	36.406%	---
Axis 3	---	---	16.316%	---	13.866%	---	---	---

* The first number refers to the number of components produced and the second number refers to the number of components saved.

DA: Unstandardized	Humerus	Radius	Ulna	Metacarpal 3	Femur	Tibia	Calcaneum	Metatarsal 3
All Sites, Partial Measurements								
# of Functions	6	8	8	6	7	6	4	6
Axis 1	74.6%	42.8%	86.5%	59.7%	63.3%	73.7%	82.1%	77.5%
Axis 2	15.1%	26.7%	5.9%	26.5%	32.2%	10.2%	8.2%	12.9%
Axis 3	6.2%	15.6%	3.2%	5.7%	2.7%	7.0%	7.1%	4.4%
Correct Assignment	90.9%	88.6%	100.0%	82.6%	100.0%	70.6%	65.7%	84.3%
Correct Cross-validation	40.9%	34.3%	56.0%	56.5%	11.8%	29.4%	42.9%	62.7%
GFS Assignment	MQ (2)	LBB (2)	LBB (2)	SQ, WQ (2)	WQ (2)	LIQ (2)	BV, MF	BV, MBB
Types with Gray								
# of Functions	2	2	2	2	2	2	2	2
Axis 1	89.9%	87.5%	73.1%	89.2%	94.7%	61.4%	78.8%	59.1%
Axis 2	10.1%	12.5%	26.9%	10.8%	5.3%	38.6%	21.2%	40.9%
Axis 3	---	---	---	---	---	---	---	---
Correct Assignment	92.9%	92.9%	100.0%	100.0%	100.0%	85.7%	100.0%	85.7%
Correct Cross-validation	50.0%	50.0%	23.1%	70.6%	0.0%	35.7%	90.0%	76.2%
GFS Assignment	LIQ (2)	LIQ (2)	LIQ (2)	LIQ, WQ (2)	MBB, WQ	LIQ, MBB	LIQ (2)	LIQ, MBB
Types with Gray, All Measurements								
# of Functions	2	2	2	2	2	2	2	2
Axis 1	99.7%	69.5%	78.0%	92.9%	91.2%	96.4%	77.8%	59.2%
Axis 2	0.3%	30.5%	22.0%	7.1%	8.8%	3.6%	22.2%	40.8%
Axis 3	---	---	---	---	---	---	---	---
Correct Assignment	100.0%	85.7%	100.0%	94.7%	100.0%	100.0%	100.0%	85.7%
Correct Cross-validation	75.0%	35.7%	84.6%	63.2%	22.2%	53.8%	72.7%	76.2%
GFS Assignment	LIQ	LIQ (2)	LIQ (2)	LIQ, WQ (2)	MBB, WQ	MBB, WQ	LIQ (2)	LIQ, MBB

DA: Standardized	Humerus	Radius	Ulna	Metacarpal 3	Femur	Tibia	Calcaneum	Metatarsal 3
All Sites, Partial Measurements								
# of Functions	5	7	8	5	7	5	3	5
Axis 1	48.8%	45.1%	49.9%	75.3%	96.7%	69.6%	46.7%	81.9%
Axis 2	36.5%	29.3%	21.9%	14.4%	1.5%	12.6%	38.3%	9.1%
Axis 3	6.8%	15.0%	14.0%	---	0.9%	9.3%	15.0%	5.1%
Correct Assignment	81.8%	85.7%	100.0%	76.1%	100.0%	55.9%	48.6%	76.5%
Correct Cross-validation	18.2%	37.1%	20.0%	58.7%	0.0%	26.5%	22.9%	51.0%
GFS Assignment	MBB (2)	LBB (2)	LIQ (2)	LIQ, MF, WQ	MBB, WQ	LIQ, MBB	BV (2)	BV, WQ
Types with Gray								
# of Functions	2	2	2	2	2	2	2	2
Axis 1	89.2%	96.2%	78.0%	86.3%	92.2%	60.8%	86.4%	55.0%
Axis 2	10.8%	3.8%	22.0%	13.7%	7.8%	39.2%	13.6%	45.0%
Axis 3	---	---	---	---	---	---	---	---
Correct Assignment	78.6%	92.9%	100.0%	100.0%	100.0%	78.6%	70.0%	85.7%
Correct Cross-validation	50.0%	50.0%	23.1%	70.6%	33.3%	35.7%	40.0%	81.0%
GFS Assignment	MBB (2)	MBB (2)	LIQ (2)	LIQ (2), WQ	MBB (2)	MBB (2)	LIQ, MBB	MBB (2)
Types with Gray, All Measurements								
# of Functions	2	2	2	2	2	2	2	2
Axis 1	88.7%	96.2%	97.0%	87.9%	93.8%	94.3%	80.9%	55.0%
Axis 2	11.3%	3.8%	3.0%	12.1%	6.2%	5.7%	19.1%	45.0%
Axis 3	---	---	---	---	---	---	---	---
Correct Assignment	100.0%	92.9%	100.0%	84.2%	100.0%	100.0%	81.8%	85.7%
Correct Cross-validation	87.5%	50.0%	7.7%	63.2%	33.3%	61.5%	36.4%	81.0%
GFS Assignment	LIQ	MBB (2)	LIQ, WQ	LIQ, WQ (2)	MBB, WQ	MBB (2)	MBB (2)	MBB (2)

APPENDIX F

Discriminant Results of Comparative Localities

DA: Unstandardized		*Teleoceras proterum*		*Teleoceras fossiger*				*Teleoceras hicksi*	
		LBB	MF	AQ	BTR	MQ	SQ	BTRh	BV
Humerus	*T. proterum*	1	0	0	0	0	0	0	---
	T. fossiger	1	1	1	0	1	0	0	---
	T. hicksi	0	0	0	1	0	1	1	---
Ulna	*T. proterum*	1	---	2	1	0	0	0	---
	T. fossiger	1	---	0	1	0	1	1	---
	T. hicksi	0	---	0	2	1	0	1	---
Radius	*T. proterum*	4	0	2	1	1	0	---	2
	T. fossiger	3	0	0	1	0	1	---	0
	T. hicksi	1	2	0	2	1	0	---	0
Metacarpal 3	*T. proterum*	0	0	---	1	0	1	---	0
	T. fossiger	10	4	---	1	2	1	---	1
	T. hicksi	0	0	---	2	1	1	---	4
Femur	*T. proterum*	0	0	---	0	0	0	---	---
	T. fossiger	0	0	---	1	0	0	---	---
	T. hicksi	1	1	---	3	1	1	---	---
Tibia	*T. proterum*	5	2	---	0	1	1	1	1
	T. fossiger	0	0	---	1	0	1	1	1
	T. hicksi	0	0	---	3	1	0	0	1
Calcaneum	*T. proterum*	3	5	---	0	0	0	---	0
	T. fossiger	3	2	---	5	2	1	---	3
	T. hicksi	1	0	---	0	0	0	---	0
Metatarsal 3	*T. proterum*	0	0	---	2	0	1	---	4
	T. fossiger	11	3	---	1	0	0	---	0
	T. hicksi	0	3	---	2	2	1	---	0
Total	*T. proterum*	14	7	4	5	2	3	1	7
	T. fossiger	29	10	1	11	5	5	2	5
	T. hicksi	3	6	0	15	7	4	2	5

DA: Standardized		*Teleoceras proterum*		*Teleoceras fossiger*				*Teleoceras hicksi*	
		LBB	MF	AQ	BTR	MQ	SQ	BTRh	BV
Humerus	*T. proterum*	0	0	0	0	0	0	0	---
	T. fossiger	2	1	1	0	1	0	0	---
	T. hicksi	0	0	0	1	0	1	1	---
Ulna	*T. proterum*	1	---	1	2	1	1	0	---
	T. fossiger	1	---	0	0	0	0	2	---
	T. hicksi	0	---	1	2	0	0	0	---
Radius	*T. proterum*	6	0	2	1	0	1	---	2
	T. fossiger	1	0	0	1	1	0	---	0
	T. hicksi	1	2	0	2	1	0	---	0
Metacarpal 3	*T. proterum*	0	0	---	2	1	1	---	0
	T. fossiger	10	4	---	1	2	1	---	1
	T. hicksi	0	0	---	1	0	1	---	4
Femur	*T. proterum*	0	0	---	1	0	0	---	---
	T. fossiger	1	1	---	0	0	1	---	---
	T. hicksi	0	0	---	3	1	0	---	---
Tibia	*T. proterum*	2	2	---	1	1	1	1	2
	T. fossiger	3	0	---	2	0	1	1	1
	T. hicksi	0	0	---	1	1	0	0	0
Calcaneum	*T. proterum*	1	2	---	3	1	1	---	1
	T. fossiger	6	5	---	2	0	0	---	2
	T. hicksi	0	0	---	0	1	0	---	0
Metatarsal 3	*T. proterum*	0	0	---	3	1	2	---	4
	T. fossiger	11	4	---	0	0	0	---	0
	T. hicksi	0	2	---	2	1	0	---	0
Total	*T. proterum*	10	4	3	13	5	7	1	9
	T. fossiger	35	15	1	6	4	3	3	4
	T. hicksi	1	4	1	12	5	2	1	4

VITA

RACHEL A. SHORT

Personal Data:	Date of Birth: July 7, 1987
	Place of Birth: Peoria, Illinois
Education:	M.S. Geosciences, East Tennessee State University, Johnson City, Tennessee 2013
	B.A. Biology, Illinois Wesleyan University, Bloomington, Illinois 2009
	Public Schools, Creve Coeur and East Peoria, Illinois
Professional Experience:	Research Assistant, Department of Geosciences, ETSU, 2012-2013
	Teaching Assistant, Department of Geosciences, ETSU, 2011
	Field and Lab Assistant, Gray Fossil Site, ETSU, 2011-2013
	David B. Jones Intern, Ashfall Fossil Beds State Historical Park, NE, 2009, 2010
Publications/Presentations:	Morphology of *Teleoceras* (Mammalia: Rhinocerotidae) from the Gray Fossil Site (Gray, Tennessee), with Comparisons to Other Hemphillian Members of the Genus, SeAVP 2012